Structural and Functional Models for [NiFe] Hydrogenase

Raja Angamuthu

Cover-page illustration:

Crystal structure of $[Ni_6(cpss)_{12}]$ (Chapter 6). Ni, green; S, red; Cl, yellow; C, gray.

Printed by:

Ridderprint BV, Ridderkerk, The Netherlands

Structural and Functional Models for [NiFe] Hydrogenase

PROEFSCHRIFT

ter verkrijging van de graad van Doctor aan de Universiteit Leiden,

op gezag van Rector Magnificus prof. mr. P. F. van der Heijden,

volgens besluit van het College voor Promoties

te verdedigen op woensdag 14 oktober 2009

klokke 16.15 uur

door

Raja Angamuthu

geboren te Karur (Tamil Nadu), India in 1980

Promotiecommissie

Promotor	Prof. Dr. J. Reedijk
Copromotor	Dr. E. Bouwman
Overige leden	Prof. Dr. M. Schröder (The University of Nottingham, UK)
	Prof. Dr. M. Fontecave (Université Joseph Fourier, Grenoble, France)
	Dr. M. C. Feiters (Radboud Universiteit Nijmegen)
	Prof. Dr. M. T. M. Koper
	Prof. Dr. J. Brouwer

Table of Contents

a.u.	Arbitrary unit
ACN	Acetonitrile
APT	Attached Proton Test
b	Broad
bpy	2,2'-Bipyridine
CoM	Coenzyme M; 2-thioethane sulfonate
COSY	Correlation Spectroscopy
CV	Cyclic voltammetry; cyclic volammogram
Cys	Cysteine
d	Doublet
dedtc	Diethyldithiocarbamate
DMF	*N,N*-Dimethylformamide
dpa	Dipicolylamine
dppe	1,2-Bis(diphenylphosphino)ethane
E_{pa}	Anodic potential; oxidation potential
E_{pc}	Cathodic potential; reduction potential
EPPG	Edge plane pyrolytic graphite (electrode)
eq.	Equivalent
ESI-MS	Electrospray ionization mass spectrometry
Et	Ethyl
FTIR	Fourier transform infra red
GC	Glassy carbon
Glu	Glutamic acid
GSH	Glutathione
H_2ase	Hydrogenase
H_2bdt	Benzene-1,2-dithiol
H_2bme*-daco	1,5-bis(mercaptoethyl)-1,5-diazacyclooctane
H_2pdt	Propane-1,3-dithiol
H_2tpdt	2-Thiapropane-1,3-dithiol
Hacac	Acetylacetone, 2,4-pentanedione
HCp	1,3-Cyclopentadiene
HER	Dihydrogen evolution reaction
HG-GSH	Hemithioacetal
His	Histidine
HS–HPT	*N*-(7-mercaptoheptanoyl)-*O*-phospho-L-threonie; coenzyme B

J	Coupling constant
LMCT	Ligand-to-metal charge transfer
m	Multiplet in NMR; medium in IR
m/z	Ratio of mass upon charge
M_d	Distal metal
Me	Methyl
MeCoM	Methyl–coenzyme M; 2-(methylthio)ethanesulfonate
MLCT	Metal-to-ligand charge transfer
M_p	Proximal metal
NMR	Nuclear magnetic resonance
NOESY	Nuclear Overhauser Effect Spectroscopy
OTf^-	Trifluoridomethanesulfonate
PEM	Proton exchange membrane
Ph	Phenyl
PMe_3	Trimethylphosphine
PPh_3	Triphenylphosphine
ppm	Parts per million
ROESY	Rotating-Frame NOE Spectroscopy
s	Singlet in NMR; strong in IR
SCE	Standard calomel electrode
SHE	Standard hydrogen electrode
t	Triplet
^{t}Bu	*tertiary*-Butyl
TEA·HCl	Triethylamine hydrochloride
THF	Tetrahydrofuran
TMS	Tetramethylsilane
tmtu	1,1,3,3-tetramethyl-2-thiourea
TOCSY	Total Correlation Spectroscopy
tpa	Tripicolylamine
$TsOH·H_2O$	*para*-Toluenesulfonic Acid monohydrate
UV-Vis	Ultra violet and visible spectrocopy
Val	Valine
w	Weak
δ	Chemical shift
τ	Trigonality index

1

General Introduction

Abstract. The main goal of the research presented in this thesis is the synthesis of suitable structural and functional models for the enzyme [NiFe] hydrogenase, which can reduce protons† into dihydrogen. This chapter starts with a brief survey of the roles of all the known nickel-containing enzymes in biological systems with a focus on the [NiFe] hydrogenases. Structure, function, physicochemical and catalytic properties of the [NiFe] hydrogenase itself and of the reported model complexes are presented. This chapter concludes with the goal of the research and modeling strategies, followed by an outline of the thesis.

---

† Although strictly speaking natural isotope ratios require the use of “hydron”, hydride etc., throughout this thesis “proton” is used.

1.1. A Prelude to Nickel Biochemistry

Nickel is a relatively abundant element, constituting approximately 8% of the earth's core and 0.01% of the earth's crust. Organisms in nature have obtained nickel by leaching the most abundant form of nickel, Ni(II), from the earth's crust. It is perhaps puzzling then as to why no protein or enzymatic system containing functionally significant nickel was known until 1975, despite the fact that nickel is readily available.[1-4] Currently there are only nine proteins or enzymatic systems known in nature that encompass functionally significant nickel; the environment around nickel within each protein is different. Several aspects in the bioinorganic chemistry of nickel-containing enzymes are unusual in the context of known coordination chemistry of common nickel salts, as well as the functions in which these enzymes are involved (See Scheme 1.1).[5,6]

1. Urease

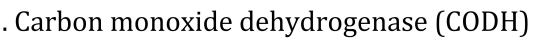

$$H_2N–CO–NH_2 + 2H_2O \longrightarrow 2NH_3 + H_2CO_3$$

2. Carbon monoxide dehydrogenase (CODH)

$$CO + H_2O \rightleftharpoons 2H^+ + CO_2 + 2e^-$$

3. Acetyl–coenzyme A synthase (ACS)

$$CH_3–CFeSP + CoA–SH + CO \rightleftharpoons CH_3–CO–SCoA + CFeSP$$

4. Glyoxalase I (GlxI)

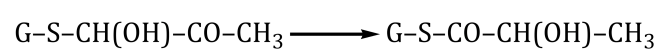

$$G–S–CH(OH)–CO–CH_3 \longrightarrow G–S–CO–CH(OH)–CH_3$$

5. Aci–reductone dioxygenase (ARD)

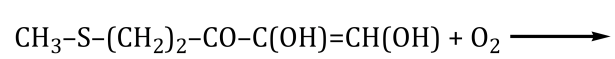

$$CH_3–S–(CH_2)_2–CO–C(OH)=CH(OH) + O_2 \longrightarrow$$
$$CH_3–S–(CH_2)_2COOH + HCOOH + CO$$

6. Methylenediurease (MDU)

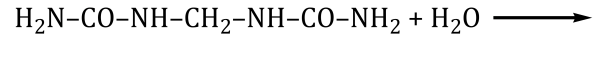

$$H_2N–CO–NH–CH_2–NH–CO–NH_2 + H_2O \longrightarrow$$
$$CO(NH_2)_2 + NH_3 + HCHO + CO_2$$

7. Methyl–coenzyme M reductase (MCR)

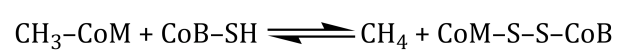

$$CH_3–CoM + CoB–SH \rightleftharpoons CH_4 + CoM–S–S–CoB$$

8. Superoxide dismutase (SOD)

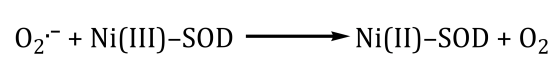

$$O_2^{\cdot -} + Ni(III)–SOD \longrightarrow Ni(II)–SOD + O_2$$

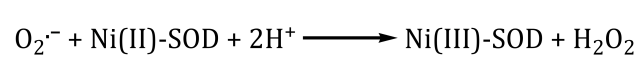

$$O_2^{\cdot -} + Ni(II)\text{-}SOD + 2H^+ \longrightarrow Ni(III)\text{-}SOD + H_2O_2$$

9. Hydrogenases (H_2ase)

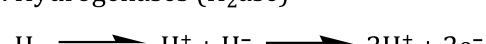

$$H_2 \rightleftharpoons H^+ + H^- \rightleftharpoons 2H^+ + 2e^-$$

Scheme 1.1. Nickel-containing enzymes and their roles in biology as known today.

1.2. Nickel-Containing Enzymes and their Role in Biological Systems

1.2.1. Introduction

Nickel-containing enzymes catalyze many critical and distinct biological processes. Most of them are industrially and environmentally significant, such as **(1)** hydrolysis of urea into ammonia and carbamate,[7-10] **(2)** reversible interconversion of carbon monoxide and carbon dioxide, **(3)** decomposition of the acetyl group into separate one-carbon units in some cells or catalyzing acetate synthesis using one-carbon precursors in others,[11-19] **(4)** detoxification of cytotoxic methylglyoxal (MG) via the isomerization of hemithioacetal,[4,20,21] **(5)** oxidation of 1,2-dihydroxy-3-keto-5-methylthiopentane (aci-reductone) into methylthio propionic acid, formic acid and carbon monoxide,[22-26] **(6)** degradation of methylenediurea (slow release fertilizer),[27] **(7)** methane generation,[28] **(8)** dismutation of toxic and cell damaging superoxide radical anions into harmless molecular oxygen[29,30] and on top of all, **(9)** reversible interconversion of dihydrogen into protons and electrons (Scheme 1.1).[31-35] The first eight enzymes are briefly discussed here. The hydrogenase enzymes are described in more detail in Section 1.3.

1.2.2. Urease

Urease (urea amidohydrolase) catalyzes the hydrolysis of urea to form ammonia and carbamate at approximately 10^{14} times the rate of the uncatalyzed reaction.[36] The carbamate formed spontaneously degrades in vivo to form a second molecule of ammonia and hydrogen carbonate.[37] This urease-catalyzed hydrolysis is in contrast with the uncatalyzed reaction, which affords ammonia and cyanic acid.[38] James B. Sumner successfully crystallized the enzyme urease from Jack bean in 1926 after almost nine years of hard work, as the first enzyme to be isolated in crystalline form.[7]

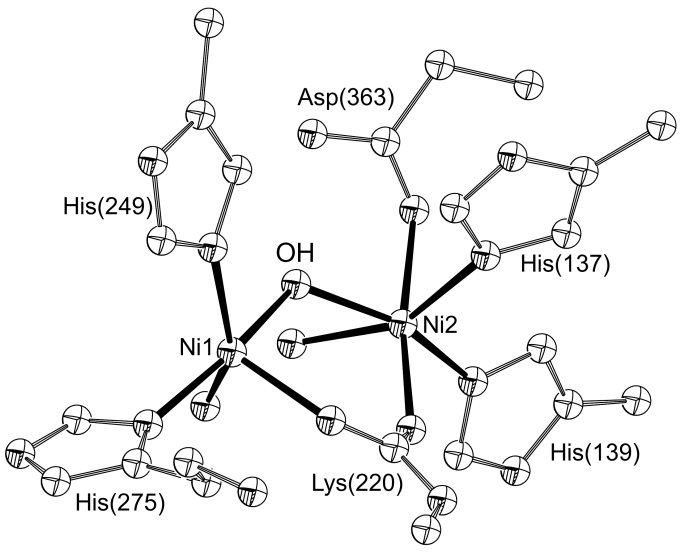

Fig. 1.1. Perspective view of the active site of urease (1FWJ).

The presence of a nickel center in the active site was discovered only fifty years after the isolation of the crystalline urease.[8] It took almost seventy years before the first crystal structure of a urease was reported.[6,9,10] The crystal structure of urease shows the active centre to contain a homodinuclear Ni_2 center. Each nickel ion is coordinated to a water molecule and two histidine nitrogen donors apart from the two bridges between the nickel centers formed by a hydroxido group and a carbamylated lysine (Fig. 1.1). Numerous dinuclear nickel(II) complexes have been reported in recent literature to mimic the structure and function of urease.[39-54]

1.2.3. CO Dehydrogenase/Acetyl-Coenzyme A Synthase (CODH/ACS)

The bifunctional enzyme CODH/ACS has an important role in the global carbon cycle as the C-cluster, an Ni–Fe–S centre, of CODH reduces carbon dioxide to carbon monoxide and the A-cluster, another Ni–Fe–S centre, of ACS assembles acetyl-CoA from a methyl group, coenzyme-A and the CO generated by the C-cluster (Scheme 1.1).[11,14,17,55-59] The A-cluster is a complex metallocofactor, containing an Fe_4S_4 group connected by cysteine bridging to M_p of a dinuclear $[M_pNi_d]$ site. The proximal metal M_p is predominantly Cu in the as-isolated enzyme from native *Moorella thermoacetica*, but [NiNi] and [ZnNi] forms are also known to be isolated and well studied (Fig. 1.2).[55-57,59,60]

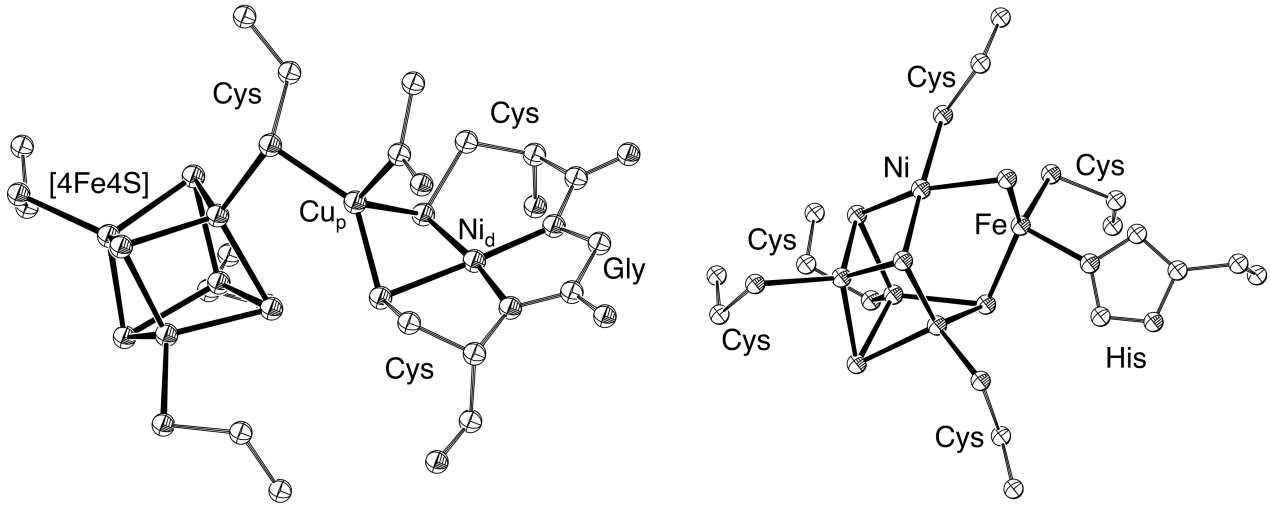

Fig. 1.2. Perspective view of the A-cluster of ACS (left, 1MJG) and the C-cluster of CODH (right, 1JJY).

The distal nickel ion Ni_d is in a square-planar (NiN_2S_2) geometry derived from two backbone carboxamido nitrogens and two Cys-S residues. The Ni_d centre is bridged through the two Cys-S donors to the proximal metal M_p that is in a tetrahedral coordination environment. A fourth nonprotein ligand (CO/acetyl) is bound to M_p to complete its coordination sphere. The C-cluster of CODH is a unique asymmetric $[NiFe_4S_5]$ assembly containing a four-coordinate square-planar nickel center linked to an

iron ion, which is extraneous to the cuboidal-like core, through a bridging sulfide (Fig. 1.2). Numerous model complexes mimicking the structure and functions of CODH/ACS, involving methyl transfer[61,62] and CO insertion[63-68] reactions, have been reported in recent years and have been recently reviewed.[69-73]

1.2.4. Glyoxalase I (GlxI)

Glyoxalase I, a member of the metalloglutathione transferase superfamily, catalyzes the first step in the detoxification of cytotoxic methyglyoxal (MG) via the conversion of nonenzymatically-produced hemithioacetals (HG-GSH) into *S*-D-lactoylglutathione and thereby plays a critical detoxification role in cells (Scheme 1.2). Yet, the mechanism of nickel incorporation into GlxI remains hard to pin down.[4,20,21] The three-dimensional structure of the enzyme is homodimeric with what appears to be two identical active sites (Fig. 1.3).[20] Each active site contains two histidine and two glutamic acid residues that coordinate to the metal ion along with two water molecules so that the catalytic metal ion has a distorted octahedral geometry.

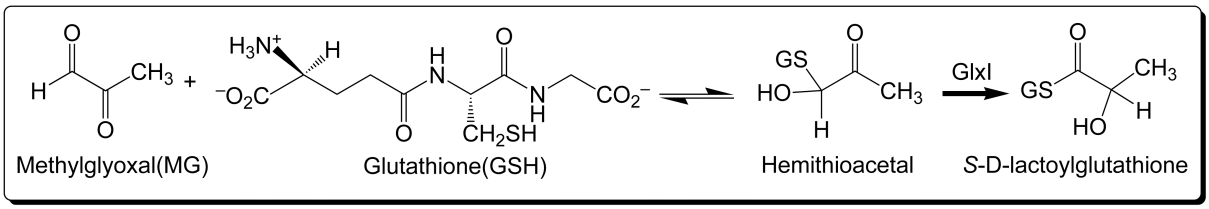

Scheme 1.2. Formation and isomerization of hemithioacetal.

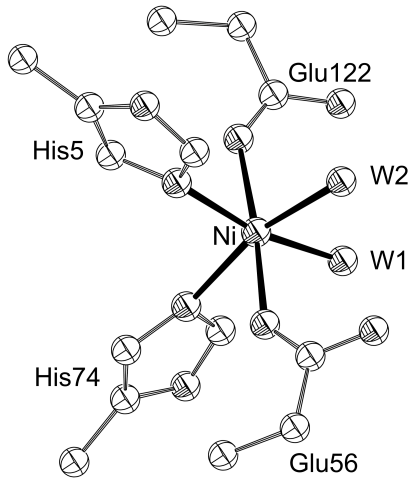

Fig. 1.3. Active site structure of glyoxalase (1F9Z).[20]

1.2.5. Aci-reductone Dioxygenase (ARD)

Aci-reductone dioxygenase was first discovered in 1993 in a study of the methionine salvage pathway in *Klebsiella pneumoniae*.[74] ARD was found to cleave the key intermediate of this pathway namely aci-reductone (1,2-dihydroxy-5-methylthiopent-1-

en-3-one) and its analogues.[75,76] Investigations using *K. pneumoniae* unveiled that aci-reductone is oxidized to two different sets of products. In the productive case, a dioxygenase activity produces formic acid and the α-ketoacid precursor of methionine.[25,75] In addition, a second, non-productive dioxygenase activity converts the aci-reductone into formate, carbon monoxide, and methylthiopropionic acid. Remarkably, these activities belong to the same protein (ARD), but result from the differences in metal content (Scheme 1.3). The reason for the presence of two isoforms of a protein with different metals is a mystery. Further investigations using recombinant protein confirmed that the productive activity is due to the iron-containing ARD and the non-productive activity is from the Ni– or Co–containing ARD.[75]

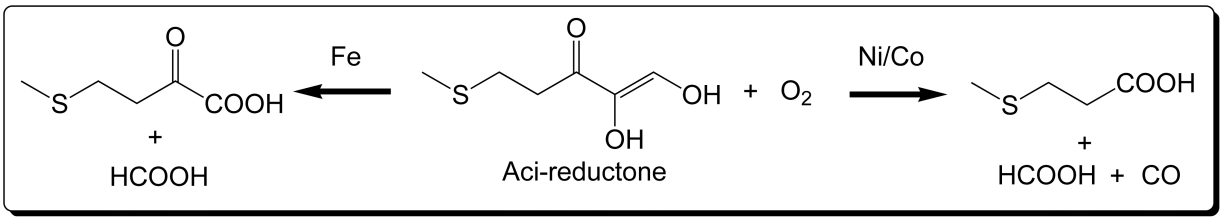

Scheme 1.3. Metal-dependent reactions carried out by ARD.

The global structure of ARD was elucidated employing high-resolution NMR spectroscopy,[24,26] while the active site structure was studied with by X-ray absorption spectroscopy.[23] The active site appears to have an octahedral geometry with three nitrogen donors provided by His96, His98 and His140 together with three oxygen donors provided by Glu102 and two water molecules. Among these six ligands, His96 and Glu102 are trans located at the paramagnetic nickel(II) ion.[23] A limited number of structural[77] and functional[78] models have been reported recently in an effort to understand the catalytic mechanism of ARD.

1.2.6. Methylenediurease (MDUase)

Methylenediurease (MDUase), isolated from *Burkholderia*, was found to be a nickel-dependent enzyme, which is able to degrade methylenediurea into urea and formaldehyde with ammonia and carbon dioxide as byproducts (Scheme 1.4).[27] Methyleneureas or ureaforms are condensation products of urea and aldehyde [(H_2N-(CO–NH–CH_2–NH)$_n$–CO–NH_2); n=1 for methylenediurea] which are potentially applied as slow-release fertilizers in bioremediation processes (more than 300,000 tons per year).[79-81] Significantly, the methylenediurease activity was resolved by anion exchange chromatography from urease activity of the same microorganism, and each enzyme was found to be specific toward its own substrate, such as *Ralstonia paucula* (methyleneureas),[80] *Burkholderia* (methylenediurea and dimethylenetriurea),[79] *Rhodococcus erythropolis* (isobutylidenediurea),[82] *Rhodococcus* (crotonylidenediurea).[79]

Further studies are necessary to characterize the structure and functional mechanism of this enzyme.

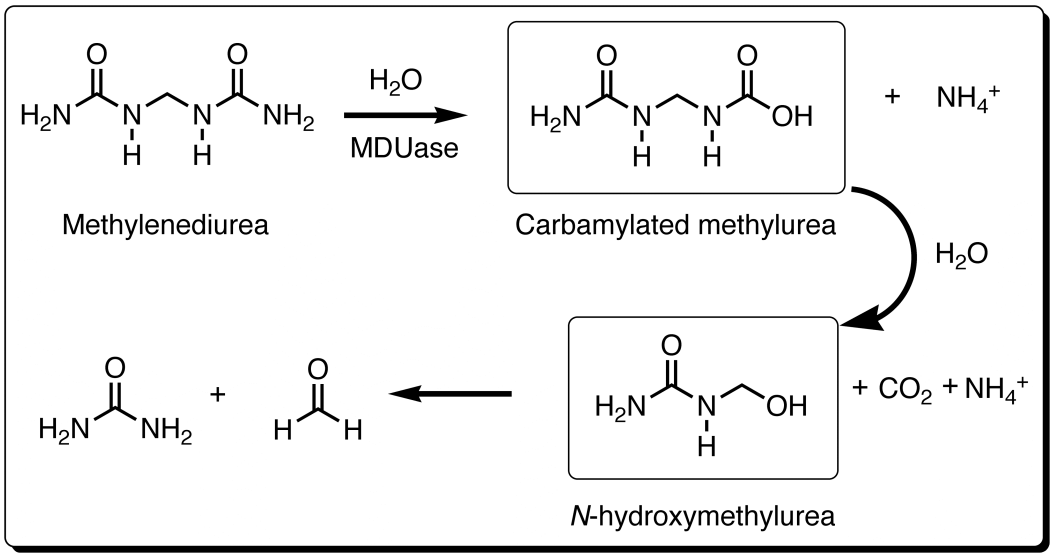

Scheme 1.4. Degradation pathway of methylenediurea by MDUase.

1.2.7. Methyl-Coenzyme M Reductase (MCR)

Methyl-coenzyme M reductase (MCR) is the key enzyme in biological methane formation by methanogenic archaea.[28,83,84] In the MCR active site, the nickel ion is present in the tightly, but non-covalently, bound tetrahydrocorphinoid complex called coenzyme F-430 (Fig. 1.4). The upper face of the F-430 cofactor forms the floor of a narrow hydrophobic well leading to the surface of the protein. The nickel ion is coordinated by the four pyrrolic nitrogens in the equatorial plane and by an oxygen of the glutamine side-chain in the lower axial position. The upper axial position contains either the thiolate or the sulfonate group of CoM, depending on the form of MCR isolated.

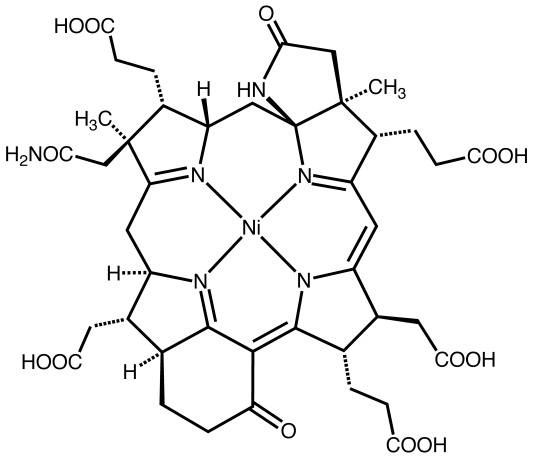

Fig. 1.4. Schematic view of coenzyme F-430 of MCR showing the extensively reduced tetrapyrrole ring in which the π chromophore only extends over three of the four nitrogens. A lactam ring and a six-membered carbocyclic ring enlarge the tetrapyrrole ring.[28,83]

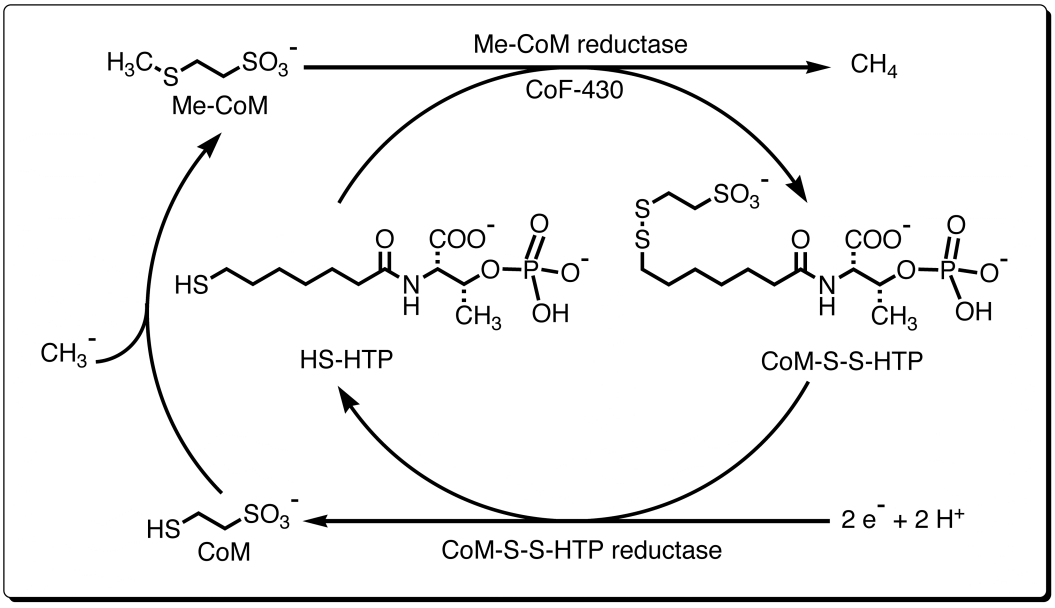

Scheme 1.5. Catalytic cycle involving the coenzyme F-430-assisted methane formation in methanogenic archaea (Adapted from the literature).[85]

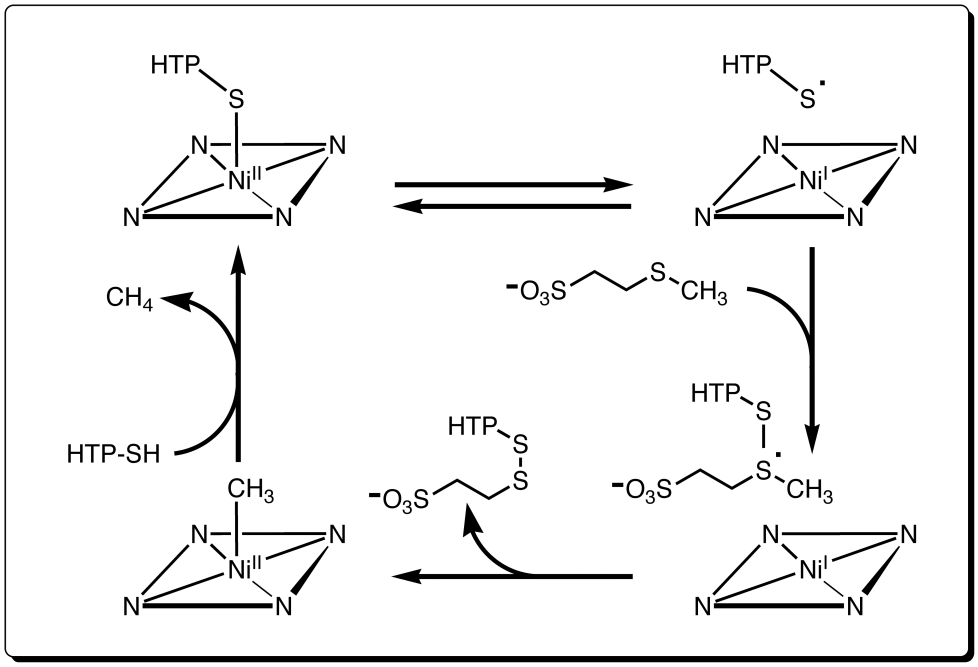

Scheme 1.6. Mechanism of F-430-catalyzed methane formation (Adapted from the literature).[85-87]

MCR catalyzes the reaction between the thioether methyl coenzyme M (MeCoM) and the thiol *N*-(7-mercaptoheptanoyl)-*O*-phospho-L-threonine (HS-HPT, coenzyme B) to give methane and the mixed disulfide CoM-S-S-HTP (Scheme 1.5). The nickel center of free coenzyme F-430, as well as its penta-ester or penta-amide derivatives, can be reduced reversibly to the Ni(I) valence state, which exhibits a characteristic quasi-axial

EPR spectrum and UV-visible absorption maxima at 380 and 750 nm. Conventional purification of MCR leads to an inactive enzyme that contains the metal in the Ni(II) valence state. The first isolation of highly active enzyme preparations from reductively preconditioned cells and the reductive reactivation of the so-called MCR_{ox1} state to active enzyme (MCR_{red1}) demonstrated that the enzyme is active only if the metal center of coenzyme F-430 is in the Ni(I) form.[88]

The mechanism shown in Scheme 1.6 postulates the formation of Ni(I) and a thiyl radical. The formed thiyl radical attacks the Me-CoM to form the sulfuranyl radical. The unpaired electron from the Ni(I) $d_{x^2-y^2}$ orbital transfers to the C-S σ^* orbital and induces the homolytic cleavage of the C-S bond to form the Ni(II) methyl-substituted coenzyme F-430 and the unsymmetrical disulfide. This methyl-substituted coenzyme F-430 is further attacked by HSCoB to release methane.

1.2.8. Nickel Superoxide Dismutase (Ni-SOD)

Nickel superoxide dismutase (Ni-SOD) is a recently discovered member of the nickel-containing metalloenzymes and of the SOD class of enzymes that catalyze the disproportionation of highly toxic superoxide ($O_2^{\bullet -}$) into peroxide (O_2^{2-}) and molecular oxygen.[29,30,89] Ni-SOD is the fourth member of this class of enzymes; the other known SODs containing Fe, Mn and Cu/Zn. Reduced Ni-SOD contains nickel(II) in a square-planar N_2S_2 coordination environment derived from the backbone terminal amino group of His1, the amide group, and the thiolate groups of Cys2 and Cys6 (Scheme 1.7).[30,90,91] The Nδ and Nε nitrogens of His1 are not involved in coordination; they are involved in hydrogen-bonding to the main-chain oxygen atom of Val8 (Nδ) and to Glu17 (Nε) of a neighboring subunit.[30] Oxidized Ni-SOD contains a Ni(III) ion in a distorted square-pyramidal N_3S_2 coordination environment derived from same units as reduced Ni-SOD and in addition the Nδ nitrogen of His1 (Scheme 1.7).

The presence of thiolate donors makes the Ni-SOD different from other SODs and the stabilization of these two thiolate ligands against sulfur-based oxidation in the presence of the highly active radical substrate remains elusive. The monomeric unit of this enzyme is a 4-helix bundle accommodating the active site at the N-terminus and six of these bundles make the whole molecule of a Ni-SOD as a homohexamer. The proposed mechanism of dismutation shows that the electron transfer from the nickel(II) ion to the axially bound superoxide must be coupled with a proton transfer to generate the dihydrogen peroxide. Site-specific mutagenesis studies confirm the significance of the histidine ligand, as altering this site tremendously decreases the dismutase activity.

A number of nickel complexes with N_2S_2 and N_3S_2 (bis-amide or bis-amine) coordination environment are available in literature before and after the report of the

crystal structure of a nickel-containing superoxide dismutase (Fig. 1.5).[92-96] NiN_2S_2 complexes can be reactive toward both H_2O_2 and O_2, often yielding S-based oxygenation products.[97] Synthetic studies have demonstrated that NiN_2S_2 complexes in bis-amine ligand environments are more stable toward oxygen than the corresponding bis-amide complexes.[70,92]

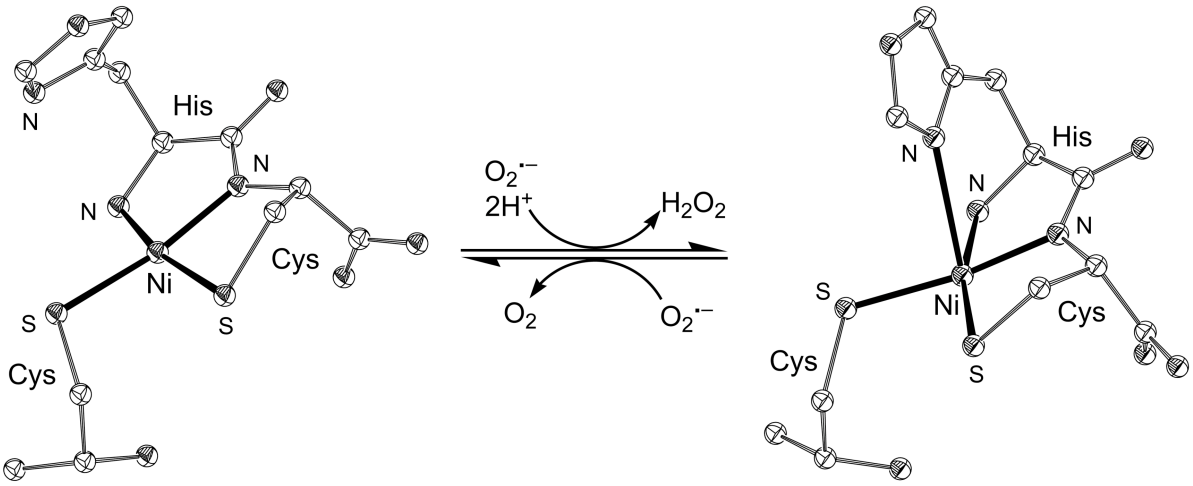

Scheme 1.7. Active site structures of reduced Ni-SOD showing the square-planar Ni(II) (1Q0K) and oxidized Ni-SOD showing the square-pyramidal Ni(III) with axially coordinated imidazole of His-1 (1Q0D) along with the detoxification reaction carried out by Ni-SOD.[30]

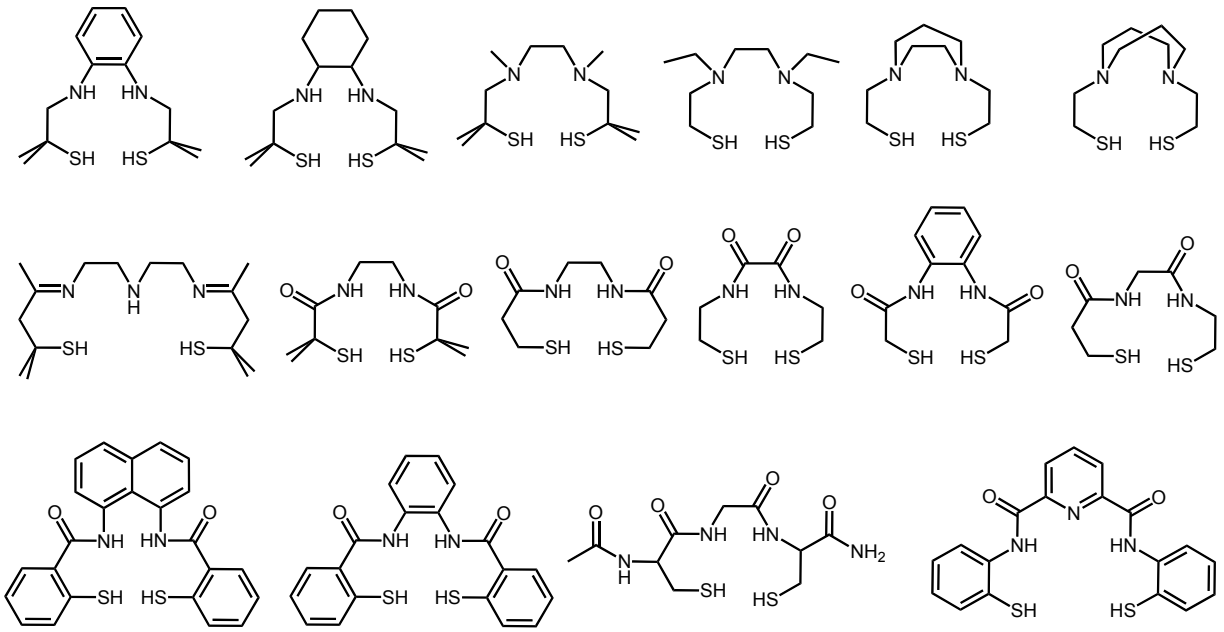

Fig. 1.5. Selection of N_2S_2 and N_3S_2 ligands used in the synthesis of nickel complexes to mimic Ni-SOD.[92-96]

Recently the first NiN_2S_2 complex $[Ni^{II}(beamm)]^-$ [H_2beamm = *N*-{2-[benzyl(2-mercapto-2-methylpropyl)amino]ethyl}-2-mercapto-2-methylpropionamide] (Fig. 1.6) containing amine/amide coordination has been reported with the studies on the difference between amine/amide and bisamide coordination on the models of Ni-SOD.[98] Bis-amine-coordinated NiN_2S_2 complex $[Ni^{II}(bmedach)]$ [H_2bmedach = *N*,*N*'-bis(2-mercaptoethyl)- 1,4-diazacycloheptane] (Fig. 1.6) possess a Ni^{II}/Ni^{III} redox potential far too positive to reduce superoxide ($E_{1/2}$ > 1.2 V *vs* Ag/Ag^+), while bis-amide-coordinated NiN_2S_2 complex $[Ni^{II}(emi)]^{2-}$ [H_2emi = *N*,*N*'-ethylenebis(2-mercaptoisobutyramide)] (Fig. 1.6) is incapable of oxidizing superoxide after accessing the Ni^{III} oxidation state.

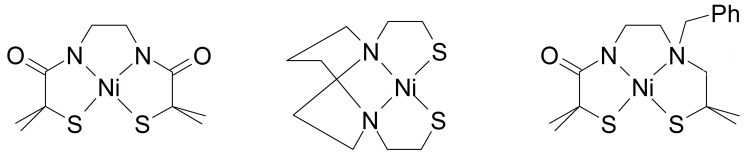

$[Ni^{II}(emi)]^{2-}$ $[Ni^{II}(bmedach)]$ $[Ni^{II}(beamm)]^{1-}$

Fig. 1.6. Comparison of NiN_2S_2 complexes with different environments.[98]

A model complex for Ni-SOD should have the Ni^{II}/Ni^{III} redox potential between 0.04 V and 1.09 V *vs* Ag/Ag^+, obviously because the oxidation and reduction potentials of the superoxide radical anion are respectively 0.04 V and 1.09 V *vs* Ag/Ag^+.[99] It has been postulated that the combination of amine and amide in an $Ni^{II}N_2S_2$ coordination environment ensures a Ni-centered one-electron oxidation process, appropriately tunes the Ni^{II}/Ni^{III} redox potential for SOD catalysis, and secures the thiolate donors from oxygenation by O_2.[98] However, $[Ni^{II}(beamm)]^-$ is not reactive towards $O_2^{\bullet-}$, even though it has an amine/amide mixed environment around the nickel ion; this suggests that the fifth axial coordination might be a key component for the SOD activity, as suggested by the site-specific mutagenesis studies.

1.3. Hydrogenases (H_2ases)

1.3.1. Introduction

Hydrogenases are a class of enzymes, which catalyze the interconversion of protons and electrons with molecular hydrogen ($H_2 \leftrightarrows H^+ + H^- \leftrightarrows 2H^+$).[100] The recent surge towards the development of cheap and clean alternatives for fossil fuels has drawn tremendous attention on the research concerning the active site structure of the hydrogenases and the mechanism behind their catalytic function.[101,102] Furthermore, the presence of biologically unusual ligands in the active sites of hydrogenases has drawn particular attention from the coordination and bioinorganic chemists.[103-110] Hydrogenases are classified into three types according to the metal content of the

active site, namely **(1)** [FeFe] hydrogenases, **(2)** [NiFe] hydrogenases and **(3)** [Fe] hydrogenases or iron-sulfur-cluster free hydrogenases. Although the main focus of this thesis is on the modeling of Ni-containing enzymes, all three classes are briefly discussed in the following sections.

1.3.2. [FeFe] Hydrogenases

[FeFe] hydrogenases and their model complexes are the most studied among the three types of hydrogenases.[111] The periplasmic [FeFe] hydrogenase is involved in H_2 uptake while the cytoplasmic [FeFe] hydrogenase is involved in dihydrogen production.[112]

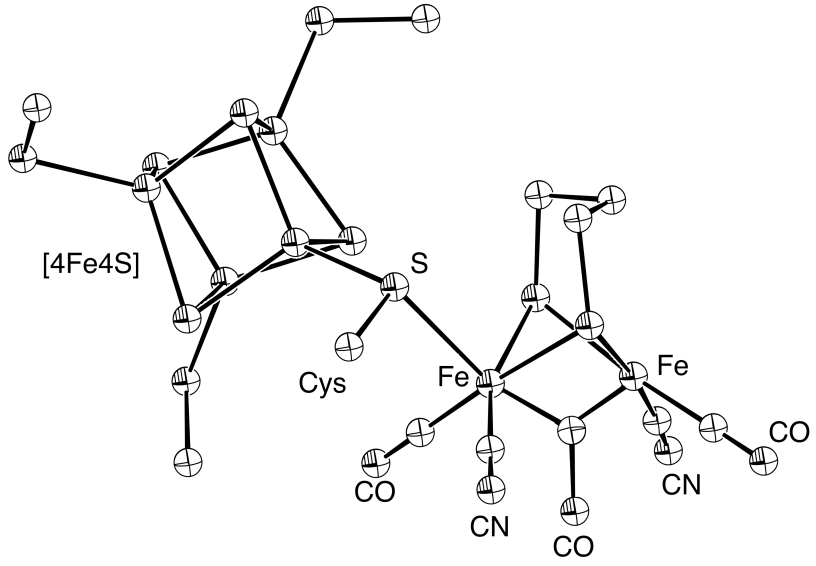

Fig. 1.7. Active site structure of [FeFe] hydrogenase (1FEH).

The H-cluster of [FeFe] hydrogenase active site is built up from two parts, namely, an [4Fe4S] cubane and a binuclear [2Fe2S] metal center bridged by a dithiolate ligand, linked to each other by a cysteinyl residue.[113,114] The metal centers in the binuclear site are bridged by the biologically unusual carbonyl ligand and a set of carbonyl and cyanide groups coordinate to each iron center. The coordination environment of the active site of [FeFe] hydrogenase can be simply formulated as $[(H_2O)(CN)(CO)Fe(SCH_2XCH_2S)Fe(CN)(CO)(\mu\text{-}S_{Cys})(Fe_4S_4)]$ (X = CH_2, NH, O). More detailed information on [FeFe] hydrogenase and its model complexes are available in recent reviews.[100,106,112,115-117]

1.3.3. [Fe] Hydrogenases

[Fe] hydrogenase is the relatively new member in the hydrogenase family, and is present in some methanogenic archaea.[118] [Fe] hydrogenase is also called iron-sulfur cluster free hydrogenase, owing to the fact that in contrast with other classes it contains

only a mononuclear iron center in the active site.[119] The [Fe] hydrogenase has been abbreviated as "Hmd" (H_2-forming methylenetetrahydromethanopterin), as it catalyzes the reversible reduction of methenyltetrahydromethanopterin (methenyl-H_4MPT^+) with dihydrogen to methylenetetrahydromethanopterin (methene-H_4MPT), which is an intermediary step in the biological conversion of CO_2 to methane (Scheme 1.8).

The iron ion in the active site of Hmd has a square-pyramidal geometry comprised of a pyridine-type nitrogen of the guanylylpyridone derivative coordinated apically to the iron center. The basal-plane comprises two *cis*-carbonyl ligands, a cysteinyl thiolate and an unknown ligand.[119] A water molecule is located *trans* to the pyridone derivative within a distance of 2.7 Å. The oxidation state of the iron center remains elusive; high-spin Fe(II) has been excluded, as the as-isolated form of the enzyme is not EPR active and Mössbauer experiments suggest low-spin Fe(0) or Fe(II).[120] More detailed information on the enzyme Hmd[118,119,121] and of its model complexes[122-125] are available in recent literature.[111]

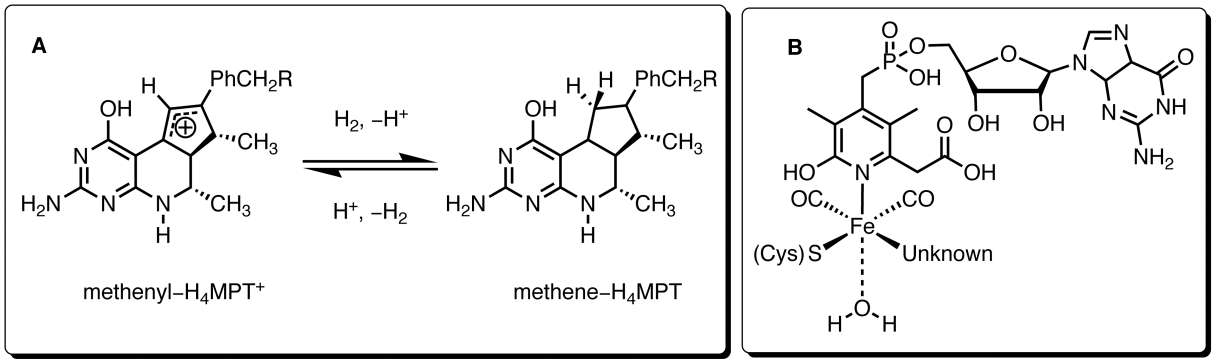

Scheme 1.8. (A) Reaction catalyzed by the [Fe] hydrogenase. (B) Schematic representation of the active site of the [Fe] hydrogenase showing the iron guanylylpridone cofactor (FeGP cofactor) from *M. jannaschii* (3DAG).[119]

1.3.4. [NiFe] Hydrogenases

[NiFe] hydrogenases are interesting among the three types of hydrogenases due the presence of the heterodinuclear active site (Fig. 1.8). They are further divided into four subclasses according to the functions in which they are involved namely, **(1)** H_2-uptake, **(2)** H_2-evolution, **(3)** bidirectional H_2-activation and **(4)** H_2-sensing. High-resolution X-ray crystal structures are available for the [NiFe] hydrogenases isolated from *D. gigas*,[31,126] *D. vulgaris*,[32,127-129] *D. fructosovorans*,[33,130,131] *D. sulfuricans*[35] and *Dm. baculatum.*[34]

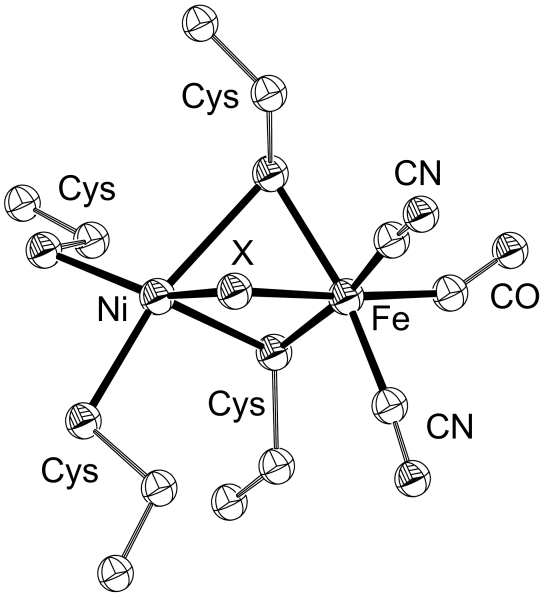

Fig. 1.8. Active site structure of [NiFe] hydrogenase from *D. gigas* (2FRV).

All the known X-ray structures have revealed a heterodinuclear active site which can be formulated as $[(Cys–S)_2Ni(\mu\text{-}S–Cys)_2Fe(CN)_2(CO)]$; it contains a NiS_4 center with four S-donors derived from cysteine residues, two of which bridge the nickel and iron center (Fig. 1.8). Surprisingly, the low-spin iron center is further coordinated by biologically unusual carbonyl and two cyanide groups. Even though the earlier studies speculated that these carbonyl and cyanide ligands are part of the catalytic center,[132] the X-ray structural studies suggest that these groups may just maintain the oxidation state of iron at 2+ in order to preserve its low-spin nature.[31]

As the "gas channel" from the surface of the enzyme ends at nickel[33,133] and the inhibitors CO and HOO^- bind at nickel,[127,128,130] the nickel ion is suggested to be the binding site of dihydrogen; yet DFT studies have shown the possibility of iron being the H_2 binding site.[117,134] Numerous studies suggest that only the nickel center is responsible for the redox state changes in the active site. All the observed redox states of the enzyme together present a highly complicated scheme of the catalytic cycle as shown in Scheme 1.9. The enzyme's different redox states in its active and inactive forms are distinguished by different notations in literature as shown in Scheme 1.9.

For the past ten years the biochemistry and modeling chemistry [NiFe] hydrogenase have grown tremendously and have been the subject of numerous reviews, from which more detailed information can be obtained.[100,104,111,112,116,117,134,135]

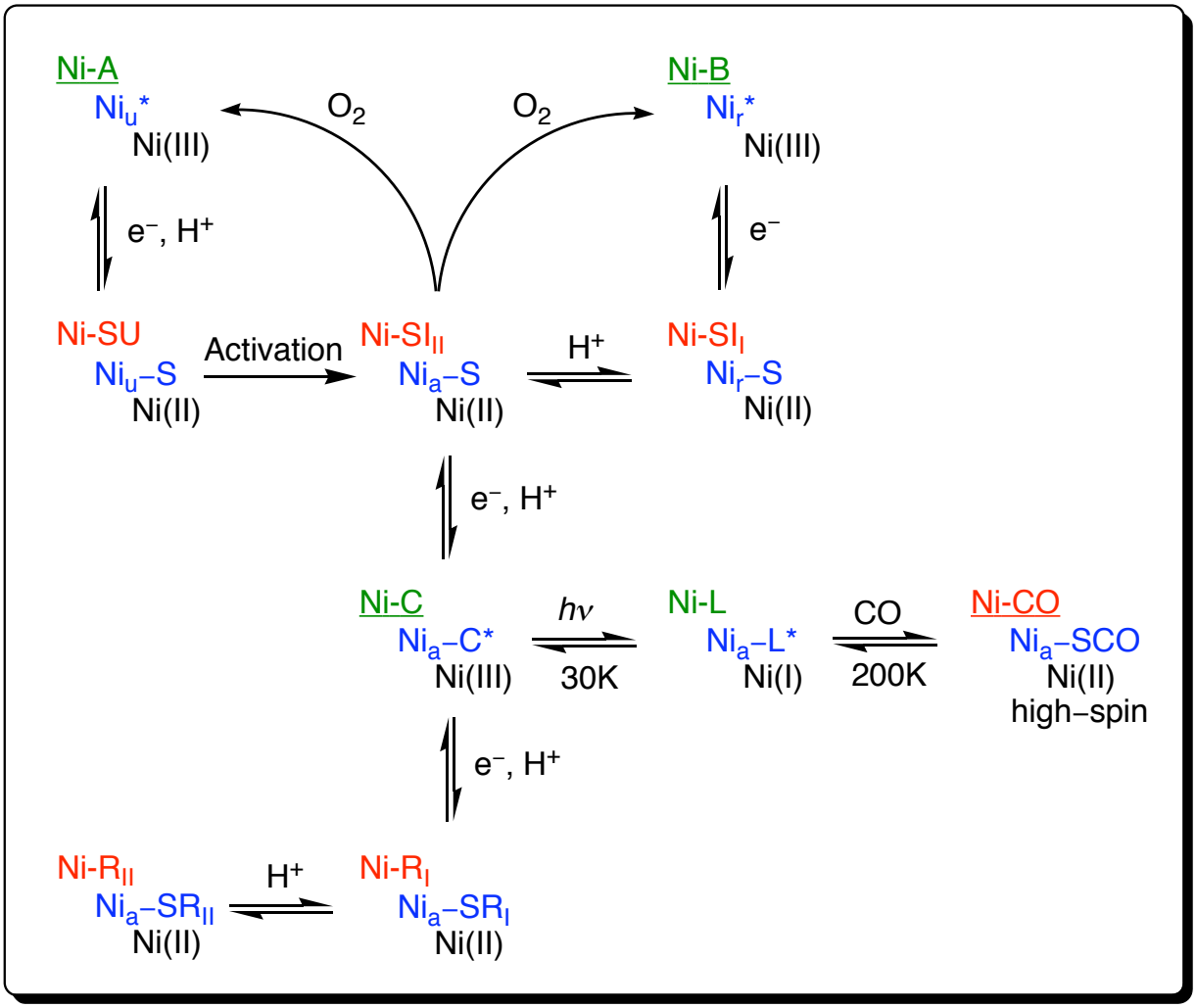

Scheme 1.9. Overview of different redox states proposed for [NiFe] hydrogenase showing various redox states of the enzyme (u, unready; r, ready; a, active; S, SI, EPR-silent).[117,134,136] EPR-active species are shown in green.[111] Diamagnetic species are shown in red. Alternative notations are denoted in blue. X-ray crystallographically characterized species are underlined.[34,126-130,137] In some reports Ni-SI$_I$ and Ni-SI$_{II}$ are denoted as Ni-SI$_{(b)}$ and Ni-SI$_{(a)}$, respectively.[138]

1.4. Modeling the Structure of [NiFe] Hydrogenases

1.4.1. Introduction

The report of the first X-ray crystal structure of a [NiFe] hydrogenase enzyme watered the surge towards better structural and functional models.[31] A large number of small molecular models comprising heterodinuclear [NiFe] complexes have been reported since the first structure report in 1996.[139] The field of heterodinuclear complexes modeling [NiFe] hydrogenases has been first reviewed in the year 2001,[110] a later review in the year 2003 focuses on both [NiFe] and [Fe-only] hydrogenases.[138] In the year 2005, Bouwman and coworkers reported a historic overview of the biomimetic models for [NiFe] hydrogenase that have been synthesized since the nickel content of the

enzyme was reported.[103] A large number of reports appeared in special issues of Chemical Reviews,[100,102,111,112,116,117,134,135,140] Coordination Chemistry Reviews[103,104,108,109,141-143] and Chemical Society Reviews,[144] that are helpful for the readers to obtain an overview of the biochemistry and structural properties of the enzyme, the model complexes and the techniques used to assess the functional activity of the model compounds. Some remarkable model systems and the major functional studies of the mimics are discussed in the following sections.

1.4.2. [NiFe] Complexes

A large number of heterodinuclear [NiFe] complexes have been reported as structural models for [NiFe] hydrogenase, since the first report of the X-ray crystal structure of the enzyme.[103,110,138,145] Darensbourg and coworkers reported the first reasonably accurate structural model for the [NiFe] hydrogenase, comprising of a Ni(II) ion in an N_2S_2 environment with one of the two thiolates bridging to an $Fe(CO)_4$ moiety (Fig. 1.9A); the Ni···Fe distance (3.76 Å) is rather large compared to the biological system (2.6-2.9 Å).[139]

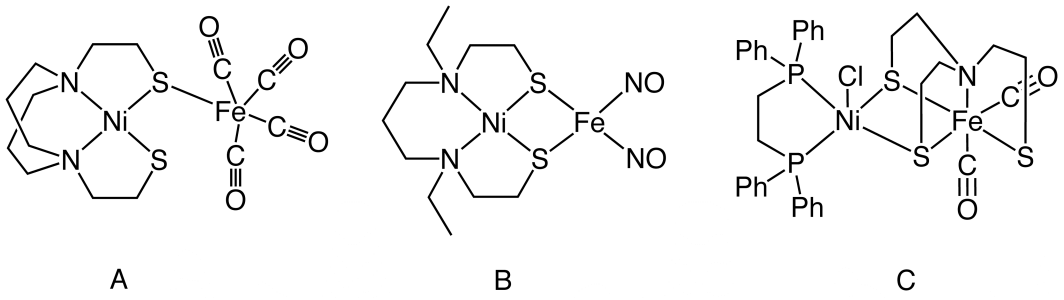

Fig. 1.9. [NiFe] complexes reported as mimics for [NiFe] hydrogenase by Darensbourg et al. (A),[139] Pohl et al. (B)[146] and Evans et al. (C).[147]

Pohl and coworkers reported the first [NiFe] complex in which two thiolates of a NiN_2S_2 metalloligand are bridging to the iron moiety resulting in a Ni to Fe distance of 2.8 Å (Fig. 1.9B).[146] Evans and coworkers reported the first [NiFe] complex containing two thiolates bridging to the iron center containing carbonyl ligands with a Ni···Fe distance of 3.3 Å (Fig. 1.9C).[147] This complex introduced the utilization of soft P-donor ligands instead of N-donor ligands to mimic the S-donor cysteinates of the [NiFe] hydrogenase.

Sellman and coworkers have reported a large series of transition-metal complexes of S-donor ligands. The first [NiFe] complex (Ni···Fe = 3.3 Å) comprising an NiS_4 coordination sphere with two thiolates bridging to the iron moiety with a carbonyl ligand was reported by Sellman and coworkers in 2002 (Fig. 1.10A).[148] In the same year, Bouwman and coworkers reported the S_4 ligand H_2xbsms

(1,2-bis(4-mercapto-3,3-dimethyl-2-thiabutyl)benzene) and its mononuclear low-spin nickel complex[149] which was the basis of a number of structural[150] and functional[145,151,152] models for [NiFe] hydrogenase. The compounds [Ni(xbsms)Fe(NO)$_2$] (Fig. 1.10B), [Ni(xbsms)Fe(CO)$_4$] (Fig. 1.10C) and [Ni(xbsms)Fe(CO)$_2$I$_2$] (Fig. 1.10D) were derived from [Ni(xbsms)] by reaction of the nickel complex with [Fe(CO)$_2$(NO)$_2$], [Fe$_2$(CO)$_9$] and [Fe(CO)$_4$I$_2$], respectively.[150]

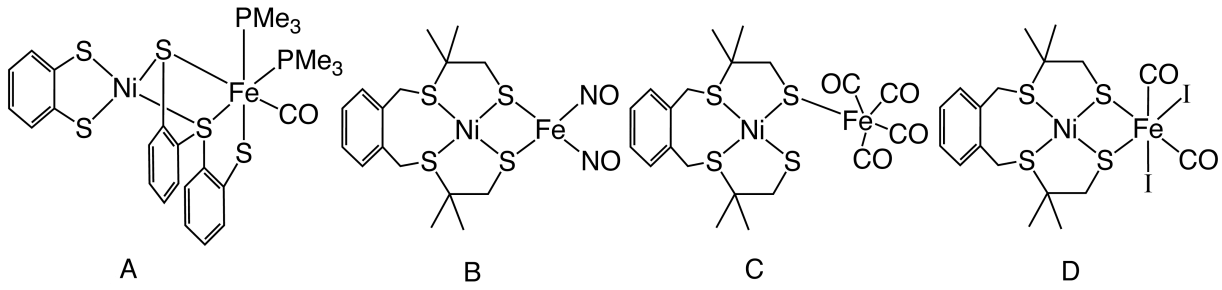

Fig. 1.10. Heterodinuclear [NiFe] complexes reported as mimics for [NiFe] hydrogenase by Sellman et al. (A)[148] and Bouwman et al. (B-D).[149,150]

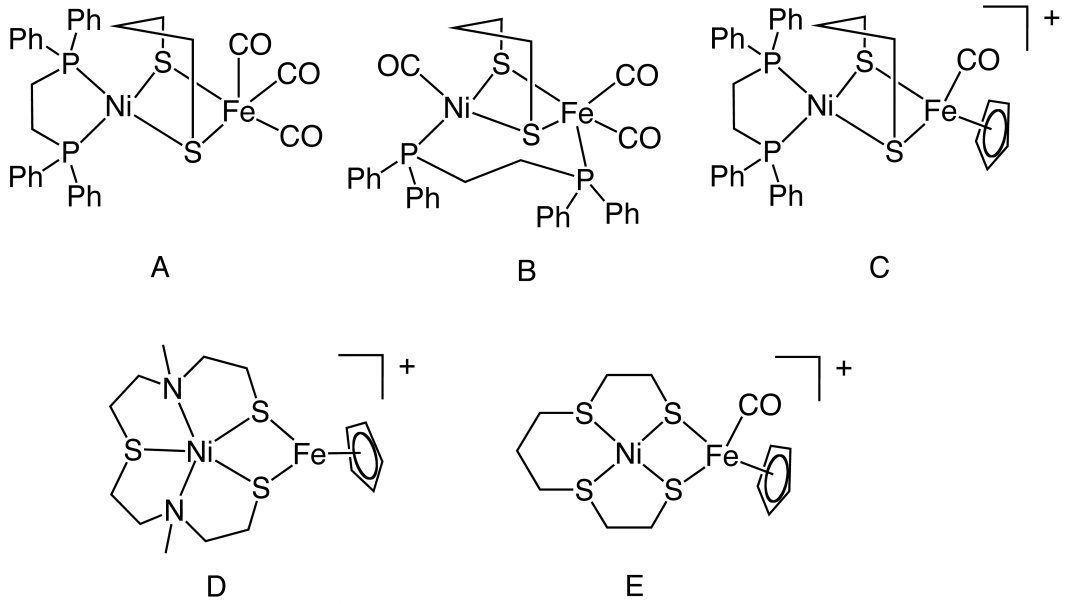

Fig. 1.11. Heterodinuclear [NiFe] complexes reported by Schröder et al.[153]

Breakthrough model complexes were reported by Schröder et al.[153] and Tatsumi et al.[154] in the year 2005. Where all the known [NiFe] complexes contain square-planar or square-based geometry around the nickel center, the complex [(dppe)Ni(μ-pdt)Fe(CO)$_3$] (dppe, 1,2bis(diphenylphosphino)ethane; pdt, propane-1,3-dithiolate) (Fig. 1.11A) interestingly was reported to have a distorted tetrahedral NiS$_2$P$_2$ coordination arrangement (Ni···Fe = 2.46 Å); surprisingly, this complex is diamagnetic.[153] Thus, the

nickel center in the square-planar precursor [Ni(pdt)(dppe)] has undergone a complete tetrahedral twist on binding of the $Fe(CO)_3$ moiety. The complex [(dppe)Ni(μ-pdt)$Fe(CO)_3$] (Fig. 1.11A) is unstable in solution and affords [(CO)Ni(μ-dppe)(μ-pdt)$Fe(CO)_2$] (Fig. 1.11B) upon rearrangement in benzene; this compound also contains a diamagnetic nickel center with the same Ni···Fe distance (2.47 Å). In addition, several other [NiFe] complexes were reported, obtained from [Fe(Cp)$(CO)_2$I] as a precursor. The [NiFe] complexes [(dppe)Ni(μ-pdt)Fe(Cp)(CO)]$^+$ (Fig. 1.11C), [Ni(N_2S_3)Fe(Cp)]$^+$ (Fig. 1.11D) and [Ni(S_4)Fe(Cp)(CO)]$^+$ (Fig. 1.11E) were reported with Ni···Fe distances of 2.78, 2.54 and 3.17 Å, respectively.[153]

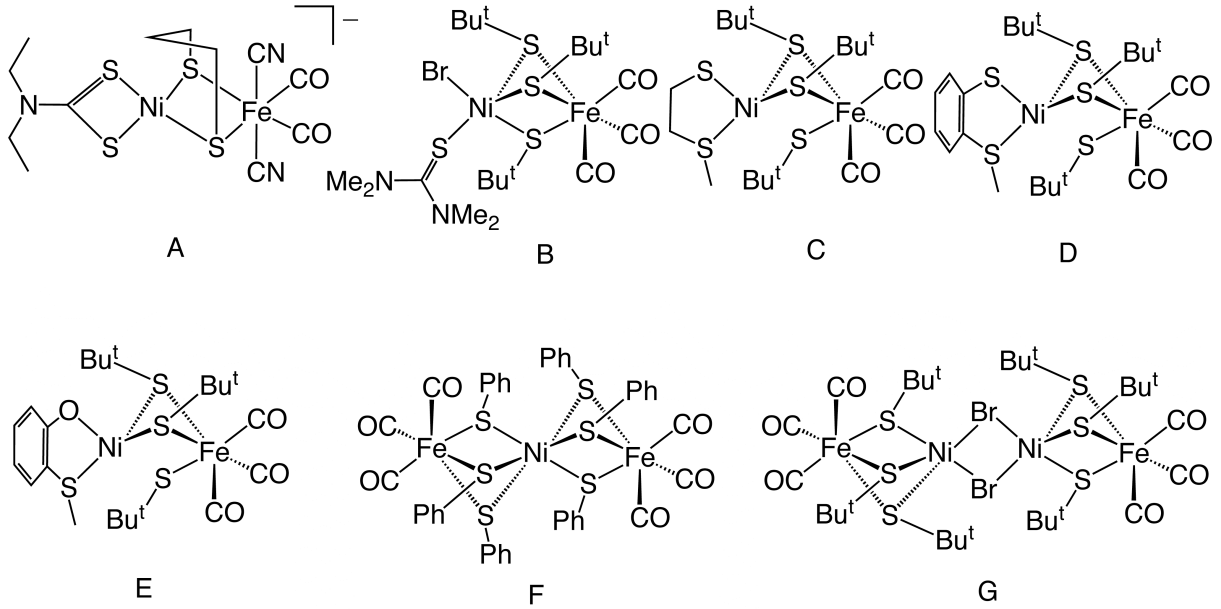

Fig. 1.12. Heterodinuclear and oligonuclear [NiFe] complexes reported by Tatsumi et al.[154,155]

The complex [(dedtc)Ni(μ-pdt)$Fe(CO)_2(CN)_2$]$^-$ (Fig. 1.12A) was reported as the closest yet structural model of that time comprising most of the elements matching the active site of [NiFe] hydrogenase; an S_4 coordination geometry around the nickel center, two thiolates bridging to the iron center (Ni···Fe = 3.05 Å) which coordinates to diatomic ligands (CO and CN).[154] Recently, Tatsumi et al. reported a number of [NiFe] complexes (Fig. 1.12B-E) formed from the reaction between the tetranuclear [Ni_2Fe_2] cluster [$(CO)_3$Fe(μ-S^{t}Bu)$_3$Ni(μ-Br)]$_2$ (Fig. 1.12G) and various S-donor ligands such as $SC(NMe_2)_2$, $NaS(CH_2)_2SMe$, $NaSC_6H_4SMe$ and $NaOSC_6H_4SMe$.[155] The linear clusters [$(CO)_3$Fe(μ-SPh)$_3$Ni(μ-SPh)$_3$$Fe(CO)_3$] (Fig. 1.12F) and [$(CO)_3$Fe($\mu$-S^{t}Bu)$_3$Ni($\mu$-Br)]$_2$ (Fig. 1.12G) were obtained from the reaction between $FeBr_2(CO)_4$ and $NiBr_2(C_2H_5OH)_4$ in the presence of the sodium salts of the corresponding thiols; both the precursors and the

resulting [NiFe] complexes were characterized by X-ray crystallography, despite the fact that these complexes were synthesized and manipulated at –40 °C.

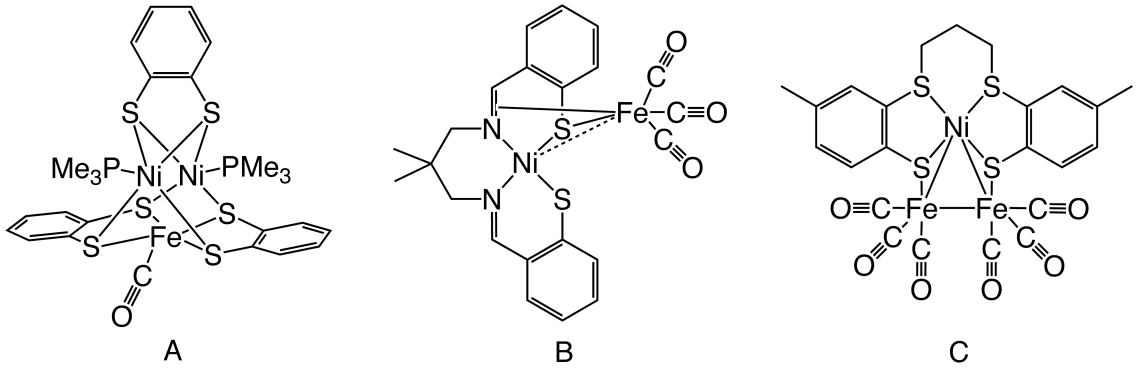

Fig. 1.13. [NiFe] complexes reported by Sellman et al. (A)[156,157] and Schröder et al. (B,C).[158-160]

The trinuclear [Ni_2Fe] complex [(bdt)($NiPMe_3$)$_2$Fe(CO)(bdt)$_2$] [bdt = benzene-1,2-dithiolate] (Fig. 1.13A) was reported as the first *functional* model for [NiFe] hydrogenase; upon reaction with HBF_4 this compound evolved molecular hydrogen and formed the stable one electron oxidized paramagnetic complex [(bdt)($NiPMe_3$)$_2$$Fe_2(CO)_2(bdt)_2$]$^+$.[156] The dinuclear complex [Ni(N_2S_2)Fe(CO)$_3$] (Fig. 1.13B) was reported by Schröder et al. with a diimine-dithiolato ligand coordinated to the nickel(II) ion and with the iron center of the Fe(CO)$_3$ moiety coordinated to the C=N π bond (Ni···Fe = 2.89 Å).[159] The two trinuclear complexes [(bdt)($NiPMe_3$)$_2$Fe(CO)(bdt)$_2$] (Fig. 1.13A) and [Ni(S_4)Fe_2(CO)$_6$] (Fig. 1.13C)[160] are so far the only [NiFe] complexes which show electrocatalytic activity in the reduction of protons into molecular hydrogen at –0.48 V *vs*. NHE[157] and –1.03 V *vs*. Fc/Fc^+,[158] respectively.

More recently, Schröder et al. reported a [$NiFe_2$] cluster (Fig. 1.14A) with interesting structural features formed from the reaction between the mononuclear nickel complex [Ni(S_5)] [H_2S_5 = bis(2-((2-mercaptophenyl)thiol)ethyl)sulfide] and [Fe_3(CO)$_{12}$] as a result of C–S and S–Ni bond cleavages.[161] The origin of and the mechanism by which the bridging sulfide ion is formed are unclear. The [$NiFe_2$] cluster comprises a NiS_3 moiety connected to two Fe(CO)$_3$ moieties by direct Ni-Fe bonds and a sulfide ion capping the [$NiFe_2$] equilateral triangle forming a trigonal pyramid (Fig. 1.14A).

Tatsumi et al.[162] reported the [NiFe] complex [(dedtc)Ni(μ-tpdt)Fe$(CN)_2$(CO)]$^-$ (Fig. 1.14B) formed from the reaction between [$(CN)_2$(CO)Fe($SCH_2CH_2SCH_2CH_2SK$)]$^-$ and [(PPh_3)NiBr(dedtc)] at –40 °C (dedtc = diethyldithiocarbamate; tpdt = 3-thiapentane-1,5-

dithiolate); the CN/CO bands in the IR spectrum of this complex reproduce those of the Ni–A, Ni–B and Ni–SU states of the [NiFe] hydrogenases.

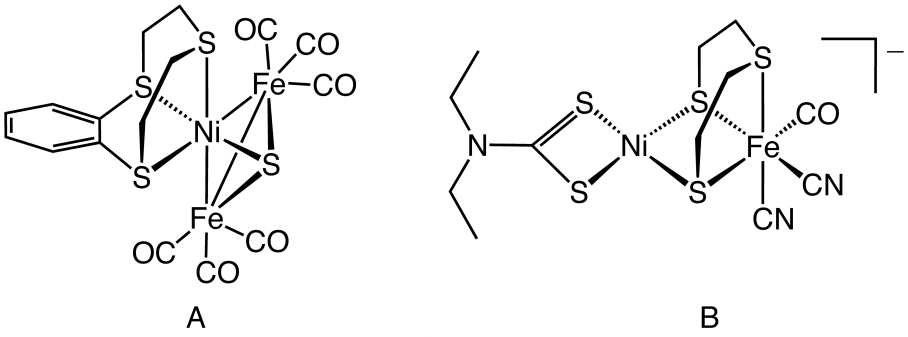

Fig. 1.14. [NiFe] complexes recently reported by Schröder et al. (A)[161] and Tatsumi et al. (B)[162].

A number of nickel-ruthenium complexes[145,151,152,163-167] have also been reported as models for [NiFe] hydrogenases (Fig. 1.15A-D), since the first report of $[Ni(S_2N_2)RuCp^*]_2(OTf)_2$ (Fig. 1.15A) and [Ni(bme*-daco)RuCp*(NCMe)]OTf (Fig. 1.15B) with NiN_2S_2 coordination geometry as models for ACS and [NiFe] hydrogenase.[163] A very recent review[111] from Pickett et al. covers many aspects of [Fe], [FeFe] and [NiFe] hydrogenase enzymes and of their model complexes. The review contains tables of CO stretching frequencies, metal-to-metal distances, redox potentials of selected complexes and other important features that may be useful for the interested readers.[111]

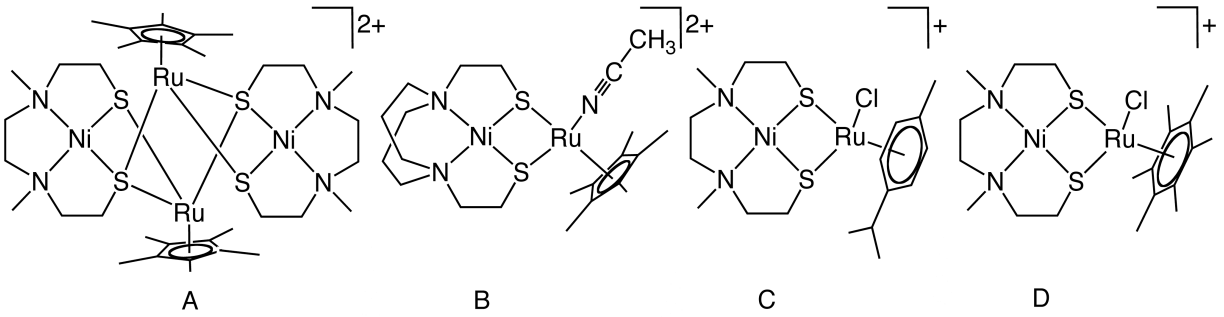

Fig. 1.15. [NiRu] complexes reported by Rauchfuss et al.[163]

1.5. Modeling the Function of Hydrogenases

1.5.1. Introduction

Most of the structural mimics of the hydrogenases discussed in the previous section are either not stable or not active towards the reduction of protons or oxidation of dihydrogen; many complexes have not been tested for their activity at all or their

reactivity was not reported. Various groups have synthesized many complexes solely in the aim of mimicking the functions of hydrogenases. Although model complexes have been reported as catalysts for proton reduction, activation of dihydrogen and H/D exchange reactions, only the complexes that are active catalysts for proton reduction are discussed in detail, in the view of the aim of this thesis.

1.5.2. Electrocatalysts for Proton Reduction

Until recently, the complexes $[(bdt)(NiPMe_3)_2Fe(CO)(bdt)_2]$ (Fig. 1.13A)[156] and $[Ni(S_4)Fe_2(CO)_6]$ (Fig. 1.13C)[160] were the only [NiFe] complexes reported to be active as electrocatalyst for proton reduction. The recent report from Rauchfuss et al.[168] presents a new type of synthetic approach towards [NiFe] complexes, with a bridging hydride ion as shown in Scheme 1.10. The hydride complex $[(CO)(dppe)Fe(pdt)(\mu\text{-H})Ni(dppe)]^+$ synthesized by this approach catalyses the reduction of protons at –1.37 V vs Fc/Fc^+ using trifluoroacetic acid as the proton source.

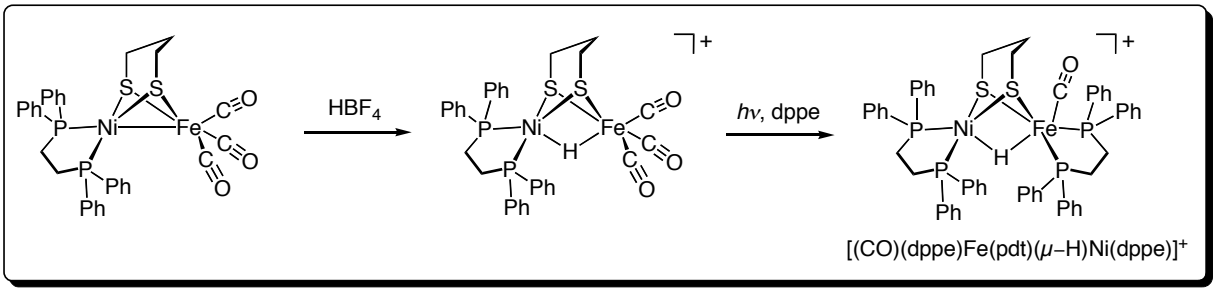

Scheme 1.10. [Ni(μ-H)Fe] complexes reported by Rauchfuss et al.[168]

Due to the pronounced stability of coordination complexes of chelating ligands, there has been considerable interest in stable and efficient electrocatalysts, such as nickel and cobalt complexes of macrocycles and multinuclear metallacrowns, as they can be potentially employed in PEM (Proton Exchange Membrane) water electrolysis cells.[169-172] A handful of transition-metal complexes, away from the interest of modeling the active site of hydrogenases, have also been reported to reduce protons into dihydrogen effectively with various overpotentials ranging between –1.5 and –0.2 V vs. SCE.[151,169,170,173-181]

A series of cobalt difluoroboryl-diglyoximate complexes have been reported recently to catalyze the electrochemical dihydrogen evolution at overpotentials as low as –0.20 V vs. SCE in acetonitrile.[170-172,182] The dinuclear complex $[(CpMo\text{-}\mu\text{-}S)_2S_2CH_2]$ has been reported as an electrocatalyst in the dihydrogen production showing almost 100% current efficiency when *p*-cyanoanilinium tetrafluoroborate was used as a proton

source.[173] The oxothiomolybdenum wheel $Li_2[Mo_8S_8O_8(OH)_8(oxalate)]$ has recently been shown to be a electrocatalyst producing dihydrogen from $HClO_4$, *p*-toluenesulfonic acid, trifluoroacetic acid and acetic acid at –1 V vs. SCE.[169]

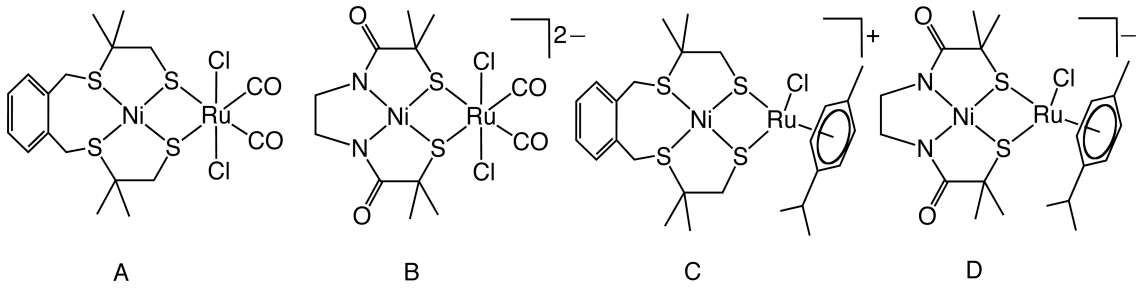

Fig. 1.16. [NiRu] complexes reported by Fontecave et al. as electrocatalysts for H_2 production.[151,152]

$[Ni(xbsms)Ru(CO)_2Cl_2]$ (Fig. 1.16A) was the first [NiRu] complex reported as a functional model for [NiFe] hydrogenase showing electrocatalytic properties to produce H_2 from a DMF solution of TEA·HCl at –1.50 V vs Ag/Ag^+.[152] $(NEt_4)_2[Ni(emi)Ru(CO)_2Cl_2]$ (Fig. 1.16B), $[Ni(xbsms)Ru(p\text{-}cymene)Cl]BF_4$ (Fig. 1.16C) and $(NEt_4)[Ni(emi)Ru(p\text{-}cymene)Cl]$ (Fig. 1.16D) were further reported with similar comparable H_2-evolution properties.[151] However, these complexes are leaving the researchers with the interesting question whether similar [NiFe] complexes can be used as electrocatalysts. A recent review from Artero et al.[141] provides detailed information about electrocatalysts for the proton-reduction reaction along with mechanistic details, while another review from Pickett et al.[111] tabulates the working potentials of a large selection electrocatalysts.

1.5.3. Photocatalysts for Proton Reduction

Due to the fact that dihydrogen production by cheaper and efficient sources is important in the context of the quest for alternative fuels, researchers have successfully made use of light-sensitive materials assisting redox systems in proton reduction. Recent reports from Artero et al.,[183,184] Reek et al.,[185] Song et al.[186,187] and Sun et al.[188-193] have demonstrated the utilization of photoactive complexes in photocatalytic dihydrogen production. These photosystems can be classified into three different types according to their constitution: **(1)** Photosensitizing systems, e.g. $Ru(bpy)_3$ covalently linked to a redox active center, such as a diiron moiety (Fig. 1.21A);[192-195] **(2)** Photosensitizing systems linked to a redox active system through non-covalent linkage such as metalloporphyrins (Fig. 1.21B);[185,186,189] **(3)** Homogeneous solutions containing photoactive materials, which can be reduced in the presence of light and a sacrificial electron donor; the reduced species then reduces the redox active species in order to

undergo the proton reduction.[183-185,190] Recent reviews provide detailed information on photocatalytic proton reduction.[107,111,188]

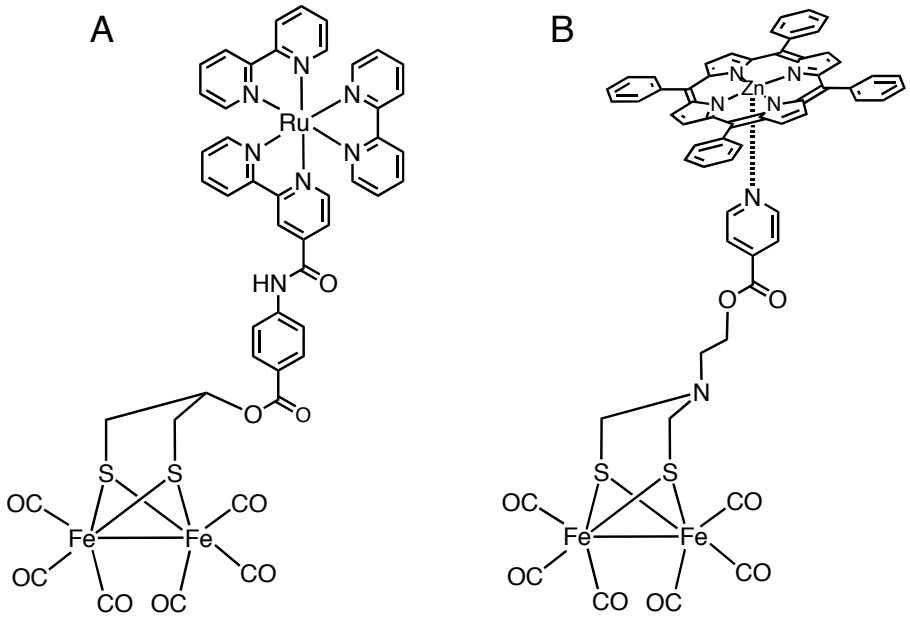

Fig. 1.17. Illustration of photocatalysts in the photoreduction of protons reported by Sun et al.[189,194]

1.5.4. Other Functional Models

Recently, the water soluble [NiRu] complex $[Ni(N_2S_2)Ru(H_2O)(C_6Me_6)](NO_3)_2$ (Fig. 1.18A) has been reported to form the hydride-bridged complex $[Ni(N_2S_2)(H_2O)(\mu\text{-}H)Ru(C_6Me_6)](NO_3)$ (Fig. 1.18B) by the reaction with H_2 in water. The latter complex catalyses the H/D exchange in acidic medium (pH 4-6).[166] Furthermore, $[Ni(N_2S_2)Ru(H_2O)(C_6Me_6)](NO_3)_2$ produces the hydroxido bridged complex $[Ni(N_2S_2)Ru(OH)(C_6Me_6)](NO_3)_2$ in basic medium (pH 7-10), which catalyses the hydrogenation of carbonyl compounds.[167]

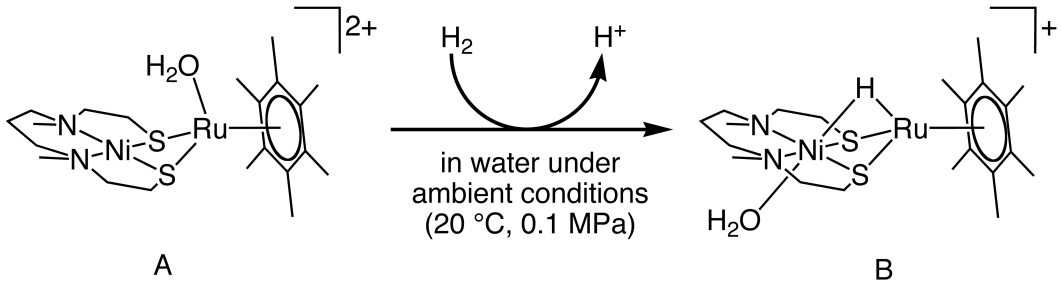

Fig. 1.18. Heterodinuclear [NiRu] complexes reported by Ogo et al.[166]

1.6. Aim and Outline of the Research

1.6.1. Aim

The aim of the research described in this thesis is the synthesis of new structural and functional models for the enzyme [NiFe] hydrogenase. By varying the steric and electronic properties of the ligands, attempts will be undertaken to tune the structural and redox properties of the [Ni] and [NiFe] complexes. Owing to the fact that the research towards the models for [NiFe] hydrogenase has led to a handful of unexpected and exciting findings, this thesis also reports structural and/or functional models of other Ni-containing enzymes such as ACS/CODH and MCR.

1.6.2. Modeling Strategy

The travel along the literature on the models complexes of hydrogenases that appeared after the report of the crystal structure of *D. gigas* provides a clear view of the gradual developments and the interesting facts about this particular discipline of chemistry.

The first phase of the modeling was to make stable mononuclear nickel complexes with NiS_4 coordination spheres, inspired by the complex [Ni(xbsms)][149] introduced by my predecessor, which formed the basis for many stable interesting [NiFe][150,196] and [NiRu][145,151,152] complexes as structural and functional models. A library of tetradentate chelating S_4-donor ligands containing two thioether and two thiolate donors were designed/selected (Fig. 1.19) to be used in the synthesis of stable low-spin nickel(II) complexes. The variation in the bridges (C2, C3 and C4) and the dimethyl substitution were introduced in the view of controlling steric and electronic properties of the complexes.

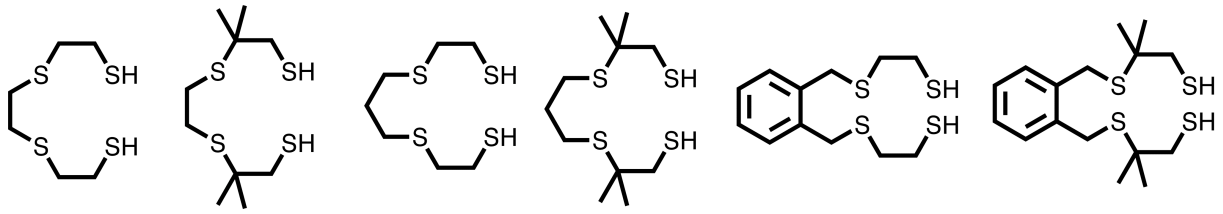

Fig. 1.19. Tetradentate chelating $S_2S'_2$-donor ligands selected for the synthesis of low-spin nickel complexes.

The second phase was to use new bidentate S_2-donor ligands for the synthesis of $Ni(S_2)_2$ complexes thereby providing flexibility around the Ni center (Fig. 1.20). The R groups were varied and the dimethyl groups were introduced in the view of fine-tuning the geometrical and electronic properties of the complexes.

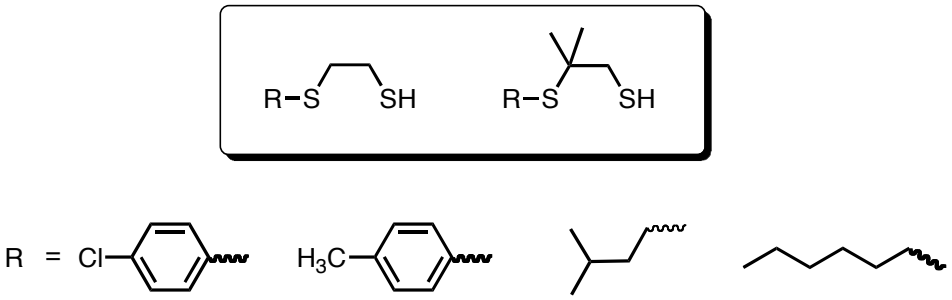

Fig. 1.20. Bidentate chelating SS'-donor ligands selected in the present study.

The third phase was using the low-spin nickel complexes synthesized with the $S_2S'_2$-donor and SS'-donor ligands in the synthesis of heterodinuclear [NiFe] complexes by reacting them with Fe moieties such as $[Fe(Cp)(CO)]^{2+}$ (Cp, cyclopentadienyl).

The final phase was to use Ru-containing moieties such as $[Ru(bpy)_2]^{2+}$ and $[Ru(tpa)]^{2+}$ instead of iron-containing moieties in order to enhance the stability of the model systems. Further to study the effect of attaching photosensitive groups directly to the redox active center (Fig. 1.21) in contrast to the conventional methods (Fig. 1.17).

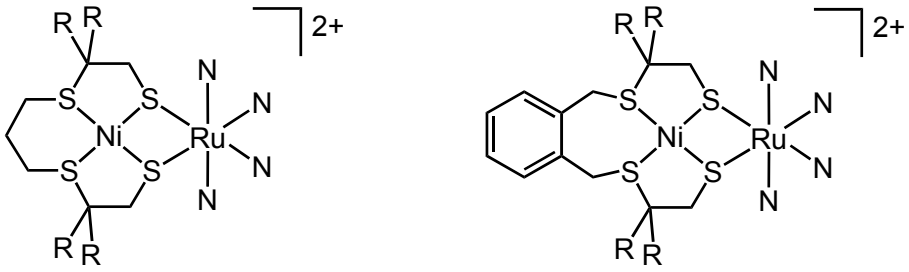

Fig. 1.21. Heterodinuclear [NiRu] complexes planned; R = H or Me; Bipyridine or tripicolylamine are used as N-donor ligands.

1.6.3. Outline of the Thesis

The design, syntheses and characterizations of new tetradentate dithioether-dithiolate ligands and bidentate thioether-thiolate ligands are presented in Chapter **2**; schemes of the syntheses of the ligands and simplified code notations for the ligands and of their precursors, and intermediates have also been provided in this Chapter.

A library of new low-spin nickel complexes of new tetradentate dithioether-dithiolate ligands are reported in Chapter **3**. These low-spin nickel complexes were reacted with $[Fe(C_5H_5)(CO)I]$ to obtain [NiFe] complexes, including one reported complex; their electrocatalytic properties towards proton reduction are also reported in Chapter **3**. Chapter **4** is devoted to analogous [NiFe] complexes based on new $[Ni(S_2)_2]$ complexes. The $[Ni(S_2)_2]$ complexes reported in this chapter were obtained by the reaction of $Ni(acac)_2$ with bidentate thioether-thiolate ligands reported in Chapter **2**.

The reactivity of four $[Ni(S_4)]$ complexes with the $[Ru(bpy)_2(EtOH)_2]$ moiety in order to make [NiRu] complexes and of their proton reducing abilities are presented in Chapter **5**. A serendipitously obtained hexanuclear Ni_6-thiolate metallacrown, its reactivity with iodine, protonation studies and the proton reduction abilities are presented in Chapter **6**. Reactivity of a new $[Ni(S_2)_2]$ complex reported in Chapter **4** towards CuI yielded a heterooctanuclear cage possessing interesting structural features including Ni–H anagostic interactions, which is reported in Chapter **7**. A light-induced C–S bond cleavage in a nickel thiolate complex with relevance to the function of methyl-coenzyme M reductase (MCR) is presented in Chapter **8**.

In Chapter **9**, a summary of all the results reported in the previous chapters, important general conclusions drawn from the studies and future prospects for further research are provided. Parts of this thesis have been published,[197-199] or have been submitted for publication;[200] some manuscripts are under preparation.[201-207]

1.7. References

1. J. C. Fontecilla-Camps and S. W. Ragsdale, *Adv. Inorg. Chem.*, 1999, **47**, 283-333.
2. J. J. R. Frausto da Silva and R. J. P. Williams, *The Biological Chemistry of the Elements*, Clarendon Press, Oxford, 1991.
3. W. Kaim and B. Schwederski, *Bioinorganic Chemistry: Inorganic Elements in the Chemistry of Life*, John Wiley & Sons Ltd., Chichester, 1994.
4. N. Sukdeo, E. Daub and J. F. Honek, Biochemistry of the Nickel-Dependent Glyoxalase I Enzymes, in *Nickel and Its Surprising Impact in Nature*, eds. A. Sigel, H. Sigel and R. K. O. Sigel, John Wiley & Sons, New York, 2007, pp. 445-471.
5. S. W. Ragsdale, *Curr. Opin. Chem. Biol.*, 1998, **2**, 208-215.
6. R. P. Hausinger, *J. Biol. Inorg. Chem.*, 1997, **2**, 279-286.
7. J. B. Sumner, *J. Biol. Chem.*, 1926, **69**, 435-441.
8. N. E. Dixon, C. Gazzola, R. L. Blakeley and B. Zerner, *J. Am. Chem. Soc.*, 1975, **97**, 4131-4133.
9. P. A. Karplus, M. A. Pearson and R. P. Hausinger, *Acc. Chem. Res.*, 1997, **30**, 330-337.
10. E. Jabrie, M. B. Carr, R. P. Hausinger and P. A. Karplus, *Science*, 1995, **268**, 998-1004.
11. T. I. Doukov, L. C. Blasiak, J. Seravalli, S. W. Ragsdale and C. L. Drennan, *Biochemistry*, 2008, **47**, 3474-3483.
12. T. I. Doukov, H. Hemmi, C. L. Drennan and S. W. Ragsdale, *J. Biol. Chem.*, 2007, **282**, 6609-6618.
13. C. L. Drennan, T. I. Doukov and S. W. Ragsdale, *J. Biol. Inorg. Chem.*, 2004, **9**, 511-515.
14. T. I. Doukov, T. M. Iverson, J. Seravalli, S. W. Ragsdale and C. L. Drennan, *Science*, 2002, **298**, 567-572.

15. C. L. Drennan, J. Y. Heo, M. D. Sintchak, E. Schreiter and P. W. Ludden, *Proc. Natl. Acad. Sci. U. S. A.*, 2001, **98**, 11973-11978.
16. H. Dobbek, V. Svetlitchnyi, L. Gremer, R. Huber and O. Meyer, *Science*, 2001, **293**, 1281-1285.
17. J. Seravalli, W. W. Gu, A. Tam, E. Strauss, T. P. Begley, S. P. Cramer and S. W. Ragsdale, *Proc. Natl. Acad. Sci. U. S. A.*, 2003, **100**, 3689-3694.
18. P. A. Lindahl, *Biochemistry*, 2002, **41**, 2097-2105.
19. E. L. Maynard and P. A. Lindahl, *J. Am. Chem. Soc.*, 1999, **121**, 9221-9222.
20. M. M. He, S. L. Clugston, J. F. Honek and B. W. Matthews, *Biochemistry*, 2000, **39**, 8719-8727.
21. Z. D. Su, N. Sukdeo and J. F. Honek, *Biochemistry*, 2008, **47**, 13232-13241.
22. G. D. Straganz and B. Nidetzky, *ChemBioChem*, 2006, **7**, 1536-1548.
23. F. Al-Mjeni, T. Ju, T. C. Pochapsky and M. J. Maroney, *Biochemistry*, 2002, **41**, 6761-6769.
24. T. C. Pochapsky, S. S. Pochapsky, T. T. Ju, H. P. Mo, F. Al-Mjeni and M. J. Maroney, *Nat. Struct. Biol.*, 2002, **9**, 966-972.
25. Y. Dai, P. C. Wensink and R. H. Abeles, *J. Biol. Chem.*, 1999, **274**, 1193-1195.
26. H. P. Mo, Y. Dai, S. S. Pochapsky and T. C. Pochapsky, *J. Biomol. NMR*, 1999, **14**, 287-288.
27. T. Jahns, R. Schepp, C. Siersdorfer and H. Kaltwasser, *Acta Biol. Hung.*, 1998, **49**, 449-454.
28. U. Ermler, W. Grabarse, S. Shima, M. Goubeaud and R. K. Thauer, *Science*, 1997, **278**, 1457-1462.
29. H. D. Youn, E. J. Kim, J. H. Roe, Y. C. Hah and S. O. Kang, *Biochem. J.*, 1996, **318**, 889-896.
30. J. Wuerges, J. W. Lee, Y. I. Yim, H. S. Yim, S. O. Kang and K. D. Carugo, *Proc. Natl. Acad. Sci. U. S. A.*, 2004, **101**, 8569-8574.
31. A. Volbeda, M. H. Charon, C. Piras, E. C. Hatchikian, M. Frey and J. C. Fontecilla-Camps, *Nature*, 1995, **373**, 580-587.
32. Y. Higuchi, T. Yagi and N. Yasuoka, *Structure*, 1997, **5**, 1671-1680.
33. Y. Montet, P. Amara, A. Volbeda, X. Vernede, E. C. Hatchikian, M. J. Field, M. Frey and J. C. FontecillaCamps, *Nat. Struct. Biol.*, 1997, **4**, 523-526.
34. E. Garcin, X. Vernede, E. C. Hatchikian, A. Volbeda, M. Frey and J. C. Fontecilla-Camps, *Structure*, 1999, **7**, 557-566.
35. P. M. Matias, C. M. Soares, L. M. Saraiva, R. Coelho, J. Morais, J. Le Gall and M. A. Carrondo, *J. Biol. Inorg. Chem.*, 2001, **6**, 63-81.
36. L. Pauling, *The Nature of the Chemical Bond*, Cornel university, Ithaca, New York, 1948.
37. R. L. Blakeley, J. A. Hinds, H. E. Kunze, E. C. Webb and B. Zerner, *Biochemistry*, 1969, **8**, 1991-2000.
38. R. L. Blakeley, A. Treston, R. K. Andrews and B. Zerner, *J. Am. Chem. Soc.*, 1982, **104**, 612-614.
39. G. Estiu and K. M. Merz, *J. Am. Chem. Soc.*, 2004, **126**, 11832-11842.
40. S. Mukherjee, T. Weyhermuller, E. Bothe, K. Wieghardt and P. Chaudhuri, *Eur. J. Inorg. Chem.*, 2003, 863-875.
41. D. Gaynor, Z. A. Starikova, S. Ostrovsky, W. Haase and K. B. Nolan, *Chem. Commun.*, 2002, 506-507.
42. A. M. Barrios and S. J. Lippard, *Inorg. Chem.*, 2001, **40**, 1250-1255.
43. A. M. Barrios and S. J. Lippard, *J. Am. Chem. Soc.*, 2000, **122**, 9172-9177.
44. S. Benini, W. R. Rypniewski, K. S. Wilson, S. Miletti, S. Ciurli and S. Mangani, *J. Biol. Inorg. Chem.*, 2000, **5**, 110-118.
45. A. M. Barrios and S. J. Lippard, *J. Am. Chem. Soc.*, 1999, **121**, 11751-11757.
46. F. Meyer, E. Kaifer, P. Kircher, K. Heinze and H. Pritzkow, *Chem.-Eur. J.*, 1999, **5**, 1617-1630.
47. D. A. Brown, L. P. Cuffe, O. Deeg, W. Errington, N. J. Fitzpatrick, W. K. Glass, K. Herlihy, T. J. Kemp and H. Nimir, *Chem. Commun.*, 1998, 2433-2434.
48. T. Koga, H. Furutachi, T. Nakamura, N. Fukita, M. Ohba, K. Takahashi and H. Okawa, *Inorg. Chem.*, 1998, **37**, 989-996.
49. S. Uozumi, H. Furutachi, M. Ohba, H. Okawa, D. E. Fenton, K. Shindo, S. Murata and D. J. Kitko, *Inorg. Chem.*, 1998, **37**, 6281-6287.

50. K. Yamaguchi, S. Koshino, F. Akagi, M. Suzuki, A. Uehara and S. Suzuki, *J. Am. Chem. Soc.*, 1997, **119**, 5752-5753.
51. D. Volkmer, B. Hommerich, K. Griesar, W. Haase and B. Krebs, *Inorg. Chem.*, 1996, **35**, 3792-3803.
52. D. Volkmer, A. Horstmann, K. Griesar, W. Haase and B. Krebs, *Inorg. Chem.*, 1996, **35**, 1132-1135.
53. A. J. Stemmler, J. W. Kampf, M. L. Kirk and V. L. Pecoraro, *J. Am. Chem. Soc.*, 1995, **117**, 6368-6369.
54. H. E. Wages, K. L. Taft and S. J. Lippard, *Inorg. Chem.*, 1993, **32**, 4985-4987.
55. S. W. Ragsdale, *Crit. Rev. Biochem. Mol. Biol.*, 2004, **39**, 165-195.
56. E. L. Hegg, *Accounts Chem. Res.*, 2004, **37**, 775-783.
57. J. Seravalli, Y. M. Xiao, W. W. Gu, S. P. Cramer, W. E. Antholine, V. Krymov, G. J. Gerfen and S. W. Ragsdale, *Biochemistry*, 2004, **43**, 3944-3955.
58. J. Seravalli and S. W. Ragsdale, *Biochemistry*, 2000, **39**, 1274-1277.
59. C. Darnault, A. Volbeda, E. J. Kim, P. Legrand, X. Vernéde, P. A. Lindahl and J. C. Fontecilla-Camps, *Nat. Struct. Biol.*, 2003, **10**, 271-279.
60. A. Volbeda and J. C. Fontecilla-Camps, *Dalton Trans.*, 2005, 3443-3450.
61. S. W. Ragsdale and C. G. Riordan, *J. Biol. Inorg. Chem.*, 1996, **1**, 489-493.
62. M. S. Ram and C. G. Riordan, *J. Am. Chem. Soc.*, 1995, **117**, 2365-2366.
63. D. Sellmann, D. Haussinger, F. Knoch and M. Moll, *J. Am. Chem. Soc.*, 1996, **118**, 5368-5374.
64. M. C. Smith, J. E. Barclay, S. C. Davies, D. L. Hughes and D. J. Evans, *Dalton Trans.*, 2003, 4147-4151.
65. C. S. Shultz, J. M. DeSimone and M. Brookhart, *Organometallics*, 2001, **20**, 16-18.
66. C. S. Shultz, J. M. DeSimone and M. Brookhart, *J. Am. Chem. Soc.*, 2001, **123**, 9172-9173.
67. G. C. Tucci and R. H. Holm, *J. Am. Chem. Soc.*, 1995, **117**, 6489-6496.
68. Y. M. Hsiao, S. S. Chojnacki, P. Hinton, J. H. Reibenspies and M. Y. Darensbourg, *Organometallics*, 1993, **12**, 870-875.
69. D. J. Evans, *Coord. Chem. Rev.*, 2005, **249**, 1582-1595.
70. O. Hatlevik, M. C. Blanksma, V. Mathrubootham, A. M. Arif and E. L. Hegg, *J. Biol. Inorg. Chem.*, 2004, **9**, 238-246.
71. C. G. Riordan, *J. Biol. Inorg. Chem.*, 2004, **9**, 542-549.
72. C. G. Riordan, *J. Biol. Inorg. Chem.*, 2004, **9**, 509-510.
73. T. C. Harrop and P. K. Mascharak, *Coord. Chem. Rev.*, 2005, **249**, 3007-3024.
74. R. W. Myers, J. W. Wray, S. Fish and R. H. Abeles, *J. Biol. Chem.*, 1993, **268**, 24785-24791.
75. Y. Dai, T. C. Pochapsky and R. H. Abeles, *Biochemistry*, 2001, **40**, 6379-6387.
76. J. W. Wray and R. H. Abeles, *J. Biol. Chem.*, 1995, **270**, 3147-3153.
77. E. Szajna, P. Dobrowolski, A. L. Fuller, A. M. Arif and L. M. Berreau, *Inorg. Chem.*, 2004, **43**, 3988-3997.
78. E. Szajna, A. M. Arif and L. M. Berreau, *J. Am. Chem. Soc.*, 2005, **127**, 17186-17187.
79. T. Jahns, H. Ewen and H. Kaltwasser, *J. Polym. Environ.*, 2003, **11**, 155-159.
80. T. Jahns and H. Kaltwasser, *J. Polym. Environ.*, 2000, **8**, 11-16.
81. T. Jahns, R. Schepp, C. Siersdorfer and H. Kaltwasser, *J. Environ. Polym. Degrad.*, 1999, **7**, 75-82.
82. T. Jahns and R. Schepp, *Biodegradation*, 2001, **12**, 317-323.
83. U. Ermler, *Dalton Trans.*, 2005, 3451-3458.
84. R. K. Thauer, *Microbiology-(UK)*, 1998, **144**, 2377-2406.
85. L. Signor, C. Knuppe, R. Hug, B. Schweizer, A. Pfaltz and B. Jaun, *Chem.-Eur. J.*, 2000, **6**, 3508-3516.
86. B. Jaun, *Helv. Chim. Acta*, 1990, **73**, 2209-2217.
87. A. Berkessel, *Bioorganic Chem.*, 1991, **19**, 101-115.
88. M. Goubeaud, G. Schreiner and R. K. Thauer, *Eur. J. Biochem.*, 1997, **243**, 110-114.
89. B. Palenik, B. Brahamsha, F. W. Larimer, M. Land, L. Hauser, P. Chain, J. Lamerdin, W. Regala, E. E. Allen, J. McCarren, I. Paulsen, A. Dufresne, F. Partensky, E. A. Webb and J. Waterbury, *Nature*, 2003, **424**, 1037-1042.

90. D. P. Barondeau, C. J. Kassman, C. K. Bruns, J. A. Tainer and E. D. Getzoff, *Protein Sci.*, 2004, **13**, 192-192.
91. D. P. Barondeau, C. J. Kassmann, C. K. Bruns, J. A. Tainer and E. D. Getzoff, *Biochemistry*, 2004, **43**, 8038-8047.
92. C. A. Grapperhaus, C. S. Mullins, P. M. Kozlowski and M. S. Mashuta, *Inorg. Chem.*, 2004, **43**, 2859-2866.
93. T. C. Harrop, M. M. Olmstead and P. K. Mascharak, *Inorg. Chem.*, 2006, **45**, 3424-3436.
94. T. C. Harrop, M. M. Olmstead and P. K. Mascharak, *Inorg. Chem.*, 2005, **44**, 9527-9533.
95. T. C. Harrop, M. M. Olmstead and P. K. Mascharak, *Inorg. Chim. Acta*, 2002, **338**, 189-195.
96. P. V. Rao, S. Bhaduri, J. F. Jiang and R. H. Holm, *Inorg. Chem.*, 2004, **43**, 5833-5849.
97. C. A. Grapperhaus and M. Y. Darensbourg, *Acc. Chem. Res.*, 1998, **31**, 451-459.
98. J. Shearer and N. F. Zhao, *Inorg. Chem.*, 2006, **45**, 9637-9639.
99. J. Shearer and L. M. Long, *Inorg. Chem.*, 2006, **45**, 2358-2360.
100. P. M. Vignais and B. Billoud, *Chem. Rev.*, 2007, **107**, 4206-4272.
101. R. Cammack, R. Frey and R. Robson, *Hydrogen as a Fuel. Learning from Nature*, Taylor & Francis, London, 2001.
102. W. Lubitz and W. Tumas, *Chem. Rev.*, 2007, **107**, 3900-3903.
103. E. Bouwman and J. Reedijk, *Coord. Chem. Rev.*, 2005, **249**, 1555-1581.
104. M. Bruschi, G. Zampella, P. Fantucci and L. De Gioia, *Coord. Chem. Rev.*, 2005, **249**, 1620-1640.
105. J.-F. Capon, F. Gloaguen, P. Schollhammer and J. Talarmin, *Coord. Chem. Rev.*, 2005, **249**, 1664-1676.
106. X. Liu, S. K. Ibrahim, C. Tard and C. J. Pickett, *Coord. Chem. Rev.*, 2005, **249**, 1641-1652.
107. L. Sun, B. Åkermark and S. Ott, *Coord. Chem. Rev.*, 2005, **249**, 1653-1663.
108. P. M. Vignais, *Coord. Chem. Rev.*, 2005, **249**, 1677-1690.
109. A. Volbeda and J. C. Fontecilla-Camps, *Coord. Chem. Rev.*, 2005, **249**, 1609-1619.
110. A. C. Marr, D. J. E. Spencer and M. Schröder, *Coord. Chem. Rev.*, 2001, **219**, 1055-1074.
111. C. Tard and C. J. Pickett, *Chem. Rev.*, 2009, **109**, 2245-2274.
112. J. C. Fontecilla-Camps, A. Volbeda, C. Cavazza and Y. Nicolet, *Chem. Rev.*, 2007, **107**, 4273-4303.
113. Y. Nicolet, C. Piras, P. Legrand, C. E. Hatchikian and J. C. Fontecilla-Camps, *Structure*, 1999, **7**, 13-23.
114. J. W. Peters, W. N. Lanzilotta, B. J. Lemon and L. C. Seefeldt, *Science*, 1998, **282**, 1853-1858.
115. J.-F. Capon, F. Gloaguen, F. Y. PÈtillon, P. Schollhammer and J. Talarmin, *Coord. Chem. Rev.*, 2009, **253**, 1476-1494.
116. W. Lubitz, E. Reijerse and M. van Gastel, *Chem. Rev.*, 2007, **107**, 4331-4365.
117. P. E. M. Siegbahn, J. W. Tye and M. B. Hall, *Chem. Rev.*, 2007, **107**, 4414-4435.
118. S. Shima and R. K. Thauer, *Chem. Rec.*, 2007, **7**, 37-46.
119. S. Shima, O. Pilak, S. Vogt, M. Schick, M. S. Stagni, W. Meyer-Klaucke, E. Warkentin, R. K. Thauer and U. Ermler, *Science*, 2008, **321**, 572-575.
120. S. Shima, E. J. Lyon, R. K. Thauer, B. Mienert and E. Bill, *J. Am. Chem. Soc.*, 2005, **127**, 10430-10435.
121. S. Vogt, E. J. Lyon, S. Shima and R. K. Thauer, *J. Biol. Inorg. Chem.*, 2008, **13**, 97-106.
122. B. V. Obrist, D. F. Chen, A. Ahrens, V. Schunemann, R. Scopelliti and X. L. Hu, *Inorg. Chem.*, 2009, **48**, 3514-3516.
123. X. Wang, Z. Li, X. Zeng, Q. Luo, D. J. Evans, C. J. Pickett and X. Liu, *Chem. Commun.*, 2008, 3555-3557.
124. Y. S. Guo, H. X. Wang, Y. M. Xiao, S. Vogt, R. K. Thauer, S. Shima, P. I. Volkers, T. B. Rauchfuss, V. Pelmenschikov, D. A. Case, E. E. Alp, W. Sturhahn, Y. Yoda and S. P. Cramer, *Inorg. Chem.*, 2008, **47**, 3969-3977.
125. A. R. Sadique, W. W. Brennessel and P. L. Holland, *Inorg. Chem.*, 2008, **47**, 784-786.
126. A. Volbeda, E. Garcia, C. Piras, A. L. deLacey, V. M. Fernandez, E. C. Hatchikian, M. Frey and J. C. FontecillaCamps, *J. Am. Chem. Soc.*, 1996, **118**, 12989-12996.

127. H. Ogata, S. Hirota, A. Nakahara, H. Komori, N. Shibata, T. Kato, K. Kano and Y. Higuchi, *Structure*, 2005, **13**, 1635-1642.
128. H. Ogata, Y. Mizoguchi, N. Mizuno, K. Miki, S. Adachi, N. Yasuoka, T. Yagi, O. Yamauchi, S. Hirota and Y. Higuchi, *J. Am. Chem. Soc.*, 2002, **124**, 11628-11635.
129. Y. Higuchi, H. Ogata, K. Miki, N. Yasuoka and T. Yagi, *Structure*, 1999, **7**, 549-556.
130. A. Volbeda, L. Martin, C. Cavazza, M. Matho, B. W. Faber, W. Roseboom, S. P. J. Albracht, E. Garcin, M. Rousset and J. C. Fontecilla-Camps, *J. Biol. Inorg. Chem.*, 2005, **10**, 239-249.
131. A. Volbeda, Y. Montet, X. Vernede, E. C. Hatchikian and J. C. Fontecilla-Camps, *Int. J. Hydrog. Energy*, 2002, **27**, 1449-1461.
132. K. A. Bagley, E. C. Duin, W. Roseboom, S. P. J. Albracht and W. H. Woodruff, *Biochemistry*, 1995, **34**, 5527-5535.
133. A. Volbeda and J. C. Fontecilla-Camps, *Dalton Trans.*, 2003, 4030-4038.
134. A. L. DeLacey, V. M. Fernandez, M. Rousset and R. Cammack, *Chem. Rev.*, 2007, **107**, 4304-4330.
135. K. A. Vincent, A. Parkin and F. A. Armstrong, *Chem. Rev.*, 2007, **107**, 4366-4413.
136. P. Jayapal, M. Sundararajan, I. H. Hillier and N. A. Burton, *Phys. Chem. Chem. Phys.*, 2008, **10**, 4249-4257.
137. F. Leroux, S. Dementin, B. Burlatt, L. Cournac, A. Volbeda, S. Champ, L. Martin, B. Guigliarelli, P. Bertrand, J. Fontecilla-Camps, M. Rousset and C. Leger, *Proc. Natl. Acad. Sci. U. S. A.*, 2008, **105**, 11188-11193.
138. D. J. Evans and C. J. Pickett, *Chem. Soc. Rev.*, 2003, **32**, 268-275.
139. C. H. Lai, J. H. Reibenspies and M. Y. Darensbourg, *Angew. Chem.-Int. Edit. Engl.*, 1996, **35**, 2390-2393.
140. G. J. Kubas, *Chem. Rev.*, 2007, **107**, 4152-4205.
141. V. Artero and M. Fontecave, *Coord. Chem. Rev.*, 2005, **249**, 1518-1535.
142. S. P. Best, *Coord. Chem. Rev.*, 2005, **249**, 1536-1554.
143. A. L. de Lacey, V. M. Fernandez and M. Rousset, *Coord. Chem. Rev.*, 2005, **249**, 1596-1608.
144. F. Gloaguen and T. B. Rauchfuss, *Chem. Soc. Rev.*, 2009, **38**, 100-108.
145. S. Canaguier, V. Artero and M. Fontecave, *Dalton Trans.*, 2008, 315-325.
146. F. Osterloh, W. Saak, D. Haase and S. Pohl, *Chem. Commun.*, 1997, 979-980.
147. S. C. Davies, D. J. Evans, D. L. Hughes, S. Longhurst and J. R. Sanders, *Chem. Commun.*, 1999, 1935-1936.
148. D. Sellmann, F. Geipel, F. Lauderbach and F. W. Heinemann, *Angew. Chem., Int. Ed. Engl.*, 2002, **41**, 632-634.
149. J. A. W. Verhagen, D. D. Ellis, M. Lutz, A. L. Spek and E. Bouwman, *J. Chem. Soc.-Dalton Trans.*, 2002, 1275-1280.
150. J. A. W. Verhagen, M. Lutz, A. L. Spek and E. Bouwman, *Eur. J. Inorg. Chem.*, 2003, 3968-3974.
151. Y. Oudart, V. Artero, J. Pecaut, C. Lebrun and M. Fontecave, *Eur. J. Inorg. Chem.*, 2007, 2613-2626.
152. Y. Oudart, V. Artero, J. Pecaut and M. Fontecave, *Inorg. Chem.*, 2006, **45**, 4334-4336.
153. W. F. Zhu, A. C. Marr, Q. Wang, F. Neese, D. J. E. Spencer, A. J. Blake, P. A. Cooke, C. Wilson and M. Schröder, *Proc. Natl. Acad. Sci. U. S. A.*, 2005, **102**, 18280-18285.
154. Z. L. Li, Y. Ohki and K. Tatsumi, *J. Am. Chem. Soc.*, 2005, **127**, 8950-8951.
155. Y. Ohki, K. Yasumura, K. Kuge, S. Tanino, M. Ando, Z. Li and K. Tatsumi, *Proc. Natl. Acad. Sci. U. S. A.*, 2008, **105**, 7652-7657.
156. D. Sellmann, F. Lauderbach, F. Geipel, F. W. Heinemann and M. Moll, *Angew. Chem., Int. Ed. Engl.*, 2004, **43**, 3141-3144.
157. F. Lauderbach, R. Prakash, A. W. Götz, M. Munoz, F. W. Heinemann, U. Nickel, B. A. Hess and D. Sellmann, *Eur. J. Inorg. Chem.*, 2007, 3385-3393.
158. A. Perra, E. S. Davies, J. R. Hyde, Q. Wang, J. McMaster and M. Schröder, *Chem. Commun.*, 2006, 1103-1105.
159. P. A. Stenson, A. Marin-Becerra, C. Wilson, A. J. Blake, J. McMaster and M. Schröder, *Chem. Commun.*, 2006, 317-319.

160. Q. Wang, J. E. Barclay, A. J. Blake, E. S. Davies, D. J. Evans, A. C. Marr, E. J. L. McInnes, J. McMaster, C. Wilson and M. Schröder, *Chem.-Eur. J.*, 2004, **10**, 3384-3396.
161. A. Perra, Q. Wang, A. J. Blake, E. S. Davies, J. McMaster, C. Wilson and M. Schroder, *Dalton Trans.*, 2009, 925-931.
162. S. Tanino, Z. Li, Y. Ohki and K. Tatsumi, *Inorg. Chem.*, 2009, **48**, 2358-2360.
163. M. A. Reynolds, T. B. Rauchfuss and S. R. Wilson, *Organometallics*, 2003, **22**, 1619-1625.
164. A. K. Justice, R. C. Linck, T. B. Rauchfuss and S. R. Wilson, *J. Am. Chem. Soc*, 2004, **126**, 13214-13215.
165. T. B. Rauchfuss, *Science*, 2007, **316**, 553-554.
166. S. Ogo, R. Kabe, K. Uehara, B. Kure, T. Nishimura, S. C. Menon, R. Harada, S. Fukuzumi, Y. Higuchi, T. Ohhara, T. Tamada and R. Kuroki, *Science*, 2007, **316**, 585-587.
167. B. Kure, T. Matsumoto, K. Ichikawa, S. Fukuzumi, Y. Higuchi, T. Yagi and S. Ogo, *Dalton Trans.*, 2008, 4747-4755.
168. B. E. Barton, C. M. Whaley, T. B. Rauchfuss and D. L. Gray, *J. Am. Chem. Soc.*, 2009, **131**, 6942-6943.
169. B. Keita, S. Floquet, J. F. Lemonnier, E. Cadot, A. Kachmar, M. Benard, M. M. Rohmer and L. Nadjo, *J. Phys. Chem. C*, 2008, **112**, 1109-1114.
170. X. Hu, B. S. Brunschwig and J. C. Peters, *J. Am. Chem. Soc.*, 2007, **129**, 8988-8998.
171. X. Hu, B. M. Cossairt, B. S. Brunschwig, N. S. Lewis and J. C. Peters, *Chem. Commun.*, 2005, 4723-4725.
172. O. Pantani, E. Anxolabéhére-Mallart, A. Aukauloo and P. Millet, *Electrochem. Commun.*, 2007, **9**, 54-58.
173. A. M. Appel, D. L. DuBois and M. R. DuBois, *J. Am. Chem. Soc.*, 2005, **127**, 12717-12726.
174. I. Bhugun, D. Lexa and J. M. Saveant, *J. Am. Chem. Soc.*, 1996, **118**, 3982-3983.
175. J. P. Collman, Y. Y. Ha, P. S. Wagenknecht, M. A. Lopez and R. Guilard, *J. Am. Chem. Soc.*, 1993, **115**, 9080-9088.
176. V. Artero and M. Fontecave, *C. R. Chim.*, 2008, **11**, 926-931.
177. Z. Yu, M. Wang, P. Li, W. B. Dong, F. J. Wang and L. C. Sun, *Dalton Trans.*, 2008, 2400-2406.
178. G. A. N. Felton, A. K. Vannucci, J. Z. Chen, L. T. Lockett, N. Okumura, B. J. Petro, U. I. Zakai, D. H. Evans, R. S. Glass and D. L. Lichtenberger, *J. Am. Chem. Soc.*, 2007, **129**, 12521-12530.
179. L. C. Song, Z. Y. Yang, Y. J. Hua, H. T. Wang, Y. Liu and Q. M. Hu, *Organometallics*, 2007, **26**, 2106-2110.
180. C. Tard, X. M. Liu, S. K. Ibrahim, M. Bruschi, L. De Gioia, S. C. Davies, X. Yang, L. S. Wang, G. Sawers and C. J. Pickett, *Nature*, 2005, **433**, 610-613.
181. S. Ott, M. Kritikos, B. Åkermark, L. C. Sun and R. Lomoth, *Angew. Chem.-Int. Edit.*, 2004, **43**, 1006-1009.
182. O. Pantani, S. Naskar, R. Guillot, P. Millet, E. Anxolabéhére-Mallart and A. Aukauloo, *Angew. Chem., Int. Ed. Engl.*, 2008, **47**, 9948-9950.
183. A. Fihri, V. Artero, A. Pereira and M. Fontecave, *Dalton Trans.*, 2008, 5567-5569.
184. A. Fihri, V. Artero, M. Razavet, C. Baffert, W. Leibl and M. Fontecave, *Angew. Chem.-Int. Edit.*, 2008, **47**, 564-567.
185. A. M. Kluwer, R. Kapre, F. Hartl, M. Lutz, A. L. Spek, A. M. Brouwer, P. W. N. M. van Leeuwen and J. N. H. Reek, *Proc. Natl. Acad. Sci. U. S. A.*, 2009.
186. L. C. Song, M. Y. Tang, S. Z. Mei, J. H. Huang and Q. M. Hu, *Organometallics*, 2007, **26**, 1575-1577.
187. L. C. Song, M. Y. Tang, F. H. Su and Q. M. Hu, *Angew. Chem.-Int. Edit.*, 2006, **45**, 1130-1133.
188. W. Gao, J. Liu, W. Jiang, M. Wang, L. Weng, B. Åkermark and L. Sun, *C. R. Chim.*, 2008, **11**, 915-921.
189. X. Q. Li, M. Wang, S. P. Zhang, J. X. Pan, Y. Na, J. H. Liu, B. Akermark and L. C. Sun, *J. Phys. Chem. B*, 2008, **112**, 8198-8202.
190. Y. Na, M. Wang, J. X. Pan, P. Zhang, B. Akermark and L. C. Sun, *Inorg. Chem.*, 2008, **47**, 2805-2810.
191. Y. Na, J. X. Pan, M. Wang and L. C. Sun, *Inorg. Chem.*, 2007, **46**, 3813-3815.
192. S. Ott, M. Kritikos, B. Akermark and L. C. Sun, *Angew. Chem.-Int. Edit.*, 2003, **42**, 3285-3288.

193. S. Ott, M. Borgstrom, M. Kritikos, R. Lomoth, J. Bergquist, B. Åkermark, L. Hammarström and L. C. Sun, *Inorg. Chem.*, 2004, **43**, 4683-4692.
194. H. Wolpher, M. Borgstrom, L. Hammarstrom, J. Bergquist, V. Sundstrom, S. Stenbjorn, L. C. Sun and B. Akermark, *Inorg. Chem. Commun.*, 2003, **6**, 989-991.
195. J. Ekström, M. Abrahamsson, C. Olson, J. Bergquist, F. B. Kaynak, L. Eriksson, S. C. Licheng, H. C. Becker, B. Åkermark, L. Hammarström and S. Ott, *Dalton Trans.*, 2006, 4599-4606.
196. J. A. W. Verhagen, M. Beretta, A. L. Spek and E. Bouwman, *Inorg. Chim. Acta*, 2004, **357**, 2687-2693.
197. R. Angamuthu, H. Kooijman, M. Lutz, A. L. Spek and E. Bouwman, *Dalton Trans.*, 2007, 4641-4643.
198. R. Angamuthu, L. L. Gelauff, M. A. Siegler, A. L. Spek and E. Bouwman, *Chem. Commun.*, 2009, 2700-2702.
199. R. Angamuthu and E. Bouwman, *Phys. Chem. Chem. Phys.*, 2009, **11**, 5578–5583.
200. R. Angamuthu, B. Byers, M. Lutz, A. L. Spek and E. Bouwman, *Submitted for publication*, Electrocatalytic CO2 fixation as oxalate by a copper complex.
201. R. Angamuthu, W. Roorda, M. A. Seigler, A. L. Spek and E. Bouwman, *Manuscript under preparation*, Chapter **3**.
202. R. Angamuthu, M. A. Seigler, A. L. Spek and E. Bouwman, *Manuscript under preparation*, Chapter **4**.
203. R. Angamuthu, M. A. Seigler, A. L. Spek and E. Bouwman, *Manuscript under preparation*, Chapter **5**.
204. R. Angamuthu, W. Roorda, M. A. Seigler, A. L. Spek and E. Bouwman, *Manuscript under preparation*, Chapter **8**.
205. R. Angamuthu, B. Byers, M. Lutz, A. L. Spek and E. Bouwman, *Manuscript under preparation*, A zinc thiolate complex of SN3 tripodal ligand.
206. R. Angamuthu, S. Ramón-Roig, M. A. Seigler, A. L. Spek and E. Bouwman, *Manuscript under preparation*, [Ni(S2S'2)Ru(tpa)](PF6)2 Complexes.
207. R. Angamuthu, M. Lutz, A. L. Spek and E. Bouwman, *Manuscript under preparation*, [Ni3(pbsms)2].

2

Ligand Design, Synthetic Procedures and Experimental Methods†

Abstract. Ligand design, guide for abbreviations of short names of ligands as well as their precursors, material and experimental methods used in the synthesis and catalysis are described in this chapter.

---

† This chapter is based on: R. Angamuthu, H. Kooijman, M. Lutz, A. L. Spek and E. Bouwman, *Dalton Trans*., **2007**, 4641-4643; R. Angamuthu, L. L. Gelauff, M. A. Siegler, A. L. Spek and E. Bouwman, *Chem. Commun*., **2009**, 2700-2702; R. Angamuthu and E. Bouwman, *Phys. Chem. Chem. Phys*., **2009**, 5578-5583, and several other unpublished reports.

2.1. Introduction

In this chapter, the synthesis of eight new bidentate and four new tetradentate ligands in combination with two other previously reported[1-4] ligands are described. In Scheme 2.1 and Scheme 2.2, the schematic structures of the ligands with their corresponding simplified code notations are shown.

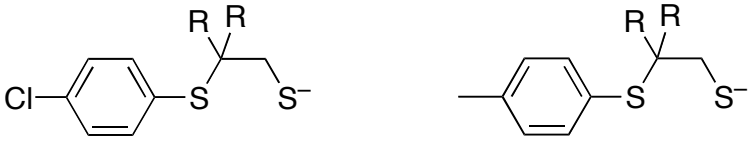

R = H; cpss
R = Me; cpsms

R = H; mpss
R = Me; mpsms

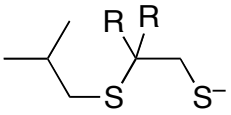

R = H; ibss
R = Me; ibsms

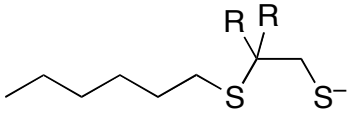

R = H; nhss
R = Me; nhsms

Scheme 2.1. Bidentate thioether-thiolate ligands used in this thesis.

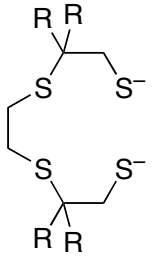

R = H; ebss
R = Me; ebsms

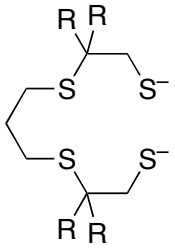

R = H; pbss
R = Me; pbsms

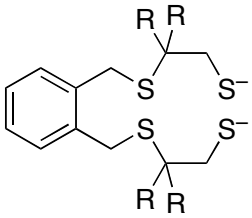

R = H; xbss
R = Me; xbsms

Scheme 2.2. Tetradentate dithioether-dithiolate ligands used in this thesis.

2.2. Guide for abbreviations

The first two letters in the abbreviations of the bidentate ligands representing the substituents on the thioether sulfur; **cp**, **mp**, **ib** and **nh** stand for 4-**c**hloro**p**henyl, 4-**m**ethyl**p**henyl, **i**so**b**utyl and **n**-**h**exyl, respectively. The "ss" in the abbreviations represent the two available sulfurs of the ligands and the 'm' in the "sms" stands for the dimethyl substitution. Likewise, the first letter in the abbreviations of the tetradentate ligands representing the bridge; **e**, **p** and **x** stand for **e**thyl, **p**ropyl and **x**ylyl groups. The second letter 'b' stands for 'bis' and the remaining part is the same as for the bidentate ligands.

2.3. Synthesis of Thiouronium Salt Precursors

In scheme 2.3, the general synthetic route applied to synthesize the thiouronium salt precursors of the bidentate ligands is shown. The hydroxo compounds formed in the first step of the synthesis have been made by the substitution reaction between the corresponding thiols and 1-chloro-2-methyl-2-propanol or between the corresponding chloro compounds and 2-mercaptoethanol in the presence of NaOH or KOH.

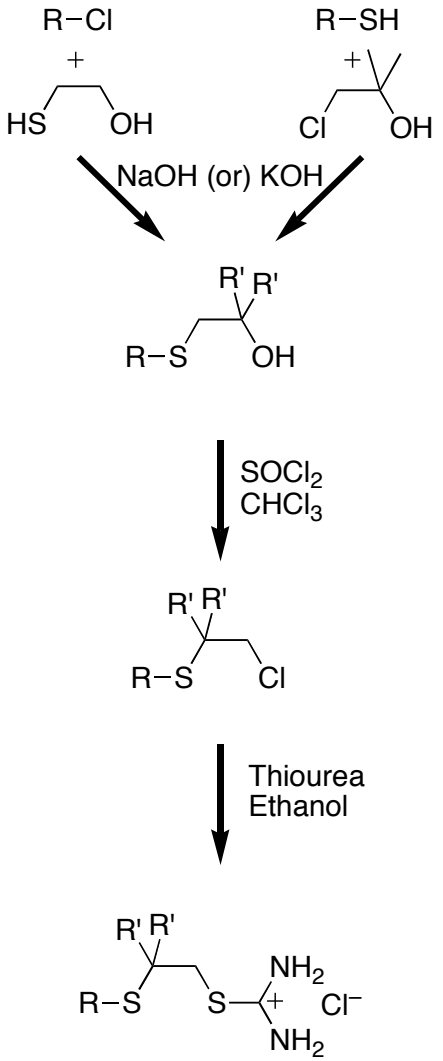

R = 4–Cl–phenyl, R' = H;	OH-cpss
R = 4–Cl–phenyl, R' = Me;	OH-cpsms
R = 4–Me–phenyl, R' = H;	OH-mpss
R = 4–Me–phenyl, R' = Me;	OH-mpsms
R = isobutyl, R' = H;	OH-ibss
R = isobutyl, R' = Me;	OH-ibsms
R = n-hexyl, R' = H;	OH-nhss
R = n-hexyl, R' = Me;	OH-nhsms
R = 4–Cl–phenyl, R' = H;	Cl-cpss
R = 4–Cl–phenyl, R' = Me;	Cl-cpsms
R = 4–Me–phenyl, R' = H;	Cl-mpss
R = 4–Me–phenyl, R' = Me;	Cl-mpsms
R = isobutyl, R' = H;	Cl-ibss
R = isobutyl, R' = Me;	Cl-ibsms
R = n-hexyl, R' = H;	Cl-nhss
R = n-hexyl, R' = Me;	Cl-nhsms
R = 4–Cl–phenyl, R' = H;	TU-cpss
R = 4–Cl–phenyl, R' = Me;	TU-cpsms
R = 4–Me–phenyl, R' = H;	TU-mpss
R = 4–Me–phenyl, R' = Me;	TU-mpsms
R = isobutyl, R' = H;	TU-ibss
R = isobutyl, R' = Me;	TU-ibsms
R = n-hexyl, R' = H;	TU-nhss
R = n-hexyl, R' = Me;	TU-nhsms

Scheme 2.3. General synthetic route applied for the synthesis of thiouronium salts.

Interestingly, during the chlorination step of the dimethyl-substituted ligands a spontaneous rearrangement takes place, by which the dimethyl groups on the α positions end up at the β positions as reported previously.[3] After the formation of the episulfonium chloride salt, the chloride ion attacks the least sterically hindered carbon,[5] thus selectively opening the ring to form the rearranged product. The chloro compounds were

reacted with thiourea to form the thiouronium salt precursors of the ligands. All the thiouronium salts reported here are crystalline powders and were found to be air-stable for many months.

2.4. Instrumental Methods

2.4.1. Analytical Techniques

Electronic absorption spectra were recorded on a Varian Cary 50 UV–Visible spectrophotometer using cuvettes of 1 cm path length. IR spectra were recorded on a Perkin-Elmer FT-IR Paragon 1000 spectrophotometer equipped with a golden gate ATR device, using the reflectance technique (4000–300 cm^{-1}, resolution 4 cm^{-1}). Elemental analyses were carried out on a Perkin-Elmer series II CHNS/O analyzer 2400. NMR spectra were recorded on a Bruker 300 DPX spectrometer. Temperature was kept constant using a variable temperature unit within the error limit of ±1 K. The software MestReNova was used for the processing of the NMR spectra.[6] Tetramethylsilane (TMS) or the solvent residual peaks were used for calibration. Mass experiments were performed on a Finnigan MAT 900 equipped with an electrospray interface. Spectra were collected by constant infusion of the sample dissolved in methanol/water or dichloromethane (with 1% HOAc). Isotopic patterns were confirmed by comparing the experimental mass spectra with the simulated mass spectra. The freely available simulating software iMass was used for the simulation of mass spectra.

2.4.2. Electrochemical Techniques

The electrochemistry measurements were performed with a computer-aided Autolab PGstat 10 potentiostat controlled by GPES4 software. A conventional three-electrode system was used, consisting of a static glassy carbon disc or platinum disc working electrode, a platinum wire auxiliary electrode and an Ag/AgCl reference electrode. Extra dry N,N-dimethylformamide (99.8%, water <50 ppm, over molecular sieves) was stored under argon and used as received. Other solvents used in the electrochemical measurements were purified following conventional procedures and stored under argon. All the solutions were deaerated by purging argon for 15 minutes prior to the measurement and the electrochemical experiments were performed at room temperature under argon atmosphere.

2.4.3. Electrocatalytic Proton Reduction Experiments

Cyclic voltammetry was used to evaluate the catalytic activity of complexes in proton reduction. Additions of acids were made by syringe using stock solutions in DMF or in acetonitrile. After each addition the electrochemical solution was deaerated by

purging argon for 3 minutes prior to the next measurement to remove the dihydrogen bubbles formed on the surface of the working electrode.

2.4.4. Electrochemical Studies Using Surface-Modified Electrodes

The pyrolitic graphite electrode was abraded using P500 and P1000 SiC sandpaper and ultrasonicated in Millipore MilliQ water for 1 min. The electrode was dried in a stream of argon for 5 sec; it was then immersed once in a 2 mM solution of a selected complex in dichloromethane for 5 minutes, after which the electrode was dried in a stream of argon for 5 seconds and this surface modified electrode was immediately utilized for the electrochemical measurements. Cyclic voltammograms were measured using 0.1 M solutions of acid in acetonitrile with a Pt wire auxiliary electrode.

2.4.5. Protonation Studies Using ^{1}H NMR Spectroscopy

Protonation experiments were performed at 25±1 °C in a 5 mm NMR tube containing 0.1 mmol of a complex in 0.75 ml of deuterated solvent. Stock solutions of acids were made using 0.1 mmol of the corresponding acid in 1 ml of deuterated solvent and 125 µl from this solution was added each time. The spectra were recorded immediately after each addition of acid.

2.5. Experimental Section

2.5.1. Chemicals

All preparations were carried out in reagent-grade solvents. All chemicals used in the syntheses were obtained from Acros or Aldrich and were used without further purification unless mentioned otherwise. All synthetic manipulations were carried under argon atmosphere using standard Schlenk techniques, unless stated otherwise. Solvents were distilled using standard techniques or deoxygenated by bubbling through a stream of argon and dried over molecular sieves.

2.5.2. Safety

Although no discomforts were noticed during the usage of the thiols mentioned in the following synthetic procedures, care should be taken while using them as most of the thiols mentioned here have an extremely pungent smell and may cause skin and respiratory disorders.

2.5.3. Synthesis of the ligand precursor TU-cpss

2-(4-chlorophenylthio)ethan-1-ol (OH-cpss). 4-Chlorobenzenethiol (8.68 g, 60 mmol) and 2-chloroethanol (4.83 g, 60 mmol) were dissolved in 60 ml ethanol. A solution of NaOH (2.4 g, 60 mmol in 10 ml H_2O) was slowly added at 0 °C. Formed NaCl was removed

by filtration after two hours of stirring at 60 °C. After evaporating the ethanol under reduced pressure, water was added and the product was extracted with chloroform (2 × 30 ml). The combined chloroform layers were dried with $MgSO_4$ and evaporated to get a colorless oil (yield: 8.46 g, 75%). **^{1}H NMR:** δ_H [300.13 MHz, DMSO-d_6, 298 K] 7.33 (s, 4H, phenyl ring), 4.96 (t, ^3J = 5.4 Hz, 1H, –O*H*), 3.55 (q, ^3J = 5.6 Hz, 2H, –S–CH$_2$–C*H*$_2$–OH), 3.03 (t, ^3J = 6.8 Hz, 2H, –S–C*H*$_2$–CH$_2$–OH). **^{13}C NMR:** δ_C [75.47 MHz, DMSO-d_6, 298 K] 135.59 (Ph–C4), 130.07 (Ph–C1), 129.47 (Ph–C3), 128.82 (Ph–C2), 59.70 (–S–CH$_2$–*C*H$_2$–OH), 34.99 (–S–*C*H$_2$–CH$_2$–OH).

2-(4-cholorophenylthio)ethyl-1-chloride (Cl-cpss). To a solution of **OH-cpss** (8.46 g, 44.8 mmol) in 30 ml chloroform was slowly added a solution of excess $SOCl_2$ (10 g, 84 mmol) in 30 ml chloroform. After an hour of stirring the chloroform and excess thionyl chloride were evaporated under reduced pressure to yield 9.28 g of a bright yellow oil (100%). **^{1}H NMR:** δ_H [300.13 MHz, $CDCl_3$, 298 K] 7.31 (d, ^3J = 6.4 Hz, 2H, phenyl ring), 7.29 (d, ^3J = 6.4 Hz, 2H, phenyl ring), 3.60 (t, 2H, ^3J = 8.3 Hz, –S–CH$_2$–C*H*$_2$–Cl). 3.19 (t, 2H, ^3J = 8.3 Hz ,–S–C*H*$_2$–CH$_2$–Cl), **^{13}C NMR:** δ_C [75.47 MHz, $CDCl_3$, 298 K] 133.08 (Ph–C4), 132.73 (Ph–C1), 131.73 (Ph–C3), 129.24 (Ph–C2), 42.03 (–S–CH$_2$–*C*H$_2$–Cl), 36.28 (–S–*C*H$_2$–CH$_2$–Cl).

2-(4-chlorophenylthio)ethyl-1-thiouronium chloride (TU-cpss). To a solution of Cl-cpss (9.28 g, 44.8 mmol) in 30 ml ethanol was added a solution of thiourea (3.04 g, 40 mmol) in 60 ml ethanol. After 3 hours of reflux the solvent was evaporated under reduced pressure, which resulted in a solid. This solid was washed with a small amount of ethanol and diethyl ether to obtain a white product in a yield of 87% based on thiourea (9.87 g). **^{1}H NMR:** δ_H [300.13 MHz, DMSO-d_6, 298 K] 9.34 (bs, 4H, –S–C(N*H*$_2$)$_2^+$Cl$^-$), 7.35 (2d, 4H, phenyl ring), 3.42 (t, ^3J = 7.5 Hz, 2H, phenyl–S–CH$_2$–C*H*$_2$–), 3.25 (t, ^3J = 7.5 Hz, 2H, phenyl–S–C*H*$_2$–CH$_2$–). **^{13}C NMR:** δ_C [75.47 MHz, DMSO-d_6, 298 K] 169.59 (–S–*C*(NH$_2$)$_2^+$), 133.78 (Ph-C4), 130.56 (Ph–C1), 129.18 (Ph–C3), 131.1 (Ph–C2), 30.1 (phenyl–S–*C*H$_2$–CH$_2$–), 31.98 (phenyl–S–CH$_2$–*C*H$_2$–). **MS (ESI):** (*m/z*) calculated for $C_9H_{12}ClN_2S_2$ $[M–Cl]^+$ requires (monoisotopic mass) 247.01, found 246.86.

2.5.4. Synthesis of the ligand precursor TU-cpsms

2-(4-chlorophenylthio)-1,1-dimethylethan-1-ol (OH-cpsms). 1-Chloro-2-methyl-2-propanol (6.51 g, 60 mmol) and 4-chlorobenzenethiol (8.68 g, 60 mmol) were dissolved in 60 ml ethanol. A solution of NaOH (2.4 g, 60 mmol in 10 ml H_2O) was slowly added to this mixture at room temperature and the reaction mixture was refluxed for two hours. The formed NaCl was removed by filtration and the solvent was evaporated. The residual oil was partitioned between water and chloroform and extracted into chloroform (2 x 25 ml). All organic layers were combined and dried over $MgSO_4$, evaporated and dried under

vacuum to get a colorless oil (11.27 g, 87%). **^{1}H NMR:** δ_H [300.13 MHz, $CDCl_3$, 298 K] 7.31 (d, ^3J = 8.5 Hz, 2H, phenyl ring), 7.22 (d, ^3J = 8.5 Hz, 2H, phenyl ring), 3.06 (s, 2H, –S–CH_2–C(CH_3)$_2$–), 2.51 (s, 1H, –OH), 1.28 (s, 6H, –S–CH_2–C(CH_3)$_2$–). **^{13}C NMR:** δ_C [75.47 MHz, $CDCl_3$, 298 K] 135.59 (Ph-C4), 131.81 (Ph–C1), 130.43 (Ph–C3), 128.83 (Ph-C2), 70.59 (–C(CH_3)$_2$–), 48.33 (-C(CH$_3$)$_2$–), 28.50 (–CH$_2$–C(CH_3)$_2$–).

2-(4-chlorophenylthio)-2,2-dimethylethyl-1-chloride (Cl-cpsms). A solution of $SOCl_2$ (7.14 g, 60 mmol in 10 ml chloroform) was slowly added to a solution of OH-cpsms (11.27 g, 52 mmol in 30 ml chloroform) at room temperature; the mixture was stirred for an hour. The chloroform and excess thionyl chloride were evaporated under reduced pressure to yield a bright yellow oil (12.25 g, 99%). **^{1}H NMR:** δ_H [300.13 MHz, $CDCl_3$, 298 K] 7.34 (d, ^3J = 8.5 Hz, 2H, phenyl ring), 7.25 (d, ^3J = 8.5 Hz, 2H, phenyl ring), 3.34 (s, 2H, -S–C(CH_3)$_2$–CH_2–), 1.64 (s, 6H, –C(CH_3)$_2$–). **^{13}C NMR:** δ_C [75.47 MHz, $CDCl_3$, 298 K] 135.18 (Ph–C4), 132.44 (Ph-C1), 131.30 (Ph–C3), 129.04 (Ph–C2), 69.36 (–C(CH_3)$_2$–), 50.20 (-CH$_2$–C(CH_3)$_2$–), 31.32 (-C(CH$_3$)$_2$–).

2-(4-chlorophenylthio)-2,2-dimethylethyl-1-thiouronium chloride (TU-cpsms). A solution of thiourea (3.81 g, 50 mmol in 30 ml ethanol) was added to a solution of Cl-cpsms (12.35 g, 50 mmol in 30 ml ethanol) and refluxed for six hours. The solvent was evaporated under reduced pressure to get a colorless oil. Addition of chloroform to this oil and standing for two hours resulted in a white crystalline solid. The solid was collected by filtration and washed with chloroform before drying under vacuum (13.54 g, 87%). **^{1}H NMR:** δ_H [300.13 MHz, DMSO-d_6, 298 K] 9.37 (s, 4H, –S–C(NH_2)$_2^+$Cl$^-$), 7.53 (d, ^3J = 8.6 Hz, 2H, phenyl ring), 7.49 (d, ^3J = 8.6 Hz, 2H, phenyl ring) 3.43 (s, 2H, –S–C(CH_3)$_2$–CH_2–), 1.29 (s, 6H, –S–C(CH_3)$_2$–CH_2–). **^{13}C NMR:** δ_C [75.47 MHz, DMSO-d_6, 298 K] 169.95 (–S–C(NH_2)$_2^+$Cl$^-$), 138.60 (Ph–C3), 134.89 (Ph–C4), 129.22 (Ph–C2), 128.91 (Ph–C1), 48.62 (–S–C(CH_3)$_2$–CH_2–), 42.18 (–S–C(CH_3)$_2$–CH$_2$–), 27.29 (–S–C(CH$_3$)$_2$–CH_2–). **MS (ESI):** (m/z) calculated for $C_{11}H_{16}ClN_2S_2$ $[M–Cl]^+$ requires (monoisotopic mass) 275.04, found 274.84.

2.5.5. Synthesis of the ligand precursor TU-mpss

2-(4-methylphenylthio)ethan-1-ol (OH-mpss). 4-Methylbenzenethiol (7.45 g, 60 mmol) and 2-chloroethanol (4.83 g, 60 mmol) were dissolved in 60 ml ethanol. A solution of NaOH (2.4 g, 60 mmol in 10 ml H_2O) was slowly added at 0 °C. The formed NaCl was removed by filtration after two hours of stirring at 60 °C. After evaporating the ethanol under reduced pressure, water was added to the oily residue and the product was extracted with chloroform (2 × 30 ml). The combined chloroform layers were dried with $MgSO_4$ and evaporated to get a colorless oil (yield: 7.56 g, 75%). **^{1}H NMR:** δ_H [300.13 MHz, $CDCl_3$, 298 K] 7.24 (d, ^3J = 8.1 Hz, 2H, phenyl ring), 7.12 (d, ^3J = 8.1 Hz, 2H, phenyl

ring), 4.96 (t, ^3J = 5.3 Hz, 1H, –O*H*), 3.55 (q, ^3J = 6.6 Hz, 2H, –S–CH$_2$–C*H*$_2$–OH), 3.03 (t, ^3J = 6.9 Hz, 2H, –S–C*H*$_2$–CH$_2$–OH). **^{13}C NMR:** δ_C [75.47 MHz, $CDCl_3$, 298 K] 135.18 (Ph–C1), 132.55 (Ph–C4), 129.62 (Ph–C2), 128.81 (Ph–C3), 60.01 (–S–CH$_2$–*C*H$_2$–OH), 35.61 (–S–*C*H$_2$–CH$_2$–OH).

2-(4-methylphenylthio)ethyl-1-chloride (Cl-mpss). To a solution of **OH-mpss** (7.5 g, 45 mmol) in 30 ml chloroform was slowly added a solution of excess $SOCl_2$ (10 g, 84 mmol) in 30 ml chloroform. After an hour of stirring the chloroform and excess thionyl chloride were evaporated under reduced pressure to yield 8.4 g of a bright yellow oil (100%). **^{1}H NMR:** δ_H [300.13 MHz, $CDCl_3$, 298 K] 7.31 (d, ^3J = 8.1 Hz, 2H, phenyl ring), 7.15 (d, ^3J = 8.1 Hz, 2H, phenyl ring), 3.60 (t, ^3J = 7.6 Hz, 2H, –S–CH$_2$–C*H*$_2$–Cl), 3.19 (t, ^3J = 7.6 Hz, 2H, –S–C*H*$_2$–CH$_2$–Cl), 2.35 (s, 3H, –CH_3). **^{13}C NMR:** δ_C [75.47 MHz, $CDCl_3$, 298 K] 132.73 (Ph–C1), 129.24 (Ph–C2), 131.73 (Ph–C3), 133.08 (Ph–C4), 42.03 (–S–CH$_2$–*C*H$_2$–Cl), 36.28 (–S–*C*H$_2$–CH$_2$–Cl), 22.04 (–*C*H$_3$).

2-(4-methylphenylthio)ethyl-1-thiouronium chloride (TU-mpss). To a solution of Cl-mpss (8.4 g, 44.8 mmol) in 30 ml ethanol was added a solution of thiourea (3.04 g, 40 mmol) in 60 ml ethanol. After 3 hours of reflux the solvent was evaporated under reduced pressure, which resulted in a solid. This solid was washed with a small amount of ethanol and diethyl ether to obtain a white product in a yield of 94% based on thiourea (9.87 g). **^{1}H NMR:** δ_H [300.13 MHz, DMSO-d_6, 298 K] 9.33 (s, 4H, –S–C(N*H*$_2$)$_2^+$Cl$^-$), 7.31 (d, ^3J = 8.1 Hz, 2H, phenyl ring), 7.17 (d, ^3J = 8.1 Hz, 2H, phenyl ring), 3.37 (t, ^3J = 7 Hz, 2H, phenyl–S–CH$_2$–C*H*$_2$–), 3.42 (t, ^3J = 7 Hz, 2H, phenyl–S–C*H*$_2$–CH$_2$–), 2.26 (s, 3H, –CH_3). **^{13}C NMR:** δ_C [75.47 MHz, DMSO-d_6, 298 K] 169.59 (–S–*C*(NH$_2$)$_2^+$Cl$^-$), 136.22 (Ph–C1), 130.70 (Ph–C4), 129.92 (Ph–C2), 129.76 (Ph–C3), 32.46 (–S–*C*H$_2$–CH$_2$–), 30.12 (–S–CH$_2$–*C*H$_2$–), 20.57 (–*C*H$_3$). MS (ESI): (*m/z*) calculated for $C_{10}H_{15}N_2S_2$ $[M\text{-}Cl]^+$ requires (monoisotopic mass) 227.07, found 226.96.

2.5.6. Synthesis of the ligand precursor TU-mpsms

2-(4-methylphenylthio)-1,1-dimethylethan-1-ol (OH-mpsms). 1-Chloro-2-methyl-2-propanol (6.51 g, 60 mmol) and 4-methylbenzenethiol (7.45 g, 60 mmol) were dissolved in 60 ml ethanol. A solution of NaOH (2.4 g, 60 mmol in 10 ml H_2O) was slowly added to this mixture at room temperature and refluxed for two hours. The formed NaCl was removed by filtration and the solvent was evaporated. The residual oil was partitioned between water and chloroform and extracted into chloroform (2 x 25 ml). All organic layers were combined and dried over $MgSO_4$, evaporated and dried under vacuum to get a colorless oil (10.72 g, 91%). **^{1}H NMR:** δ_H [300.13 MHz, $CDCl_3$, 298 K] 7.31 (d, ^3J = 8.1 Hz, 2H, phenyl ring), 7.07 (d, ^3J = 8.1 Hz, 2H, phenyl ring), 3.05 (s, 2H, –S–C*H*$_2$–C(CH$_3$)$_2$–), 2.51 (s, 1H, –O*H*), 2.28 (s, 3H, C*H*$_3$–phenyl–), 1.26 (s, 6H, –S–CH$_2$–C(C*H*$_3$)$_2$–). **^{13}C NMR:** δ_C

[75.47 MHz, $CDCl_3$, 298 K] 136.08 (Ph-C1), 133.23 (Ph–C4), 129.94 (Ph–C2), 129.59 (Ph–C3), 70.62 (–*C*$(CH_3)_2$–), 48.97 (–*C*H_2–C$(CH_3)_2$–), 28.48 (–C(*C*$H_3)_2$–), 20.81 (*p*-*C*H_3).

2-(4-methylphenylthio)-2,2-dimethylethyl-1-chloride (Cl-mpsms). A solution of $SOCl_2$ (7.14 g, 60 mmol in 10 ml chloroform) was slowly added to the solution of OH-mpsms (10.01 g, 51 mmol in 30 ml chloroform) at room temperature and stirred for an hour. The chloroform and excess thionyl chloride were evaporated under reduced pressure to yield a bright yellow oil (10.95 g, 100%). **^{1}H NMR:** δ_H [300.13 MHz, $CDCl_3$, 298 K] 7.37 (d, ^3J = 8.00 Hz, 2H, phenyl ring), 7.14 (d, ^3J = 8 Hz, 2H, phenyl ring), 3.39 (s, 2H, –S–C$(CH_3)_2$–C*H*$_2$–), 2.35 (s, 3H, C*H*$_3$–phenyl–), 1.68 (s, 6H, –C(C*H*$_3)_2$–). **^{13}C NMR:** δ_C [75.47 MHz, $CDCl_3$, 298 K] 136.54 (Ph–C1), 132.96 (Ph–C4), 130.61 (Ph–C2), 130.03 (Ph–C3), 69.78 (–*C*$(CH_3)_2$–), 50.66 (–*C*H_2–C$(CH_3)_2$–), 31.23 (–C(*C*$H_3)_2$–), 20.90 (*C*H_3–phenyl–).

2-(4-methylphenylthio)-2,2-dimethylethyl-1-thiouronium chloride (TU-mpsms). A solution of thiourea (3.81 g, 50 mmol in 30 ml ethanol) was added to a solution of Cl-mpsms (10.74 g, 50 mmol in 30 ml ethanol) and refluxed for six hours. The solvent was evaporated under reduced pressure to get a colorless oil. Addition of chloroform to this oil and standing for two hours resulted white crystalline solid. The solid was collected by filtration and washed with chloroform before drying under vacuum (13.38 g, 92%). **^{1}H NMR:** δ_H [300.13 MHz, DMSO-d_6, 298 K] 9.40 (s, 4H, –S–C(N*H*$_2)_2^+Cl^-$), 7.39 (d, ^3J = 8 Hz, 2H, phenyl ring), 7.23 (d, ^3J = 8 Hz, 2H, phenyl ring) 3.33 (s, 2H, –S–C$(CH_3)_2$–C*H*$_2$–), 2.30 (s, 3H, C*H*$_3$–phenyl–), 1.26 (s, 6H, –S–C(C*H*$_3)_2$–CH_2–). **^{13}C NMR:** δ_C [75.47 MHz, DMSO-d_6, 298 K] 170.17 (-S-*C*$(NH_2)_2^+Cl^-$), 139.44 (Ph–C1), 136.93 (Ph–C3), 129.88 (Ph–C2), 126.52 (Ph–C4), 48.04 (–S–*C*$(CH_3)_2$–CH_2–), 42.26 (–S–C$(CH_3)_2$–*C*H_2–), 27.31 (–S–C(*C*$H_3)_2$–CH_2–), 20.83 (*C*H_3–phenyl–). **MS (ESI):** (*m/z*) calculated for $C_{12}H_{19}N_2S_2$ $[M–Cl]^+$ requires (monoisotopic mass) 255.10, found 254.91.

2.5.7. Synthesis of the ligand precursor TU-ibss

2-(isobutylthio)ethan-1-ol (OH-ibss). 1-Bromo-2-methylpropane (12.33 g, 90 mmol) and 2-mercaptoethanol (7.03 g, 90 mmol) were dissolved in 60 ml ethanol. A solution of KOH (5.05 g, 90 mmol in 10 ml H_2O) was slowly added to this mixture at room temperature and refluxed for two hours. The formed KBr was removed by filtration and the solvent was evaporated. The residual oil was partitioned between water and chloroform and extracted into chloroform (2 x 25 ml). All organic layers were combined and dried over $MgSO_4$, evaporated and dried under vacuum to get colorless oil (11.11 g, 92%). **^{1}H NMR:** δ_H [300.13 MHz, $CDCl_3$, 298 K] 3.64 (t, ^3J = 6.1 Hz, 2H, –CH_2–S–CH_2–C*H*$_2$–), 2.78 (s, 1H, –O*H*), 2.64 (t, ^3J = 6.1 Hz, 2H, –CH_2–S–C*H*$_2$–CH_2–), 2.34 (d, ^3J = 6.9 Hz, 2H, -C*H*$_2$–S–CH_2–CH_2–), 1.73 (septet, ^3J = 6.7 Hz, 1H, $(CH_3)_2$–C*H*–), 2.34 (d, ^3J = 6.64 Hz, 6H,

($C\mathit{H}_3$)$_2$–CH–). **^{13}C NMR:** δ_C [75.47 MHz, $CDCl_3$, 298 K] 60.22 (–CH_2–S–CH_2–$\mathit{C}H_2$–), 40.77 (-CH_2–S–$\mathit{C}H_2$–CH_2–), 35.50 (–$\mathit{C}H_2$–S–CH_2–CH_2–), 28.52 ((CH_3)$_2$–CH–), 21.78 (($\mathit{C}H_3$)$_2$–CH–).

2-(isobutylthio)ethyl-1-chloride (Cl-ibss). A solution of $SOCl_2$ (17.85 g, 150 mmol in 50 ml chloroform) was slowly added to a solution of OH-ibss (11 g, 82 mmol in 100 ml chloroform) at room temperature and stirred for an hour. The chloroform and excess thionyl chloride were evaporated under reduced pressure to yield a bright yellow oil (12.27 g, 98%). **^{1}H NMR:** δ_H [300.13 MHz, $CDCl_3$, 298 K] 3.61 (t, ^3J = 7.8 Hz, 2H, –CH_2–S–CH_2–CH_2–), 2.83 (t, ^3J = 7.8 Hz, 2H, –CH_2–S–CH_2–CH_2–), 2.44 (d, ^3J = 6.9 Hz, 2H, –CH_2–S–CH_2–CH_2–), 2.34 (septet, ^3J = 6.7 Hz, 1H, (CH_3)$_2$–CH–), 1.73 (d, ^3J = 6.6 Hz, 6H, (CH_3)$_2$–CH-). **^{13}C NMR:** δ_C [75.47 MHz, $CDCl_3$, 298 K] 43.06 (–CH_2–S–CH_2–$\mathit{C}H_2$–), 41.68 (–CH_2–S–$\mathit{C}H_2$–CH_2–), 34.79 (–$\mathit{C}H_2$–S–CH_2–CH_2–), 28.75 ((CH_3)$_2$–CH–), 21.89 (($\mathit{C}H_3$)$_2$–CH–).

2-(isobutylthio)ethyl-1-thiouronium chloride (TU-ibss). A solution of thiourea (6.09 g, 80 mmol in 30 ml ethanol) was added to the solution of Cl-ibss (12.21 g, 80 mmol in 30 ml ethanol) and refluxed for six hours. The solvent was evaporated under reduced pressure to get a colorless oil. Addition of chloroform to this oil and standing for two hours resulted in a white crystalline solid. The solid was collected by filtration and washed with chloroform before drying under vacuum (15.19 g, 83%). **^{1}H NMR:** δ_H [300.13 MHz, DMSO-d_6, 298 K] 9.35 (s, 4H, –S–C(NH_2)$_2^+$$Cl^-$), 3.42 (t, ^3J = 7.6 Hz, 2H, –CH_2–S–CH_2–CH_2–), 2.73 (t, ^3J = 7.6 Hz, 2H, -CH_2–S–CH_2–CH_2–), 2.45 (d, ^3J = 6.8 Hz, 2H, –CH_2–S–CH_2–CH_2–), 1.71 (septet, ^3J = 6.7 Hz, 1H, (CH_3)$_2$–CH–), 0.91 (d, ^3J = 6.6 Hz, 6H, (CH_3)$_2$–CH–). **^{13}C NMR:** δ_C [75.47 MHz, DMSO-d_6, 298 K] 171.04 (–S–C(NH_2)$_2^+$$Cl^-$), 41.21 (–$CH_2$–S–$CH_2$–$\mathit{C}H_2$–), 32.05 (–$CH_2$–S–$\mathit{C}H_2$–$CH_2$–), 31.90 (-$\mathit{C}H_2$–S–$CH_2$–$CH_2$–), 29.27 (($CH_3$)$_2$–$\mathit{C}$H–), 22.96 (($\mathit{C}H_3$)$_2$–CH–). **MS (ESI):** (*m/z*) calculated for $C_7H_{17}N_2S_2$ $[M–Cl]^+$ requires (monoisotopic mass) 193.08, found 192.95.

2.5.8. Synthesis of the ligand precursor TU-ibsms

2-(isobutylthio)-1,1-dimethylethan-1-ol (OH-ibsms). 2-Methyl-1-propanethiol (8.12 g, 90 mmol) and 1-chloro-2-methyl-2-propanol (9.77 g, 90 mmol) were dissolved in 60 ml ethanol. A solution of NaOH (3.6 g, 90 mmol in 10 ml H_2O) was slowly added to this mixture at room temperature and refluxed for two hours. The formed NaCl was removed by filtration and the solvent was evaporated. The residual oil was partitioned between water and chloroform and extracted into chloroform (2 x 25 ml). All organic layers were combined and dried over $MgSO_4$. The solvent was evaporated and the colorless oil was dried under vacuum (10.4 g, 71%). **^{1}H NMR:** δ_H [300.13 MHz, $CDCl_3$, 298 K] 2.62 (s, 2H, –S–CH_2–C(CH_3)$_2$–OH), 2.45 (d, ^3J = 6.8 Hz, 2H, (CH_3)$_2$CH–CH_2–S–), 2.26 (s, 1H, –S–CH_2–C(CH_3)$_2$–OH), 1.75 (septet, ^3J = 6.7 Hz, 1H, (CH_3)$_2$CH–CH_2–S–), 1.23 (s, 6H, –S–CH_2–C(CH_3)$_2$–OH), 0.96 (d, ^3J = 6.7 Hz, 6H, (CH_3)$_2$CH–CH_2–S–). **^{13}C NMR:** δ_C [75.47 MHz, $CDCl_3$,

298 K] 70.33 (–S–CH_2–*C*$(CH_3)_2$–OH), 47.63 (–S–*C*H_2–C$(CH_3)_2$–OH), 43.84 (($(CH_3)_2$CH–*C*H_2–S–), 28.97 (($(CH_3)_2$*C*H–CH_2–S–), 28.54 (–S–CH_2–C(*C*$H_3)_2$–OH), 21.88 (($(CH_3)_2$CH–CH_2–S–).

2-(isobutylthio)-2,2-dimethylethyl-1-chloride (Cl-ibsms). A solution of $SOCl_2$ (17.85 g, 150 mmol in 50 ml chloroform) was slowly added to a solution of OH-ibsms (10.22 g, 63 mmol in 100 ml chloroform) at room temperature and stirred for an hour. The chloroform and excess thionyl chloride were evaporated under reduced pressure to yield a bright yellow oil (11.35 g, 100%). **^{1}H NMR:** δ_H [300.13 MHz, $CDCl_3$, 298 K] 2.91 (s, 2H, –S–C$(CH_3)_2$–C*H*$_2$–Cl), 2.48 (d, ^3J = 6.8 Hz, 2H, $(CH_3)_2$CH–C*H*$_2$–S–), 1.78 (septet, ^3J = 6.7 Hz, 1H, $(CH_3)_2$C*H*–CH_2–S–), 1.64 (s, 6H, –S–C(C*H*$_3)_2$–CH_2–Cl), 0.97 (d, ^3J = 6.7 Hz, 6H, (C*H*$_3)_2$CH–CH_2–S–). **^{13}C NMR:** δ_C [75.47 MHz, $CDCl_3$, 298 K] 70.35 (–S–*C*$(CH_3)_2$–CH_2–Cl), 48.75 (–S–C$(CH_3)_2$–*C*H_2–Cl), 43.88 (($(CH_3)_2$CH–*C*H_2–S–), 31.28 (–S–C(*C*$H_3)_2$–CH_2–Cl), 28.81 (($(CH_3)_2$–*C*H–CH_2–S–), 21.88 (($(CH_3)_2$CH–CH_2–S–).

2-(isobutylthio)-2,2-dimethylethyl-1-thiouronium chloride (TU-ibsms). A solution of thiourea (4.57 g, 60 mmol in 60 ml ethanol) was added to the solution of Cl-ibsms (10.84 g, 60 mmol in 60 ml ethanol) and refluxed for six hours. The solvent was evaporated under reduced pressure to get a colorless oil. Addition of chloroform to this oil and standing for two hours resulted in a white crystalline solid. The solid was collected by filtration and washed with chloroform before drying under vacuum (13.27 g, 86%). **^{1}H NMR:** δ_H [300.13 MHz, DMSO-d_6, 298 K] 9.33 (s, 4H, –S–C(N*H*$_2)_2^+Cl^-$), 3.51 (t, ^3J = 7.7 Hz, 2H, –S-C$(CH_3)_2$–C*H*$_2$–), 2.42 (d, ^3J = 6.9 Hz, 2H, –C*H*$_2$–S–C$(CH_3)_2$–CH_2–), 1.51 (septet, ^3J = 6.7 Hz, 1H, $(CH_3)_2$–C*H*–), 1.31 (2H, –CH_2–S–C(C*H*$_3)_2$–CH_2–), 0.92 (d, ^3J = 6.7 Hz, 6H, (C*H*$_3)_2$–CH–). **^{13}C NMR:** δ_C [75.47 MHz, DMSO-d_6, 298 K] 170.14 (–S–*C*$(NH_2)_2^+Cl^-$), 44.52 (–CH_2–S–*C*$(CH_3)_2$–CH_2–), 42.41 (-*C*H_2–S–C$(CH_3)_2$–CH_2–), 36.10 (–CH_2–S–C$(CH_3)_2$–*C*H_2–), 28.29 (($(CH_3)_2$–*C*H–), 27.57 (($(CH_3)_2$–*C*H–), 22.05 (($(CH_3)_2$–CH–). **MS (ESI):** (*m/z*) calculated for $C_9H_{21}N_2S_2$ $[M–Cl]^+$ requires (monoisotopic mass) 221.11, found 220.97.

2.5.9. Synthesis of the ligand precursor TU-nhss

2-(*n*-hexylthio)ethan-1-ol (OH-nhss). 1-Hexanethiol (11.09 g, 90 mmol) and 2-chloroethanol (7.25 g, 90 mmol) were dissolved in 60 ml ethanol. A solution of NaOH (3.6 g, 90 mmol in 10 ml H_2O) was slowly added to this mixture at room temperature and refluxed for two hours. The formed NaCl was removed by filtration and the solvent was evaporated. The residual oil was partitioned between water and chloroform and extracted into chloroform (2 x 25 ml). All organic layers were combined and dried over $MgSO_4$, evaporated and dried under vacuum to get a colorless oil (11.83 g, 81%). **^{1}H NMR:** δ_H [300.13 MHz, $CDCl_3$, 298 K] 3.68 (t, ^3J = 6.1 Hz, 2H, –S–CH_2–C*H*$_2$–OH), 2.68 (t, ^3J = 6.1 Hz, 2H, -S–C*H*$_2$–CH_2–OH), 2.50 (s, 1H, –O*H*), 2.48 (t, ^3J = 7.5 Hz, 2H, CH_3–$(CH_2)_4$–C*H*$_2$–S–), 1.55 (p, ^3J = 6.7 Hz, 2H, CH_3–$(CH_2)_3$–C*H*$_2$–CH_2–S–), 1.3 (m, 6H, CH_3–(C*H*$_2)_3$–

$(CH_2)_2$–S–), 0.85 (t, ^3J = 6.6 Hz, 2H, CH_3–). **^{13}C NMR:** δ_C [75.47 MHz, $CDCl_3$, 298 K] 60.16 (–S–CH_2–CH_2–OH), 35.09 (CH_3–$(CH_2)_3$–CH_2–CH_2–S–), 31.56 (–S–CH_2–CH_2–OH), 31.29 (CH_3–CH_2–CH_2–$(CH_2)_3$–S–), 29.6 (CH_3–$(CH_2)_4$–CH_2–S–), 28.41 (CH_3–$(CH_2)_2$–CH_2–$(CH_2)_2$–S–), 22.42 (CH_3–CH_2–$(CH_2)_4$–S–), 13.91 (CH_3–).

2-(*n*-hexylthio)ethyl-1-chloride (Cl-nhss). A solution of $SOCl_2$ (17.85 g, 150 mmol in 30 ml chloroform) was slowly added to a solution of OH-nhss (11.69 g, 72 mmol in 30 ml chloroform) at room temperature and stirred for an hour. The chloroform and excess thionyl chloride were evaporated under reduced pressure to yield a bright yellow oil (13 g, 99%). **^{1}H NMR:** δ_H [300.13 MHz, $CDCl_3$, 298 K] 3.61 (t, ^3J = 7.8 Hz, 2H, –S–CH_2–CH_2–Cl), 2.83 (t, ^3J = 7.8 Hz, 2H, –S–CH_2–CH_2–Cl), 2.54 (t, ^3J = 7.3 Hz, 2H, CH_3–$(CH_2)_4$–CH_2–S–), 1.6 (p, ^3J = 7.7 Hz, 2H, CH_3–$(CH_2)_3$–CH_2–CH_2–S–), 1.3 (m, 6H, CH_3–(CH_2)$_3$–$(CH_2)_2$–S–), 0.88 (t, ^3J = 6.6 Hz, 2H, CH_3–). **^{13}C NMR:** δ_C [75.47 MHz, $CDCl_3$, 298 K] 43.05 (–S–CH_2–CH_2–Cl), 34.19 (–S–CH_2–CH_2–Cl), 32.41 (CH_3–$(CH_2)_4$–CH_2–S–), 31.34 (CH_3–CH_2–CH_2–$(CH_2)_3$–S–), 29.68 (CH_3–$(CH_2)_3$–CH_2–CH_2–S–), 28.42 (CH_3–$(CH_2)_2$–CH_2–$(CH_2)_2$–S–), 22.49 (CH_3–CH_2–$(CH_2)_4$–S–), 13.98 (CH_3–).

2-(*n*-hexylthio)ethyl-1-thiouronium chloride (TU-nhss). A solution of thiourea (5.48 g, 72 mmol in 30 ml ethanol) was added to a solution of Cl-nhss (13 g, 72 mmol in 30 ml ethanol) and refluxed for six hours. The solvent was evaporated under reduced pressure to get a colorless oil. Addition of chloroform to this oil and standing for two hours resulted in a white crystalline solid. The solid was collected by filtration and washed with chloroform before drying under vacuum (16.08 g, 87%). **^{1}H NMR:** δ_H [300.13 MHz, DMSO-d_6, 298 K] 9.35 (s, 4H, –S–C(NH_2)$_2^+$$Cl^-$), 3.42 (t, ^3J = 7.8 Hz, 2H, –CH_2–S–C(NH_2)$_2^+$), 2.73 (t, ^3J = 7.8 Hz, 2H, –CH_2–CH_2–S–C(NH_2)$_2^+$$Cl^-$), 2.55 (t, ^3J = 7.2 Hz, 2H, CH_3–$(CH_2)_4$–CH_2–S–), 1.48 (p, ^3J = 7.4 Hz, 2H, CH_3–$(CH_2)_3$–CH_2–CH_2–S–), 1.3 (m, 6H, CH_3–(CH_2)$_3$–$(CH_2)_2$–S–), 0.83 (t, ^3J = 6.5 Hz, 2H, CH_3–). **^{13}C NMR:** δ_C [75.47 MHz, DMSO-d_6, 298 K] 169.8 (–S–C(NH_2)$_2^+$$Cl^-$), 30.91 (–$CH_2$–$CH_2$–S–C(N$H_2$)$_2^+$$Cl^-$), 30.83 ($CH_3$–$(CH_2)_4$–$CH_2$–S–), 30.59 ($CH_3$–$CH_2$–$CH_2$–$(CH_2)_3$–S–), 30.27 ($CH_3$–$(CH_2)_3$–$CH_2$–$CH_2$–S–), 29.01 ($CH_3$–$(CH_2)_2$–$CH_2$–$(CH_2)_2$–S–), 27.87 ($CH_3$–$CH_2$–$(CH_2)_4$–S–), 22.05 (–$CH_2$–$CH_2$–S–C(N$H_2$)$_2^+$$Cl^-$), 13.91 ($CH_3$–). **MS (ESI):** (*m/z*) calculated for $C_9H_{21}N_2S_2$ $[M–Cl]^+$ requires (monoisotopic mass) 221.11, found 220.95.

2.5.10. Synthesis of the ligand precursor TU-nhsms

2-(*n*-hexylthio)-1,1-dimethylethan-1-ol (OH-nhsms). 1-Hexanethiol (11.09 g, 90 mmol) and 1-chloro-2-methyl-2-propanol (9.77 g, 90 mmol) were dissolved in 60 ml ethanol. A solution of NaOH (3.6 g, 90 mmol in 10 ml H_2O) was slowly added to this mixture at room temperature and refluxed for two hours. The formed NaCl was removed by filtration and the solvent was evaporated. The residual oil was partitioned between

water and chloroform and extracted into chloroform (2 x 25 ml). All organic layers were combined and dried over $MgSO_4$, evaporated and dried under vacuum to get a colorless oil (13.37 g, 78%). **^{1}H NMR:** δ_H [300.13 MHz, $CDCl_3$, 298 K] 2.62 (s, 2H, –S–CH_2–C$(CH_3)_2$–OH), 2.53 (t, ^3J = 7.3 Hz, 2H, CH_3–$(CH_2)_4$–CH_2–S–), 2.41 (s, 1H, –O*H*), 1.55 (p, ^3J = 7.5 Hz, 2H, CH_3–$(CH_2)_3$–CH_2–CH_2–), 1.3 (m, 6H, CH_3–(CH_2)$_3$–$(CH_2)_2$–S–), 1.23 (s, 6H, –C(CH_3)$_2$–), 0.85 (t, ^3J = 6.7 Hz, 2H, CH_3–). **^{13}C NMR:** δ_C [75.47 MHz, $CDCl_3$, 298 K] 70.25 (–*C*$(CH_3)_2$–), 64.9 (–S–*C*H_2–C$(CH_3)_2$–OH), 34.5 (CH_3–$(CH_2)_4$–*C*H_2–S–), 31.34 (CH_3–CH_2–*C*H_2–$(CH_2)_3$–S–), 29.91 (CH_3–$(CH_2)_3$–*C*H_2–CH_2–S–), 28.52 (-C(*C*H_3)$_2$–), 28.4 (CH_3–$(CH_2)_2$–*C*H_2–$(CH_2)_2$–S–), 22.46 (CH_3–*C*H_2–$(CH_2)_4$–S–), 13.94 (*C*H_3–).

2-(*n*-hexylthio)-2,2-dimethylethyl-1-chloride (Cl-nhsms). A solution of $SOCl_2$ (17.85 g, 150 mmol in 10 ml chloroform) was slowly added to a solution of OH-nhsms (13.33 g, 70 mmol in 30 ml chloroform) at room temperature and stirred for an hour. The chloroform and excess thionyl chloride were evaporated under reduced pressure to yield a bright yellow oil (14.58 g, 99%). **^{1}H NMR:** δ_H [300.13 MHz, $CDCl_3$, 298 K] 2.94 (m, 2H, –S–C$(CH_3)_2$–CH_2–Cl), 2.6 (m, 2H, CH_3–$(CH_2)_4$–CH_2–S–), 1.65 (m, 6H, –S–C(CH_3)$_2$–CH_2–Cl), 1.59 (m, 2H, CH_3–$(CH_2)_3$–CH_2–CH_2–S–), 1.3 (m, 6H, CH_3–(CH_2)$_3$–$(CH_2)_2$–S–), 0.88 (t, ^3J = 6.8 Hz, 2H, CH_3–). **^{13}C NMR:** δ_C [75.47 MHz, $CDCl_3$, 298 K] 70.39 (–S–*C*$(CH_3)_2$–CH_2–Cl), 48.11 (–S–C$(CH_3)_2$–*C*H_2–Cl), 34.64 (CH_3–$(CH_2)_3$–*C*H_2–CH_2–S–), 31.4 (CH_3–CH_2–*C*H_2–$(CH_2)_3$–S–), 31.33 (–S–C(*C*H_3)$_2$–CH_2–Cl), 29.74 (CH_3–$(CH_2)_2$–*C*H_2–$(CH_2)_2$–S–), 28.45 (CH_3–$(CH_2)_4$–*C*H_2–S–), 22.51 (CH_3-*C*H_2-$(CH_2)_4$–S–), 14.00 (*C*H_3–).

2-(*n*-hexylthio)-2,2-dimethylethyl-1-thiouronium chloride (TU-nhsms). A solution of thiourea (5.25 g, 69 mmol in 30 ml ethanol) was added to the solution of Cl-nhsms (14.42 g, 69 mmol in 30 ml ethanol) and refluxed for six hours. The solvent was evaporated under reduced pressure to get colorless oil. Addition of chloroform to this oil and standing for two hours resulted white crystalline solid. The solid was collected by filtration and washed with chloroform before drying under vacuum (17.11 g, 87%). **^{1}H NMR:** δ_H [300.13 MHz, DMSO-d_6, 298 K] 9.34 (s, 4H, –S–C(N*H*$_2$)$_2^+$$Cl^-$), 3.52 (s, 2H, –S–C$(CH_3)_2$–C$H_2$–S–), 2.52 (t, ^3J = 7.4 Hz, 2H, CH_3–$(CH_2)_4$–CH_2–S–), 1.45 (p, ^3J = 7.5 Hz, 2H, CH_3–$(CH_2)_3$–CH_2–CH_2–S–), 1.31 (s, 6H, –S–C(CH_3)$_2$–CH_2–S–), 1.25 (m, 6H, CH_3–(CH_2)$_3$–$(CH_2)_2$–S–), 0.83 (t, ^3J = 6.6 Hz, 2H, CH_3–). **^{13}C NMR:** δ_C [75.47 MHz, DMSO-d_6, 298 K] 170.42 (–S–*C*(NH_2)$_2^+$$Cl^-$), 44.69 (–S–*C*$(CH_3)_2$–$CH_2$–S–), 42.43 (–S–C$(CH_3)_2$–*C*$H_2$–S–), 30.88 ($CH_3$–$(CH_2)_3$–*C*$H_2$–$CH_2$–S–), 28.96 ($CH_3$–$CH_2$–*C*$H_2$–$(CH_2)_3$–S–), 28.2 ($CH_3$–$(CH_2)_2$–*C*$H_2$–$(CH_2)_2$–S–), 27.56 (–S–C(*C*$H_3$)$_2$–$CH_2$–S–), 27.45 ($CH_3$–$(CH_2)_4$–*C*$H_2$–S–), 20.05 ($CH_3$–*C*$H_2$–$(CH_2)_4$–S–), 13.94 (*C*$H_3$-). **MS (ESI):** (*m/z*) calculated for $C_{11}H_{25}N_2S_2$ $[M–Cl]^+$ requires (monoisotopic mass) 249.15, found 248.46.

2.5.11. Synthesis of the ligand precursor TU-ebss

3,6-(dithia)octyl-1,8-dichloride (Cl-ebss): To a solution of 3,6-dithiaoctane-1,8-diol (5.47 g, 30 mmol) in 40 ml $CHCl_3$ was added drop-wise a solution of 4.35 ml $SOCl_2$ in 10 ml $CHCl_3$. The suspension was stirred for 1.5 h at room temperature. Then the chloroform and excess $SOCl_2$ were evaporated under reduced pressure to yield 6.56 g of a sticky yellowish product (100%). **^{1}H NMR:** δ_H [300.13 MHz, $CDCl_3$, 298 K] 3.74 (t, 4H, –C*H*$_2$–Cl), 2.91 (t, 4H, –S–*CH*$_2$–CH$_2$–Cl), 2.77 (s, 4H, –S–C*H*$_2$–C*H*$_2$–S–). **^{13}C NMR:** δ_C [75.47 MHz, $CDCl_3$, 298 K] 43.9 (–*C*H$_2$–Cl), 33.3 (–S–*C*H$_2$–CH$_2$–Cl), 31.5 (–S–*C*H$_2$–*C*H$_2$–S–). **IR (neat):** 2956w, 2933w, 1435m, 1418m, 1436m, 1306w, 1231w, 1196m, 1140m, 1042w, 758ws, 699s, 677s, 420w, 370w cm^{-1}.

3,6-(dithio)octyl-1,8-dithiouronuim dichloride (TU-ebss): To a solution of Cl-ebss (5.82 g, 26.55 mmol) in 40 ml ethanol was added a solution of thiourea (3.84 g, 50.45 mmol) in 40 ml ethanol. The mixture was refluxed for one hour and the formed white precipitate was collected by filtration. The product was washed with cold ethanol and diethyl ether to yield 9.2 g of white powder (93% based on thiourea). **^{1}H NMR:** δ_H [300.13 MHz, DMSO-d$_6$, 298 K] 9.25 (s, 8H, –SC$^+$(N*H*$_2$)$_2$Cl$^-$), 3.43 (t, 4H, –C*H*$_2$–SC$^+$(NH$_2$)$_2$Cl$^-$), 2.83 (m, 8H, –S–C*H*$_2$–C*H*$_2$–S– and –C*H*$_2$–CH$_2$–SC$^+$(NH$_2$)$_2$Cl$^-$). **^{13}C NMR:** δ_C [75.47 MHz, DMSO-d$_6$, 298 K] 170.8 (–S*C*$^+$(NH$_2$)$_2$Cl$^-$), 32.4 (–*C*H$_2$–SC$^+$(NH$_2$)$_2$Cl$^-$), 31.9 (–*C*H$_2$–CH$_2$–SC$^+$(NH$_2$)$_2$Cl$^-$), 31.5 (–S–*C*H$_2$–*C*H$_2$–S–). **IR (neat):** 3192m, 3050m, 1663s, 1560w, 1436m, 1227w, 1195m, 1148w, 1083w, 668s, 464s, 310w cm^{-1}. **MS (ESI):** (*m/z*) calculated for $C_8H_{18}S_4N_4$ [M–2Cl] requires (monoisotopic mass) 298.04, found 298.81.

2.5.12. Synthesis of the ligand precursor TU-ebsms

4,7-dithia-2,9-dimethyldecane-2,9-diol (OH-ebsms): To a solution of 1,2-ethanedithiol (5.65 g, 60 mmol) in 70 ml ethanol was added 1-chloro-2-methyl-2-propanol (13.03 g, 120 mmol) and NaOH (4.81 g, 120 mmol) in 45 ml water. After refluxing for two hours, the formed NaCl was removed by filtration. After evaporating the ethanol under reduced pressure, water was added and the product was extracted with chloroform. The combined chloroform layers were dried with $MgSO_4$ and evaporated to get 10.68 g of colorless oil (98 %). **^{1}H NMR:** δ_H [300.13 MHz, $CDCl_3$, 298 K] 2.78 (m, 2H, –O*H*), 2.70 (s, 4H, –S–C*H*$_2$–C(CH$_3$)$_2$OH), 2.57 (s, 4H, –S–C*H*$_2$–C*H*$_2$–S–) 1.62 (s, 12H, –C(C*H*$_3$)$_2$OH). **^{13}C NMR:** δ_C [75.47 MHz, $CDCl_3$, 298 K] 70.3 (–*C*(CH$_3$)$_2$OH), 46.4 (–S–*C*H$_2$–C(CH$_3$)$_2$OH), 34.1 (–S–*C*H$_2$–*C*H$_2$–S–), 28.3 (–(*C*H$_3$)$_2$OH).

1,8-dichloro-3,6-dithia-2,2,7,7-tetramethyloctane (Cl-ebsms): To a solution of OH-ebsms (10.68 g, 58.72 mmol) in 20 ml $CHCl_3$ was added drop-wise a solution of $SOCl_2$ (17.85 g, 150 mmol) in $CHCl_3$. The solution turned into yellow color initially and orange at the final stage of the addition of $SOCl_2$. After an hour stirring the chloroform and excess

$SOCl_2$ were evaporated under reduced pressure to yield 12.33 g of a yellow oil (100%). **^{1}H NMR:** δ_H [300.13 MHz, $CDCl_3$, 298 K] 2.93 (s, 4H, –C*H*$_2$–Cl), 2.81 (s, 4H, –S–C*H*$_2$–C*H*$_2$–S–), 1.62 (s, 12H, -C*H*$_3$). **^{13}C NMR:** δ_C [75.47 MHz, $CDCl_3$, 298 K] 70.0 (–*C*H$_2$–Cl), 48.01 (–S–CH$_2$–CH$_2$–*C*(CH$_3$)$_2$Cl), 34.3 (–S–*C*H$_2$–*C*H$_2$–S), 31.3 (–*C*H$_3$).

1,8-dithiouronium-3,6-dithia-2,2,7,7-tetramethyloctane dichloride (TU-ebsms): Thiourea (7.99 g, 105 mmol) and Cl-ebsms (12.11 g, 55.24 mmol) were dissolved in ethanol (85 ml) and refluxed for an hour. After refluxing for half an hour an off-white precipitate was formed. After cooling down to the room temperature, the formed precipitate was filtered off and washed with cold ethanol and diethyl ether and dried under vacuum to get 17.64 g of pure crystalline white solid (76% based on thiourea). **^{1}H NMR:** δ_H [300.13 MHz, DMSO-d_6, 298 K] 9.33 (d, 8H, –SC$^+$(N*H*$_2$)$_2$Cl$^-$) 3.56 (s, 4H, –C*H*$_2$–SC$^+$(NH$_2$)$_2$Cl$^-$), 2.71 (s, 4H, –S–C*H*$_2$–C*H*$_2$–S–), 1.31 (s, 12H, -C*H*$_3$). **^{13}C NMR:** δ_C [75.47 MHz, DMSO-d_6, 298 K] 170.3 (-CH$_2$-S*C*$^+$(NH$_2$)$_2$), 45.5 (–*C*H$_2$–SC$^+$(NH$_2$)$_2$), 42.5 (–S–*C*(CH$_3$)$_2$–) 28 (–S–*C*H$_2$–*C*H$_2$–S–), 27.5 (–*C*H$_3$). **IR (neat):** 3023bm, 2716w, 1979w, 1634m, 1652vs, 1558w, 1538w, 1463w, 1436m, 1418m, 1382m, 13668m, 1198w, 1110w, 859w, 718s, 696s, 668s, 637s, 606s, 496w, 461m cm^{-1}. **MS (ESI):** (*m/z*) calculated for $C_{12}H_{28}S_4N_4$ [M–2HCl] requires (monoisotopic mass) 354.10, found 354.74.

2.5.13. Synthesis of H_2pbss

3,7-dithianonane-1,9-diol (OH-pbss): Propane-1,3-dithiol (1.62 g, 15 mmol) and 2-chloroethanol (2.41 g, 30 mmol) were dissolved in 60 ml ethanol. A solution of NaOH (1.2 g, 30 mmol in 10 ml H_2O) was slowly added to this mixture at room temperature and the reaction mixture was refluxed for two hours. The formed NaCl was removed by filtration and the solvent was evaporated. The residual oil was partitioned between water and chloroform and extracted into chloroform (2 x 25 ml). All organic layers were combined and dried over $MgSO_4$, evaporated and dried under vacuum to get a yellow colored oil (2.53 g, 86%). **^{1}H NMR:** δ_H [300.13 MHz, $CDCl_3$, 298 K] 3.65 (q, 4H, ^3J = 5.97 Hz, –S–CH$_2$–C*H*$_2$–OH), 2.87 (s, 2H, -O*H*), 2.65 (t, 4H, ^3J = 6.12 Hz, –S-C*H*$_2$-CH$_2$-OH), 2.59 (t, 4H, ^3J = 7.05 Hz, –S–C*H*$_2$–CH$_2$–C*H*$_2$–S–), 1.81 (t, 4H, ^3J = 7.11 Hz, –S–CH$_2$–C*H*$_2$–CH$_2$–S–). **^{13}C NMR:** δ_C [75.47 MHz, $CDCl_3$, 298 K] 60.6 (-S–CH$_2$–*C*H$_2$–OH), 34.9 (–S–CH$_2$–*C*H$_2$–CH$_2$–S–), 30.4 (–S–*C*H$_2$–CH$_2$–OH), 29.3 (–S–*C*H$_2$–CH$_2$–*C*H$_2$–S–).

1,9-dichloro-3,7-dithianonane (Cl-pbss): A solution of $SOCl_2$ (3.57 g, 30 mmol in 10 ml chloroform) was slowly added to a solution of OH-pbss (2.53 g, 12.9 mmol in 30 ml chloroform) at room temperature and stirred for an hour. The chloroform and excess thionyl chloride were evaporated under reduced pressure to yield an orange colored oil (3.01 g, 100%). **^{1}H NMR:** δ_H [300.13 MHz, $CDCl_3$, 298 K] 3.75 (t, 4H, –S–CH$_2$–C*H*$_2$–Cl), 2.72 (t, 2H, –S–C*H*$_2$–CH$_2$–Cl), 2.44 (t, 4H, –S–C*H*$_2$–CH$_2$–C*H*$_2$–S–), 2.03 (t, 4H, –S–CH$_2$–C*H*$_2$–CH$_2$–

S–). **^{13}C NMR:** δ_C [75.47 MHz, $CDCl_3$, 298 K] 43.0 (–S–CH_2–*C*H_2–Cl), 34.8 (–S–*C*H_2–CH_2–Cl), 31.3 (–S–*C*H_2–CH_2–*C*H_2–S–), 29.7 (–S–CH_2–*C*H_2–CH_2–S–).

1,9-dithiouronium-3,7-dithianonane dichloride (TU-pbss): A solution of thiourea (1.52 g, 20 mmol in 30 ml ethanol) was added to the solution of Cl-pbss (2.8 g, 12 mmol in 30 ml ethanol) and refluxed for six hours. The solvent was evaporated under reduced pressure to get an orange colored solid mass (3.3 g, 86%). **^{1}H NMR:** δ_H [300.13 MHz, DMSO-d_6, 298 K] 9.35 (s, 8H, –$SC^+(NH_2)_2$), 3.42 (t, 4H, ^3J = 6.93 Hz, –S–C*H*$_2$–CH_2–C*H*$_2$–S–), 2.76 (t, 4H, ^3J = 6.83 Hz, –C*H*$_2$–$SC^+(NH_2)_2Cl^-$), 2.63 (t, 4H, ^3J = 7.13 Hz, –C*H*$_2$–CH_2–$SC^+(NH_2)_2Cl^-$), 1.74 (t, 4H, ^3J = 7.12 Hz, –S–CH_2–C*H*$_2$–CH_2–S–). **^{13}C NMR:** δ_C [75.47 MHz, DMSO-d_6, 298 K] 169.8 (–S*C*$^+(NH_2)_2Cl^-$), 30.6 (–S–*C*H_2–CH_2–*C*H_2–S–), 30.2 (–*C*H_2–CH_2–$SC^+(NH_2)_2Cl^-$), 29.6 (–CH_2–*C*H_2–$SC^+(NH_2)_2Cl^-$), 29.1 (–S–CH_2–*C*H_2–CH_2–S–). **MS (ESI):** (*m/z*) calculated for $C_9H_{20}S_4N_4$ [M–2HCl] requires (monoisotopic mass) $C_{15}H_{25}S_4NiFe$ 312.06, found 312.80.

3,7-dithianonane-1,9-dithiol (H_2pbss): The synthesis was carried out using modified literature procedure.[2,3] To a solution of TU-pbss (14.9 mmol, 5.40 g) in 50 ml water was added a solution of excess NaOH (30 mmol, 1.20 g) in 20 ml water. The resulting white mixture was refluxed for 2 h. After allowing the mixture to cool down concentrated HCl was added to neutralize the product. The resulting solution was extracted twice with 50 ml CH_2Cl_2. The combined organic layers were dried over $MgSO_4$ and evaporated under vacuum to yield 1.87 g of a grey colored oil (55%). Due to the rapid oxidation in air, the successive reaction with nickel was carried out immediately and the characterization of H_2pbss was not carried out.

2.5.14. Synthesis of the ligand precursor TU-pbsms

4,8-dithia-2,10-dimethylundecane-2,10-diol (OH-pbsms): Propane-1,3-dithiol (1.62 g, 15 mmol) and 1-chloro-2-methylpropan-2-ol (3.26 g, 30 mmol) were dissolved in 60 ml ethanol. A solution of NaOH (1.2 g, 30 mmol in 10 ml H_2O) was slowly added to this mixture at room temperature and the reaction mixture was refluxed for two hours. The formed NaCl was removed by filtration and the solvent was evaporated. The residual oil was partitioned between water and chloroform and extracted into chloroform (2 x 25 ml). All organic layers were combined and dried over $MgSO_4$, evaporated and dried under vacuum to get a colorless oil (2.84 g, 72%). **^{1}H NMR:** δ_H [300.13 MHz, $CDCl_3$, 300 K] 2.64 (t, ^3J = 7.08 Hz, 4H, –CH_2–C*H*$_2$–S–), 2.61 (s, 4H, –S–C*H*$_2$–C$(CH_3)_2$–), 2.38 (s, 2H, –O*H*), 1.84 (p, ^3J = 7.09 Hz, 2H, –C*H*$_2$–CH_2–S–), 1.23 (s, 6H, –S–CH_2–C(C*H*$_3$)$_2$–). **^{13}C NMR:** δ_C [75.47 MHz, $CDCl_3$, 300 K] 70.34 (–S–CH_2–*C*$(CH_3)_2$–), 46.40 (–S–*C*H_2–C$(CH_3)_2$–), 32.70 (–CH_2–*C*H_2–S–), 29.48 (–*C*H_2–CH_2–S–), 28.34 (–S–CH_2–*C*$(CH_3)_2$–).

1,9-dichloro-3,7-dithia-2,2,8,8-tetramethylnonane (Cl-pbsms): A solution of $SOCl_2$ (3.57 g, 30 mmol in 10 ml chloroform) was slowly added to a solution of OH-pbsms (2.84 g, 11.25 mmol in 30 ml chloroform) at room temperature and stirred for an hour. The chloroform and excess thionyl chloride were evaporated under reduced pressure to yield a bright yellow oil (3.25 g, 100%). **^{1}H NMR:** δ_H [300.13 MHz, $CDCl_3$, 300 K] 2.89 (s, 4H, –S–C(CH_3)$_2$–CH_2–), 2.68 (t, ^3J = 7.12 Hz, 4H, –CH$_2$–CH_2–S–), 1.84 (p, ^3J = 7.05 Hz, 2H, –CH_2–CH$_2$–S–), 1.60 (s, 6H, -S–C(CH_3)$_2$–CH$_2$–). **^{13}C NMR:** δ_C [75.47 MHz, $CDCl_3$, 300 K] 70.07 (–S–*C*(CH_3)$_2$–), 47.96 (-S–C(CH_3)$_2$–*C*H$_2$–), 32.98 (–CH$_2$–*C*H$_2$–S–), 31.26 (–S–C(*C*H$_3$)$_2$–CH$_2$–), 29.44 (–*C*H$_2$–CH$_2$–S–).

1,9-dithiouronium-3,7-dithia-2,2,8,8-tetramethylnonane dichloride (TU-pbsms): A solution of thiourea (1.68 g, 22 mmol in 30 ml ethanol) was added to the solution of Cl-pbsms (3.18 g, 11 mmol in 30 ml ethanol) and refluxed for six hours. The solvent was evaporated under reduced pressure to get a colorless oil. Addition of methanol/n-hexane (1:1) to this oil and standing for a night resulted in a white crystalline solid (4.23 g, 87%). **^{1}H NMR:** δ_H [300.13 MHz, DMSO-d_6, 300 K] 9.28 (s, 8H, –SC$^+$(NH_2)$_2$Cl$^-$), 3.51 (s, 4H, –S–C(CH_3)$_2$–CH_2–), 2.63 (t, ^3J = 7.32 Hz, 4H, –CH$_2$–CH_2–S–), 1.70 (p, ^3J = 7.19 Hz, 2H, –CH_2–CH$_2$–S–), 1.33 (s, 6H, –S–C(CH_3)$_2$–CH$_2$–). **^{13}C NMR:** δ_C [75.47 MHz, DMSO-d_6, 300 K] 170.17 (–S*C*$^+$ (NH$_2$)$_2$Cl$^-$), 45.05 (–S–*C*(CH_3)$_2$–CH$_2$–), 42.42 (–S–C(CH_3)$_2$–*C*H$_2$–), 29.63 (–*C*H$_2$–CH$_2$–S–), 27.56 (–S–C(*C*H$_3$)$_2$–CH$_2$–), 26.68 (–CH$_2$–*C*H$_2$–S–). **MS (ESI):** (*m/z*) calculated for $C_{13}H_{28}S_4N_4$ [M–2HCl] requires (monoisotopic mass) 368.12, found 368.87.

2.5.15. Synthesis of the ligand precursor TU-xbss

1,2-bis(4-hydroxy-2-thia-1-butyl)benzene (OH-xbss): A solution of NaOH (4.80 g, 120 mmol) in 15 ml water was added to a solution of α,α'-dichloro-*o*-xylene (10.50 g, 60 mmol) and 2-mercaptoethanol (9.38 g, 120 mmol) in 100 ml ethanol. After two hours refluxing, the formed NaCl was removed by filtration, and the solvents were evaporated under reduced pressure. Water was added and the product was extracted thrice with 50 ml $CHCl_3$. All the organic layers were combined and dried with $MgSO_4$. After evaporating the $CHCl_3$, the product was dried under vacuum to yield 14.40 g of a yellow oil (93%). **^{1}H NMR:** δ_H [300.13 MHz, DMSO-d_6, 298 K] 7.23 (m, ^3J = 3.70 Hz, 2H, phenyl ring), 7.17 (m, ^3J = 3.65 Hz, 2H, phenyl ring), 4.76 (s, 2H, –O*H*), 3.86 (s, 4H, Ph–CH_2–), 3.52 (t, ^3J = 6.83 Hz, 4H, –CH_2–OH), 2.47 (t, ^3J = 6.84 Hz, 4H, –CH_2–CH$_2$–OH). **^{13}C NMR:** δ_C [75.47 MHz, DMSO-d_6, 298 K] 136.9 (Ph–C1, Ph–C2), 130.6 (Ph–C3, Ph–C6), 127.3 (Ph–C4, Ph–C5), 61.0 (–*C*H$_2$–OH), 34.2 (Ph–CH_2–S–), 33.0 (–S–CH_2–CH$_2$–OH).

1,2-bis(4-chloro-2-thia-1-butyl)benzene (Cl-xbss): The synthesis was carried out by following a previously reported procedure.[3] Yield: 100%. **^{1}H NMR:** δ_H [75.47 MHz, DMSO-d_6, 298 K] 7.34 (m, 2H, phenyl ring), 7.26 (m, 2H, phenyl ring), 3.95 (s, 2H, Ph–

C*H*$_2$–S–), 3.70 (s, ^3J = 7.69 Hz , 4H, –C*H*$_2$–Cl), 2.78 (t, ^3J = 7.27 Hz, 4H, –S–C*H*$_2$–CH$_2$–Cl), **^{13}C NMR:** δ_C [300.13 MHz, DMSO-d$_6$, 298 K] 136.2 (Ph–C1, Ph–C2), 130.4 (Ph–C3, Ph–C6), 127.3 (Ph–C4, Ph–C5), 43.4 (–C*H*$_2$–Cl), 33.2 (–S–*C*H$_2$–CH$_2$–Cl), 32.2 (–S–CH$_2$–*C*H$_2$–Cl).

1,2-bis(4-thiouronium-2-thia-1-butyl)benzene dichloride (TU-xbss): To a suspension of Cl-xbss (15.40 g, 52.2 mmol) in 80 ml ethanol was added two equivalents of thiourea (8.04 g, 104.4 mmol). The mixture was then refluxed for two hours and the ethanol was evaporated under reduced pressure to obtain a dark oil. The oil was suspended in chloroform (60 ml) and diethyl ether (15 ml) to yield a greasy purple solid, which was filtered and washed with chloroform and ether to yield 19.66 g of a grey powder (85%). **^{1}H NMR:** δ_H [75.47 MHz, DMSO-d$_6$, 298 K] 9.33 (s, 8H, –SC$^+$(N*H*$_2$)$_2$Cl$^-$), 7.32 (m, 2H, phenyl ring), 7.22 (m, 2H, phenyl ring), 3.97 (s, 4H, Ph–C*H*$_2$–S–), 3.49 (t, ^3J = 7.67 Hz, 4H, –C*H*$_2$–SC$^+$(NH$_2$)$_2$Cl$^-$), 2.71 (t, ^3J = 7.60 Hz, 4H, –C*H*$_2$–CH$_2$–SC$^+$(NH$_2$)$_2$Cl$^-$). **^{13}C NMR:** δ_C [300.13 MHz, DMSO-d$_6$, 298 K] 169.6 (-S*C*$^+$(NH$_2$)$_2$Cl$^-$), 136.2 (Ph–C1, Ph–C2), 130.6 (Ph–C3, Ph–C6), 127.3 (Ph–C4, Ph–C5), 32.1 (-*C*H$_2$–CH$_2$–SC$^+$(NH$_2$)$_2$Cl$^-$), 30.4 (–*C*H$_2$–SC$^+$(NH$_2$)$_2$Cl$^-$), 30.4 (Ph–*C*H$_2$–S–). **IR (neat):** 3013bs, 2706w, 2020w, 1652vs, 1558w, 1489w, 1417m, 1268w, 1209w, 1079w, 910w, 701s, 668s, 595s, 461s, 452s, 398m, 384w cm^{-1}. **MS (ESI):** (*m/z*) calculated for C$_{14}$H$_{22}$S$_4$N$_4$ [M–2HCl] requires (monoisotopic mass) 374.07, found 374.86.

2.6. References

1. W. F. Zhu, A. C. Marr, Q. Wang, F. Neese, D. J. E. Spencer, A. J. Blake, P. A. Cooke, C. Wilson and M. Schröder, *Proc. Natl. Acad. Sci. U. S. A.*, 2005, **102**, 18280-18285.
2. V. Guyon, A. Guy, J. Foos, M. Lemaire and M. Draye, *Tetrahedron*, 1995, **51**, 4065-4074.
3. J. A. W. Verhagen, D. D. Ellis, M. Lutz, A. L. Spek and E. Bouwman, *J. Chem. Soc.-Dalton Trans.*, 2002, 1275-1280.
4. T. Yamamura, H. Arai, N. Nakamura and H. Miyamae, *Chem. Lett.*, 1990, 2121-2124.
5. G. H. Schmid, M. Strukelj, S. Dalipi and M. D. Ryan, *J. Org. Chem.*, 1987, **52**, 2403-2407.
6. MestReNova, Version 5.1.2, Mestrelab Research S.L., Santiago de Compostela, Spain, www.mestrelab.com, 2009.

3

$[Ni(S_4)Fe(C_5H_5)(CO)](PF_6)$ Complexes Containing $S_2S'_2$-donor Tetradentate ligands: Synthesis, Characterization and Electrocatalytic Dihydrogen Production†

Abstract. Six tetradentate chelating $S_2S'_2$-donor ligands – abbreviated as H_2ebss, H_2ebsms, H_2pbss, H_2pbsms, H_2xbss and H_2xbsms – have been synthesized that differ in both steric and electronic properties. These ligands have been reacted with $[Ni(acac)_2]$ (acac = acetylacetonate) and the low-spin nickel complexes $[Ni(S_2S'_2)]$ have been obtained. Reaction of these low-spin nickel complexes with $[Fe(C_5H_5)(CO)_2I]$ (C_5H_5 = cyclopentadienyl) and anion exchange with NH_4PF_6 yielded six [NiFe] complexes of general formula $[Ni(S_2S'_2)Fe(C_5H_5)(CO)](PF_6)$, of which the complex $[Ni(pbss)Fe(C_5H_5)(CO)](PF_6)$ has been previously reported. All the nickel and [NiFe] complexes have been characterized using ESI-MS spectrometry, electronic, IR and NMR spectroscopy, and cyclic voltammetric techniques. The X-ray structures of two of the nickel complexes are reported; $[Ni(ebsms)]_2$ crystallizes as a dimer with two bridging thiolate donors and with the nickel(II) ion in a square-pyramidal geometry. [Ni(pbsms)] crystallizes as a mononuclear compound with a square-planar geometry. All the six [NiFe] complexes show electrocatalytic activity to produce dihydrogen in the presence of acetic acid. Catalytic reduction of H^+ is shown at potentials as low as –1.19 V *vs*. Ag/AgCl for $[Ni(pbss)Fe(CO)Cp](PF_6)$ in acetonitrile. It was found that increased flexibility of the bridge of the ligands leads to electrocatalysts that need lower overpotentials whereas electron-donating dimethyl-substitution of the ligands leads to the need of higher overpotentials.

---

† R. Angamuthu, W. Roorda, M. A. Siegler, M. Lutz, A. L. Spek and E. Bouwman, *manuscripts in preparation*.

3.1. Introduction

Structural and functional models mimicking the active site of the hydrogenases have drawn tremendous interest recently as the models may shed light onto the mechanism of dihydrogen production and may result in the development of new effective catalytic systems of environmental and industrial importance.[1-5] The reactivity of thiolates coordinated to metals, towards small molecules such as O_2, H_2O_2, I_2, Br_2, CH_2Cl_2 and NO have been well studied in recent years.[6-9] Furthermore, nickel thiolate complexes have been frequently used as metalloligands in the synthesis of oligonuclear complexes as models for nickel-containing enzymes.[10-23] Darensbourg et al.[6,7,10-14] and Schröder[15,24,25] et al. have studied NiN_2S_2 complexes extensively while Bouwman et al. specifically studied the NiS_4 complexes.

Many heteronuclear model complexes have been investigated containing [FeFe], [NiFe], [NiRu], [NiCu], [NiZn] and [NiW] moieties, of which some [NiFe],[24,26-28] [FeFe],[29] [NiRu][1,30,31] and [Fe][29,32] complexes are known for their reactivity with protons and/or H_2, either catalytically or electro-catalytically.[29] Even though a large number of electrocatalysts containing [FeFe] and [NiRu] moieties have been reported in recent literature to reduce protons,[1,2,29] only three electrocatalysts are known based on nickel and iron having [$NiFe_2$],[24] [Ni_2Fe][26,27] and [NiFe][28] moieties. The most recently reported catalytically active [NiFe] complex contains a P_2S_2 donor set around the nickel(II) center.[28]

This chapter reports the syntheses and characterisations of four new tetradentate $S_2S'_2$-donor ligands and of nickel(II) complexes of six such ligands (Fig. 3.1). These six nickel(II) complexes have been reacted with [$Fe(C_5H_5)(CO)_2I$] forming a series of [NiFe] complexes with different flexibility and electronic properties. The chemistry of this series of [NiFe] complexes and their ability to produce dihydrogen electro-catalytically is reported.

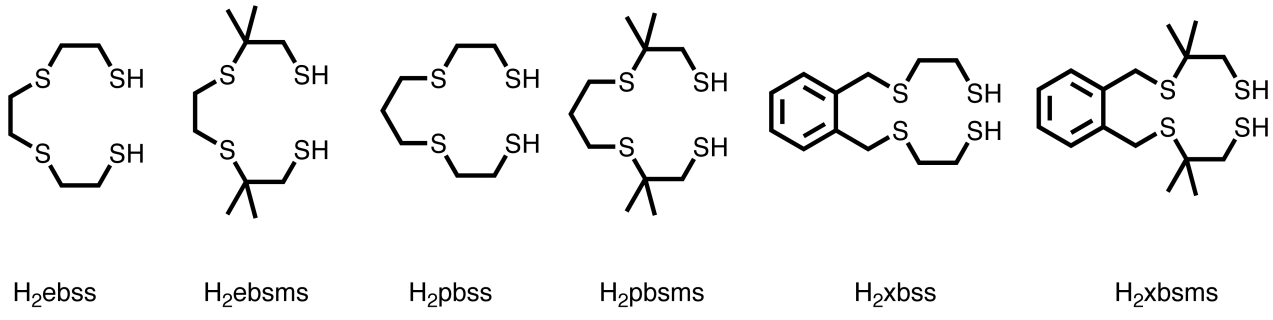

Fig. 3.1. Tetradentate chelating ligands used in the present study (see Chapter 2, section 2.2 for the abbreviation of the names of ligands).

3.2. Results

3.2.1. Synthesis

The syntheses of the ligand precursor thiouronium salts are discussed in detail in Chapter **2**. All the nickel complexes, except [Ni(pbss)], were synthesized by the reactions of $Ni(acac)_2$ with the thiouronium salts in the presence of a mild base such as tetramethylammonium hydroxide in toluene, THF or ethanol. The hydroxide ion attacks at the cationic carbon of the thiouronium salt resulting in urea and a thiolate ligand, which then coordinates to the nickel center. The isolation and manipulation of oxidation-sensitive thiol ligands is thus circumvented by the direct use of the thiouronium salts.[33] The anhydrous $Ni(acac)_2$ does not dissolve well in ethanol at RT, however, the complexes could be formed after refluxing for some time. This method was not successful for [Ni(pbss)]. The complex [Ni(pbss)] was synthesized from the reaction of H_2pbss with $NiCl_2{\cdot}6H_2O$ and four equivalents of NaOH in aqueous ethanol and the complex was obtained in pure crystalline form by filtering and cooling the reaction mixture.[34] All the mononuclear nickel complexes except [Ni(pbss)] were purified over an alumina column to remove any by-products, disulfide or unwanted oligomers formed during the reaction.

All the complexes were synthesized and handled in an inert argon atmosphere, and were found to be stable in air for several months. The light-sensitivity of the complex $[Ni(ebsms)]_2$ is discussed in detail in Chapter **9**.

The reaction of [Ni(pbss)] with $[Fe(C_5H_5)(CO)_2I]$ yielding $[Ni(pbss)Fe(C_5H_5)(CO)]I$ has been reported by Schröder et al.[16] The [NiFe] complexes were synthesized by slightly modifying the procedure reported by Schröder's group (Scheme 3.1). All the six nickel complexes reported in this chapter have been reacted with $[Fe(C_5H_5)(CO)_2I]$ in order to form [NiFe] complexes of general formula $[Ni(S_2S'_2)Fe(C_5H_5)(CO)]I$. The iodide anions are exchanged with PF_6^- anions using an exactly stoichiometric amount of NH_4PF_6; using an excess of NH_4PF_6 results in the formation of trinuclear $[Ni_3(S_2S'_2)_2](PF_6)_2$ species. The formed ammonium iodide and any unwanted precipitates are removed by passing the solution through a Celite column. The analytically pure [NiFe] complexes are obtained by passing the acetonitrile solutions of the complexes through neutral alumina column. The [NiFe] complexes have been characterized by ESI-MS spectrometry, electronic, IR and NMR spectroscopy, elemental analysis and electrochemical techniques. Single crystals suitable for X-ray diffraction were obtained for $[Ni(ebsms)]_2$ and [Ni(pbsms)]. Furthermore, the reactivity of the [NiFe] complexes with protons has been studied using electrochemistry.

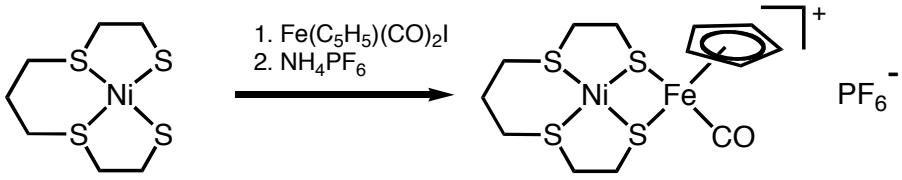

Scheme 3.1. Illustrative synthetic route used in the synthesis of heterodinuclear [NiFe] complexes.[16]

3.2.2. Molecular Structure of the Nickel Complexes

[Ni(ebsms)]$_2$: The asymmetric unit of [Ni(ebsms)]$_2$ contains one crystallographically independent molecule of the dinuclear complex; a molecule of dichloromethane is present in the crystal lattice. The two Ni(II) centers are in slightly distorted square-pyramidal environments with three thiolate donors and two thioether sulfurs coordinated to each nickel center (Fig. 3.2). Two thiolate sulfurs from the same ligand coordinate to a nickel center in *trans* position of each NiS_4 square-plane. One of these two thiolate sulfurs is bound in a terminal position and the other sulfur is bridging to the adjacent nickel center. One thioether sulfur of the same ligand and a thiolate bridging sulfur from the other ligand occupy the remaining two *trans* positions; the remaining thioether of the ligand binds axially to the Ni(II) center. The Ni–$S_{thiolate}$ distances (bridging, 2.2096(8)–2.2344(8) Å; terminal, 2.1928(8) and 2.1965(10) Å) are shorter than the Ni–$S_{thioether}$ distances (equatorial, 2.2360(8) and 2.246(3) Å; axial, 2.6011(8) and 2.7039(9) Å), as expected. However, a surprisingly short Ni–S distance (Ni1A–S19B, 2.139(3) Å) and unusual disorder is observed for the thioether site S19 (S19A and S19B; site occupancy = 0.6 : 0.4).

Both NiS_4 basal planes in the complex [Ni(ebsms)]$_2$ have a considerable degree of tetrahedral distortions with dihedral angles of 17.81° for Ni1 (between the planes S6–Ni1–S6A and S16–Ni1–S19) and 20.01 and 10.89° for Ni1A (between the planes S6–Ni1A–S6A and S16A–Ni1A–S19B/S16A–Ni1A–S19A). These tetrahedral distortions are interesting in the context of the active sites of [NiFe] hydrogenase enzymes, as these have highly distorted tetracoordinated NiS_4 geometry around the Ni(II) center in the reduced active form and a distorted pentacoordinated NiS_4X (X = HOO^- in Ni-A and HO^- in Ni-B) geometry around the Ni(III) center in the oxidized inactive form of the active site. In contrast to other dinuclear nickel thiolate complexes,[35,36] the molecular structure of complex [Ni(ebsms)]$_2$ exhibits an unusual coplanar structure instead of a butterfly or folded structure**.** The dihedral angle of the two NiS_4 planes in the complex [Ni(ebsms)]$_2$ is only 7.42° (3.05°). This coplanarity may be due to the steric hindrance rendered by the dimethyl groups of the ligand, reflected by the Ni-H_{Me} anagostic interactions (2.66 and 2.74 Å), which may be strong enough to not allow the NiS_4 planes to fold (Fig. 3.2).

Table 3.1. Selected distances (Å) and angles (°) for $[Ni(ebsms)]_2$ and [Ni(pbsms)] along with the data from [Ni(pbss)] for comparison.[37]

	$[Ni(ebsms)]_2$		
Ni1–S6	2.2345(8)	Ni1–S6A	2.2096(9)
Ni1–S9	2.6010(8)	Ni1A–S9A	2.7039(9)
Ni1–S16	2.1928(9)	Ni1A–S16A	2.1965(10)
Ni1–S19	2.2360(9)	Ni1A–S6	2.2139(8)
Ni1A–S6A	2.2284(8)	Ni1A–S19A	2.246(3)
		Ni1A–S19B	2.139(3)
S6–Ni1–S6A	83.70(3)	S6–Ni1A–S6A	83.74(3)
S6–Ni1–S9	87.41(3)	S6A–Ni1A–S9A	85.63(3)
S6–Ni1–S16	170.97(3)	S6A–Ni1A–S16A	168.42(4)
S6–Ni1–S19	94.84(3)	S6A–Ni1A–S19A	95.77(7)
		S6A–Ni1A–S19B	89.28(11)
S6A–Ni1–S9	108.47(3)	S6–Ni1A–S9A	100.52(3)
S6A–Ni1–S19	163.27(3)	S6–Ni1A–S19A	177.25(9)
S6A–Ni1–S16	89.66(3)	S6–Ni1A–S16A	91.49(3)
		S6–Ni1A–S19B	162.23(16)
S9–Ni1–S19	88.07(3)	S9A–Ni1A–S19A	82.12(9)
		S9A–Ni1A–S19B	95.19(14)
S9–Ni1–S16	100.53(3)	S9A–Ni1A–S16A	105.66(3)
S16–Ni1–S19	89.76(3)	S16A–Ni1A–S19A	88.49(7)
		S16A–Ni1A–S19B	92.21(10)

	[Ni(pbsms)]	[Ni(pbss)][37]		[Ni(pbsms)]	[Ni(pbss)][37]
Ni1–S6	2.1722(11)	2.179(2)	Ni1–S9	2.1646(11)	2.173(1)
Ni1–S16	2.1769	2.177(2)	Ni1–S19	2.1617(11)	2.166(2)
S6–Ni1–S9	90.30(4)	90.17(6)	S6–Ni1–S16	87.68(4)	87.05(6)
S6–Ni1–S19	176.54(4)	175.85(6)	S9–Ni1–S16	175.21(5)	177.02(6)
S9–Ni1–S19	91.74(4)	92.85(5)	S16–Ni1–S19	90.07(4)	89.87(5)

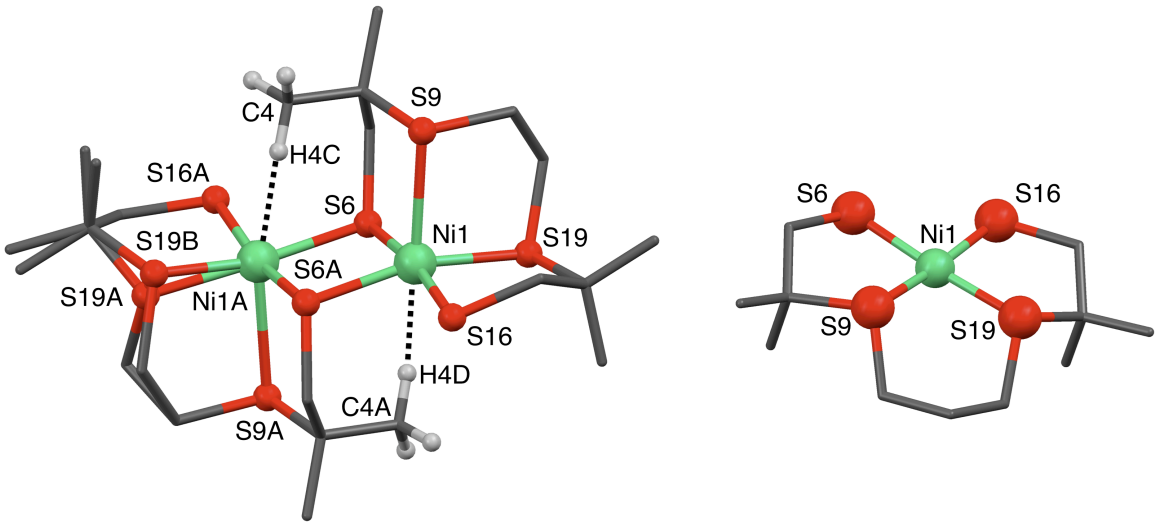

Fig. 3.2. Perspective views of the molecular structures of $[Ni(ebsms)]_2$ (left) and [Ni(pbsms)] (right). Ni, green; S, red; C, gray. Solvent and hydrogens are omitted for clarity. Selected distances (Å) and angles (°) for $[Ni(ebsms)]_2$: Ni1···Ni1A, 3.3090(5); anagostic Ni1···H4D, 2.66; Ni1A···H4C, 2.74 Å. Further details are provided in Table 3.1.

[Ni(pbsms)]: The mononuclear low-spin complex [Ni(pbsms)] crystallizes in the space group *P*21; the asymmetric unit contains one crystallographically independent ordered molecule (Fig. 3.2), no solvent molecules are present in the crystal lattice. The complex contains a Ni(II) centre which is in square-planar surroundings with an $S_2S'_2$ coordination sphere. Two thiolate donors and two thioether sulfurs are coordinated to the nickel centre, and are in enforced *cis* positions. The Ni–$S_{thiolate}$ distances (2.1722(11) and 2.1769(11) Å) are slightly longer than the Ni–$S_{thioether}$ distances (2.1646(11) and 2.1617(11) Å), as exhibited by [Ni(pbss)] (Table 3.1).[37] However, these distances are in contrast to the normal observation; usually, the Ni–$S_{thioether}$ distances are longer than (or similar to) the Ni-$S_{thiolate}$ distances.[38,39] The nickel(II) center has a slight tetrahedral distortion with a dihedral angle of 5.21° as defined by the triangular planes S6–Ni1–S9 and S16–Ni1–S19.

The X-ray crystal structures of [Ni(pbss)][37] and [Ni(xbsms)][33] have been reported in literature and reveal similar coordination environments as found for [Ni(pbsms)] with square-planar geometry around the low-spin nickel(II) center (Fig. 3.3). The efforts to crystallize [Ni(ebss)] and [Ni(xbss)] were not fruitful.

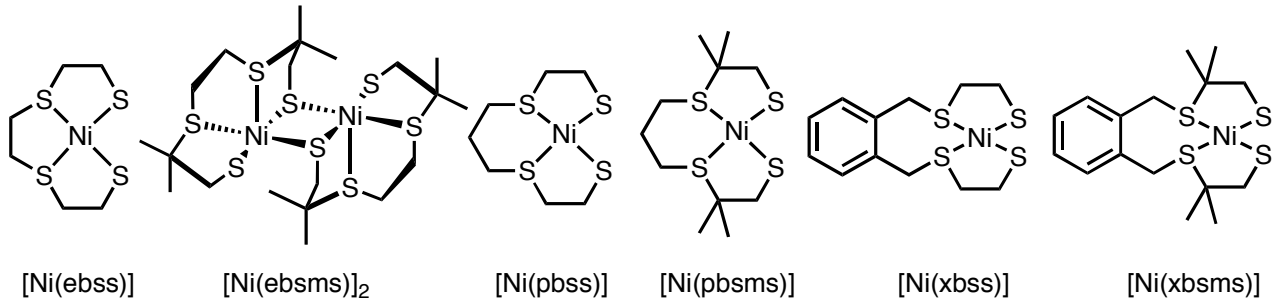

Fig. 3.3. Molecular structures of [Ni($S_2S'_2$)] complexes. The complexes $[Ni(ebsms)]_2$, [Ni(pbss)],[37] [Ni(pbsms)] and [Ni(xbsms)][33] have been characterised by X-ray crystallography.

3.2.3. Electronic, NMR and ESI-MS Spectra of the Nickel Complexes

The electronic absorption spectroscopic data of the nickel complexes in chloroform are presented in Table 3.2. All the six complexes exhibit two characteristic bands between 14000 cm^{-1} ($^1E' \leftarrow {}^1A_1'$) and 24000 cm^{-1} ($^1E'' \leftarrow {}^1A_1'$) due to d←d transitions, consistent with the square-planar geometry with an NiS_4 chromophore. The absorption maxima of the dimethyl-substituted complexes are shifted to higher energy due to the increase in the electron donation of the ligands.

Due to the fluxional behaviour of the nickel centers between square-planar and tetrahedral geometries, the ^1H NMR signals are significantly broadened at room temperature. However, the signals gradually sharpen and split upon cooling of the

samples. The axial and equatorial methyl groups in [Ni(pbsms)] show a single broad resonance around 1.6 ppm at 293 K (Fig. 3.4), but two comparatively narrow resonances at 243 K. Likewise, the protons of methylene groups next to the thiolate or thioether sulfurs show broad resonances at 293 K, whereas at 243 K they show typical AB pattern resonances. The Ni–H_{Me} interactions observed in the X-ray crystal structure of $[Ni(ebsms)]_2$ are also visible in the low-temperature ^{1}H NMR spectra and are discussed in detail in Chapter **9**.

Table 3.2. Electronic absorption maxima for the nickel complexes measured in chloroform.

Complex	$\nu/10^3$ cm^{-1} (ε/mol^{-1} l cm^{-1})			
Ni(ebss)]	14.1(150)		23.4 (1200)	
$[Ni(ebsms)]_2$	14.2 (100)	19.7 (1000)	23.4 (1200)	26.4 (1400)
[Ni(pbss)]	15.8 (70)	19.7 (sh)	23.8 (500)	26.5 (sh)
[Ni(pbsms)]	15.9 (90)	19.7 (sh)	23.6 (700)	26.3 (sh)
[Ni(xbss)]	14.5 (90)	19.3 (sh)	24.0 (sh)	
[Ni(xbsms)]	15.6 (69)	19.8 (sh)	25.6 (sh)	

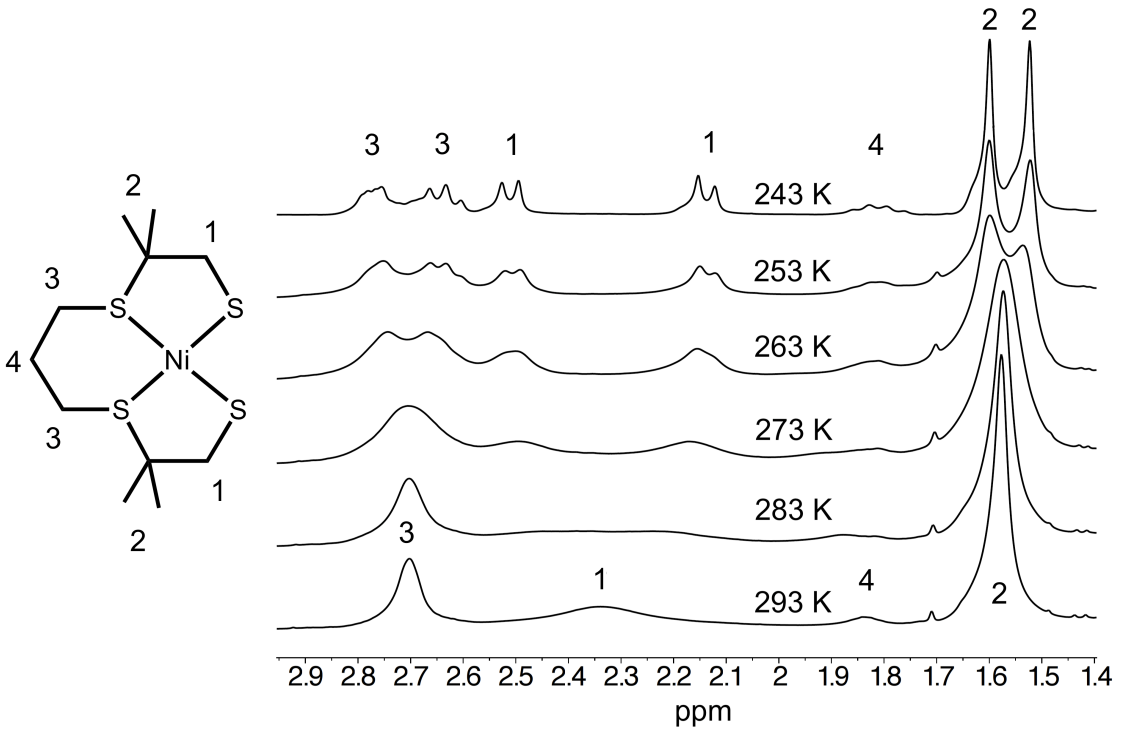

Fig. 3.4. ^{1}H NMR spectra of [Ni(pbsms)] in $CDCl_3$ recorded at different temperatures ranging between 243 and 293 K with the schematic structure of [Ni(pbsms)] showing the assignments of protons.

ESI-MS spectra of all the complexes were obtained from either a dichloromethane solution or acetonitrile solution with a trace amount of acetic acid. In all the cases $[M+H]^+$ molecular ion peaks, perfectly matching with calculated isotopic distributions, were observed. The complex $[Ni(ebsms)]_2$ exhibits a signal at $m/z = 651.59$ for $[M+H]^+$

(calculated m/z = 651.96) in addition to m/z = 326.76 (calculated m/z = 326.99) for $[0.5M+H]^+$, consistent with the observed solid-state dinuclear structure.

3.2.4. Electrochemical Behaviour of the Nickel Complexes

The redox properties of the nickel(II) complexes in dimethylformamide solutions were investigated using cyclic voltammetry; the relevant data are presented in Table 3.3. At a scan rate of 200 mV s^{-1} only irreversible oxidations of the complexes are observed at potentials ranging between 0.52 and 0.65 V *vs*. Ag/AgCl (Fig. 3.5). This implies that the nickel(III) state is not discernible within the timescale of the experiment or it is inaccessible for these complexes. The complex [Ni(ebss)] oxidized at more positive potential (1.09 V *vs*. Ag/AgCl) than the other five complexes indicating the difficulty in structural reorganisation upon oxidation. The oxidation potentials of the dimethyl-substituted complexes are less positive than the unsubstituted complexes, obviously due to the increased electron density on the nickel center caused by the substitution of the electron-donating dimethyl groups on the ligands. The reversible and quasi-reversible redox couples observed at negative potentials cannot be unambiguously assigned, as the thiolate and thioether donors are redox-non-innocent ligands. These irreversible or reversible reductions may originate from Ni^{II}/Ni^{I} redox couple or from the non-innocent sulfur donors.

Table 3.3. Electrochemical data of the nickel complexes obtained for 1 mM solutions of complexes (0.5 mM for $[Ni(ebsms)]_2$) in DMF containing 0.1 M $(NBu_4)PF_6$. Scan rate 200 mV s^{-1}. Static GC disc working electrode, Pt wire counter electrodes with a Ag/AgCl (satd. KCl) reference electrode.

Complex	E_{pa}(V)	E_{pc}(V)	ΔE(V)
[Ni(ebss)]	1.09		
		-1.12	
		-1.41	
$[Ni(ebsms)]_2$	0.65		
	-0.82	-0.96	0.14
	-1.33	-1.41	0.08
[Ni(pbss)]	0.57		
	-0.48		
	-1.48	-1.56	0.08
[Ni(pbsms)]	0.52		
	-0.80	-0.93	0.13
	-1.56	-1.67	0.09
[Ni(xbss)]	0.62		
	-0.62	-0.82	0.19
	-1.42	-1.55	0.13
[Ni(xbsms)]	0.54		
	-0.78	-0.92	0.14
		-1.09	

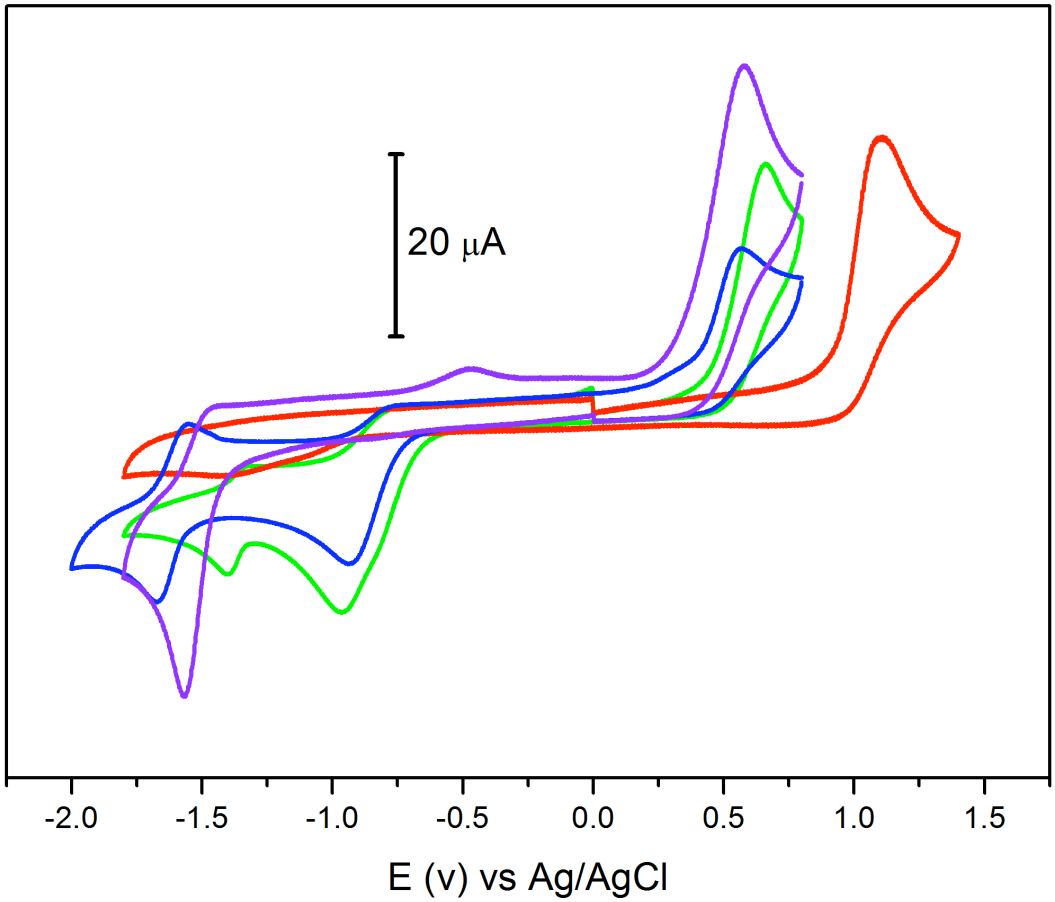

Fig. 3.5. Cyclic voltammograms of [Ni(ebss)] (red), $[Ni(ebsms)]_2$ (green), [Ni(pbss)] (violet) and [Ni(pbsms)] (blue); see Table 3.3 for detailed information.

3.2.5. FTIR and ESI-MS Spectra of the [NiFe] Complexes

The initial characterisations of the [NiFe] complexes were made using ESI-MS spectrometry in acetonitrile. All the [NiFe] complexes exhibit the $[Ni(S_2S'_2)Fe(C_5H_5)(CO)]^+$ and $[Ni(S_2S'_2)Fe(C_5H_5)]^+$ signals as parent molecular ion peak and fragment, respectively, in their corresponding positive-ion ESI-MS spectrum in agreement with formula $[Ni(S_2S'_2)Fe(C_5H_5)(CO)](PF_6)$. The [NiFe] complex of the ligand H_2ebsms, however, shows a molecular ion peak at m/z = 502.83 that can be assigned to the complex $[Ni(ebsms)Fe(C_5H_5)(CO)_2]^+$ i.e., with one additional CO ligand and fragments assigned to $[Ni(ebsms)Fe(C_5H_5)(CO)]^+$ (m/z = 474.62) and $[Ni(ebsms)Fe(CO)]^+$ (m/z = 409.67). The peak for $[Ni(S_2S'_2)Fe(C_5H_5)]^+$ is observed as the fragment of lowest molecular weight in five of the six [NiFe] complexes where the [NiFe] complex of the ligand H_2ebsms exhibit $[Ni(S_2S'_2)Fe(C_5H_5)(CO)]^+$ fragment at 10 V and $[Ni(ebsms)Fe(CO)]^+$ at 20 V.

Table 3.4. Comparison of the carbonyl IR stretching frequencies of the [NiFe] complexes in dichloromethane and the observed *m/z* values of the parent molecular ion peaks in ESI-MS.

Complex	ν(CO)	ν(PF_6^-)	m/z exptl. (calcd.)
[Ni(ebss)Fe(C_5H_5)(CO)](PF_6)	2042, 1997	828	418.56 (418.89)
[Ni(ebsms)Fe(C_5H_5)($CO)_2$](PF_6)	2046, 2001, 1959	830	502.83 (502.94)
[Ni(pbss)Fe(C_5H_5)(CO)](PF_6)	2045, 1998	822	432.50 (432.90)
[Ni(pbsms)Fe(C_5H_5)(CO)](PF_6)	2044, 1999, 1931	829	488.67 (488.96)
[Ni(xbss)Fe(C_5H_5)(CO)](PF_6)	2060, 2042, 1998	830	494.57 (494.92)
[Ni(xbsms)Fe(C_5H_5)(CO)](PF_6)	2046, 1999	835	550.69 (550.98)

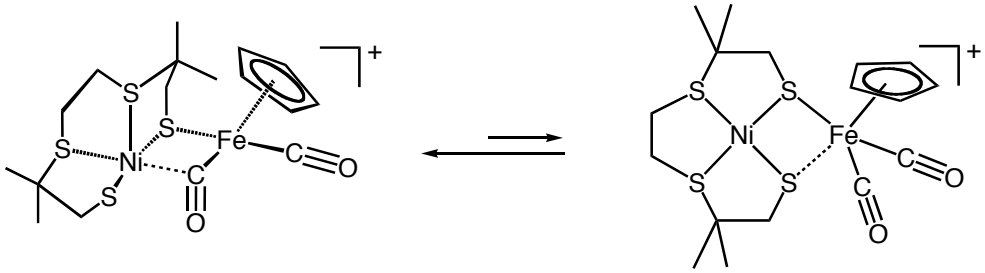

Fig. 3.6. Postulated molecular structure of [Ni(ebsms)Fe(C_5H_5)($CO)_2$](PF_6).

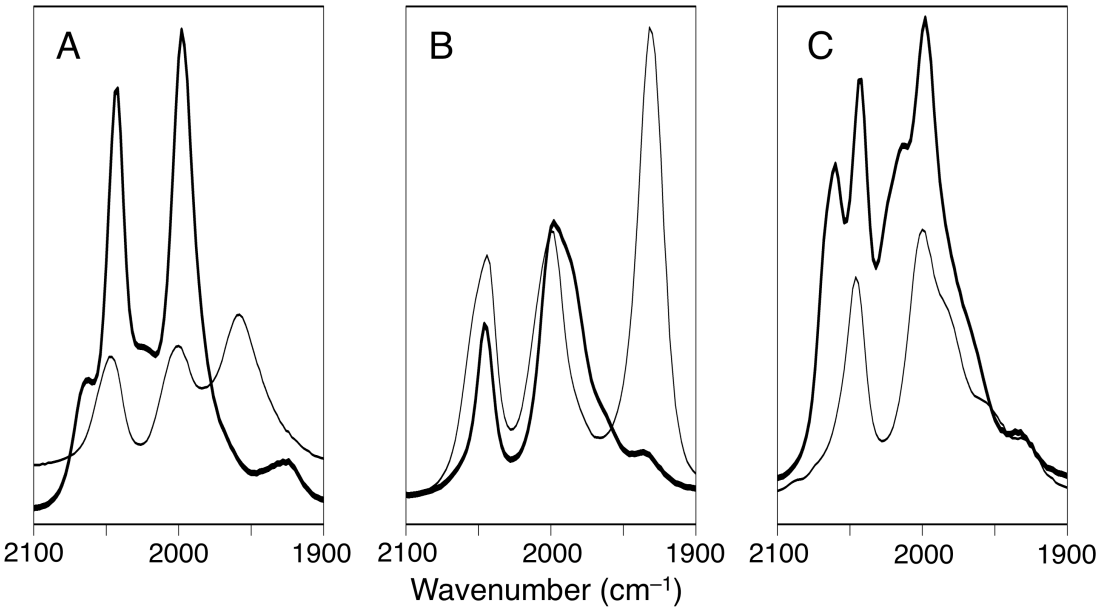

Fig. 3.7. Comparison of the solution IR spectra of [NiFe] complexes in dichloromethane showing the carbonyl stretching region. (A) [Ni(ebss)Fe(C_5H_5)(CO)]PF_6 (thick), [Ni(ebsms)Fe(C_5H_5)($CO)_2$]PF_6 (thin); (B) [Ni(pbss)Fe(C_5H_5)(CO)]PF_6 (thick), [Ni(pbsms)Fe(C_5H_5)(CO)]PF_6 (thin); (C) [Ni(xbss)Fe(C_5H_5)(CO)]PF_6 (thick) and [Ni(xbsms)Fe(C_5H_5)(CO)]PF_6 (thin).

The available structural data in combination with the ESI-MS spectrometric results indicate that the molecular structure of five [NiFe] complexes are as expected as reported for [Ni(pbss)Fe(C_5H_5)(CO)](PF_6)[16] as shown in Fig. 3.1. The [NiFe] complex of the ligand H_2ebsms may have two carbonyls as shown in Fig. 3.6 due to the fact that the iron(II) ion may not be able to bind to both of the available thiolates of the [Ni(ebsms)] moiety caused by the strain in the $[Ni(ebsms)]_2$ as observed in the X-ray crystal structure (Fig. 3.2). Fragmentations $[Ni(ebsms)Fe(C_5H_5)(CO)]^+$ and $[Ni(ebsms)Fe(CO)]^+$ may indicate that one CO is bridging as shown in Fig. 3.6(left). The carbonyl regions of the FTIR spectra of the [NiFe] complexes recorded in dichloromethane solutions are shown in Fig. 3.7. The shifts in the wavenumbers of the dimethyl-substituted complexes are indicative of the increase in the electron density on the iron center (Table 3.4).

3.2.6. NMR and Electronic Spectra of the [NiFe] Complexes

Despite the predicted low-spin square-planar nickel(II) and low-spin iron(II), the signal in the NMR spectra of [NiFe] complexes in acetonitrile or in dichloromethane are broad, and difficult to discern unequivocally. Unlike the nickel complexes, cooling down the NMR samples did not result in sharpening of the signals. This may be caused by the fluxional behaviour of the complexes or paramagnetic impurities. Therefore, the NMR spectroscopic data of the [NiFe] complexes are not helpful in the description of the solution structures and are not further discussed.

Table 3.5. Electronic absorption maxima for the [NiFe] complexes measured using acetonitrile solutions.

Complex	$\nu/10^3$ cm^{-1} (ε/mol^{-1}Lcm^{-1})					
[Ni(ebss)Fe(C_5H_5)(CO)]PF_6	19.1 (430)		29.9 (2900)	35.0 (3800)	41.5 (7100)	46.8 (10100)
[Ni(ebsms)Fe(C_5H_5)($CO)_2$]PF_6	19.0 (1100)	24.3 (3200)	29.8 (6100)	34.2 (10500)	40.7 (19400)	47.6 (22200)
[Ni(pbss)Fe(C_5H_5)(CO)]PF_6	20.2 (1100)	24.7 2500)	28.2 (3600)	34.0 (7200)	40.1 (15300)	46.9 (12400)
[Ni(pbsms)Fe(C_5H_5)(CO)]PF_6	20.3 (1000)	24.7 (2000)	28.0 (2900)	32.5 (5600)	40.5 (12900)	47.3 (13800)
[Ni(xbss)Fe(C_5H_5)(CO)]PF_6			29.400 (5900)	35.700 (11600)	41.150 (18900)	46.3 (26700)
[Ni(xbsms)Fe(C_5H_5)(CO)]PF_6	19.6 (1200)	23.6 (2000)	29.200 (4300)	33.400 (6900)	41.000 (16100)	47.4 (27300)

The UV-VIS spectra of the [NiFe] complexes have been recorded in acetonitrile (Table 3.5) and are not compared to spectra in non-coordinating solvents due to the low solubility in these solvents. So, it cannot be concluded that solvent coordination does not take place. The d←d bands of the nickel complexes shift to higher energy in the [NiFe] complexes compared to the corresponding mononuclear nickel complexes, which is in

agreement with the incorporation of the electron-rich $[Fe(C_5H_5)(CO)]^+$ moiety. Furthermore, a number of higher energy bands corresponding to π-π* transitions of the Cp^- ring are observed between 28000 cm^{-1} and 47000 cm^{-1}. The d←d transition bands of the complex $[Ni(xbss)Fe(CO)Cp]PF_6$ could not be observed due to solubility problems and the low concentration of the solutions.

3.2.7. Electrochemical Behaviour of the [NiFe] Complexes and Reduction of Protons

The electrochemical behaviour of the [NiFe] complexes in acetonitrile was investigated using cyclic voltammetry. For all the six [NiFe] complexes several quasi-reversible and irreversible redox couples are observed (Table 3.6). As an example, the CV of complex $[Ni(ebss)Fe(C_5H_5)(CO)](PF_6)$ is shown in Fig. 3.8. In all the six [NiFe] complexes, an irreversible anodic peak can be seen around 0.6 V vs Ag/AgCl corresponding to the oxidation of the nickel(II) ion to nickel(III) and a quasi-reversible or irreversible redox couple around 0.3 V vs Ag/AgCl is observed ascribed to the Fe(II)/Fe(III) couple for some complexes. However, the oxidations or reductions observed are not unequivocally assignable due to the presence multiple redox-active atoms in the [NiFe] complexes, and the redox changes may be distributed among the redox-active members of the [NiFe] complexes.[26]

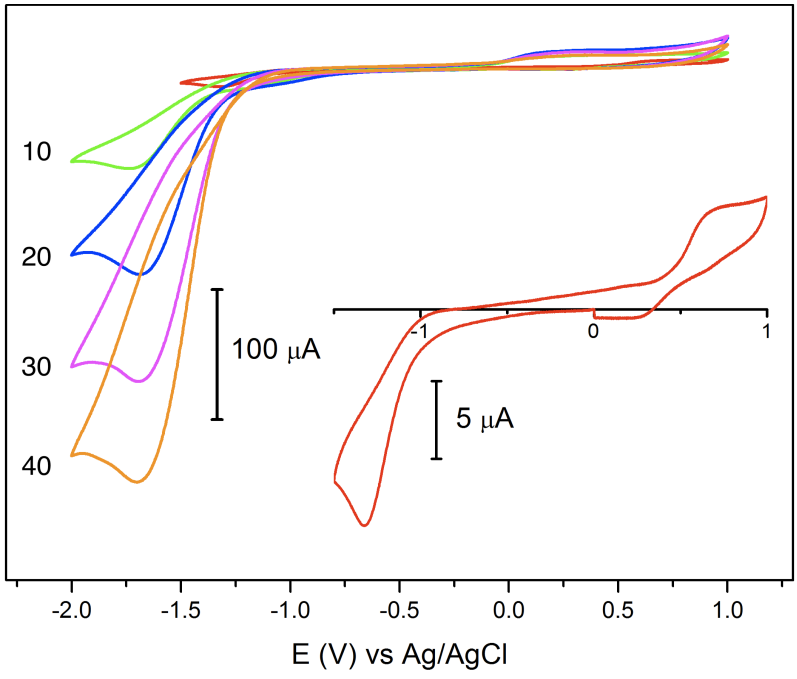

Fig. 3.8. Cyclic voltammograms of $[Ni(ebss)Fe(C_5H_5)(CO)](PF_6)$ (0.5 mM) in acetonitrile in the presence of 10, 20, 30, 40 equivalents of acetic acid. Inset: Cyclic voltammogram of $[Ni(ebss)Fe(C_5H_5)(CO)](PF_6)$ in the absence of acid. Further details are provided in Table 3.6.

Table 3.6. Electrochemical data of [NiFe] complexes (0.5 mM) in acetonitrile.*

	E_{pa}(V)	E_{pc}(V)	ΔE(V)	E_{HER}(V)#
$[Ni(ebss)Fe(C_5H_5)(CO)]PF_6$	0.68			
		0.28		
		-1.33		-1.74
$[Ni(ebsms)Fe(C_5H_5)(CO)_2]PF_6$	0.62			
		-1.33		-1.65
$[Ni(pbss)Fe(C_5H_5)(CO)]PF_6$	0.53			
		0.01		
		-1.05		-1.19
$[Ni(pbsms)Fe(C_5H_5)(CO)]PF_6$	0.63			
	0.29			
		-1.12		
		-1.28		-1.69
$[Ni(xbss)Fe(C_5H_5)(CO)]PF_6$	0.70	0.54	0.15	
	0.47	0.21	0.26	
		-1.27		-1.44
$[Ni(xbsms)Fe(C_5H_5)(CO)]PF_6$	0.69			
	0.26			
		-1.24		-1.52

* Measured vs. Ag/AgCl reference electrode; Static glassy carbon disc working electrode; Pt-wire counter electrode; Scan rate 200 mV s^{-1}; Supporting electrolyte 0.05 M Bu_4NPF_6.
\# E_{HER}: potential at which hydrogen evolution reaction occurs.

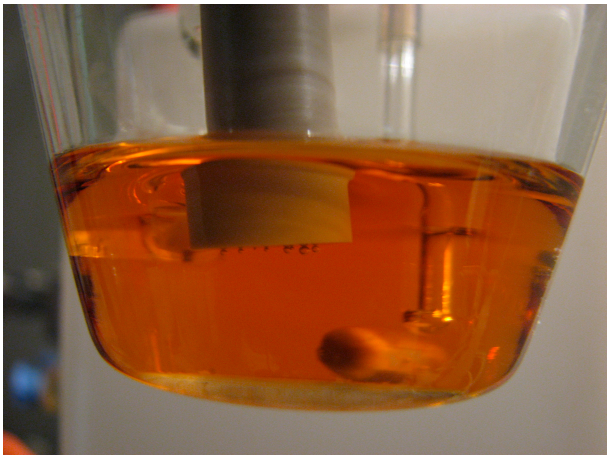

Fig. 3.9. Dihydrogen bubbles formed on the surface of the glassy carbon working electrode during the electrocatalysis of 0.5 mM $[Ni(pbss)Fe(C_5H_5)(CO)]PF_6$ in the presence of acetic acid. Object at the bottom of the cell is a stir-bar; the Pt wire counter electrode and the Ag/AgCl reference electrode are behind the working electrode.

The hydrogenase activity of all the six [NiFe] complexes was tested by means of electrocatalytic reduction of protons in the presence of acetic acid as a mild source of protons. A new irreversible cathodic wave corresponding to the reduction of protons with concurrent evolution of dihydrogen gas appears in the cyclic voltammograms of the [NiFe] complexes in the presence of acetic acid, which rises in height and shifts to more negative potential upon increasing concentrations of acetic acid (Fig. 3.8). After some

time the bubbles of formed dihydrogen gas can be observed on the surface of the glassy carbon working electrode (Fig. 3.9). At lower H^+ concentrations, the catalytic wave appears with a sigmoidial shape, indicating that the catalytic reaction proceeds sufficiently rapid and that the current is controlled by the diffusion of acid to the electrode surface. This is confirmed by the linearity of the plots of the catalytic peak current against the concentration of the added acetic acid. The potential at proton reduces varies between –1.19 V and –1.74 V *vs*. Ag/AgCl and found to be affected by the structural and electronic properties of the [NiFe] complexes used.

3.3. Discussion

The molecular structures of the nickel(II) complexes $[Ni(ebsms)]_2$ and [Ni(pbsms)] are unequivocally derived from the X-ray crystallographic data to have a thiolate bridged square-pyramidal dinuclear and square-planar mononuclear structure, respectively. In general, $[Ni(ebsms)]_2$ appears to be the only coplanar dinuclear nickel thiolate structure. The structures of [Ni(pbss)][37] and [Ni(xbsms)][33] have been reported to have square-planar geometry around the NiS_4 coordination sphere. The complexes [Ni(ebss)] and [Ni(xbss)] probably also have mononuclear square-planar structures according to the available spectroscopic and ESI-MS spectrometric data. The square-pyramidal geometry of the nickel centers in the complex $[Ni(ebsms)]_2$ may be caused by the strain in the structure rendered by the dimethyl groups. The molecular structures of the [NiFe] complexes of the ligand H_2ebss, H_2pbsms, H_2xbss and H_2xbsms are expected to have the molecular structure as reported for the complex $[Ni(pbss)Fe(C_5H_5)(CO)](PF_6)$ according to the available spectroscopic and ESI-MS spectrometric data. In contrast, the analyses of the [NiFe] complex of the ligand H_2ebsms are indicative of the presence of two CO groups and the expected structure might be either one or a mixture of the two structures shown in Fig. 3.6.

The electron-donating dimethyl-substituted complexes [Ni(pbsms)] and [Ni(xbsms)] are oxidized more easily compared to the unsubstituted counterparts. For example, the oxidation potential of [Ni(pbss)] is 0.57 V *vs*. Ag/AgCl whereas for [Ni(pbsms)] it is 0.52 V *vs*. Ag/AgCl (Table 3.3). Likewise, the oxidation potential of [Ni(xbss)] is 0.62 V *vs*. Ag/AgCl and 0.54 V *vs*. Ag/AgCl for [Ni(xbsms)].

All the six [NiFe] complexes are found to be active in the reduction of H^+ into dihydrogen. It appears that increased flexibility of the nickel coordination sphere favours the electrocatalytic proton reduction at more positive potentials. A longer and more flexible carbon bridge usually increases the flexibility around the nickel center. The complex with C_2 bridge, $[Ni(ebss)Fe(C_5H_5)(CO)](PF_6)$, shows dihydrogen evolution at -1.74 V *vs*. Ag/AgCl whereas the complex with C_3 bridge, $[Ni(pbss)Fe(C_5H_5)(CO)](PF_6)$,

reduces protons at comparatively more positive value of –1.19 V *vs*. Ag/AgCl. However, [Ni(pbsms)Fe(C_5H_5)(CO)](PF_6) (E_{HER}, –1.69 V *vs*. Ag/AgCl) and [Ni(ebsms)Fe(C_5H_5)$(CO)_2$](PF_6) (E_{HER}, –1.65 V *vs*. Ag/AgCl) differs from the expected trend: the complex [Ni(ebsms)Fe(C_5H_5)$(CO)_2$](PF_6) may have more flexibility around the nickel(II) as the iron may not bind to both the thiolates of [Ni(ebsms)] moiety. The complexes [Ni(xbss)Fe(C_5H_5)(CO)](PF_6) and [Ni(xbsms)Fe(C_5H_5)(CO)](PF_6) cannot be compared with the other four complexes as they have different electronic properties due to the aromatic xylyl bridging group.

The presence of electron-donating dimethyl substitution on the ligands moves the reduction of protons to more negative potentials; this may be due to higher electron density on the nickel(II) ion. For example, the complex [Ni(pbss)Fe(C_5H_5)(CO)](PF_6) reduces protons at –1.19 V *vs*. Ag/AgCl whereas the analogous complex [Ni(pbsms)Fe(C_5H_5)(CO)](PF_6) reduces protons at –1.69 V *vs*. Ag/AgCl. Likewise, the complex [Ni(xbss)Fe(C_5H_5)(CO)](PF_6) reduces protons at –1.44 V *vs*. Ag/AgCl whereas the analogous complex [Ni(xbsms)Fe(C_5H_5)(CO)](PF_6) reduces protons at –1.52 *vs*. Ag/AgCl.

Cooperativity between the nickel and iron centers or dinuclearity of the [NiFe] complexes seems to be important as there was catalytic behaviour found for neither of the precursor mononuclear nickel complexes nor for the mononuclear compound [Fe(C_5H_5)$(CO)_2$I]. However, [Ni(xbsms)][30] and [Fe(C_5H_5)$(CO)_2$I][32] have been reported to electrocatalyse proton reduction under different conditions by the group of Fontecave. The mononuclear complex [Ni(xbsms)] is reported to electrocatalyse the dihydrogen evolution from $(C_2H_5)_3$NHCl at –1.45 V *vs*. Ag/AgCl in dimethylformamide.[30] The solvated species of the mononuclear complex [Fe(C_5H_5)$(CO)_2$I], [Fe(C_5H_5)$(CO)_2$(THF)]$^+$, (THF = tetrahydrofuran) is reported to electrocatalyse proton reduction from trichloroacetic acid at –0.8 V *vs*. Ag/AgCl in dimethylformamide.[32]

Heterogeneous catalysis due to the coating of nickel on the glassy carbon electrode can be excluded as there was no activity with the electrode after washing and there was no precipitation after the electrochemical experiments. The active species in the electrocatalysis may be a metal hydride compound formed from the reaction of dissolved protons with a reduced heterodinuclear complex. However, the fact that the catalytic wave develops at potentials lower than that required for the initial reduction of the [NiFe] complexes suggests that this metal-hydride species should be further reduced for activation as stated in the literature.[2,40] Thus the [NiFe] complexes are pre-catalysts that need activation prior to catalysis. Hence, the electrocatalysis may follow an ECEC route for the proton reduction.

3.4. Conclusions

In summary, the presented six heterodinuclear [NiFe] complexes are the first series of functional models of [NiFe] hydrogenase which have S_4 coordination around the nickel(II) ion and a carbonyl ligand coordinated to the iron center. All the six [NiFe] complexes are electro-catalytically active in the reduction of protons using acetic acid as a proton source at working potentials as low as -1.19 V *vs.* Ag/AgCl. By systematically varying the structural and electronic properties of these six [NiFe] complexes, the influence of these properties on the working potentials in the proton reduction has been demonstrated. An increased flexibility around the nickel coordination sphere and a decreased electron density on the metal centers move the proton reduction potential to more positive values. Hence, the next Chapter is devoted to a series of heterodinuclear [NiFe] complexes comprising SS'-donor bidentate ligands, whereby the flexibility of the complexes is further enhanced in order to make better functional models.

3.5. Experimental Procedures

3.5.1. General Remarks

The syntheses of the ligand precursor thiouronium salts TU-ebss, TU-ebsms, TU-pbsms, TU-xbss are described in Chapter **2** along with the characterizations. The mononuclear nickel(II) complexes [Ni(pbss)][34,37,41] and [Ni(xbsms)],[33] and the heterodinuclear complex [Ni(pbss)Fe(C_5H_5)(CO)](PF_6)[16] were synthesized according to the previous reports.

3.5.2. Synthesis of [Ni(ebss)]

To a two-necked flask charged with a solution of Ni(acac)$_2$ (2.57 g, 10 mmol) in 60 mL THF was added TU-ebss (3.71 g, 10 mmol). After 10 minutes stirring at 50 °C, NMe_4OH (9.1 ml, 20 mmol) was added to the green solution. After the immediate formation of a dark brown colour, the solution was refluxed for five hours. After cooling down, the mixture was filtered and the precipitate was washed with THF to get a light brown powder. It was then dissolved in chloroform; the insoluble by-products were removed by filtration and the filtrate was evaporated under reduced pressure to yield 0.754 g of a dark brown powder. The powder was then dissolved in CH_2Cl_2 (4ml) and passed through Al_2O_3. The first band (dark red) was collected to yield 0.41 g of pure [Ni(ebss)] (15%). **Elemental analysis (%):** Calculated for $C_6H_{12}S_4Ni$ (271.12); C 26.58, H 4.46, S 47.31, found: C 26.55, H 4.56, S 47.25. **^{1}H NMR:** δ_H (300 MHz, $CDCl_3$, 298 K): 3.59 (m, 4H, –CH_2–S–(CH_2)$_2$–S–CH_2–), 2.92 (m, 8H, –CH_2–S–(CH_2)$_2$–S–). **IR (neat):** 3019w, 2994w, 1491s, 1404m, 1254w, 960m, 950s, 851w, 819w, 751w, 457w cm^{-1}. **MS (ESI):** (*m/z*) calcd for $C_6H_{13}S_4Ni$ [M+H$^+$] requires (monoisotopic mass) 270.93, found 270.78.

3.5.3. Synthesis of [Ni(ebsms)]$_2$

To a two-necked flask charged with a solution of $Ni(acac)_2$ (0.768g, 3 mmol) in 60 ml dry toluene was added TU-ebsms (1.284 g, 3 mmol). After 10 minutes stirring at 50 °C, NMe_4OH (2.73 ml, 6 mmol) was added to the mint-green colour solution. This immediately formed a dark brown solution, which was refluxed for three hours. After evaporating the solvent, CH_2Cl_2 was added and the insoluble by-products were removed by filtering. The filtrate was passed through alumina and the first dark-red band was collected and evaporated to get 0.14 g of pure [Ni(ebsms)] (15%). **Elemental analysis (%):** Calculated for $C_{20}H_{40}S_8Ni_2(654.45)\bullet 0.4CH_2Cl_2$; C 35.59, H 5.97, S 37.26, found: C 35.57, H 5.98, S 37.19. **^{1}H NMR:** δ_H (400 MHz, $CDCl_3$, 293 K): 4.14 (bs, 2H, 2 × –C(H_2)*H*), 3.09–2.21 (m, 8H, 4 × -CH_2-), 1.57 (4H, 2 × -C(*H_2*)H), 1.39 (6H, 2 × –C*H_3*). **IR (neat):** 2956m, 2903m, 2360m, 1684w, 1652w, 1558w, 1456s, 1418s, 1378m, 1361s, 1260m, 1195m, 1114s, 1080s, 932w, 887w, 842s, 728m, 668w, 630w, 575w, 388s, 374s cm^{-1}. **MS (ESI):** (*m/z*) calculated for $C_{20}H_{40}S_8Ni_2$ $[M]^+$ requires (monoisotopic mass) 651.96, found 651.59; $[1/2M+H^+]$ requires 326.99, found 326.65.

3.5.4. Synthesis of [Ni(pbsms)]

The synthesis was carried out according to the procedure described in the literature.[33] **[Ni(pbsms)]:** Yield: 72%. **Elemental analysis (%):** Calcd for $C_{11}H_{22}S_4Ni$ (341.24); C 38.72, H 6.50, S 37.59, found: C 38.56, H 6.79, S 37.33. **^{1}H NMR:** δ_H (300 MHz, $CDCl_3$, 298 K): 2.68 (t, 4H, –S–C*H_2*–CH_2–C*H_2*–S–), 2.31 (bs, 6H, –S–CH_2–C*H_2*–CH_2–S– and –S–C(CH_3)$_2$–C*H_2*–S–), 1.56 (s, 12H, –C*H_3*). **IR (neat):** 3388w, 2920w, 2172w, 1652w, 1585s, 1558m, 1516s, 1506m, 1489m, 1456s, 1404s, 1362s, 1254m, 1134m, 1080m, 1020w, 951m, 915w, 890w, 668w, 575m, 384w cm^{-1}. **MS (ESI):** (*m/z*) calculated for $C_{11}H_{23}S_4Ni$ $[M+H^+]$ requires (monoisotopic mass) 341.00, found 340.72.

3.5.5. Synthesis of [Ni(xbss)]

The synthesis was carried out according to the procedure described in the literature.[33] **[Ni(xbss)]:** Yield: 37.2%. **Elemental analysis:** Calcd (%) for $C_{12}H_{16}S_4Ni$, 347.21: C 41.51, H 4.64, S 36.94, found: C, 41.43; H, 4.82; S, 36.63. **^{1}H NMR:** δ_H (400 MHz, $CDCl_3$, 293 K): 7.33 (d, 2H, phenyl), 7.24 (d, 2H, phenyl), 3.88 (s, 4H, Ar–C*H_2*–S–), 2.87 (m, 4H, –CH_2–S–C*H_2*–CH_2–S–), 2.43 (m, 4H, –CH_2–S–CH_2–C*H_2*–S–). **IR (neat):** 3309w, 3187w, 3026w, 2917w, 2144w, 1654w, 1586s, 1515s, 1464m, 1398s, 1254m, 1193w, 1110w, 1013m, 950m, 918m, 765w, 730m, 699w, 654w, 559w, 546m, 452w, 406m cm^{-1}. **MS (ESI):** (*m/z*) calculated for $C_{12}H_{17}S_4Ni$ $[M+H^+]$ requires (monoisotopic mass) 345.95, found 346.65.

3.5.6. Synthesis of [Ni(ebss)Fe(C_5H_5)(CO)](PF_6)

The synthesis was carried out by modifying the procedure described in the literature.[16] Yield: 20%. **Elemental analysis (%):** Calcd for $C_{12}H_{17}S_4ONiFePF_6$ (565.02); C 25.51, H 3.03, S 22.7, found: C 25.42, H 2.95, S 22.53. **IR (neat):** 3054w, 2223w, 2038m, 1992m, 1424m, 828s, 603w, 556s, 418w cm^{-1}. **MS (ESI):** (*m/z*) calculated for $C_{12}H_{17}S_4ONiFe$ [M-PF_6] requires (monoisotopic mass) 418.89, found 418.49; (*m/z*) calculated for $C_{11}H_{17}S_4NiFe$ [M–(CO+PF_6)] requires 390.89, found 390.60

3.5.7. Synthesis of [Ni(ebsms)Fe(C_5H_5)($CO)_2$](PF_6)

The synthesis was carried out by modifying the procedure described in the literature.[16] Yield: 23%. **Elemental analysis:** Calcd (%) for $C_{17}H_{25}S_4O_2NiFePF_6$, 621.13: C 31.45, H 3.88, S 19.76, found: C 31.25, H 3.68, S 19.38. **IR (neat):** 2967w, 2360w, 2034w, 1948w, 1458w, 1369w, 1116w, 830vs, 556s, 418w cm^{-1}. **MS (ESI):** (*m/z*) calculated for $C_{17}H_{25}S_4O_2NiFe$ [M–PF_6] requires (monoisotopic mass) 502.94, found, 502.63; $C_{16}H_{25}S_4ONiFe$ [M–(CO+PF_6)] requires 474.95, found 474.62.

3.5.8. Synthesis of [Ni(pbsms)Fe(C_5H_5)(CO)](PF_6)

The synthesis was carried out by modifying the procedure described in the literature.[16] Yield: 18%. **Elemental analysis:** Calcd (%) for $C_{17}H_{27}S_4ONiFePF_6$, 635.15: C 32.15, H 4.28, S 20.19, found: C 32.02, H 4.10, S 19.70. **IR (neat):** 2924w, 2042m, 1995m, 1563w, 1558w, 1428w, 1371w, 829vs, 740w, 6044w, 556s, 352w cm^{-1}. **MS (ESI):** (*m/z*) calculated for $C_{17}H_{27}S_4ONiFe$ [M–PF_6] requires (monoisotopic mass) 488.96, found 488.67; calculated for $C_{16}H_{27}S_4NiFe$ [M–(CO+PF_6)] requires 460.97, found 460.68.

3.5.9. Synthesis of [Ni(xbss)Fe(C_5H_5)(CO)](PF_6)

The synthesis was carried out by modifying the procedure described in the literature.[16] Yield: 9%. **Elemental analysis:** Calcd (%) for $C_{18}H_{21}S_4ONiFePF_6$, 641.13: C 33.72, H 3.30, S 20.01, found: C 33.77, H 3.19, S 19.62. **IR (neat):** 3383bw, 2218w, 2052w, 1990w, 1662w, 1652w, 1568m, 1558m, 1520m, 1506m, 1418m, 1362m, 1279w, 1162w, 1020w, 934w, 830vs, 667w, 608w, 556vs, 418w, 310w cm^{-1}. **MS (ESI):** (*m/z*) calculated for $C_{18}H_{21}S_4ONiFe$ [M–PF_6] requires (monoisotopic mass) 494.92, found 494.99; calculated for $C_{17}H_{21}S_4NiFe$ [M–(CO+PF_6)] requires 466.92, found 466.50.

3.5.10. Synthesis of [Ni(xbsms)Fe(C_5H_5)(CO)](PF_6)

The synthesis was carried out by modifying the procedure described in the literature.[16] Yield 18%. **Elemental analysis:** Calcd (%) for $C_{22}H_{29}OS_4NiFePF_6$, 697.22: C 37.90, H 4.19, S 18.40, found: C 37.45 H 4.23 S 17.98. **IR (neat):** 3331bw, 2212w, 1992w, 1592w, 1558w, 1436m, 1452w, 835vs, 557s, 374w, 366w cm^{-1}. **MS (ESI):** (*m/z*)

calculated for $C_{22}H_{29}S_4ONiFe$ [M–PF_6] requires (monoisotopic mass) 550.98, found 550.69; calculated for $C_{21}H_{29}S_4NiFe$ [M–(CO+PF_6)] requires 522.99, found 522.64.

3.5.11. Crystallographic data of Complex [Ni(ebsms)]$_2$

$C_{20}H_{40}Ni_2S_8 \cdot CH_2Cl_2$, Fw = 739.35, black block, 0.60 x 0.42 x 0.36 mm^3, orthorhombic, $Pna2_1$ (no. 33), a = 10.5534(3), b = 23.6789(8), c = 12.4717(3) Å, V = 3116.58(16) Å^3, Z = 4, D_x = 1.576 g/cm^3, μ = 1.93 mm^{-1}. 32767 Reflections were measured up to a resolution of $(\sin\theta/\lambda)_{max}$ = 0.61 Å^{-1} at a temperature of 110(2) K. Absorption correction range 0.43-0.50. 5805 Reflections were unique (R_{int} = 0.042), of which 5617 were observed [I>2σ(I)]. The thioether group involving S19A/S19B was disordered over two conformations. 346 Parameters were refined with 72 restraints concerning the disordered group (distance and angle restraints and restraints to approximate isotropic behaviour of the displacement parameters). R_1/wR_2 [I > 2σ(I)]: 0.0246 / 0.0596. R_1/wR_2 [all refl.]: 0.0264 / 0.0607. S = 1.072. Flack parameter[42] x = 0.588(10). Residual electron density between -0.39 and 0.82 e/Å^3.

3.5.12. Crystallographic data of Complex [Ni(pbsms)]

$C_{11}H_{22}NiS_4$, Fw = 341.24, green plates, 0.02 × 0.13 × 0.31 mm^3, monoclinic, *P21* (no. 4), a = 6.3677(4), b = 10.6954(8), c = 11.2505(6) Å, α = 90, β = 104.822(5), γ = 90 °, V = 740.72(8) Å^3, Z = 2, D_x = 1.530 g cm^{-3}, μ = 1.846 mm^{-1}. 12390 Reflections were measured up to a resolution of $(\sin\theta/\lambda)_{max}$ = 0.65 Å^{-1}. An absorption correction based on multiple measured reflections was applied (0.33–0.86 correction range). 2907 Reflections were unique (R_{int} = 0.052), of which 2907 were observed [$I > 2\sigma(I)$]. 149 Parameters were refined with no restraints. $R1/wR2$ [$I > 2\sigma(I)$]: 0.0203/0.0387. $R1/wR2$ [all refl.]: 0.0319/0.0413. S = 1.05. Residual electron density between −0.47 and 0.46 eÅ^{-3}.

3.6. References

1. S. Canaguier, V. Artero and M. Fontecave, *Dalton Trans.*, 2008, 315-325.
2. V. Artero and M. Fontecave, *Coord. Chem. Rev.*, 2005, **249**, 1518-1535.
3. E. Bouwman and J. Reedijk, *Coord. Chem. Rev.*, 2005, **249**, 1555-1581.
4. D. J. Evans and C. J. Pickett, *Chem. Soc. Rev.*, 2003, **32**, 268-275.
5. A. C. Marr, D. J. E. Spencer and M. Schröder, *Coord. Chem. Rev.*, 2001, **219**, 1055-1074.
6. C. A. Grapperhaus and M. Y. Darensbourg, *Acc. Chem. Res.*, 1998, **31**, 451-459.
7. V. E. Kaasjager, E. Bouwman, S. Gorter, J. Reedijk, C. A. Grapperhaus, J. H. Reibenspies, J. J. Smee, M. Y. Darensbourg, A. Derecskei-Kovacs and L. M. Thomson, *Inorg. Chem.*, 2002, **41**, 1837-1844.
8. Q. Wang, A. C. Marr, A. J. Blake, C. Wilson and M. Schröder, *Chem. Commun.*, 2003, 2776-2777.
9. T. Kruger, B. Krebs and G. Henkel, *Angew. Chem.-Int. Edit. Engl.*, 1992, **31**, 54-56.
10. M. L. Golden, M. V. Rampersad, J. H. Reibenspies and M. Y. Darensbourg, *Chem. Commun.*, 2003, 1824-1825.
11. M. L. Golden, C. M. Whaley, M. V. Rampersad, J. H. Reibenspies, R. D. Hancock and M. Y. Darensbourg, *Inorg. Chem.*, 2005, **44**, 875-883.

12. S. P. Jeffery, K. N. Green, M. V. Rampersad, J. H. Reibenspies and M. Y. Darensbourg, *Dalton. Trans.*, 2006, 4244-4252.
13. S. P. Jeffery, M. L. Singleton, J. H. Reibenspies and M. Y. Darensbourg, *Inorg. Chem.*, 2007, **46**, 179-185.
14. K. N. Green, S. M. Brothers, B. Lee, M. Y. Darensbourg and D. A. Rockcliffe, *Inorg. Chem.*, 2009, **48**, 2780-2792.
15. A. J. Amoroso, S. S. M. Chung, D. J. E. Spencer, J. P. Danks, M. W. Glenny, A. J. Blake, P. A. Cooke, C. Wilson and M. Schröder, *Chem. Commun.*, 2003, 2020-2021.
16. W. F. Zhu, A. C. Marr, Q. Wang, F. Neese, D. J. E. Spencer, A. J. Blake, P. A. Cooke, C. Wilson and M. Schröder, *Proc. Natl. Acad. Sci. U. S. A.*, 2005, **102**, 18280-18285.
17. Y. Ohki, K. Yasumura, K. Kuge, S. Tanino, M. Ando, Z. Li and K. Tatsumi, *Proc. Natl. Acad. Sci. U. S. A.*, 2008, **105**, 7652-7657.
18. J. A. W. Verhagen, C. Tock, M. Lutz, A. L. Spek and E. Bouwman, *Eur. J. Inorg. Chem.*, 2006, 4800-4808.
19. J. A. W. Verhagen, M. Beretta, A. L. Spek and E. Bouwman, *Inorg. Chim. Acta*, 2004, **357**, 2687-2693.
20. J. A. W. Verhagen, M. Lutz, A. L. Spek and E. Bouwman, *Eur. J. Inorg. Chem.*, 2003, 3968-3974.
21. R. Krishnan and C. G. Riordan, *J. Am. Chem. Soc.*, 2004, **126**, 4484-4485.
22. R. Krishnan, J. K. Voo, C. G. Riordan, L. Zahkarov and A. L. Rheingold, *J. Am. Chem. Soc.*, 2003, **125**, 4422-4423.
23. R. C. Linck, C. W. Spahn, T. B. Rauchfuss and S. R. Wilson, *J. Am. Chem. Soc.*, 2003, **125**, 8700-8701.
24. A. Perra, E. S. Davies, J. R. Hyde, Q. Wang, J. McMaster and M. Schröder, *Chem. Commun.*, 2006, 1103-1105.
25. Q. Wang, A. J. Blake, E. S. Davies, E. J. L. McInnes, C. Wilson and M. Schröder, *Chem. Commun.*, 2003, 3012-3013.
26. F. Lauderbach, R. Prakash, A. W. Götz, M. Munoz, F. W. Heinemann, U. Nickel, B. A. Hess and D. Sellmann, *Eur. J. Inorg. Chem.*, 2007, 3385-3393.
27. D. Sellmann, F. Lauderbach, F. Geipel, F. W. Heinemann and M. Moll, *Angew. Chem., Int. Ed. Engl.*, 2004, **43**, 3141-3144.
28. B. E. Barton, C. M. Whaley, T. B. Rauchfuss and D. L. Gray, *J. Am. Chem. Soc.*, 2009, **131**, 6942-6943.
29. C. Tard and C. J. Pickett, *Chem. Rev.*, 2009, **109**, 2245-2274.
30. Y. Oudart, V. Artero, J. Pecaut, C. Lebrun and M. Fontecave, *Eur. J. Inorg. Chem.*, 2007, 2613-2626.
31. Y. Oudart, V. Artero, J. Pecaut and M. Fontecave, *Inorg. Chem.*, 2006, **45**, 4334-4336.
32. V. Artero and M. Fontecave, *C. R. Chim.*, 2008, **11**, 926-931.
33. J. A. W. Verhagen, D. D. Ellis, M. Lutz, A. L. Spek and E. Bouwman, *J. Chem. Soc.-Dalton Trans.*, 2002, 1275-1280.
34. F. Osterloh, W. Saak and S. Pohl, *J. Am. Chem. Soc.*, 1997, **119**, 5648-5656.
35. C. Zhang, S. Takada, M. Kölzer, T. Matsumoto and K. Tatsumi, *Angew. Chem.-Int. Edit. Engl.*, 2006, **45**, 3768-3772.
36. R. Angamuthu, H. Kooijman, M. Lutz, A. L. Spek and E. Bouwman, *Dalton Trans.*, 2007, 4641-4643.
37. T. Yamamura, H. Arai, N. Nakamura and H. Miyamae, *Chem. Lett.*, 1990, 2121-2124.
38. M. A. Halcrow and G. Christou, *Chem. Rev.*, 1994, **94**, 2421-2481.
39. D. Sellmann, D. Haussinger and F. W. Heinemann, *Eur. J. Inorg. Chem.*, 1999, 1715-1725.
40. G. A. N. Felton, A. K. Vannucci, J. Z. Chen, L. T. Lockett, N. Okumura, B. J. Petro, U. I. Zakai, D. H. Evans, R. S. Glass and D. L. Lichtenberger, *J. Am. Chem. Soc.*, 2007, **129**, 12521-12530.
41. V. Guyon, A. Guy, J. Foos, M. Lemaire and M. Draye, *Tetrahedron*, 1995, **51**, 4065-4074.
42. H. D. Flack, *Acta Crystallogr. Sect. A*, 1983, **39**, 876-881.

4

Synthesis, Characterization and Electrocatalytic Properties of $[Ni(S_4)Fe(C_5H_5)(CO)](PF_6)$ Complexes Containing Bidentate SS'-donor Ligands†

Abstract. Five bidentate chelating SS'-donor ligands – abbreviated as Hbsms, Hmpsms, Hcpsms, Hibsms and Hnhsms – have been synthesized that differ in electronic properties. These ligands have been reacted with $[Ni(acac)_2]$ (acac = acetylacetonate) and the low-spin nickel complexes of general formula $[Ni(SS')_2]$ have been obtained. Reaction of these low-spin nickel complexes with $[Fe(C_5H_5)(CO)_2I]$ (C_5H_5 = cyclopentadienyl) and anion exchange with NH_4PF_6 yielded five new [NiFe] complexes of general formula $[Ni(SS')_2Fe(C_5H_5)(CO)](PF_6)$. All the nickel and [NiFe] complexes have been characterized using ESI-MS spectrometry, electronic absorption and IR spectroscopy, and cyclic voltammetric techniques. The X-ray structure of the nickel complex with the ligand Hcpsms is reported; the compound crystallizes as the trimer $[Ni_3(cpsms)_6]$ with two different NiS_4 coordination environments as four of the six ligands bind as monodentate and the remaining two bind as chelating bidentate ligands. Three of the five [NiFe] complexes show electrocatalytic activity to produce dihydrogen in the presence of acetic acid. Catalytic reduction of H^+ is found to occur at potentials as low as –0.9 V *vs*. Ag/AgCl for $[Ni(mpsms)_2Fe(C_5H_5)(CO)](PF_6)$, $[Ni(ibsms)_2Fe(C_5H_5)(CO)](PF_6)$ and $[Ni(nhsms)_2Fe(C_5H_5)(CO)](PF_6)$ in acetonitrile. It is thus concluded that increased flexibility in the S_4 coordination sphere of the nickel(II) ion favors the lower overpotentials. The thioether donors of the chelating bidentate ligands are more readily protonated than in the chelating tetradentate ligands reported in Chapter **3**; this leads to the rapid decomposition of the complexes $[Ni(bsms)_2Fe(C_5H_5)(CO)](PF_6)$ and $[Ni(cpsms)_2Fe(C_5H_5)(CO)](PF_6)$.

---

† This chapter is based on: R. Angamuthu, M. A. Siegler, A. L. Spek and E. Bouwman, *manuscript in preparation*.

4.1. Introduction

The [NiFe] complexes of $S_2S'_2$-donor tetradentate ligands reported in Chapter **3** are electrocatalytically reducing protons at potentials in the range of –1.74 to –1.19 V *vs*. Ag/AgCl. It was found that the potential at which proton reduction occurs is shifted positively upon increasing the flexibility of the ligands. Furthermore, the [NiFe] complexes $[Ni(bsms)_2Fe(CO)_2I_2]$ (E_{pc} = –0.8 V *vs*. Ag/AgCl), $[Ni(bss)_2Fe(CO)_2I_2]$ (E_{pc} = –0.92 V *vs*. Ag/AgCl) and $[Ni(bsms)_2FeI_2]_2$ (E_{pc} = –0.79 V *vs*. Ag/AgCl) containing bidentate ligands (Fig. 4.2), synthesized by Bouwman and coworkers exhibit less negative reduction potentials compared to the [NiFe] complexes reported in Chapter **3**.[1] Hence, the bidentate SS'-donor ligands, of which the synthesis is described in Chapter **2,** have been used in the synthesis of [NiFe] complexes in order to evaluate the effect of the increased flexibility in these new complexes on their proton reduction capability.

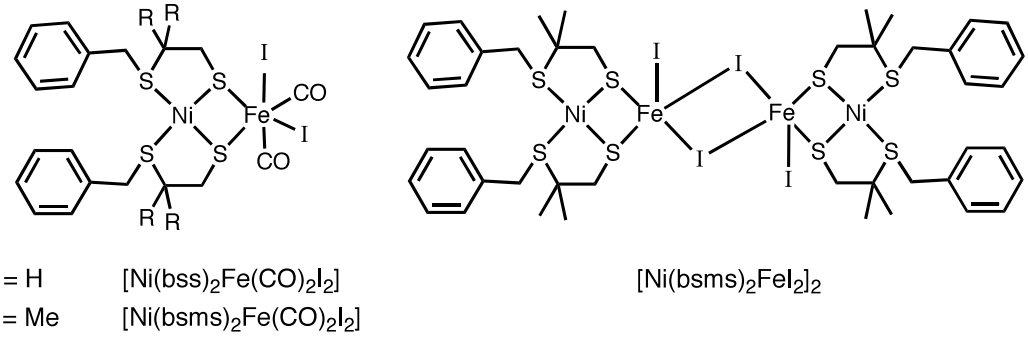

Fig. 4.1. Schematic representations of the complexes synthesized by Bouwman and coworkers.[1]

A number of nickel complexes are known to have bidentate S_2- and PS-donor ligands[1-15], these ligands mostly tend to produce either tetrahedral $[Ni(SS)_2]^-$ mononuclear, or oligonuclear complexes. This Chapter deals with the syntheses and characterizations of four new $[Ni(SS')_2]$ complexes of the bidentate SS'-donor ligands Hmpsms, Hcpsms, Hibsms and Hnhsms (Fig. 4.2). Also, the syntheses, characterizations and electrocatalytic properties of five new complexes of general formula $[Ni(SS')_2Fe(C_5H_5)(CO)](PF_6)$ are discussed.

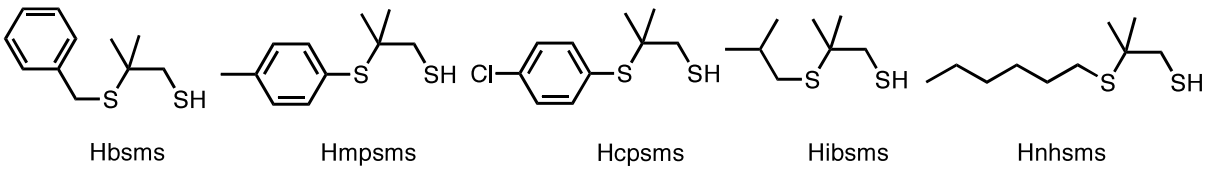

Fig. 4.2. Bidentate chelating ligands used in the present study (see Chapter-**2**, section 2.2 for the abbreviation of the names of ligands).

4.2. Results

4.2.1. Synthesis

The syntheses of ligand precursor thiouronium salts are discussed in detail in Chapter **2**. The low-spin square-planar $[Ni(SS')_2]$ complexes are synthesized by the reaction of $Ni(acac)_2$ with two equivalents of the thiouronium chloride salt of the ligands, in the presence of two equivalents of tetramethylammonium hydroxide. Even though these complexes could be synthesized in protic solvents, such as ethanol in relatively high yields, using toluene as the solvent leads to further improvement. The complexes $[Ni(bsms)_2]$ (shiny brick-red crystalline)[12] and $[Ni(mpsms)_2]$ (dark brown microcrystalline) are very stable as solid and in solution under air, whereas the complexes $[Ni(cpsms)_2]$, $[Ni(ibsms)_2]$, and $[Ni(nhsms)_2]$ are slightly hygroscopic in air, but stable in an argon atmosphere for months. The syntheses of nickel(II) complexes of the unsubstituted ligands Hcpss and Hmpss yielded the hexanuclear $[Ni_6(cpss)_{12}]$ metallacrown and an insoluble brick-red precipitate, respectively. The synthesis, structure and electrocatalytic properties of the hexanuclear complex $[Ni_6(cpss)_{12}]$ has been studied in detail and will be reported in Chapter **6**.

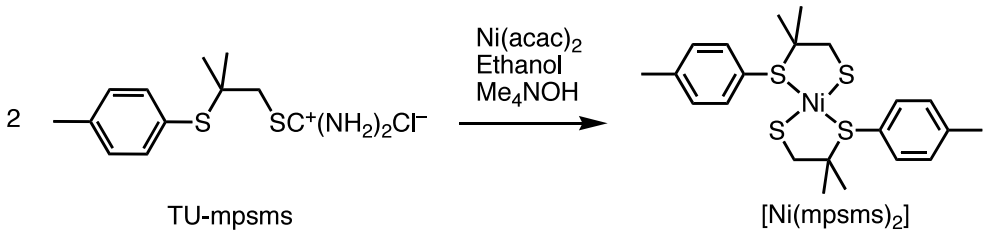

Fig. 4.3. Illustrative synthetic route used in the synthesis of $[Ni(SS')_2]$ complexes.

The [NiFe] complexes were synthesized following the same procedure as reported in Chapter **3** for the tetradentate ligands. All five nickel complexes reported in this chapter have been reacted with $[Fe(C_5H_5)(CO)_2I]$ for 12 hours in order to form [NiFe] complexes of general formula $[Ni(SS')_2Fe(C_5H_5)(CO)]I$. Performing this initial step of the reaction in a closed argon atmosphere gives rise to a mixture of complexes analyzed as $[Ni(SS')_2Fe(C_5H_5)(CO)]^+$ and $[Ni(SS')_2Fe(C_5H_5)(CO)_2]^+$, as observed from the ESI-MS spectra, and eventually this mixture decomposes in air. To avoid the formation of this mixture, argon was purged into the solution throughout the reaction time and the evaporated dichloromethane was regularly replaced; this yielded relatively pure monocarbonyl derivatives, which are stable enough to be manipulated in air for weighing and transferring. The iodide anions are exchanged with PF_6^- anions using an exact stoichiometric amount of NH_4PF_6. The formed ammonium iodide and any unwanted

precipitates are removed by passing the solution through a Celite column. The analytically pure [NiFe] complexes are obtained as their PF_6 salts, by passing the acetonitrile solutions of the complexes through a neutral alumina column.

4.2.2. Molecular Structure of the [Ni(SS')$_2$] Complexes

The molecular structure of the complex [Ni(bsms)$_2$] has been reported by Bouwman and coworkers.[12] Single crystals suitable for X-ray diffraction were obtained for [Ni(mpsms)$_2$]$_3$. The complex [Ni(cpsms)$_2$]$_3$ crystallizes in the space group C2/c; the asymmetric unit contains one crystallographically independent ordered molecule and a molecule of dichloromethane. Even though the complex of nickel(II) with the ligand Hcpsms is observed to be monomeric in solution, the X-ray crystal determination revealed a linear trinuclear [Ni$_3$(cpsms)$_6$] molecule, containing three square-planar NiS_4 units joined by edge sharing, in which only two of the ligands are chelating and the remaining four are coordinating as monodentate via the thiolate sulfur (Fig. 4.4). The observed structural reorganization may be caused by the protic solvent (ethanol) used in the crystallization process. The coordination environments of the two terminal NiS_4 units differ from the central NiS_4 unit. The terminal nickel(II) centers (Ni2, Ni3) are coordinated by a chelating ligand and two μ-S thiolate donors of two monodentate ligands, whereas the central nickel(II) ion Ni1 is coordinated to four μ-S thiolate donors.

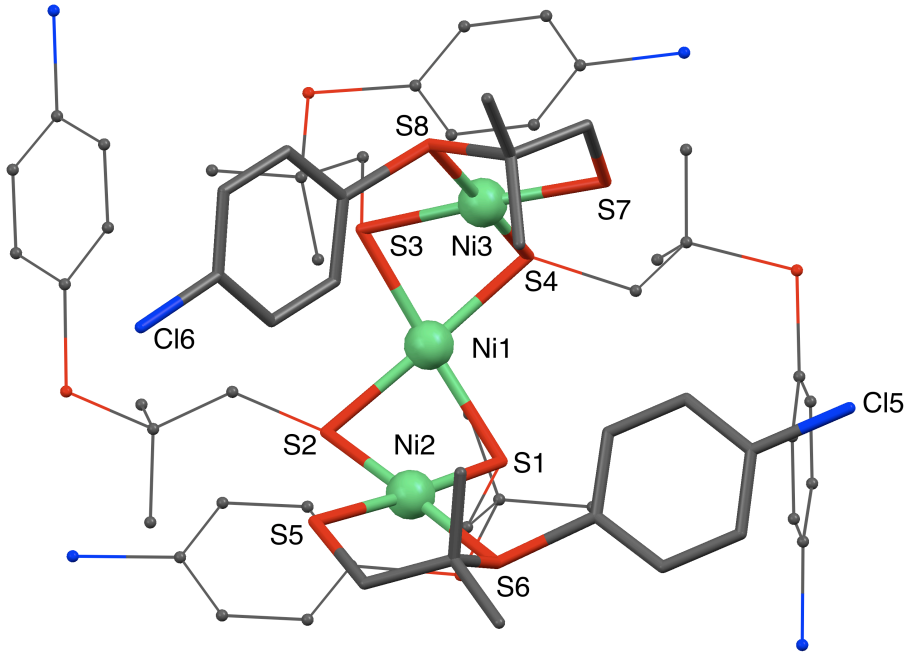

Fig. 4.4. Perspective view of [Ni$_3$(cpsms)$_6$]. Ni, green; S, red, C, gray, Cl, blue. Chelating ligands shown in capped stick model, monodentate ligands shown in minimized ball and stick model for the sake of clarity. Dichloromethane and hydrogen atoms have been omitted for clarity. Ni1···Ni2, 2.9104(6) Å; Ni1···Ni3, 2.8774(7) Å; Ni2···Ni3, 4.8856(7) Å. Further details are provided in Table 4.1

The two Ni–$S_{thiolate}$ distances (2.1655(11), 2.1670(12) Å) of the chelating ligands are shorter than (or equal to) the two Ni–$S_{thioether}$ distances (2.1647(10), 2.1700(11) Å), as expected. These two Ni–$S_{thiolate}$ distances are shorter than those of the bridging monodentate ligands (2.1751(9)–2.2388(9) Å). Owing to the geometrical restrictions introduced by the thiolate and thioether donors, the NiS_4 units are not strictly planar; the nickel ions Ni1, Ni2 and Ni3 are 0.069, 0.035 and 0.030 Å above their corresponding S_4 planes, respectively. The central NiS_4 basal plane has a considerably high degree of tetrahedral distortion with a dihedral angle of 13.74° (between the planes S1–Ni1–S2 and S3–Ni1–S4), whereas smaller dihedral angles of 3.68° for Ni2 (between the planes S1–Ni2–S2 and S5–Ni2–S6) and 3.07° for Ni3 (between the planes S3–Ni3–S4 and S7–Ni3–S8) are observed. The S–Ni–S *cis* bond angles range from 80.31(4) to 100.07(4).

The X-ray crystal structure of $[Ni(bsms)_2]$ has been reported in literature and revealed a perfectly planar mononuclear structure – due to the inversion center at the nickel ion – comprising the two thiolate donors and two thioether donors coordinated to the nickel(II) center in *trans* positions.[12] The X-ray crystal structure of a derivative of the complex $[Ni(mpsms)_2]$ has been reported recently and is discussed in detail in Chapter **7**. This compound contains two $[Ni(mpsms)_2]$ units bridged together *via* six CuI units in which each $[Ni(mpsms)_2]$ unit has two thiolate donors and two thioether donors coordinated to the nickel(II) center in enforced *cis* positions.[16]

Table 4.1. Selected distances (Å) and angles (°) for $[Ni_3(cpsms)_6]$.

Ni1–S1	2.2233(10)	Ni2–S1	2.2388(9)	Ni3–S3	2.2353(11)
Ni1–S2	2.1897(10)	Ni2–S2	2.1827(10)	Ni3–S4	2.1751(9)
Ni1–S3	2.2269(11)	Ni2–S5	2.1655(11)	Ni3–S7	2.1670(12)
Ni1–S4	2.1931(10)	Ni2–S6	2.1647(10)	Ni3–S8	2.1700(11)
S1–Ni1–S2	81.51(4)	S1–Ni2–S2	81.31(3)	S3–Ni3–S4	80.76(4)
S1–Ni1–S3	168.05(4)	S1–Ni2–S5	175.09(4)	S3–Ni3–S7	174.96(4)
S1–Ni1–S4	100.07(4)	S1–Ni2–S6	96.15(4)	S3–Ni3–S8	95.75(4)
S2–Ni1–S3	98.89(4)	S2–Ni2–S5	93.78(4)	S4–Ni3–S7	94.20(4)
S2–Ni1–S4	175.04(4)	S2–Ni2–S6	175.53(4)	S4–Ni3–S8	175.36(4)
S3–Ni1–S4	80.56(4)	S5–Ni2–S6	88.76(4)	S7–Ni3–S8	89.28(4)
Ni1–S1–Ni2	81.42(3)	Ni1–S2–Ni2	83.46(4)		
Ni1–S3–Ni3	80.31(4)	Ni1–S4–Ni3	82.40(3)		

4.2.3. Electronic, NMR and ESI-MS Spectra of the Nickel Complexes

The electronic spectra of the nickel(II) complexes have been recorded in chloroform solutions (Table 4.2). All the five nickel complexes exhibit two characteristic bands between 14000 cm^{-1} ($^1E' \leftarrow {}^1A_1'$) and 24000 cm^{-1} ($^1E'' \leftarrow {}^1A_1'$) due to d←d transitions, consistent with the square-planar geometry expected for an NiS_4 chromophore. The absorption maxima of these complexes are at slightly higher energies

compared to those of the [Ni($S_2S'_2$)] complexes reported in Chapter **3**; this may be caused by the *trans* location of the thiolates and the freedom of having perfect square-planarity, as observed in the X-ray crystal structure of [Ni(bsms)$_2$].[12] Furthermore, the bands observed around 19000 and 24000 cm^{-1} for the [Ni($S_2S'_2$)] complexes are located around 21000 and 28000 cm^{-1}, respectively, for the nickel complexes of the bidentate ligands. The absorption maxima of [Ni(cpsms)$_2$] are shifted to slightly lower energy than those of [Ni(mpsms)$_2$] due to the electron-withdrawing *p*-chlorophenyl ring in [Ni(cpsms)$_2$].

Table 4.2. Electronic absorption maxima for the nickel complexes measured in chloroform and the *m/z* values of the parent molecular ion peaks observed in ESI-MS.

Complex	$\nu/10^3$ cm^{-1} (ε/mol^{-1} l cm^{-1})						*m/z* of [M+H$^+$] exptl. (calcd.)
[Ni(bsms)$_2$]	14.4 (96)	22.0 (360)	28.2 (6600)	33.6 (12900)	38.1 (15000)		480.78 (481.07)
[Ni(mpsms)$_2$]	14.8 (47)	21.4 (230)	29.4 (6500)	33.9 (11600)	36.6 (13800)		480.80 (481.07)
[Ni(cpsms)$_2$]	14.8 (39)	20.1 (281)	28.6 (1514)	33.6 (5300)	37.5 (6900)		520.75 (520.96)
[Ni(ibsms)$_2$]	14.5 (25)	21.1 (121)	28.6 (3900)	33.0 (5800)	35.6 (6500)	39.1 (6700)	412.93 (413.10)
[Ni(nhsms)$_2$]	14.8 (46)	20.3 (570)	28.6 (4500)	33.0 (5900)	35.6 (6800)	39.1 (7760)	468.98 (469.16)

The room temperature ^{1}H NMR spectra of the complexes [Ni(mpsms)$_2$], [Ni(cpsms)$_2$] and [Ni(nhsms)$_2$] show relatively sharp signals compared to the complexes [Ni(ibsms)$_2$] and [Ni(bsms)$_2$]. This is probably due to the interesting fact that the *ortho*-protons of the 4-methylphenyl and 4-chlorophenyl rings of the complexes [Ni(mpsms)$_2$] and [Ni(cpsms)$_2$], respectively, interact with the axial positions of the nickel(II) ion. This is evident from the broad signal observed at around 8 ppm in the ^{1}H NMR spectra of the complexes [Ni(mpsms)$_2$] and [Ni(cpsms)$_2$] at 303 K. This interesting phenomenon is also observed in the derived cluster compound [{Ni(mpsms)$_2$}(CuI)$_6$], both in the solid-state structure (Ni···H = 2.626 to 2.781 Å) and in solution (7.8 ppm at 303 K, 9.5 ppm at 183 K), as studied by variable temperature ^{1}H NMR spectroscopy. The sharp signals observed in the case of [Ni(nhsms)$_2$] can be explained by the fact that the relatively long *n*-hexyl groups may restrict the fast *cis*-*trans* isomerisation. More detailed NMR studies including variable temperature and 2D NMR techniques are necessary to shed light into these interesting phenomena in solution.

ESI-MS spectra of all the complexes were obtained from dichloromethane solutions containing trace amounts of acetic acid. Despite the fact that the complex [Ni(cpsms)$_2$] exhibits a trinuclear structure in the solid state, in all the cases the

$[Ni(SS')_2+H]^+$ molecular ion peaks were observed, perfectly matching with calculated isotopic distributions.

Table 4.3. Electrochemical data of the $[Ni(SS')_2]$ complexes obtained for 1 mM solutions in dichloromethane containing 0.1 M $(NBu_4)PF_6$. Scan rate 200 mV s^{-1}. Static GC disc working electrode, Pt wire counter electrodes with a Ag/AgCl (satd. KCl) reference electrode.

Complex	E_{pa}(V)	E_{pc}(V)
$[Ni(bsms)_2]$	0.63	
	−0.35	
		−0.83
$[Ni(mpsms)_2]$	0.62	
	−0.31	
		−0.80
$[Ni(cpsms)_2]$	0.73	
		−0.61
$[Ni(ibsms)_2]$	0.61	
	−0.37	
	−0.50	
		−0.79
$[Ni(nhsms)_2]$	0.58	
	−0.38	
	−0.53	
		−0.84

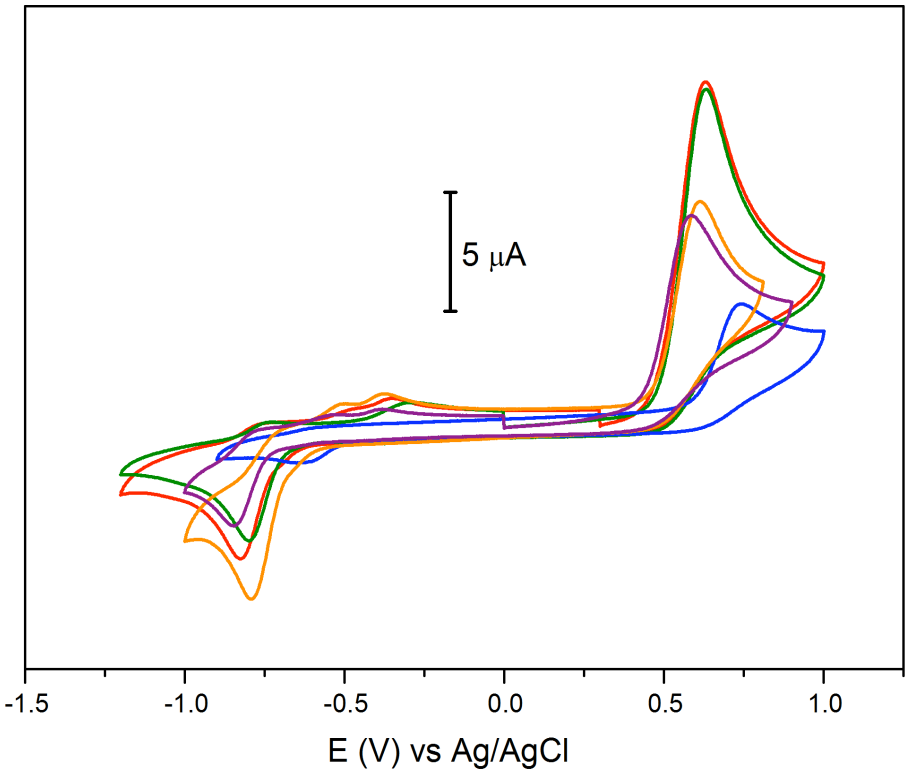

Fig. 4.5. Cyclic voltammograms of $[Ni(bsms)_2]$ (red), $[Ni(mpsms)_2]$ (green), $[Ni(cpsms)_2]$ (blue), $[Ni(ibsms)_2]$ (orange) and $[Ni(nhsms)_2]$ (purple); see Table 4.3 for more details.

4.2.4. Electrochemical Behaviour of the Nickel Complexes

The electrochemical properties of the $[Ni(SS')_2]$ complexes were investigated (Fig. 4.5) using cyclic voltammetry; the relevant data are presented in Table 4.3. At a scan rate of 200 mV s^{-1} only irreversible oxidations of the complexes are observed at potentials ranging between 0.58 and 0.73 V *vs*. Ag/AgCl (Table 4.5), which are comparable to the $[Ni(S_2S'_2)]$ complexes reported in Chapter **3**. The oxidation potential of $[Ni(cpsms)_2]$ is 0.11 V higher than that of $[Ni(mpsms)_2]$ due to the electron-withdrawing *p*-chlorophenyl ring in $[Ni(cpsms)_2]$. This trend is also reflected in the reduction potentials of the complexes $[Ni(mpsms)_2]$ and $[Ni(cpsms)_2]$; the complex $[Ni(cpsms)_2]$ (–0.61 V *vs*. Ag/AgCl) is more readily reduced than the complex $[Ni(mpsms)_2]$ (–0.80 V *vs*. Ag/AgCl).

4.2.5. ESI-MS, FTIR and Electronic Spectra of the [NiFe] Complexes

The characterization of the [NiFe] complexes using ESI-MS spectrometry was performed using freshly prepared acetonitrile solutions. In all the cases molecular ion and fragmentation peaks in agreement with the formulations $[Ni(SS')_2Fe(C_5H_5)(CO)]^+$, $[Ni(SS')_2Fe(C_5H_5)]^+$ and $[Ni(SS')_2Fe]^+$ were observed. The calculated and observed *m/z* values of the fragment $[Ni(SS')_2Fe(C_5H_5)(CO)]^+$ are provided in Table 4.4 along with the observed carbonyl stretching frequencies.

The carbonyl stretching frequencies of the [NiFe] complexes appear at slightly higher energies than that of the [NiFe] complexes of the tetradentate $S_2S'_2$-donor ligands reported in Chapter **3**, suggesting that iron(II) ions possess relatively less electron density in $[Ni(SS')_2Fe(C_5H_5)(CO)](PF_6)$ complexes. This is probably due to the global electron-withdrawing effect of the aromatic groups attached to the thioether sulfurs.

The ^1H NMR spectra of the $[Ni(SS')_2Fe(C_5H_5)(CO)](PF_6)$ complexes in dichloromethane exhibit broad signals, similar to the $[Ni(S_2S'_2)Fe(C_5H_5)(CO)](PF_6)$ complexes. Hence, the NMR spectroscopic data of he [NiFe] complexes are not helpful in the description of the solution structures and are not further discussed.

The UV-VIS spectra of the [NiFe] complexes have been recorded in acetonitrile and the relevant data are reported in Table 4.5. The d←d bands of the NiS_4 moiety shift to lower energy in the $[Ni(SS')_2Fe(C_5H_5)(CO)](PF_6)$ complexes compared to the corresponding mononuclear nickel complexes, which is in contrast to the $[Ni(S_2S'_2)Fe(C_5H_5)(CO)](PF_6)$ complexes. A number of higher energy bands corresponding to π-π* transitions of the Cp^- ring are observed between 28000 cm^{-1} and 44000 cm^{-1}.

Table 4.4. Comparison of the carbonyl IR stretching frequencies of the [NiFe] complexes in dichloromethane and the observed *m/z* values of the parent molecular ion peaks $[Ni(SS')_2Fe(C_5H_5)(CO)]^+$ in ESI-MS.

Complex	ν(CO)			ν(PF_6^-)	m/z exptl. (calcd.)
$[Ni(bsms)_2Fe(C_5H_5)(CO](PF_6)$	2051,	2042,	1998	847	628.72 (629.03)
$[Ni(mpsms)_2Fe(C_5H_5)(CO](PF_6)$	2055,	2046,	2001	847	628.76 (629.03)
$[Ni(cpsms)_2Fe(C_5H_5)(CO](PF_6)$	2055,	2042,	1998	848	668.60 (668.92)
$[Ni(ibsms)_2Fe(C_5H_5)(CO](PF_6)$		2042,	1998	846	560.79 (561.06)
$[Ni(nhsms)_2Fe(C_5H_5)(CO](PF_6)$		2042,	1998	848	616.94 (617.12)

Table 4.5. Electronic absorption maxima for the $[Ni(SS')_2Fe(C_5H_5)(CO)](PF_6)$ complexes in acetonitrile solutions.

Complex	$\nu/10^3$ cm^{-1} (ε/mol^{-1} l cm^{-1})					
$[Ni(bsms)_2Fe(C_5H_5)(CO](PF_6)$	13.6 (91)	19.6 (sh)	26.0 (3100)	33.2 (9000)	37.9 (sh)	40.1 (sh)
$[Ni(mpsms)_2Fe(C_5H_5)(CO](PF_6)$	14.8 (106)	19.8 (sh)	26.0 (sh)	33.4 (11.6)	38.8 (sh)	44.4 (40.4)
$[Ni(cpsms)_2Fe(C_5H_5)(CO](PF_6)$	14.8 (39)	19.6 (281)		33.6 (5300)	38.8 (6900)	44.4 (30.3)
$[Ni(ibsms)_2Fe(C_5H_5)(CO](PF_6)$	13.6 (88)	19.6 (sh)	25.6 (sh)	33.3 (9000)	41.2 (13800)	44.6 (sh)
$[Ni(nhsms)_2Fe(C_5H_5)(CO](PF_6)$	13.6 (116)	19.5 (sh)	25.9 (4600)	33.6 (12700)	38.0 (13700)	39.1 (sh)

4.2.6. Electrochemical Behaviour of the [NiFe] Complexes and Reduction of Protons

The electrochemical behavior of the [NiFe] complexes in acetonitrile was investigated using cyclic voltammetry. For all the five [NiFe] complexes several quasi-reversible and irreversible redox couples are observed (Table 4.6). As an example, the CV of the complex $[Ni(ibsms)_2Fe(C_5H_5)(CO)](PF_6)$ is shown in Fig. 4.6. In all the five [NiFe] complexes, an irreversible anodic peak is observed around 0.5 V vs Ag/AgCl corresponding to the oxidation of the nickel(II) ion to nickel(III). An irreversible reduction is observed around –1 V *vs*. Ag/AgCl, except for the complex $[Ni(cpsms)_2Fe(C_5H_5)(CO)](PF_6)$ which exhibits a reduction wave at –0.58 V *vs*. Ag/AgCl. Unfortunately, the observed oxidations and reductions cannot be unequivocally assigned, due to the presence of multiple redox-active partners in the [NiFe] complexes, and the redox changes may be distributed among the redox-active members of the [NiFe] complexes.[17]

Table 4.6. Electrochemical data of $[Ni(SS')_2Fe(C_5H_5)(CO)](PF_6)$ complexes (0.5 mM) in acetonitrile.*

Complex	E_{pa}(V)	E_{pc}(V)	E_{HER}(V)#
$[Ni(bsms)_2Fe(C_5H_5)(CO)](PF_6)$	0.99		
	0.50		
	0.33		
	−0.35		
		−0.93	
$[Ni(mpsms)_2Fe(C_5H_5)(CO)](PF_6)$	0.45		
		−0.95	−0.93
$[Ni(cpsms)_2Fe(C_5H_5)(CO)](PF_6)$	1.05		
	0.64		
		−0.58	
$[Ni(ibsms)_2Fe(C_5H_5)(CO)](PF_6)$	0.47		
		−1.04	−0.92
$[Ni(nhsms)_2Fe(C_5H_5)(CO)](PF_6)$	0.47		
	0.26		
		−0.64	
		−1.11	−0.94

* Measured vs. Ag/AgCl reference electrode; Static glassy carbon disc working electrode; Pt-wire counter electrode; Scan rate 200 mV s^{-1}; Supporting electrolyte 0.05 M Bu_4NPF_6.

\# E_{HER}: potential at which hydrogen evolution reaction occurs.

The electrocatalytic properties of all the five [NiFe] complexes were investigated by means of the reduction of protons using acetic acid as a relatively mild source of protons. A new irreversible cathodic wave, corresponding to the reduction of protons with concurrent evolution of dihydrogen gas, appears in the cyclic voltammograms of the [NiFe] complexes in the presence of acetic acid, which rises in height upon increasing concentrations of acetic acid (Fig. 4.6) for the complexes $[Ni(mpsms)_2Fe(C_5H_5)(CO)](PF_6)$, $[Ni(ibsms)_2Fe(C_5H_5)(CO)](PF_6)$ and $[Ni(nhsms)_2Fe(C_5H_5)(CO)](PF_6)$. The potential at which proton reduction occurs lies around −0.9 V *vs*. Ag/AgCl. These proton reduction potentials (E_{HER}) are less negative than those observed for the $[Ni(S_2S'_2)Fe(C_5H_5)(CO)](PF_6)$ complexes with tetradentate ligands, as was expected. Unlike the $[Ni(S_2S'_2)Fe(C_5H_5)(CO)](PF_6)$ complexes reported in Chapter **3**, the electrocatalytic waves appeared slightly lower than the reduction potentials of the $[Ni(S_2S'_2)Fe(C_5H_5)(CO)](PF_6)$ complexes with a slight increase in the height of the oxidation waves. This is probably due to the protonation of the thioether sulfurs prior to the reduction making the $[Ni(S_2S'_2)Fe(C_5H_5)(CO)](PF_6)$ complexes easily reducible and more active than the $[Ni(S_2S'_2)Fe(C_5H_5)(CO)](PF_6)$ complexes.[18-20] This hypothesis is also supported by the observed increase in the current of the reduction wave in the range of −0.6 to −0.8 V *vs*. Ag/AgCl, before the electrocatalytic wave begins to appear (Fig. 4.6). The complexes $[Ni(bsms)_2Fe(C_5H_5)(CO)](PF_6)$ and

$[Ni(cpsms)_2Fe(C_5H_5)(CO)](PF_6)$ are not stable in acidic solutions and eventually decompose with an accompanying change in color from brown to greenish yellow.

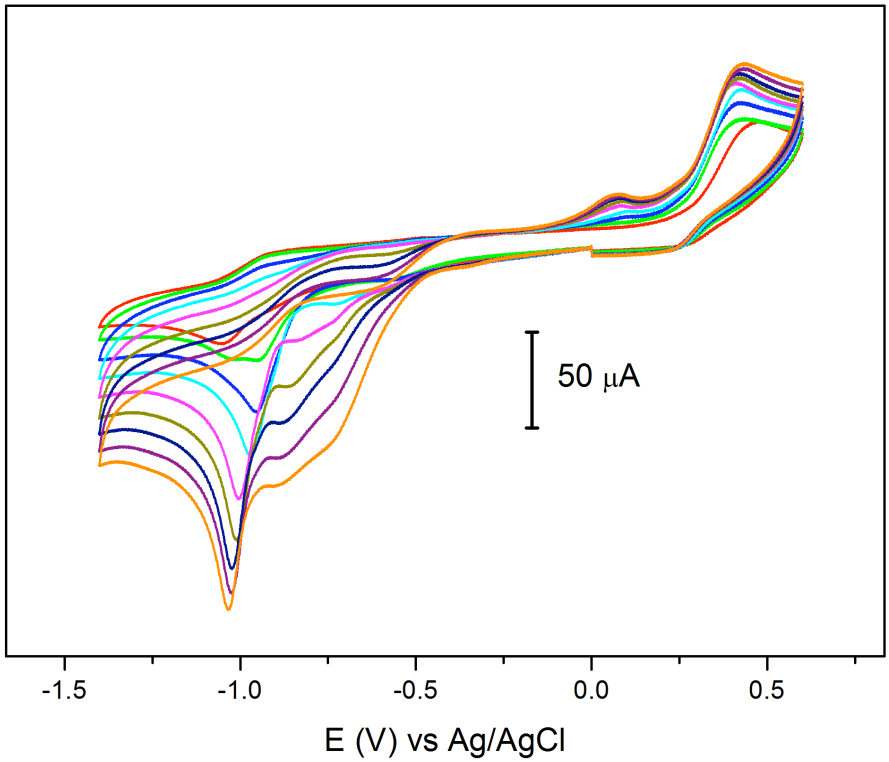

Fig. 4.6. Cyclic voltammograms of $[Ni(ibsms)_2Fe(C_5H_5)(CO)](PF_6)$ (0.5 mM) in acetonitrile in the presence of 0–16 equivalents of acetic acid; additions were made with increments of 2 equivalents. Further details are provided in Table 4.6.

4.3. Discussion

The new nickel(II) complexes of the bidentate ligands all are mononuclear in solution, as they all exhibit the $[Ni(SS')_2+H]^+$ peak as the parent molecular ion peak in the ESI-MS spectra. However, the complex of nickel(II) with the ligand Hcpsms crystallizes as a linear trinuclear molecule with two different NiS_4 coordination environments by utilizing the ligand $cpsms^-$ not only as a monodentate, but also as a chelating bidentate ligand. This may be due to the electron-withdrawing properties of the *p*-chlorophenyl group, reducing the coordination strength of the thioether sulfur, and predominating the electron-donating ability of the dimethyl substituents. The trimerization may also be ascribed to the use of the protic solvent used in the crystallization process (ethanol/hexane). The bidentate ligand Hcpss – the unsubstituted analog of the ligand Hcpsms –exhibits the same versatility in binding to the nickel(II) center as a monodentate and chelating bidentate ligand, as will be described in Chapter **6**.[19,21] However, the nickel(II) complex of the ligand Hcpss remains a hexanuclear molecule both in solid state

and in solution and the mononuclear compound [Ni(cpss)$_2$] is not observed in ESI-MS spectrometry.

The molecular structure of the nickel(II) complex [Ni(bsms)$_2$] is reported by Bouwman and coworkers to have a perfectly square-planar NiS$_4$ geometry.[1] The complex [Ni(mpsms)$_2$] yields a hetero-octaanuclear compound upon reacting with CuI in which the thiolate and thioether donors are bound to the nickel(II) ion in an enforced *cis* fashion on binding to the copper(I) ions (see Chapter **7**). Hence, it is evident that the five [Ni(SS')$_2$] complexes can have either *cis* or *trans* geometry according to the situation and most probably they all remain in the highly favored *trans* forms in the mononuclear complex in solution, or in a dynamic equilibrium of these two forms. The [NiFe] complexes formed with these five [Ni(SS')$_2$] complexes most likely have a structure similar to that reported for the complex [Ni(pbss)Fe(C$_5$H$_5$)(CO)](PF$_6$)[22] with a *cis* NiS$_4$ moiety bound to the [Fe(C$_5$H$_5$)(CO)]$^+$ group, as suggested by the available data.

The reduction potentials of the [Ni(SS')$_2$] complexes are found to be sensitive to the substituent groups on the thioether sulfur as observed from the cyclic voltammograms of the complexes (see section 0). Also, these reduction potentials are less negative compared to those of the [Ni(S$_2$S'$_2$)] complexes with the more rigid tetradentate ligands reported in Chapter **3**.

The complexes [Ni(bsms)$_2$Fe(C$_5$H$_5$)(CO)](PF$_6$) and [Ni(cpsms)$_2$Fe(C$_5$H$_5$)(CO)](PF$_6$) are not stable in the presence of protic acids and decompose immediately upon the addition of acids. This is probably due to the fact that the thioether donors are now highly prone to undergo protonation that may lead to decomposition.[19] However, the complexes [Ni(mpsms)$_2$Fe(C$_5$H$_5$)(CO)](PF$_6$), [Ni(ibsms)$_2$Fe(C$_5$H$_5$)(CO)](PF$_6$) and [Ni(nhsms)$_2$Fe(C$_5$H$_5$)(CO)](PF$_6$) are found to be active electrocatalysts in the reduction of protons into dihydrogen. Interestingly, the three active [Ni(SS')$_2$Fe(C$_5$H$_5$)(CO)](PF$_6$) complexes are able to reduce protons at less negative potentials, as compared to the [Ni(S$_2$S'$_2$)Fe(C$_5$H$_5$)(CO)](PF$_6$) complexes with tetradentate ligands as expected; most likely the increased flexibility of the NiS$_4$ coordination sphere might be responsible for this behavior. However, the E_{HER} does not seem to be affected by the electronic properties of the ligands in these complexes as they all work around –0.9 V *vs*. Ag/AgCl; it is possible that the flexibility of the ligands is predominant over the electronic properties of the ligands affecting the E_{HER}.

It appears – according to the available observations – that the [Ni(S$_2$S'$_2$)Fe(C$_5$H$_5$)(CO)](PF$_6$) complexes readily undergo protonation on the thioether sulfurs of the bidentate SS'-donor ligands; this protonation is advantageous, as this behavior assists in reducing the complexes easily; on the other hand it is disadvantageous

because it leads to the decomposition of the complexes $[Ni(bsms)_2Fe(C_5H_5)(CO)](PF_6)$ and $[Ni(cpsms)_2Fe(C_5H_5)(CO)](PF_6)$.

4.4. Conclusions

Four new $[Ni(SS')_2]$ complexes comprising bidentate SS'-donor ligands have been successfully synthesized. The ^1H NMR spectra of the complexes $[Ni(mpsms)_2]$ and $[Ni(cpsms)_2]$ reveal the presence of Ni···H anagostic interactions.[16] The $[Ni(SS')_2Fe(C_5H_5)(CO)](PF_6)$ complexes are more efficient electrocatalysts than the $[Ni(S_2S'_2)Fe(C_5H_5)(CO)](PF_6)$ complexes based on the tetradentate ligands described in Chapter 3, most likely due to the increased flexibility of the NiS_4 coordination spheres. However, two of the $[Ni(SS')_2Fe(C_5H_5)(CO)](PF_6)$ complexes are found to be less tolerant to the protic acids, since the thioether donors of these complexes are more readily protonated.[19] Hence, the next Chapter will be devoted to the study of a new class of [NiRu] complexes with the aim of making more stable and improved electrocatalysts.

4.5. Experimental Procedures

4.5.1. General Remarks

The synthesis of the ligand precursor thiouronium salts TU-cpsms, TU-mpsms, TU-ibsms, and TU-nhsms are described in Chapter **2** along with the characterizations. The mononuclear nickel complex $[Ni(bsms)_2]$ has been synthesized as reported in literature.[12] The complexes of general formula $[Ni(SS')_2Fe(C_5H_5)(CO)](PF_6)$ have been synthesized by slightly modifying the reported procedure.[22]

4.5.2. Synthesis of $[Ni(mpsms)_2]$

A two-necked round bottom flask was charged with $Ni(acac)_2$ (0.771 g, 3 mmol) and the thiouronium salt TU-mpsms (1.745 g, 6 mmol). To this 60 ml ethanol was added under argon atmosphere. After 10 minutes stirring at 60 °C, NMe_4OH (0.547 g, 6 mmol) was added to the green solution. After the immediate formation of a dark brown colour, the solution was refluxed for two hours, and then the reaction mixture was evaporated to dryness under reduced pressure. Dichloromethane was added to the residue and filtered through Celite until the filtrate was colourless, in order to remove the tetramethylammonium salt. The filtrate was concentrated to 1 ml before adding 100 ml hexane and the mixture was kept at 4 °C overnight. Analytically pure, dark-brown flocculent needles were collected by filtration and dried under vacuum (1.3 g, 91%). **^{1}H NMR:** δ_H [399.51 MHz, CD_2Cl_2, 303 K]) 7.92 (bs, 4H, phenyl–*ortho*–*H*), 7.52 (d, 4H, phenyl–*meta*–*H*), 2.36 (s, 6H, C*H*$_3$–Ph), 2.28 (s, 4H, –C*H*$_2$–S–), 1.28 (s, 12H, –C(C*H*$_3$)$_2$–). **Elemental Analysis (%):** calculated for $C_{22}H_{30}S_4Ni$, C 54.89, H 6.28, S 26.64, found,

C 55.17, H 6.66 S 24.55. **MS (ESI):** (*m/z*) calculated for $C_{22}H_{31}S_4Ni$ $[MH]^+$ requires 481.07, found 480.80.

4.5.3. Synthesis of [Ni(cpsms)$_2$]

The synthesis was carried out similar to that of [Ni(mpsms)$_2$]. Yield: 78%. **^{1}H NMR:** δ_H [399.51 MHz, CD_2Cl_2, 303 K]) 8.13 (bs, 4H, phenyl–*ortho–H*), 7.25 (d, 4H, phenyl–*meta–H*), 2.42 (s, 4H, –CH_2–S–), 1.37 (s, 12H, –C(CH_3)$_2$–). **Elemental Analysis (%):** calculated for $C_{20}H_{24}S_4NiCl_2$, C 46.00, H 4.63, S 24.56, found, C 45.17, H 4.56 S 24.15. **MS (ESI):** (*m/z*) calculated for $C_{20}H_{25}S_4NiCl_2$ $[MH]^+$ requires 520.96, found 520.75.

4.5.4. Synthesis of [Ni(ibsms)$_2$]

The synthesis was carried out similar to that of [Ni(mpsms)$_2$]. Yield: 63%. **Elemental Analysis (%):** calculated for $C_{16}H_{34}S_4Ni$, C 46.49, H 8.29, S 31.03, found, C 46.31.17, H 8.16 S 29.55. **MS (ESI):** (*m/z*) calculated for $C_{16}H_{35}S_4Ni$ $[MH]^+$ requires 413.10, found 412.93.

4.5.5. Synthesis of [Ni(nhsms)$_2$]

The synthesis was carried out similar to that of [Ni(mpsms)$_2$]. Yield: 72%. **^{1}H NMR:** δ_H [399.51 MHz, CD_2Cl_2, 303 K]) 3.11 (s, 4H, –S–C(CH_3)$_2$–CH_2–S–), 2.71 (t, 4H, CH_3–(CH_2)$_4$–CH_2–S–), 1.91 (p, 2H, CH_3–(CH_2)$_3$–CH_2–CH_2–S–), 1.58 (s, 6H, –S–C(CH_3)$_2$–CH_2–S–), 1.39 (m, 6H, CH_3–(CH_2)$_3$–(CH_2)$_2$–S–), 0.89 (t, 6H, CH_3–). **Elemental Analysis (%):** calculated for $C_{20}H_{42}S_4Ni$, C 51.16, H 9.02, S 27.32, found, C 52.17, H 9.36 S 26.55. **MS (ESI):** (*m/z*) calculated for $C_{20}H_{43}S_4Ni$ $[MH]^+$ requires 469.16, found 468.98.

4.5.6. Synthesis of [Ni(bsms)$_2$Fe(C_5H_5)CO](PF_6)

The synthesis was carried out by modifying the procedure described in the literature.[22] Yield 27%. **Elemental analysis:** Calcd (%) for $C_{28}H_{35}OS_4NiFePF_6$, 775.35: C 43.37, H 4.55, S 16.54, found: C 42.91 H 4.23 S 16.18. **MS (ESI):** (*m/z*) calculated for $C_{28}H_{35}S_4ONiFe$ [M–PF_6] requires (monoisotopic mass) 629.03, found 628.72; calculated for $C_{27}H_{35}S_4NiFe$ [M–(CO+PF_6)] requires 601.03, found 600.80; calculated for $C_{22}H_{30}S_4NiFe$ [M–(C_5H_5+CO+PF_6)] requires 535.99, found 535.70.

4.5.7. Synthesis of [Ni(mpsms)$_2$Fe(C_5H_5)CO](PF_6)

The synthesis was carried out by modifying the procedure described in the literature.[22] Yield 24%. **Elemental analysis:** Calcd (%) for $C_{28}H_{35}OS_4NiFePF_6$, 775.35: C 43.37, H 4.55, S 16.54, found: C 43.11 H 4.28 S 16.31. **MS (ESI):** (*m/z*) calculated for $C_{28}H_{35}S_4ONiFe$ [M–PF_6] requires (monoisotopic mass) 629.03, found 628.76; calculated for $C_{27}H_{35}S_4NiFe$ [M–(CO+PF_6)] requires 601.03, found 600.58; calculated for $C_{22}H_{30}S_4NiFe$ [M–(C_5H_5+CO+PF_6)] requires 535.99, found 535.73

4.5.8. Synthesis of $[Ni(cpsms)_2Fe(C_5H_5)CO](PF_6)$

The synthesis was carried out by modifying the procedure described in the literature.[22] Yield 19%. **Elemental analysis:** Calcd (%) for $C_{26}H_{29}OS_4NiCl_2FePF_6$, 816.19: C 38.26, H 3.58, S 15.72, found: C 37.85 H 3.23 S 15.48. **MS (ESI):** (*m/z*) calculated for $C_{22}H_{29}S_4ONiCl_2Fe$ [M–PF_6] requires (monoisotopic mass) 668.92, found 668.60; calculated for $C_{22}H_{29}S_4NiCl_2Fe$ [M–(CO+PF_6)] requires 604.92, found 604.62.

4.5.9. Synthesis of $[Ni(ibsms)_2Fe(C_5H_5)CO](PF_6)$

The synthesis was carried out by modifying the procedure described in the literature.[22] Yield 17%. **Elemental analysis:** Calcd (%) for $C_{22}H_{39}OS_4NiFePF_6$, 707.32: C 37.36, H 5.56, S 18.13, found: C 37.25 H 5.33 S 17.99. **MS (ESI):** (*m/z*) calculated for $C_{22}H_{39}S_4ONiFe$ [M–PF_6] requires (monoisotopic mass) 561.06, found 560.79; calculated for $C_{21}H_{39}S_4NiFe$ [M–(CO+PF_6)] requires 533.06, found 532.90.

4.5.10. Synthesis of $[Ni(nhsms)_2Fe(C_5H_5)CO](PF_6)$

The synthesis was carried out by modifying the procedure described in the literature.[22] Yield 21%. **Elemental analysis:** Calcd (%) for $C_{26}H_{47}OS_4NiFePF_6$, 763.43: C 40.91, H 6.21, S 16.80, found: C 41.07.45 H 6.33 S 16.58. **MS (ESI):** (*m/z*) calculated for $C_{26}H_{47}S_4ONiFe$ [M–PF_6] requires (monoisotopic mass) 617.12, found 616.94; calculated for $C_{25}H_{47}S_4NiFe$ [M–(CO+PF_6)] requires 589.13, found 588.87.

4.5.11. Crystallographic Data of Complex $[Ni_3(cpsms)_6]$

$C_{60}H_{72}Cl_6Ni_3S_{12}\cdot CH_2Cl_2$, Fw = 1651.65, brown plates, 0.06 × 0.14 × 0.34 mm^3, monoclinic, *C2c* (no. 15), a = 52.445(2), b = 11.5078(7), c = 27.6319(10) Å, α = 90, β = 116.548(2), γ = 90 °, V = 14918.2(12) Å^3, Z = 8, D_x = 1.471 g cm^{-3}, μ = 1.409 mm^{-1}. 102595 Reflections were measured up to a resolution of (sin $\theta/\lambda)_{max}$ = 0.65 Å^{-1}. An absorption correction based on multiple measured reflections was applied (0.33–0.86 correction range). 14648 Reflections were unique (R_{int} = 0.061), of which 10522 were observed [$I > 2\sigma(I)$]. 797 Parameters were refined with no restraints. $R1/wR2$ [$I > 2\sigma(I)$]: 0.0203/0.0387. $R1/wR2$ [all refl.]: 0.0496/0.0890. S = 1.04. Residual electron density was found between −0.84 and 1.25 eÅ^{-3}.

4.6. References

1. J. A. W. Verhagen, PhD Thesis, *Structural Models of Nickel-Containing Enzymes*, Leiden University, 2004.
2. J. R. Nicholson, G. Christou, J. C. Huffman and K. Folting, *Polyhedron*, 1987, **6**, 863-870.
3. N. Baidya, P. K. Mascharak, D. W. Stephan and C. F. Campagna, *Inorg. Chim. Acta*, 1990, **177**, 233-238.
4. T. Yamamura, H. Kurihara, N. Nakamura, R. Kuroda and K. Asakura, *Chem. Lett.*, 1990, 101-104.

5. B. S. Snyder, C. P. Rao and R. H. Holm, *Aust. J. Chem.*, 1986, **39**, 963-974.
6. D. Sellmann, S. Funfgelder, F. Knoch and M. Moll, *Z.Naturforsch.(B)*, 1991, **46**, 1601-1608.
7. M. Y. Cha, C. L. Catlin, S. C. Critchlow and J. A. Kovacs, *Inorg. Chem.*, 1993, **32**, 5868-5877.
8. M. Cha, J. Sletten, S. Critchlow and J. A. Kovacs, *Inorg. Chim. Acta*, 1997, **263**, 153-159.
9. T. Yamamura, H. Arai, H. Kurihara and R. Kuroda, *Chem. Lett.*, 1990, 1975-1978.
10. E. Erkizia and R. R. Conry, *Inorg. Chem.*, 2000, **39**, 1674-1679.
11. S. Fox, Y. Wang, A. Silver and M. Millar, *J. Am. Chem. Soc.*, 1990, **112**, 3218-3220.
12. J. A. W. Verhagen, D. D. Ellis, M. Lutz, A. L. Spek and E. Bouwman, *J. Chem. Soc.-Dalton Trans.*, 2002, 1275-1280.
13. J. A. W. Verhagen, M. Beretta, A. L. Spek and E. Bouwman, *Inorg. Chim. Acta*, 2004, **357**, 2687-2693.
14. J. A. W. Verhagen, C. Tock, M. Lutz, A. L. Spek and E. Bouwman, *Eur. J. Inorg. Chem.*, 2006, 4800-4808.
15. J. S. Kim, J. H. Reibenspies and M. Y. Darensbourg, *J. Am. Chem. Soc.*, 1996, **118**, 4115-4123.
16. R. Angamuthu, L. L. Gelauff, M. A. Siegler, A. L. Spek and E. Bouwman, *Chem. Commun.*, 2009, 2700-2702.
17. F. Lauderbach, R. Prakash, A. W. Götz, M. Munoz, F. W. Heinemann, U. Nickel, B. A. Hess and D. Sellmann, *Eur. J. Inorg. Chem.*, 2007, 3385-3393.
18. S. Ott, M. Kritikos, B. Åkermark, L. C. Sun and R. Lomoth, *Angew. Chem.-Int. Edit.*, 2004, **43**, 1006-1009.
19. R. Angamuthu and E. Bouwman, *Phys. Chem. Chem. Phys.*, 2009, **11**, 5578–5583.
20. B. Keita, S. Floquet, J. F. Lemonnier, E. Cadot, A. Kachmar, M. Benard, M. M. Rohmer and L. Nadjo, *J. Phys. Chem. C*, 2008, **112**, 1109-1114.
21. R. Angamuthu, H. Kooijman, M. Lutz, A. L. Spek and E. Bouwman, *Dalton Trans.*, 2007, 4641-4643.
22. W. F. Zhu, A. C. Marr, Q. Wang, F. Neese, D. J. E. Spencer, A. J. Blake, P. A. Cooke, C. Wilson and M. Schröder, *Proc. Natl. Acad. Sci. U. S. A.*, 2005, **102**, 18280-18285.

5

Heterodinuclear [NiRu] Complexes Comprising Ruthenium Bis-Bipyridine: Synthesis, Characterisation and Electrocatalytic Dihydrogen Production†

Abstract. Three new heterodinuclear $[Ni(S_2S'_2)Ru(bpy)_2](PF_6)_2$ complexes have been synthesized by the reaction between $[Ni(S_2S'_2)]$, *in situ* formed *cis*-$[Ru(bpy)_2(EtOH)_2]Cl_2$, and NH_4PF_6 in which $[Ni(S_2S'_2)]$ is [Ni(pbss)], [Ni(pbsms)] and [Ni(xbsms)]. The three $[Ni(S_2S'_2)Ru(bpy)_2](PF_6)_2$ complexes have been characterized by ESI-MS spectrometry, electronic absorption and NMR spectroscopy, electrochemical techniques and elemental analysis. The complex $[Ni(pbss)Ru(bpy)_2](PF_6)_2$ crystallizes in the space group $P2_1/c$; the heterodinuclear molecules are connected through a number of strong non-classical hydrogen bonds such as C–H···F, C–H···S and C–H···N, and as well as π···π interactions in the crystal lattice. All the three $[Ni(S_2S'_2)Ru(bpy)_2](PF_6)_2$ complexes have been found to reduce protons electrocatalytically in the presence of trifluoroacetic acid at potentials as low as –1.0 V *vs*. Ag/AgCl in acetonitrile. The complexes have been found to be tolerant towards higher concentrations of acid.

---

† R. Angamuthu, M. A. Siegler, A. L. Spek and E. Bouwman, *manuscript in preparation*.

5.1. Introduction

Heterodinuclear [NiRu][1-6] and homodinuclear [RuRu][7,8] complexes reported in recent literature exhibit exciting properties, such as suitable structural and functional mimics of nickel-containing enzymes, especially hydrogenases. Even though high-resolution X-ray crystal structures are available for the [NiFe] hydrogenases isolated from *D. gigas*,[9,10] *D. vulgaris*,[11-14] *D. fructosovorans*,[15-17] *D. sulfuricans*[18] and *Dm. baculatum*[19] and studying [NiFe] complexes as models would be meaningful, the following reasons can be considered to use Ru(II) instead of Fe(II) in the model complexes: **(1)** Ru(II) shows high affinity towards H_2,[20] **(2)** Ru(II) complexes are comparatively much more stable with respect to the corresponding Fe(II) counterparts, and **(3)** Ru(II) complexes of amine ligands are well known for their photoactivity in combination with their redox activity while the Fe(II) counterparts are only redox-active.

The photocatalytic splitting of water into dihydrogen and dioxygen, and the light-driven proton reduction into molecular hydrogen are both known to have been catalyzed by combining a light-absorbing photoactive center with a redox-active center. Three common approaches reported in the literature to develop light-assisted redox reactions are: **(1)** a photo-active center, e.g. $[Ru(bpy)_3]^{2+}$, is connected to the redox-active center by a conjugated system (see Fig. 1.17A);[21-24] **(2)** the photo-active center is separated from the redox-active center by a non-covalently binding linker (see Fig. 1.17B);[25-27] **(3)** the photo-active center is active in combination with sacrificial electron donors.[25,28-30]

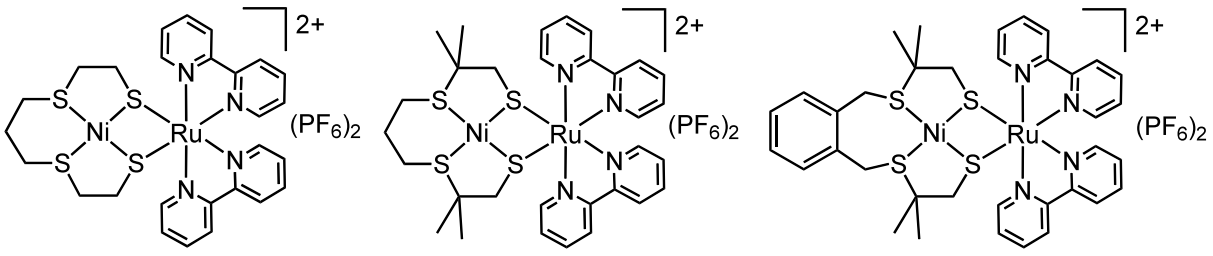

$[Ni(pbss)Ru(bpy)_2](PF_6)_2$ $[Ni(pbsms)Ru(bpy)_2](PF_6)_2$ $[Ni(xbsms)Ru(bpy)_2](PF_6)_2$

Fig. 5.1 Schematic structures of the heterodinuclear [NiRu] complexes described in this Chapter.

This Chapter is devoted to the study of a new approach by designing heterodinuclear [NiRu] complexes containing a redox-active NiS_4 unit directly connected to a photoactive group such as $[Ru(bpy)_2]^{2+}$, as shown in Fig. 5.1. The synthesis, structure and electrocatalytic properties of the three [NiRu] complexes $[Ni(pbss)Ru(bpy)_2](PF_6)_2$,

[Ni(pbsms)Ru(bpy)$_2$](PF$_6$)$_2$ and [Ni(xbsms)Ru(bpy)$_2$](PF$_6$)$_2$, synthesized using the mononuclear nickel complexes [Ni(pbss)], [Ni(pbsms)] and [Ni(xbsms)], respectively, are reported in this Chapter (Fig. 5.1).

5.2. Results

5.2.1. Synthesis

The syntheses and characterizations of the $S_2S'_2$-donor ligands and of their mononuclear low-spin nickel(II) complexes have been discussed in Chapters **2** and **3**, respectively. The complex [Ru(bpy)$_2$(EtOH)$_2$]Cl$_2$ is formed *in situ* and reacted with mononuclear nickel(II) complexes [Ni(pbss)], [Ni(pbsms)] and [Ni(xbsms)] in 1:1 ratio in ethanol to obtain the complexes [Ni(pbss)Ru(bpy)$_2$]Cl$_2$, [Ni(pbsms)Ru(bpy)$_2$]Cl$_2$ and [Ni(xbsms)Ru(bpy)$_2$]Cl$_2$, respectively (Scheme 5.1). The chloride anions are exchanged with PF_6^- anions using an excess (amount) of NH_4PF_6. The [NiRu] complexes have been isolated in analytically pure crystalline form and were used without further purifications. The presence of the PF_6^- anions is visible in the IR spectra of the complexes with strong bands around 830 cm^{-1}.

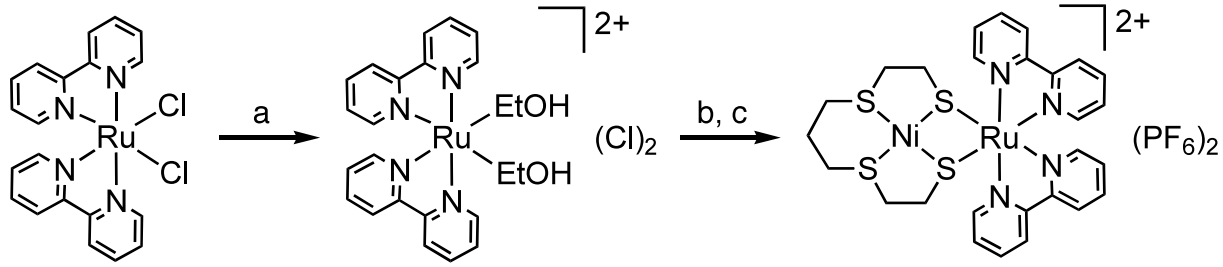

Scheme 5.1. Illustrative synthetic route used in the synthesis of [NiRu] complexes; (a) ethanol, reflux, 2 hrs; (b) [Ni(pbss)], reflux, 6 hrs; (c) NH_4PF_6, stirring, 15 minutes.

5.2.2. Molecular Structure of the [NiRu] Complexes

Perspective views of the molecular structure of the cation [Ni(pbss)Ru(bpy)$_2$]$^{2+}$ are shown in Fig. 5.2; selected interatomic distances and angles are provided in Table 5.1 along with the data of [Ni(pbss)][31] for comparison. The asymmetric unit of [Ni(pbss)Ru(bpy)$_2$](PF$_6$)$_2$ contains one crystallographically independent, ordered molecule. The [Ni(pbss)] unit in [Ni(pbss)Ru(bpy)$_2$]$^{2+}$ retains the square-planar geometry around the Ni(II) ion with two thiolate donors and two thioether sulfurs in enforced *cis* positions. The two thiolate donors of [Ni(pbss)] are connected to the *cis*-[Ru(bpy)$_2$]$^{2+}$ unit making a NiS_2Ru metallacycle through two Ni–S–Ru bridges; the [Ru(bpy)$_2$]$^{2+}$ group is situated at the same side of the Ni(II) coordination plane as the propylene-bridge of the pbss ligand, the four remaining sulfur lone pairs are all below the plane of coordination.

The Ni–$S_{thiolate}$ distances [2.1632(6), 2.1748(6) Å] are slightly shorter than the Ni–$S_{thioether}$ distances [2.1827(6)-2.1893(6) Å], as expected. However, this observation is in contrast to the parent complex [Ni(pbss)], where the Ni–$S_{thiolate}$ distances are slightly longer than the Ni–$S_{thioether}$ distances; usually, the Ni–$S_{thioether}$ distances are longer than (or similar to) the Ni–$S_{thiolate}$ distances (Table 5.1).[32,33] The fact that the two Ni–$S_{thiolate}$ bonds are slightly shorter in [Ni(pbss)Ru(bpy)$_2$](PF_6)$_2$ compared to the parent complex [Ni(pbss)], must be induced by the binding of thiolate sulfurs with ruthenium; the minimised repulsion between the π orbitals of nickel and the thiolate sulfurs upon binding to ruthenium allows for stronger Ni–$S_{thiolate}$ bonds. This observation is in line with the reported structure of [Ni(pbss)Fe(C_5H_5)(CO)](PF_6), in which the binding of the [Fe(C_5H_5)(CO)]$^+$ moiety also results in shortening of the Ni–$S_{thiolate}$ distances.[34]

Table 5.1. Selected distances (Å) and angles (°) for [Ni(pbss)Ru(bpy)$_2$](PF_6)$_2$. Distances and angles found in [Ni(pbss)] are provided in square brackets for comparison.[31]

Ni1–S6	2.1632(6) [2.179(2)]	Ni1–S9	2.1827(6) [2.173(1)]
Ni1–S16	2.1748(6) [2.177(2)]	Ni1–S19	2.1893(6) [2.166(2)]
Ru1–S6	2.4006(5)	Ru1–S16	2.3769(6)
Ru1–N1	2.0599(17)	Ru1–N2	2.0671(18)
Ru1–N3	2.066(2)	Ru1–N4	2.053(2)
S6–Ni1–S9	91.66(2) [90.17(6)]	S6–Ni1–S16	85.05(2) [87.05(6)]
S6–Ni1–S19	174.99(2) [175.85(6)]	S9–Ni1–S16	176.41(3) [177.02(6)]
S9–Ni1–S19	91.73(2) [92.85(5)]	S16–Ni1–S19	91.46(2) [89.87(5)]
Ru1–S6–Ni1	92.17(2)	Ru1–S16–Ni1	92.53(2)
S6–Ru1–S16	75.72(2)	S6–Ru1–N1	173.51(5)
S6–Ru1–N2	103.11(5)	S6–Ru1–N3	86.02(5)
S6–Ru1–N4	97.64(5)	S16–Ru1–N1	97.92(5)
S16–Ru1–N2	92.75(5)	S16–Ru1–N3	95.45(6)
S16–Ru1–N4	171.88(5)	N1–Ru1–N2	78.20(7)
N1–Ru1–N3	93.42(7)	N1–Ru1–N4	88.59(7)
N2–Ru1–N3	169.02(7)	N2–Ru1–N4	93.33(7)
N3–Ru1–N4	79.24(8)		

The nickel center has a slight tetrahedral distortion with a dihedral angle of 3.99°, as defined by the triangular planes S6Ni1S9 and S16Ni1S19. The S–Ni–S angles in [Ni(pbss)Ru(bpy)$_2$](PF_6)$_2$ have undergone a considerable degree of reorganization upon binding to the *cis*-[Ru(bpy)$_2$]$^{2+}$ moiety. Especially the S6–Ni1–S16 angle has decreased with almost 2.5° and the S9–Ni1–S19 angle enlarged nearly 3.5°, to accommodate the formation of the S6–Ru1–S16 hinge. The ruthenium center is in a distorted octahedral geometry with an N_4S_2 chromophore; the Ru–N [2.053(2)–2.0671(18) Å] and Ru–S [2.4006(5) and 2.3769(6) Å] distances are in the expected range and similar to related compounds.[35,36] The Ru–N bonds *trans* to the thiolate sulfur [Ru1–N1, 2.0599(17); Ru1–N4, 2.053(2) Å] are slightly shorter than the two other Ru–N bonds [Ru1–N2, 2.0671(18);

Ru1–N3, 2.066(2) Å]. The pyridyl ring A is tilted towards the methylene protons of the C1 and C3 carbons of the ligand pbss with H···H distances of 2.12 and 2.24 Å, respectively (Fig 5.2, right). The extended solid-state structure of [Ni(pbss)Ru(bpy)$_2$](PF$_6$)$_2$ is formed by a mixture of Δ and Λ enantiomers connected through a number of non-classical inter- and intra-molecular hydrogen-bonding networks of distances (H···A) ranging between 2.44 and 2.82 Å, and π···π stacking interactions of centroid-to-centroid distances ranging between 3.8202(15) and 5.8998(16) Å.

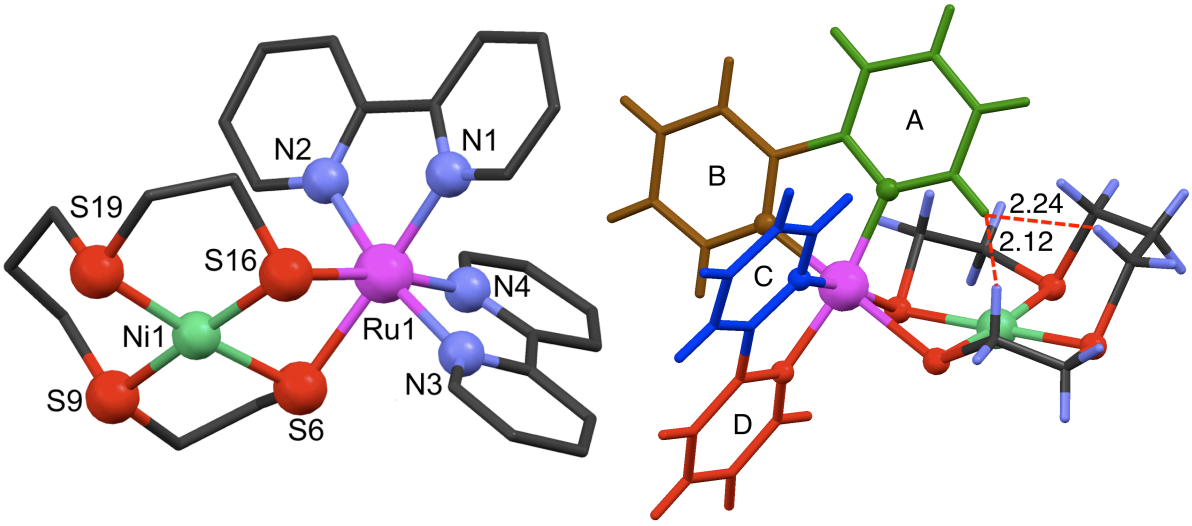

Fig. 5.2. Perspective views of the cationic part of [Ni(pbss)Ru(bpy)$_2$](PF$_6$)$_2$ showing the atomic numbering scheme; Ni1···Ru1, 3.2919(3) Å. Further details are provided in Table 5.1.

5.2.3. ESI-MS and Electronic Absorption Spectra of the [NiRu] Complexes

The ESI-MS spectrometric, and electronic absorption spectroscopic data of the [NiRu] complexes in acetonitrile and dichloromethane are provided in Table 5.2. All the three [NiRu] complexes exhibit the parent molecular-ion peak at *m/z* = [M-(PF$_6$)$_2$]$^{2+}$ in their corresponding ESI–MS spectra confirming the formulation [Ni($S_2S'_2$)Ru(bpy)$_2$]$^{2+}$.

In the electronic absorption spectra, all the [NiRu] complexes exhibit strong sharp absorption maxima around 34000 cm^{-1} corresponding to the intraligand (bpy) π–π* transition and a shoulder 28000 cm^{-1} corresponding to the LMCT of the NiS_4 chromophore. These complexes also show broad bands between 20000 and 22000 cm^{-1} with an extended shoulder (~18000 cm^{-1}) that are ascribed to Ru(4dπ)→π*(bpy) MLCT transition or a mixture of Ru(4dπ)→π*(bpy) MLCT transition and the characteristic d-d transition ($1E' \leftarrow {}^1A_1'$) of the NiS_4 chromophore. The removal of part of the electron density of the π-donating sulfur lone pairs by the coordination of the ruthenium center results in a slight blue-shift of the d-d transition of the nickel ion, as compared to the parent [Ni(pbss)] complex.

A recent report with a combination of experimental studies and DFT calculations of electronic absorption spectroscopic transitions from the group of Lever assigned the low intensity shoulders around 15000 cm^{-1} to Ru(4d)/S→π* bpy transitions;[37] the report concluded that an impressive number of actual electronic transitions are lying underneath the simple band envelope observed in the electronic absorption spectra of the ruthenium bis-bipyridine complexes. The interaction of coordinating solvents, such as acetonitrile, can be excluded, as the electronic spectra of the three [NiRu] complexes are quite similar in both acetonitrile and dichloromethane, and peaks for acetonitrile-solvated species are not observed in the ESI-MS spectra.

Table 5.2. Electronic absorption maxima for the $[Ni(S_2S'_2)Ru(bpy)_2](PF_6)_2$ complexes and the observed *m/z* values of the parent molecular-ion peaks.

Complex	$\nu/10^3$ cm^{-1} ($\varepsilon/10^3$ mol^{-1} l cm^{-1})		*m/z*
	Acetonitrile	Dichloromethane	exptl. (calcd.)
$[Ni(pbss)Ru(bpy)_2](PF_6)_2$	41.8(17.5) 34.5(32.6) 28.3(sh) 22.0(4.4) 17.9(sh) 14.9(sh)	40.3(sh) 34.6(39.2) 28.1(sh) 21.6(5.6) 18.0(sh) 14.9(sh)	348.80 (348.99)
$[Ni(pbsms)Ru(bpy)_2](PF_6)_2$	41.3(29.8) 34.6(50.8) 28.2(sh) 21.7(7) 17.9(sh) 15.1(sh)	40.2(sh) 34.5(49.4) 28.3(sh) 20.9(7.2) 18.0(sh) 14.9(sh)	376.86 (377.02)
$[Ni(xbsms)Ru(bpy)_2](PF_6)_2$	41.3(28.1) 34.6(50) 28.2(sh) 21.5(6.4) 18.0(sh) 15.0(sh)	39.8(sh) 34.4(4.5) 28.1(sh) 20.5(5.7) 18.0(sh) 15.0(sh)	407.72 (408.03)

5.2.4. NMR Spectroscopic Studies of the [NiRu] Complexes

The NMR spectra of the [NiRu] complexes were recorded using acetone-d6 solutions at different temperatures ranging between 223 and 303 K. The assignments of the protons and carbons are made unequivocally, based on the 1D ^1H and ^{13}C, and 2D homonuclear ^1H-^1H COSY, TOCSY, NOESY (T_{mix} = 1 s and 0.5 s), ROESY and heteronuclear ^1H–^{13}C HSQC spectra of the [NiRu] complexes. The assignments of the proton resonances are provided in Table 5.3. The numbering scheme of the protons and carbons of the three [NiRu] complexes is shown in Fig. 5.3.

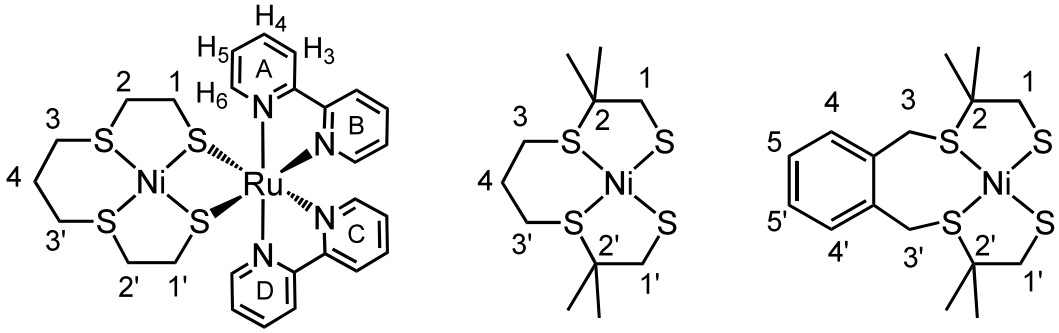

Fig. 5.3. Numbering scheme followed in the assignments of protons and carbons in the NMR spectra of the [NiRu] complexes.

The ^{1}H NMR spectra of the complexes [Ni(pbss)Ru(bpy)$_2$](PF$_6$)$_2$ and [Ni(xbsms)Ru(bpy)$_2$](PF$_6$)$_2$ show four sets of individual resonances for the four available pyridyl rings at all temperatures ranging from 233 to 303 K. The ^{1}H NMR spectrum of [Ni(xbsms)Ru(bpy)$_2$](PF$_6$)$_2$ in acetone-d6 is given in Fig. 5.4 as an example. The complex [Ni(pbsms)Ru(bpy)$_2$](PF$_6$)$_2$, however, shows four sets of broad resonances at 303 K, which resolve to eight sharp sets of resonances upon cooling the sample down to 233 K. The methylene protons of all the three complexes show sharp AB pattern signals (dd), due to the geminal coupling at low temperatures and broad signals/doublets at room temperature.

Table 5.3. ^{1}H NMR spectral data for the [Ni(S$_2$S'$_2$)Ru(bpy)$_2$](PF$_6$)$_2$ complexes recorded in acetone-d6 solutions.*

Complex	Chemical shift δ (ppm)					
	Pyridyl protons					Other protons
	Ring	H_3	H_4	H_5	H_6	
[Ni(pbss)Ru(bpy)$_2$](PF$_6$)$_2$	A	8.38	8.13	7.6	10.02	3.65 (3), 3.43 (3') 3.16–2.89 (2,2',4,4'), 2.1 & 1.84 (1), 1.3 & 0.8 (1')
	B	8.32	8.04	7.5	9.37	
	C	8.23	7.8	7.13	7.68	
	D	8.18	7.7	7.1	7.52	
[Ni(pbsms)Ru(bpy)$_2$](PF$_6$)$_2$	A	8.95	8.55	8.25	10.7	3.6–3.25 (3,3'), 2.9 (1), 2.8 (1), 2.53 (1), 2.55 (1), 1.94 (1'), 1.83 (1'), 1.2 (1'), 1.1 & 0.8 (1'), 1.9 (4), 1.66–1.19 (8Me),
		8.9		8.15	10.6	
	B	8.81	8.45	8.0	9.7	
		8.79			9.6	
	C	8.74	8.36	7.49	7.9	
		8.7		7.45		
	D	8.68	8.32	7.42	7.86	
		8.64		7.39	7.78	
[Ni(xbsms)Ru(bpy)$_2$](PF$_6$)$_2$	A	8.9	8.4	8.03	10.63	7.65 (4), 7.6 (4'), 7.54 (5), 7.5 (5'), 4.97 & 4.94 (3), 4.26 & 4.16 (3'), 2.51 & 1.85 (1), 1.82 (2Me, eq), 1.67 (2Me, ax), 1.64 (2'Me, eq), 1.61 (3'), 1.55 & 0.75 (1'), 1.46 (2'Me, ax),
	B	8.85	8.4	7.99	9.81	
	C	8.72	8.1	7.45	8.26	
	D	8.72	8.09	7.4	7.85	

* Presented data obtained for [Ni(pbss)Ru(bpy)$_2$](PF$_6$)$_2$ at 293 K, and for [Ni(pbsms)Ru(bpy)$_2$](PF$_6$)$_2$ and [Ni(xbsms)Ru(bpy)$_2$](PF$_6$)$_2$ at 233 K; see Fig. 5.3 for the numbering scheme.

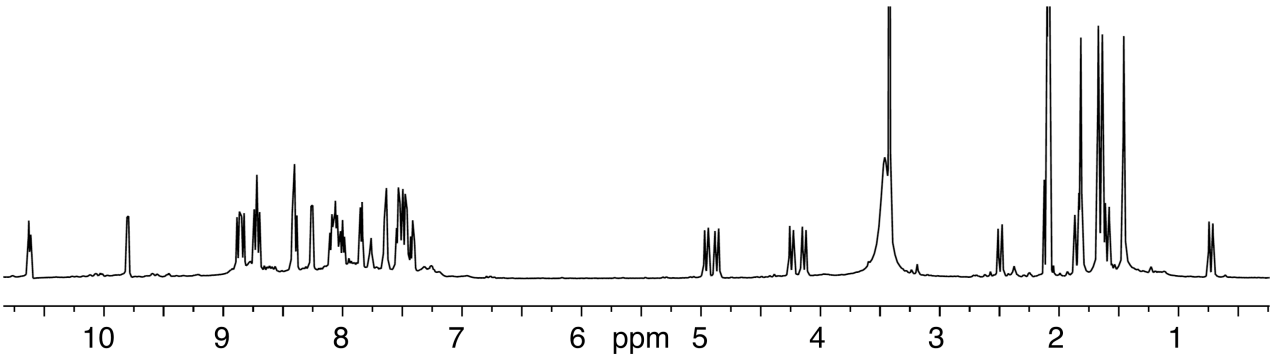

Fig. 5.4. ^{1}H NMR spectra of [Ni(xbsms)Ru(bpy)$_2$](PF$_6$)$_2$ recorded in acetone-d6 at 233 K.

Even though the complex [Ni(pbss)Ru(bpy)$_2$]$^{2+}$ could adopt different conformations in solution, the conformation found in the X-ray structure is fully retained in solution. As the ruthenium(II) ion is kinetically inert, dissociation and conformational reorganisation – necessary for the ruthenium center and the propylene bridge to bind to opposite sides of the nickel coordination plane – are not expected and indeed not observed. Fluxional behaviour of the propylene bridge, giving rise to boat/chair conformations, or flipping of the ethylene side arms of the ligand should be possible in solution. However, this is not observed in the NMR spectra. This may be caused by the relatively strong interaction between the nickel(II) ion and the *ortho*-proton (H$_6$) of the pyridyl ring A (Ni···H, 2.858 Å, see Fig. 5.2) that is pertained in solution, as supported by the observed downfield resonance at 10.02 ppm at 293 K. The interaction of the ortho-proton of pyridyl ring A with the methylene protons of the C1 and C3 carbons as seen in the X-ray crystal structure, makes the four pyridyl rings and all the methylene protons unequal; these interactions were unequivocally identified by the cross peaks observed in NOESY experiments with different mixing times.

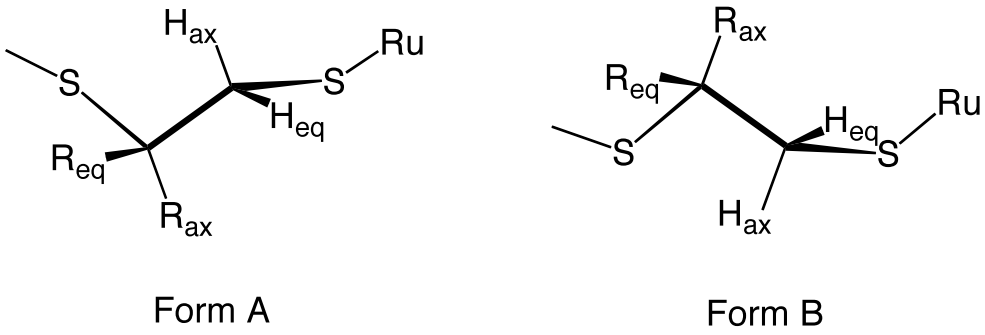

Fig. 5.5. Two observed conformations of [Ni(pbsms)Ru(bpy)$_2$](PF$_6$)$_2$ caused by the possible dynamic flipping of dimethylethylene arms.

The same type of interactions in solution are also exhibited by the complex [Ni(xbsms)Ru(bpy)$_2$](PF$_6$)$_2$ as e.g. shown by the resonance at 10.63 ppm, ascribed to the ortho H$_6$ proton of ring A, shifted downfield due to interaction with the nickel center, at

all the temperatures ranging between 233 and 303 K. Due to an interaction with the *ortho*-proton (H_6) of the pyridyl ring A, the methylene protons of the xylyl bridge are also shifted downfield to 4.97 ppm (Fig. 5.4). Thus also for [Ni(xbsms)Ru(bpy)$_2$]$^{2+}$ only one conformation of the compound is present in solution.

In contrast, for [Ni(pbsms)Ru(bpy)$_2$](PF$_6$)$_2$ eight sets of resonances are observed in the NMR spectra at low temperatures, which means that two different conformations of the complex are present in solution. In contrast to the two other complexes, interactions between the methylene protons of the C3 carbon in the propylene bridge and the ortho-protons of the pyridyl rings are not observed in both conformations of [Ni(pbsms)Ru(bpy)$_2$](PF$_6$)$_2$; this might suggest that the propylene bridge and the ruthenium center are now on opposite sides of the nickel coordination plane. An interaction between the pyridyl H_6 proton and a methylene proton of the dimethylethylene C1 carbon is observed in one of the two conformations, but not in the other, suggesting a dynamic flipping of the -CH_2–C(CH_3)$_2$– arms of the ligand pbsms. Based upon the observations it is concluded that the complex [Ni(pbsms)Ru(bpy)$_2$](PF$_6$)$_2$ shows one set of signals for form A, and another set of signals for form B as drawn in Fig. 5.5. This fluxional behaviour is not observed in the complex [Ni(xbsms)Ru(bpy)$_2$](PF$_6$)$_2$, possibly because the presence of the xylyl group prevents flipping of the dimethylethylene side arms; related complexes also show only one conformation in their ^{1}H NMR spectra.[2,3]

5.2.5. Electrochemical Behaviour of the [NiRu] Complexes

The cyclic voltammograms of the [NiRu] complexes were recorded in acetonitrile and dichloromethane solutions; relevant data are presented in Table 5.4. All three [NiRu] complexes exhibit a major reversible or quasi-reversible metal-based oxidation at around 1 V *vs*. Ag/AgCl in their cyclic voltammogram. This oxidation event is in the usual range for the Ru^{II}/Ru^{III} couple and these potentials are almost 400 mV more positive than the oxidation wave observed in the parent mononuclear nickel(II) complexes in dimethylformamide. The oxidation events are more reversible in dichloromethane solutions than in acetonitrile solutions for all three [NiRu] complexes. In contrast, the reduction waves are more reversible in acetonitrile. The complexes [Ni(pbsms)Ru(bpy)$_2$](PF$_6$)$_2$ and [Ni(xbsms)Ru(bpy)$_2$](PF$_6$)$_2$ show some minor redox couples around 0.6 V and 0.4 V *vs*. Ag/AgCl; these reductions are difficult to assign, due to the presence of multiple redox active partners. Also the [NiRu] complexes exhibit reduction waves around –0.90 V *vs*. Ag/AgCl, which are slightly less negative than in the parent mononuclear nickel(II) complexes in dimethylformamide. The complex [Ni(xbsms)Ru(bpy)$_2$](PF$_6$)$_2$ shows one more reduction wave at a more negative potential

(–1.39 V *vs*. Ag/AgCl) which may be caused by a reduction of the xylyl ligands; this reduction is not observed in the two other [NiRu] complexes.[37]

Table 5.4. Electrochemical data of the [NiRu] complexes in acetonitrile (dichloromethane). Measured using 0.5 mM solutions of complexes in acetonitrile containing 0.05 M $(NBu_4)PF_6$.*

Complex	E_{pa} (V)		E_{pc} (V)		ΔE (V)		E_{HER} (V)
$[Ni(pbss)Ru(bpy)_2](PF_6)_2$	1.02	(1.08)	0.79	(0.94)	0.166	(0.137)	–1.01
	–0.94	(–0.88)	–1.01	(–1.03)	0.073	(0.147)	
$[Ni(pbsms)Ru(bpy)_2](PF_6)_2$	0.93	(1.04)	0.80	(0.91)	0.132	(0.132)	–1.06
	0.64	(0.75)		(0.66)		(0.084)	
	0.38	(0.41)	0.32	(0.33)	0.056	(0.076)	
	–0.98	(–0.97)	–1.06	(–1.12)	0.080	(0.151)	
$[Ni(xbsms)Ru(bpy)_2](PF_6)_2$	0.91	(1.04)	0.79	(0.94)	0.115	(0.103)	–1.43
	0.70	(0.77)	0.62	(0.70)	0.081	(0.093)	
	0.36	(0.43)	0.31	(0.35)	0.048	(0.085)	
	–0.92		–1.01	(–0.99)	0.088		
	–1.39		–1.53		0.142		

* Scan rate 200 mV s^{-1}. Static GC disc working, Pt wire counter electrodes used with a Ag/AgCl (satd. KCl) reference electrode. The values in parenthesis are obtained using dichloromethane (0.5 mM) solutions of the [NiRu] complexes and are presented for comparison. E_{HER}: potential at which dihydrogen evolution reaction occurs.

The electrocatalytic proton reduction property of the $[Ni(S_2S'_2)Ru(bpy)_2](PF_6)_2$ complexes has been investigated using trifluoroacetic acid as the proton source. The addition of increasing amounts of trifluoroacetic acid to the solutions of the [NiRu] complexes results in an increase in the height of the reduction peaks in the case of $[Ni(pbss)Ru(bpy)_2](PF_6)_2$ (E_{HER} = –1.01 V *vs*. Ag/AgCl) and $[Ni(pbsms)Ru(bpy)_2](PF_6)_2$ (E_{HER} = –1.06 V *vs*. Ag/AgCl), whereas in the case of the complex $[Ni(xbsms)Ru(bpy)_2](PF_6)_2$ a new catalytic wave emerges and grows at –1.43 V *vs*. Ag/AgCl. The potential at which the proton reduction occurs is independent of the concentration of acid, unlike the [NiFe] complexes discussed in Chapter **3**, and only slightly moves to more negative potentials at higher concentrations of the acid. An interesting observation is that the oxidation potential of the complex $[Ni(pbss)Ru(bpy)_2](PF_6)_2$ shifts towards negative direction by 100 mV upon the addition of acid and thereafter remains stable at 0.91 V *vs*. Ag/AgCl. For the other two complexes the oxidation event stays unchanged even after the addition of increasing amounts of acid. Surprisingly, all three [NiRu] complexes are stable in the presence of 20 equivalents of trifluoroacetic acid for months as determined by ESI-MS spectrometry, showing the high acid tolerance of the complexes.

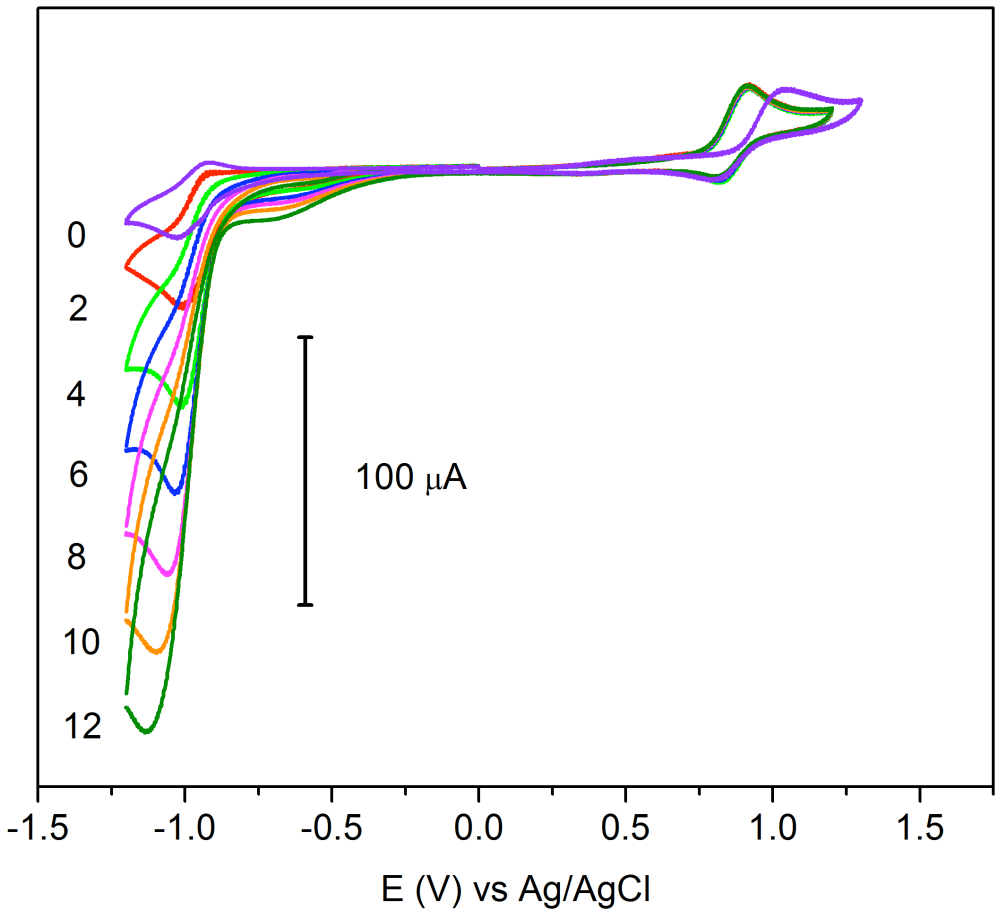

Fig. 5.6. Cyclic voltammograms of [Ni(pbss)Ru(bpy)$_2$](PF$_6$)$_2$ (0.5 mM) in acetonitrile in the presence of 0–12 equivalents of trifluoroacetic acid. Further details are provided in Table 5.4.

5.3. Discussion

The molecular structure of the complex [Ni(pbss)Ru(bpy)$_2$](PF$_6$)$_2$ is fully retained in solution, as indicated by ^{1}H NMR spectroscopy. The unsymmetrical nature of the molecular structure of the [Ni(pbss)Ru(bpy)$_2$](PF$_6$)$_2$, which leads to the four different sets of resonances for the four pyridyl rings in the ^{1}H NMR spectra, can be explained from the interaction between the nickel(II) ion and the *ortho*-proton of the one of the pyridyl rings as observed from the X-ray crystal structure data. The ortho proton H$_6$ of ring A (Fig. 5.2) is only 2.858 Å away from the nickel(II) ion in the crystal structure. This interaction is clearly reflected in the ^{1}H NMR spectra of the complex [Ni(pbss)Ru(bpy)$_2$](PF$_6$)$_2$ with the downfield shifted aromatic signal at 10.02 ppm (Table 5.3). The complexes [Ni(pbsms)Ru(bpy)$_2$](PF$_6$)$_2$ and [Ni(xbsms)Ru(bpy)$_2$](PF$_6$)$_2$ also exhibit the same interaction, as clearly indicated by resonances in the NMR spectra at 10.7 and 10.63 ppm, respectively.

The low-temperature ^{1}H NMR spectrum of complex [Ni(pbsms)Ru(bpy)$_2$](PF$_6$)$_2$ reveals the presence of two conformations in solution. Based on the available data it is proposed that these conformations are the A and B forms shown in Fig. 5.5; dynamic flipping of the dimethylethylene arms of the ligand is responsible for the two different forms. These two forms rapidly interconvert at room temperature, resulting in broad signals in the ^{1}H NMR spectra.

The NMR spectra of the complex [Ni(xbsms)Ru(bpy)$_2$](PF$_6$)$_2$ also show only one set of signals, indicating that in solution only one conformation is present. The related complex [Ni(xbsms)Ru(CO)$_2$Cl$_2$] has been structurally characterized; because of the steric repulsion of the methyl groups with the xylyl methylene groups of the Ni(xbsms) fragment, the ruthenium moiety is located on the same side of the nickel coordination plane as the aromatic ring of the [Ni(xbsms)] unit.[3] Flipping of the dimethylethylene arms is not observed and can be explained from this structure.[3]

Even though electron-donating dimethyl-substitution did not affect the reduction potentials to a large extent, the reduction potential of the complex [Ni(pbss)Ru(bpy)$_2$](PF$_6$)$_2$ (E_{pc}, –1.01 V *vs*. Ag/AgCl) is 0.05 V less negative than that of the complex [Ni(pbsms)Ru(bpy)$_2$](PF$_6$)$_2$ (E_{pc}, –1.06 V *vs*. Ag/AgCl) in acetonitrile. This difference also observed in the electrocatalytic reduction potential of these two complexes (Table 5.4). The electrocatalytic potential corresponding to the proton reduction is located at the same potential as the reduction of the complexes [Ni(pbss)Ru(bpy)$_2$](PF$_6$)$_2$ and [Ni(pbsms)Ru(bpy)$_2$](PF$_6$)$_2$, whereas for [Ni(xbsms)Ru(bpy)$_2$](PF$_6$)$_2$ the electrocatalytic wave appears 0.42 V more negative than the reduction potential of the complex. This difference may be indicative of different mechanisms followed by these complexes in the electrocatalytic proton reduction.

The protonation of the two thioether donors[38] leading to a metal-hydride intermediate can be excluded as these two thioether donors are most likely inert toward such protonation. However, the formation of metal-hydride species after protonation of the two thiolate bridging sulfur donors is more likely, as these bridging thiolates are known to bind with oxygen even in the form of Ni(μ–S$_2$)Ru. The reaction of benzene–1,2–dithiol with *cis*-[Ru(bpy)$_2$Cl$_2$] under argon followed by work-up in air produced the sulfinato complex [Ru(bpy)$_2$(C$_6$H$_4$S·SO$_2$)], which produced the complex [Ru(bpy)$_2$(C$_6$H$_4$SO$_2$·SO$_2$)] upon reaction with air.[37] However, extensive studies of combined spectroscopic methods are necessary to give further information concerning the electrocatalytic mechanism.

5.4. Conclusions

In summary, three novel [Ni($S_2S'_2$)Ru(bpy)$_2$](PF_6)$_2$ complexes have been synthesized and extensive structural characterisations have been made using NMR spectroscopy and X-ray crystallography. These complexes can be regarded as a new class of heterodinuclear [NiRu] compounds, which mimic the activity of the enzyme [NiFe] hydrogenase. All the three [NiRu] complexes have been shown to electrocatalyse the proton reduction and are highly stable in relatively high acid concentrations.

5.5. Experimental Procedures

5.5.1. General Remarks

The complexes [Ni(pbss)][31], [Ni(xbsms)][39] and *cis*-Ru(bpy)$_2$Cl$_2$·2H$_2$O[40] were synthesized according to the literature procedure. Synthesis and characterization of the mononuclear nickel complex [Ni(pbsms)] has been reported in Chapter **3**.

5.5.2. Synthesis of [Ni(pbss)Ru(bpy)$_2$](PF_6)$_2$

The *cis*-Ru(bpy)$_2$Cl$_2$·2H$_2$O (145 mg, 0.3 mmol) was refluxed in 10 ml ethanol for two hours to form [Ru(bpy)$_2$(EtOH)$_2$]Cl$_2$ in situ. Ni(pbss) (103 mg, 0.3 mmol) was added to this solution and the reaction mixture was refluxed overnight. NH_4PF_6 (97.8 mg, 0.6 mmol) was added to this reaction mixture when it was still hot and stirred for 10 minutes. The formed precipitate was filtered off and dried under vacuum to get the purple coloured powder of [Ni(pbss)Ru(bpy)$_2$](PF_6)$_2$ (222 mg, 75%). Purple coloured needles suitable for X-ray diffraction were obtained in one day by diffusing ether into acetone solution of the complex. **Elemental analysis (%):** calculated for $C_{27}H_{30}N_4NiRuS_4F_{12}P_2$·0.7$CH_2Cl_2$: C 31.75, H 3.02, N 5.35, S 12.24; found: C 31.75, H 2.92, N 5.32, S 12.11. **MS (ESI):** (*m/z*) calculated for $NiRuC_{27}H_{30}N_4S_4$ [M–(PF_6)$_2$]$^{2+}$ requires (monoisotopic mass) 348.99, found 348.80 (with expected isotopic distribution).

5.5.3. Synthesis of [Ni(pbsms)Ru(bpy)$_2$](PF_6)$_2$

This complex was synthesized by following the same procedure as in section 5.5.2. **Yield:** 69%. **Elemental analysis (%):** calculated for $C_{31}H_{38}N_4NiRuS_4F_{12}P_2$: C 35.64, H 3.67, N 5.36, S 12.28; found: C 35.87, H 3.58, N 5.48, S 12.07. **MS (ESI):** (*m/z*) calculated for $NiRuC_{27}H_{30}N_4S_4$ [M-(PF_6)$_2$]$^{2+}$ requires (monoisotopic mass) 377.02, found 376.86 (with expected isotopic distribution).

5.5.4. Synthesis of [Ni(xbsms)Ru(bpy)$_2$](PF_6)$_2$

This complex was synthesized by following the same procedure as in section 5.5.2. **Yield:** 81%. **Elemental analysis (%):** calculated for $C_{36}H_{40}N_4NiRuS_4F_{12}P_2$: C 39.07, H 3.64,

N 5.06, S 11.59; found: C 39.09, H 3.66, N 5.11, S 11.38. **MS (ESI):** (*m/z*) calculated for $NiRuC_{27}H_{30}N_4S_4$ $[M-(PF_6)_2]^{2+}$ requires (monoisotopic mass) 408.03, found 407.72 (with expected isotopic distribution).

5.5.5. X-ray crystal structure determinations

Crystallographic data for $[Ni(pbss)Ru(bpy)_2][PF_6]_2$. $C_{27}H_{30}N_4NiRuS_4F_{12}P_2$, Fw = 988.51, dark brown needles, 0.10 × 0.22 × 0.24 mm^3, monoclinic, $P2_1/c$ (no. 14), a = 17.8350(2), b = 9.0801(1), c = 26.2556(6) Å, β = 112.470(2), V = 3929.12(12) $Å^3$, Z = 4, D_x = 1.671 g cm^{-3}, μ = 1.240 mm^{-1}. 59429 Reflections were measured up to a resolution of $(\sin\theta/\lambda)_{max}$ = 0.65 $Å^{-1}$. An absorption correction based on multiple measured reflections was applied (0.33–0.0.86 correction range). 9004 Reflections were unique (R_{int} = 0.038), of which 7225 were observed [I > 2σ(I)]. 460 Parameters were refined with no restraints. $R1/wR_2$ [I > 2σ(I)]: 0.0203/0.0387. $R1/wR_2$ [all refl.]: 0.0303/0.0619. S = 1.05. Residual electron density between −0.62 and 0.57 $eÅ^{-3}$. The program SQUEEZE (PLATON) was used to eliminate the electronic contribution of ill-defined solvent.

5.6. References

1. S. Canaguier, V. Artero and M. Fontecave, *Dalton Trans.*, 2008, 315-325.
2. Y. Oudart, V. Artero, J. Pecaut, C. Lebrun and M. Fontecave, *Eur. J. Inorg. Chem.*, 2007, 2613-2626.
3. Y. Oudart, V. Artero, J. Pecaut and M. Fontecave, *Inorg. Chem.*, 2006, **45**, 4334-4336.
4. M. A. Reynolds, T. B. Rauchfuss and S. R. Wilson, *Organometallics*, 2003, **22**, 1619-1625.
5. B. Kure, T. Matsumoto, K. Ichikawa, S. Fukuzumi, Y. Higuchi, T. Yagi and S. Ogo, *Dalton Trans.*, 2008, 4747-4755.
6. S. Ogo, R. Kabe, K. Uehara, B. Kure, T. Nishimura, S. C. Menon, R. Harada, S. Fukuzumi, Y. Higuchi, T. Ohhara, T. Tamada and R. Kuroki, *Science*, 2007, **316**, 585-587.
7. A. K. Justice, R. C. Linck and T. B. Rauchfuss, *Inorg. Chem.*, 2006, **45**, 2406-2412.
8. A. K. Justice, R. C. Linck, T. B. Rauchfuss and S. R. Wilson, *J. Am. Chem. Soc*, 2004, **126**, 13214-13215.
9. A. Volbeda, E. Garcia, C. Piras, A. L. deLacey, V. M. Fernandez, E. C. Hatchikian, M. Frey and J. C. FontecillaCamps, *J. Am. Chem. Soc.*, 1996, **118**, 12989-12996.
10. A. Volbeda, M. H. Charon, C. Piras, E. C. Hatchikian, M. Frey and J. C. Fontecilla-Camps, *Nature*, 1995, **373**, 580-587.
11. H. Ogata, S. Hirota, A. Nakahara, H. Komori, N. Shibata, T. Kato, K. Kano and Y. Higuchi, *Structure*, 2005, **13**, 1635-1642.
12. H. Ogata, Y. Mizoguchi, N. Mizuno, K. Miki, S. Adachi, N. Yasuoka, T. Yagi, O. Yamauchi, S. Hirota and Y. Higuchi, *J. Am. Chem. Soc.*, 2002, **124**, 11628-11635.
13. Y. Higuchi, H. Ogata, K. Miki, N. Yasuoka and T. Yagi, *Structure*, 1999, **7**, 549-556.
14. Y. Higuchi, T. Yagi and N. Yasuoka, *Structure*, 1997, **5**, 1671-1680.
15. A. Volbeda, L. Martin, C. Cavazza, M. Matho, B. W. Faber, W. Roseboom, S. P. J. Albracht, E. Garcin, M. Rousset and J. C. Fontecilla-Camps, *J. Biol. Inorg. Chem.*, 2005, **10**, 239-249.
16. A. Volbeda, Y. Montet, X. Vernede, E. C. Hatchikian and J. C. Fontecilla-Camps, *Int. J. Hydrog. Energy*, 2002, **27**, 1449-1461.
17. Y. Montet, P. Amara, A. Volbeda, X. Vernede, E. C. Hatchikian, M. J. Field, M. Frey and J. C. FontecillaCamps, *Nat. Struct. Biol.*, 1997, **4**, 523-526.
18. P. M. Matias, C. M. Soares, L. M. Saraiva, R. Coelho, J. Morais, J. Le Gall and M. A. Carrondo, *J. Biol. Inorg. Chem.*, 2001, **6**, 63-81.

19. E. Garcin, X. Vernede, E. C. Hatchikian, A. Volbeda, M. Frey and J. C. Fontecilla-Camps, *Structure*, 1999, **7**, 557-566.
20. J. K. Law, H. Mellows and D. M. Heinekey, *J. Am. Chem. Soc.*, 2002, **124**, 1024-1030.
21. S. Ott, M. Borgstrom, M. Kritikos, R. Lomoth, J. Bergquist, B. Åkermark, L. Hammarström and L. C. Sun, *Inorg. Chem.*, 2004, **43**, 4683-4692.
22. S. Ott, M. Kritikos, B. Akermark and L. C. Sun, *Angew. Chem.-Int. Edit.*, 2003, **42**, 3285-3288.
23. H. Wolpher, M. Borgstrom, L. Hammarstrom, J. Bergquist, V. Sundstrom, S. Stenbjorn, L. C. Sun and B. Akermark, *Inorg. Chem. Commun.*, 2003, **6**, 989-991.
24. J. Ekström, M. Abrahamsson, C. Olson, J. Bergquist, F. B. Kaynak, L. Eriksson, S. C. Licheng, H. C. Becker, B. Åkermark, L. Hammarström and S. Ott, *Dalton Trans.*, 2006, 4599-4606.
25. A. M. Kluwer, R. Kapre, F. Hartl, M. Lutz, A. L. Spek, A. M. Brouwer, P. W. N. M. van Leeuwen and J. N. H. Reek, *Proc. Natl. Acad. Sci. U. S. A.*, 2009.
26. L. C. Song, M. Y. Tang, S. Z. Mei, J. H. Huang and Q. M. Hu, *Organometallics*, 2007, **26**, 1575-1577.
27. X. Q. Li, M. Wang, S. P. Zhang, J. X. Pan, Y. Na, J. H. Liu, B. Akermark and L. C. Sun, *J. Phys. Chem. B*, 2008, **112**, 8198-8202.
28. A. Fihri, V. Artero, A. Pereira and M. Fontecave, *Dalton Trans.*, 2008, 5567-5569.
29. A. Fihri, V. Artero, M. Razavet, C. Baffert, W. Leibl and M. Fontecave, *Angew. Chem.-Int. Edit.*, 2008, **47**, 564-567.
30. Y. Na, M. Wang, J. X. Pan, P. Zhang, B. Åkermark and L. C. Sun, *Inorg. Chem.*, 2008, **47**, 2805-2810.
31. T. Yamamura, H. Arai, N. Nakamura and H. Miyamae, *Chem. Lett.*, 1990, 2121-2124.
32. M. A. Halcrow and G. Christou, *Chem. Rev.*, 1994, **94**, 2421-2481.
33. D. Sellmann, D. Haussinger and F. W. Heinemann, *Eur. J. Inorg. Chem.*, 1999, 1715-1725.
34. W. F. Zhu, A. C. Marr, Q. Wang, F. Neese, D. J. E. Spencer, A. J. Blake, P. A. Cooke, C. Wilson and M. Schröder, *Proc. Natl. Acad. Sci. U. S. A.*, 2005, **102**, 18280-18285.
35. T. Yoshimura, A. Shinohara, M. Hirotsu, K. Ueno and T. Konno, *Bull. Chem. Soc. Jpn.*, 2006, **79**, 1745-1747.
36. T. Yoshimura, A. Shinohara, M. Hirotsu and T. Konno, *Chem. Lett.*, 2005, **34**, 1310-1311.
37. R. A. Begum, A. A. Farah, H. N. Hunter and A. B. P. Lever, *Inorg. Chem.*, 2009, **48**, 2018-2027.
38. R. Angamuthu and E. Bouwman, *Phys. Chem. Chem. Phys.*, 2009, **11**, 5578–5583.
39. J. A. W. Verhagen, D. D. Ellis, M. Lutz, A. L. Spek and E. Bouwman, *J. Chem. Soc.-Dalton Trans.*, 2002, 1275-1280.
40. B. P. Sullivan, D. J. Salmon and T. J. Meyer, *Inorg. Chem.*, 1978, **17**, 3334-3341.

6

Hexanuclear (Ni_6-)Metallacrown as Functional Model for [NiFe] Hydrogenase†

Abstract. The hexanuclear $[Ni_6(cpss)_{12}]$ (cpss = μ–S–CH_2–CH_2–S–C_6H_4–Cl) wheel-type cluster adopts an unusual structural motif whereby four NiS_4 square-planar and two NiS_5 square-pyramidal units are conjoined by edge sharing; the NiS_5 units resemble the inactive state of the Ni centre in [NiFe] hydrogenase. In addition, the hexanuclear metallacrown has been demonstrated to functionally resemble the [NiFe] hydrogenases. Protonation of the cluster was studied employing ^{1}H NMR spectroscopy by the sequential additions of dichloroacetic acid or *p*-toluenesulfonic acid monohydrate into solutions of $[Ni_6(cpss)_{12}]$ in CD_2Cl_2 and DMF-d_7, respectively; protonation takes place on the thioether sulfurs available in the metallacrown. Electrochemical properties of both the parent and protonated $[Ni_6(cpss)_{12}]$ species have been studied using cyclic voltammetry. Protonated $[Ni_6(cpss)_{12}]$ shows an interesting electrocatalytic property, as it catalyses the reduction of protons into molecular hydrogen in the presence of protic acids, such as dichloroacetic acid and chloroacetic acid at –1.5 and –1.6 V *vs*. Ag/AgCl in DMF, respectively. A catalytic cycle has been proposed based on the observations from the NMR spectroscopic and electrochemical studies of the metallacrown. The behavior of this electrocatalyst was further studied by its immobilization on the surface of a edge plane pyrolytic graphite electrode; reduction of a dichloroacetic acid solution in acetonitrile on the surface of the modified electrode occurs at 220 mV more positive potential compared to the unmodified electrode.

---

† This chapter is based on: R. Angamuthu, H. Kooijman, M. Lutz, A. L. Spek and E. Bouwman, *Dalton Trans.*, **2007**, 4641-4643; R. Angamuthu and E. Bouwman, *Phys. Chem. Chem. Phys.*, **2009**, 5578-5583.

6.1. Introduction

Metal thiolates, including nickel thiolates, are of interest in the context of their rich redox chemistry[1,2] and structural diversity in supramolecular architectures;[3] moreover, as synthetic models for environmentally and industrially significant enzymes like hydrogenases.[4-6] Despite the fact that there are plenty of examples for the ubiquitous O- and/or N-bridged metallacrowns,[7-15] few literature reports are available concerning S-bridged supramolecules.[16-19] Cyclic structures $[(Ni(\mu\text{-}SR)_2)_n]$ (n = 4-11) with a range of monodentate thiolates and bidentate (NS,[17,18] S_2[16]) thiolates are known since the first report[19] of a hexanuclear wheel. Noticeably all these reported cyclic structures are composed of square-planar NiS_4 units as building blocks. Interestingly, an example of a decanuclear cluster crystallized with an encapsulated benzene molecule as a guest has recently been reported.[3]

On the other hand, growing concerns about global warming and the threat regarding to the depletion of conventional fossil fuels induces the surge towards sustainable energy sources. Dihydrogen is generally accepted to be one of the most promising and sustainable energy alternatives for fossil fuels. Researchers are toiling in different directions to find viable ways to produce dihydrogen, effectively and economically.[20-26] One of the ways suggested by Nature is using the ideas and insights from enzymes such as hydrogenases; these efficiently reduce protons into dihydrogen.[27] Numerous structural and functional models of hydrogenases have been reported[1,2,4,28,29] in the past decade since the report of the crystal structure of a hydrogenase.[30] A number of [NiRu] complexes, based on [Ni(xbsms)][31] [H_2xbsms = *α*,*α*'-bis(4-mercapto-3,3-methyl-2-thiabutyl)-*o*-xylene] and [Ni(emi)][32] [H_2emi = 1,2-ethylenebis(2-mercaptoisobutyramide)] have been recently reported as electrocatalysts to produce dihydrogen around –1.5 V vs. Ag/AgCl in DMF, using triethylamine hydrochloride as a proton source.[23,33,34]

Some of the recently reported heterodinuclear [NiFe] model complexes are structurally similar to the active site of the [NiFe] hydrogenase. However, they are stable only at low temperatures, possibly due to the presence of multiple carbonyl ligands.[35,36] Consequently, there has been considerable interest in stable and efficient electrocatalysts, such as nickel and cobalt complexes of macrocycles and multinuclear metallacrowns, as they can be potentially employed in PEM (Proton Exchange Membrane) water electrolysis cells.[21,24,37,38] A handful of transition-metal complexes, away from the interest of modeling the active site of hydrogenases, have also been reported to reduce protons into dihydrogen effectively with various overpotentials ranging between –1.5 and –0.2 V vs. SCE.[20-26,28,29,39-41]

A series of cobalt difluoroboryl-diglyoximate complexes have been reported recently to catalyze the electrochemical dihydrogen evolution at overpotentials as low as –0.20 V vs. SCE in acetonitrile.[24,37,38,42] The dinuclear complex [$(CpMo–\mu–S)_2S_2CH_2$] has been reported as an electrocatalyst in the dihydrogen production showing almost 100% current efficiency when *p*-cyanoanilinium tetrafluoroborate was used as a proton source.[26] The oxothiomolybdenum wheel $Li_2[Mo_8S_8O_8(OH)_8(oxalate)]$ has recently been shown to be a electrocatalyst producing dihydrogen from $HClO_4$, *p*-toluenesulfonic acid, trifluoroacetic acid and acetic acid at –1 V vs. SCE.[21] However, a credible comparison of the electrocatalytic efficiency cannot be made among the reported electrocatalysts as they work in different environments and produce dihydrogen from various proton sources.

This chapter reports on the synthesis, reactivity and structural features of the first example of a hexanuclear cluster having square-planar, as well as square-pyramidal coordinated nickel ions in the same molecule. In addition, the protonation and electrocatalytic dihydrogen evolution studies of this extremely stable low-spin hexanuclear nickel thiolate metallacrown are assessed with the assistance of various techniques.

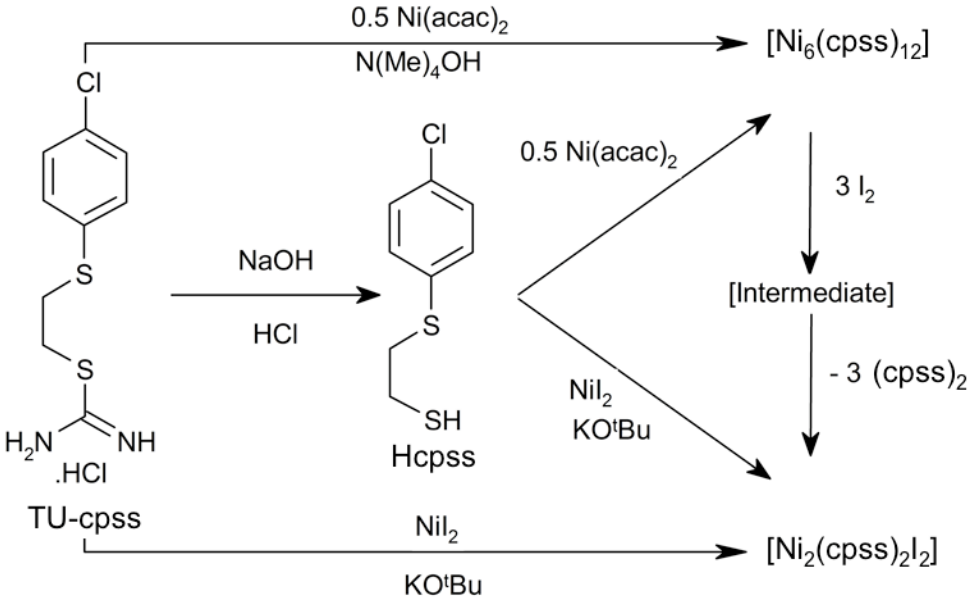

Scheme 6.1. Synthesis of complexes [$Ni_6(cpss)_{12}$] and [$Ni_2(cpss)_2I_2$] from TU-cpss, and the chemical oxidation of [$Ni_6(cpss)_{12}$] by iodine.

6.2. Results and Discussion

6.2.1. Synthesis

The reaction of $Ni(acac)_2$ with two equivalents of the thiouronium salt TU-cpss (Scheme 6.1) in the presence of two equivalents of tetramethylammonium hydroxide led

to an immediate colour change to deep brown and the thiolate-bridged hexanuclear nickel complex $[Ni_6(cpss)_{12}]$ was isolated as reddish-brown crystals. Reaction of three equivalents of iodine with one equivalent of $[Ni_6(cpss)_{12}]$ in dichloromethane resulted in a color change from dark brown to deep greenish brown. Filtration and slow evaporation of the solvent in air yielded dark brown hexagonal plates of the complex $[Ni_2(cpss)_2I_2]$ suitable for X-ray diffraction.

6.2.2. X-ray Crystal Structure Description of $[Ni_6(cpss)_{12}]$

The X-ray crystal structure determination of reddish–brown rectangular-shaped crystals revealed a hexanuclear metallacrown $[Ni_6(cpss)_{12}]$ framework (Fig. 6.1) containing four square-planar NiS_4 and two square-pyramidal NiS_5 units joined by edge sharing. The whole molecule resides on a crystallographic inversion centre. Although the ligand has been synthesized to act as a bidentate chelate, it is coordinating only via the thiolate sulfur in 10 out of the 12 ligands that are present in $[Ni_6(cpss)_{12}]$. Each nickel ion is surrounded by four thiolate sulfurs of the μ-$SCH_2CH_2SC_6H_4Cl$ ligands with Ni–S distances of 2.1895(17)–2.2161(16) Å in a distorted square-planar fashion. However, one of the four ligands coordinated to Ni(3) acts as a chelating bidentate ligand; its thioether sulfur is coordinated at the apical position making the coordination geometry of Ni(3) square-pyramidal with a τ value[43] of 0.15.

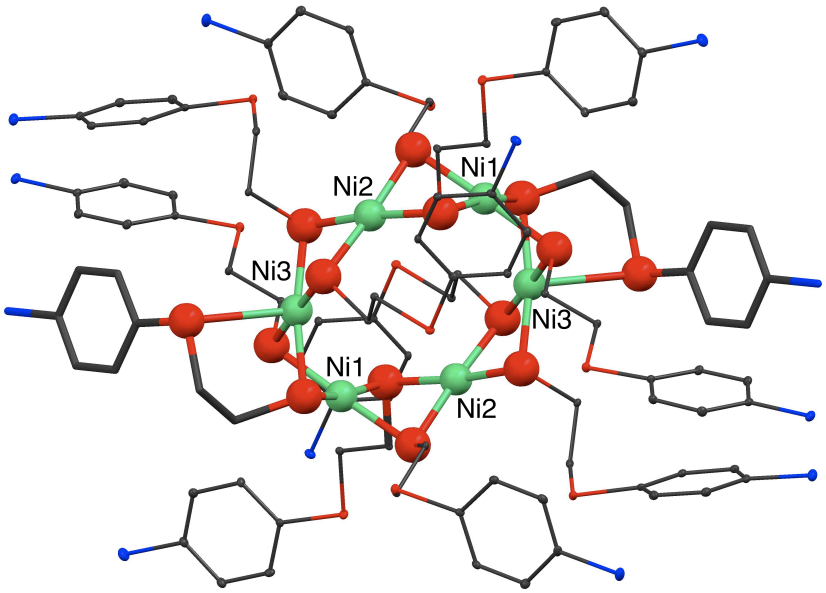

Fig. 6.1. Perspective view of $[Ni_6(cpss)_{12}]$. Ni, green; S, red; Cl, blue; C, grey. Hydrogens are omitted for clarity. Symmetry operation a: −x, 1−y, −z. Selected bond lengths (Å): Ni–S, 2.1895(17)–2.2161(16); Ni···Ni, 2.8220(11)–3.1022(12).

The two NiS_5 units resemble the Ni centre of the oxidized inactive state in the [NiFe] hydrogenase.[44] The nickel ions approximately form a hexagon, with Ni···Ni separations in the range of 2.8220(11)–3.1022(12) Å. Two μ-S bridges from two ligands connect adjacent nickel ions. The twelve μ-S atoms form double crowns, one above and the other below the Ni_6 ring. Owing to the geometrical restrictions introduced by the bridging sulfur atoms, the NiS_4 units are not strictly planar; the nickel ions Ni(1), Ni(2) and Ni(3) are 0.121, 0.026 and 0.119 Å above their corresponding S_4 planes, respectively. The S–Ni–S *cis* bond angles range from 81.88(6) to 98.31(6)°. The ellipsoidal Ni_6 ring with Ni–Ni–Ni vertex angles of 118.84(3)–129.39(4)°, has a distance range between 5.4081(12) and 6.3316(13) Å for opposite nickel ions. The Ni(2)···Ni(2) distance is noticeably shorter (5.4081(12) Å) in comparison with the Ni(1)···Ni(1) distance (6.3316(13) Å). The ligands that are coordinated to Ni(1) are involved in π–π stacking to a neighboring hexanuclear molecule with a stacking distance of 3.854(4) Å. On the other hand, the chelating ligand coordinated to the Ni(3) ion shows a comparatively weaker stacking (3.902(4) Å) while the non-chelating ligand coordinated to the same nickel ion is involved in a comparatively stronger stacking interaction (3.771(4) Å). These asymmetric π–π stacking interactions may contribute to the ellipsoidal shape of the Ni_6 hexagon and the orientation of the ligands as present in the solid-state structure.

6.2.3. Reactivity of [$Ni_6(cpss)_{12}$] with Iodine and the Structure of [$Ni_2(cpss)_2I_2$]

In order to shed light on the solution structure and to make use of the reactive axial sites of the nickel ions of complex [$Ni_6(cpss)_{12}$], its oxidation with three equivalents of iodine was performed in dichloromethane, which resulted in a color change of the dichloromethane solution from dark brown to deep greenish brown. Filtration and slow evaporation of the solvent in air yielded dark brown hexagonal plates of the complex [$Ni_2(cpss)_2I_2$] suitable for X-ray diffraction.

The ability of the ligand to coordinate via the thioether sulfur is evidenced by the formation of [$Ni_2(cpss)_2I_2$]. The X-ray crystal structure determination revealed a dinuclear structure with crystallographic twofold symmetry (Fig. 6.2), in which two ligands bridge the two Ni ions through the thiolate sulfurs, and the thioether sulfurs and iodide ions occupy the terminal positions of the nickel ions. Thus, two NiS_3I square-planar units are conjoined at an edge, and the Ni_2S_2 rhombus is folded with a dihedral angle of 66.28(2)° with an intramolecular Ni···Ni separation of 2.8602(4) Å. The Ni–S distances are quite normal in [$Ni_2(cpss)_2I_2$], the Ni–S thioether distance (2.1940(7) Å) is slightly longer than the Ni–S thiolate distances (2.1658(7) and 2.1902(7) Å). The crystal packing of [$Ni_2(cpss)_2I_2$] along the *c* axis shows a one-dimensional chain formed by the intermolecular interaction between the chlorides and the centroids of the electron-

deficient aromatic rings (C-Cl···Cg(π-ring)) at a distance of 3.696 Å.[45,46] ^{1}H and ^{13}C NMR spectra of $[Ni_2(cpss)_2I_2]$ reveal more or less the same chemical shift values, as interpreted for the chelating ligand in $[Ni_6(cpss)_{12}]$.

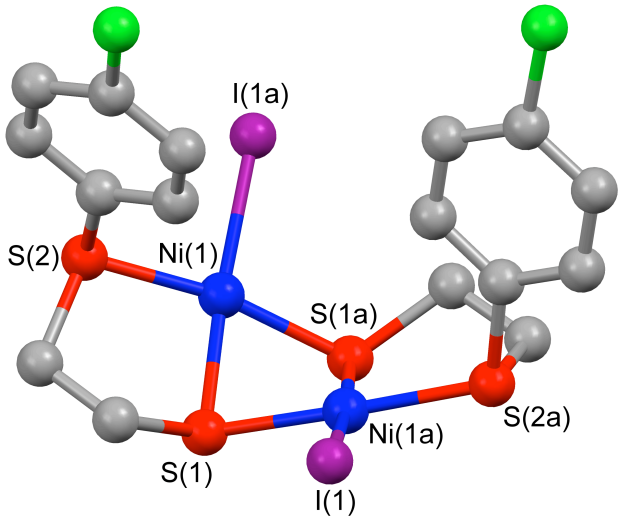

Fig. 6.2. Perspective view of $[Ni_2(cpss)_2I_2]$. Ni, blue; S, red; Cl, green; I, violet; C, grey. Hydrogens are omitted for clarity. Symmetry operation a: 1 − x, y, 0.5 − z. Selected bond lengths (A˚): Ni(1)–S(1), 2.1658(7); Ni(1a)–S(1), 2.1902(7); Ni(1)–S(2), 2.1940(7); Ni(1)···Ni()1a, 2.8602(4).

6.2.4. Electrochemical Studies of $[Ni_6(cpss)_{12}]$ and $[Ni_2(cpss)_2I_2]$

The electrochemistry of $[Ni_6(cpss)_{12}]$ in a dichloromethane solution shows only an irreversible oxidation process, observed at 0.77 V vs. Ag/AgCl (Fig. 6.3). The chemical oxidation of $[Ni_6(cpss)_{12}]$ has been achieved by adding three equivalents of iodine to a dichloromethane solution of $[Ni_6(cpss)_{12}]$ in an electrochemical cell. The CV of the unstable oxidized species has been recorded immediately. The quasi-reversible reduction of the Ni(III) species is observed at 0.60 V with reoxidation at 0.66 V. Within a few minutes, a white sediment is deposited at the bottom of the cell, which by NMR proved to be the disulfide of the ligand. The complex $[Ni_2(cpss)_2I_2]$ shows a quasi-reversible oxidation at 0.740 V, of which the reduction occurs at 0.46 V.

In addition, the cyclic voltammograms of $[Ni_6(cpss)_{12}]$ (0.5 mM) were recorded at a static glassy carbon working electrode in a DMF solution containing 0.05 M tetra-*n*-butylammonium hexafluoridophosphate in order to assess the effect of coordinating solvent. This solution displays a reductive event at –1.12 V, which is attributed to the irreversible reduction process of Ni^{II} to Ni^{I}, and an irreversible oxidation process of Ni^{II} to Ni^{III} at 0.72 V vs Ag/AgCl.

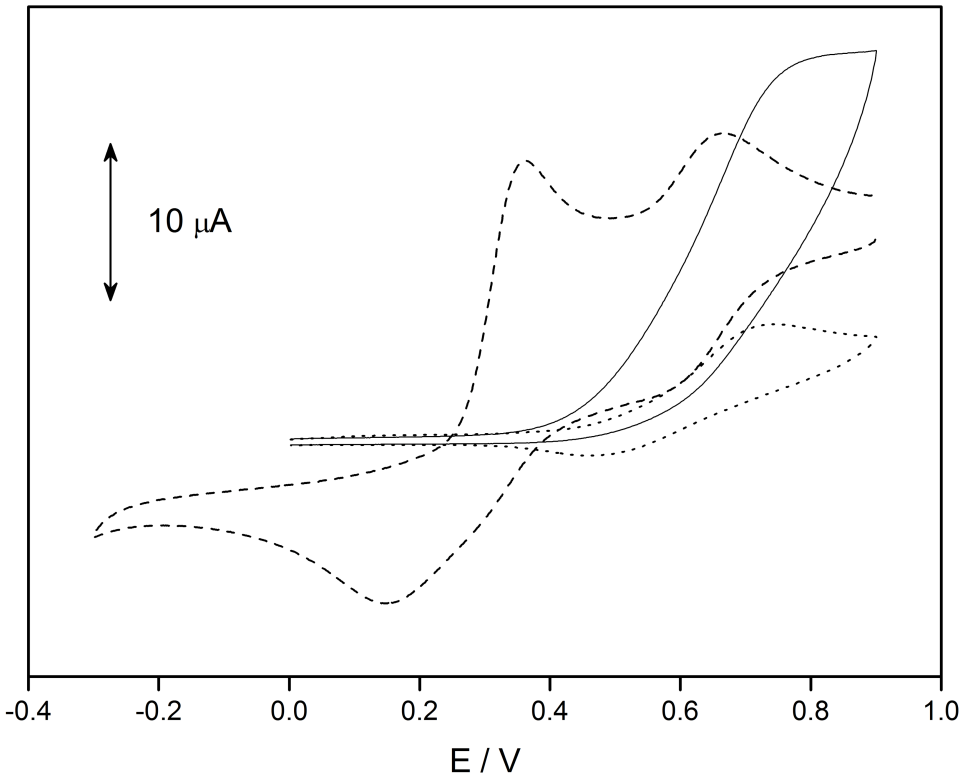

Fig. 6.3. Cyclic voltammograms of 1 mM solutions of $[Ni_6(cpss)_{12}]$ (−),$[Ni_6(cpss)_{12}]$ + $3I_2$ (---) and $[Ni_2(cpss)_2I_2]$ (· · ·) in CH_2Cl_2 containing 0.1M$(NBu_4)PF_6$. Scan rate 200 mV s^{-1}. Pt disc working, Pt wire counter electrodes used with a Ag/AgCl reference electrode.

6.2.5. Electronic Spectroscopic Studies of $[Ni_6(cpss)_{12}]$ in the Presence of H^+

To investigate the stability of the complex $[Ni_6L_{12}]$ in DMF, an electronic absorption spectrum was recorded; it displays three absorption bands at 29900 (LMCT), 24200 ($^1E''\leftarrow{}^1A_1'$) and 18200 ($^1E'\leftarrow{}^1A_1'$) cm^{-1} characteristic of a low-spin nickel(II) ion with a NiS_4 chromophore. The intensities of these absorptions remain unchanged in DMF solution for a prolonged period even after the addition of 12 equivalents of *p*-toluenesulfonic acid monohydrate ($TsOH{\cdot}H_2O$); they slowly decrease upon the addition of an excess of acid (>12 eq.) before they completely vanish only after several days (Fig. 6.4). Three new low-intensity peaks at 25600 (CT, obscuring $^3T_{1g}(P)\leftarrow{}^3A_{2g}$), 15000 ($^3T_{1g}\leftarrow{}^3A_{2g}$) and 13500 ($^1E_g\leftarrow{}^3A_{2g}$) cm^{-1} are observed after a week, associated with a change in the color of the solution from dark brown to light greenish-yellow. This change is ascribed to the disintegration of $[Ni_6L_{12}]$ upon protonation and by the excess acid present in the solution, resulting in the formation of solvent coordinated high-spin Ni(II) species. The same features are observed when dichloromethane is used as a solvent.

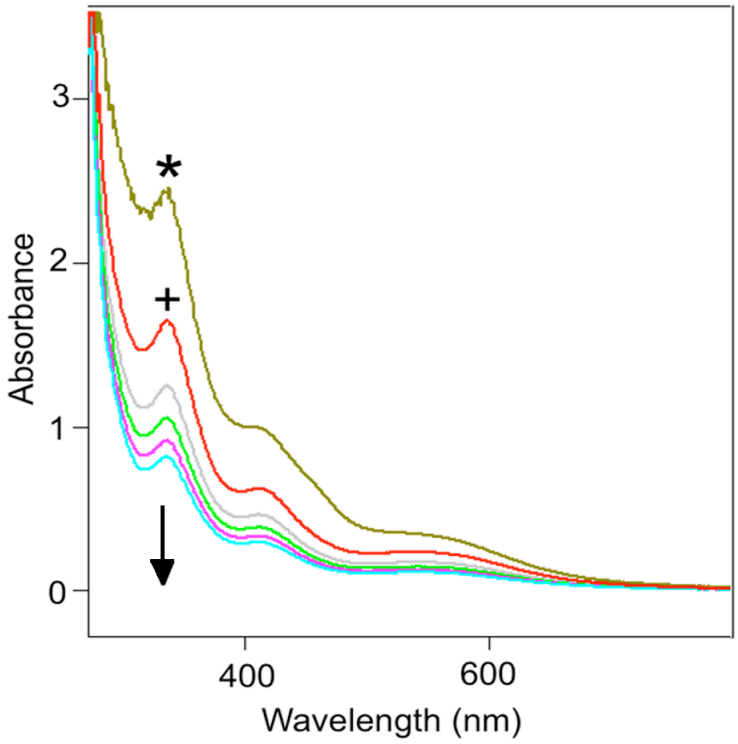

Fig. 6.4. Electronic absorption spectra of $[Ni_6(cpss)_{12}]$ (✱) and in the presence of a large excess of $[TsOH{\cdot}H_2O]$ (✚) in DMF; the remaining four spectra were recorded with 24 hour intervals between each.

6.2.6. ^{1}H NMR Spectroscopic Studies of $[Ni_6(cpss)_{12}]$

^{1}H NMR spectra of $[Ni_6(cpss)_{12}]$ have been recorded in DMF-d_7 solution to assess its stability in the presence of coordinating solvents (Fig. 6.5). Interestingly, the pattern of the ^{1}H NMR spectrum of $[Ni_6L_{12}]$ in DMF-d_7 completely resembles that recorded in CD_2Cl_2, ruling out a solvent interaction by coordination in the axial positions of Ni(II) ions in exchange for the axial coordination of the thioether donors. All the six axial positions present in the outer side of the Ni_6 ring of $[Ni_6(cpss)_{12}]$ are occupied by thioether sulfurs of the ligands alternatingly directed from above and below the Ni_6 ring (Fig. 6.5); six of the twelve ligands are monodentate and six ligands are bidentate as they use the thioether sulfur for the axial coordination.

The two doublets (7.49 and 7.37 ppm) and one singlet (7.32 ppm) of equal intensity in the aromatic region of the ^{1}H NMR spectra belong to the chelating ligands and the monodentate ligands, respectively. The aromatic protons of the monodentate ligands are showing a singlet, as the rings are free to rotate, while the aromatic protons of the chelating ligands show two doublets as a result of the restricted rotation. Furthermore, the room temperature ^{1}H NMR spectra of $[Ni_6(cpss)_{12}]$ in DMF-d_7 or in CD_2Cl_2 remain unchanged for several days, confirming the high stability of $[Ni_6(cpss)_{12}]$ in these solvents.

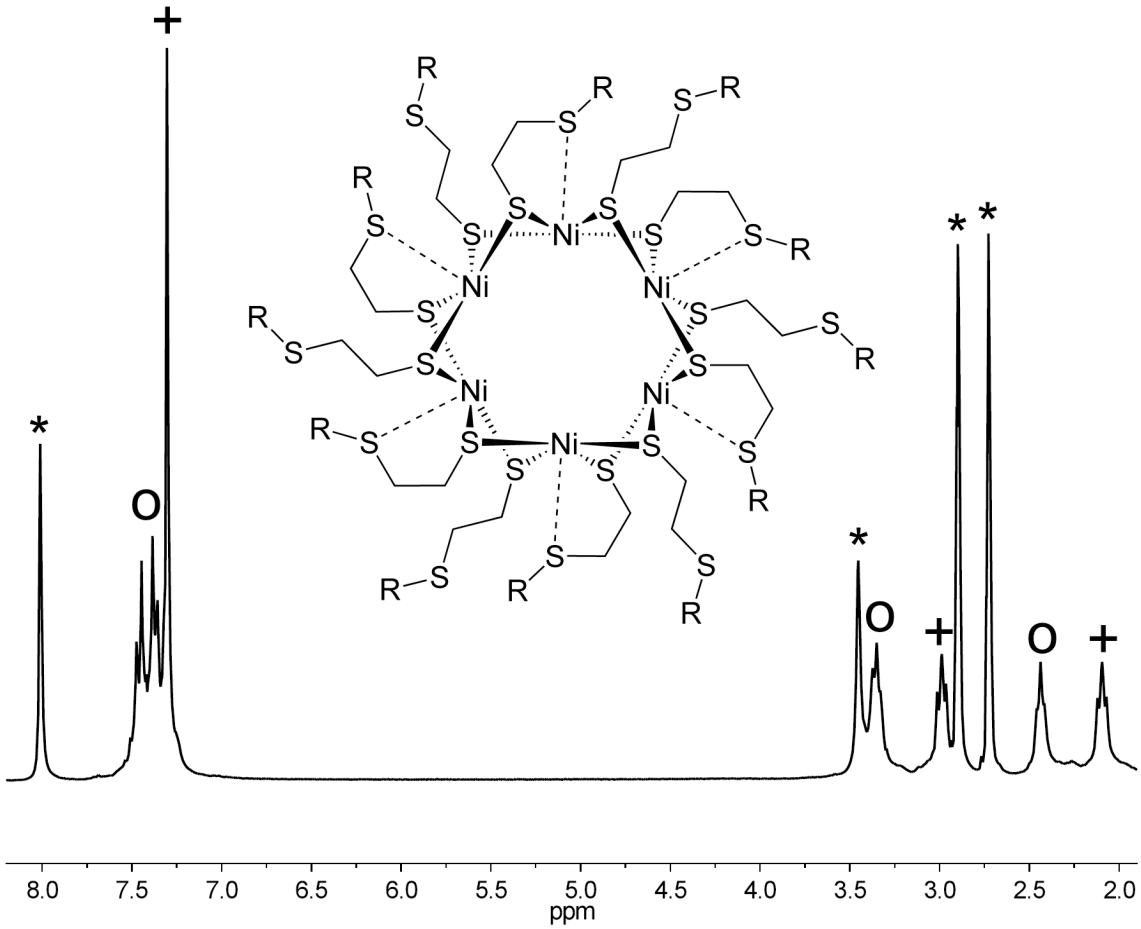

Fig. 6.5. ^{1}H NMR of [$Ni_6(cpss)_{12}$] in DMF-d_7 solution and the schematic diagram of the solution structure of [$Ni_6(cpss)_{12}$] (inset). R indicates the 4-chlorophenyl groups of the ligand; **+**, signals from monodentate ligands; **O**, signals from chelating ligands; ★, signals from residual protons of the solvent.

6.2.7. Protonation of [$Ni_6(cpss)_{12}$] as Studied by ^{1}H NMR Spectroscopy

The effect of the addition of protic acids to the CD_2Cl_2 solution of [$Ni_6(cpss)_{12}$] has been studied employing ^{1}H NMR spectroscopy. The gradual changes in the ^{1}H NMR spectrum upon the increasing addition of dichloroacetic acid to the solution of [$Ni_6(cpss)_{12}$] are shown in Fig. 6.6. Interestingly, the intensities of the signals of the monodentate ligands at 7.12, 2.87 and 2.01 ppm decrease in the initial stage of additions of the acid followed by the signals of the chelating ligands upon further additions. Simultaneously, a new set of signals grows at 7.30, 3.12 and 2.73 ppm, due to the protonation of the thioether sulfurs available from the twelve ligands. The same changes are observed when DMF-d_7 and *p*-toluenesulfonic acid monohydrate ($TsOH{\cdot}H_2O$) are used. Protonation of the cluster was further confirmed by the isotopic distribution patterns of the ESI-MS spectra: signals are found at m/z 467.75 and 468.11 for [$M+6H^+$]

(Fig. 6.7) and [M+6D⁺] (using DCl), respectively. The ^{1}H NMR spectrum of the protonated $[Ni_6L_{12}]$ in both CD_2Cl_2 (with dichloroacetic acid) and DMF-d_7 (with $TsOH{\cdot}H_2O$) remained unchanged even after two days, again confirming the high stability of the protonated $[Ni_6L_{12}]$ compound in solution. The signals slowly broaden upon the addition of a large excess of acid due to the formation of paramagnetic high-spin Ni(II) species, as also observed from the electronic absorption spectra.

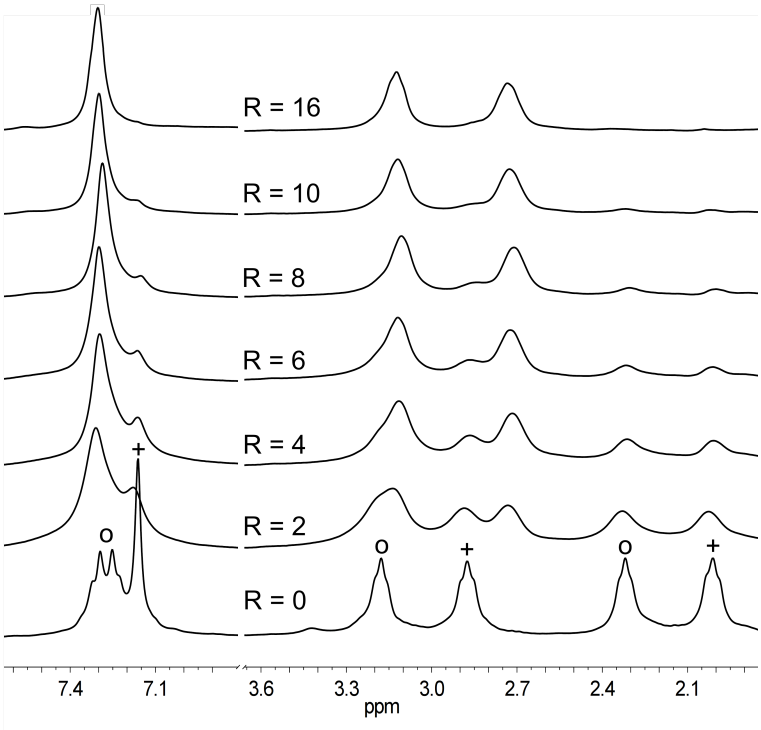

Fig. 6.6. ^{1}H NMR spectra of $[Ni_6(cpss)_{12}]$ in CD_2Cl_2 upon the addition of dichloroacetic acid in CD_2Cl_2 in various Ni to H^+ ratios. R = [acid]/[Ni]. **+**, signals from monodentate ligands; **O**, signals from chelating ligands.

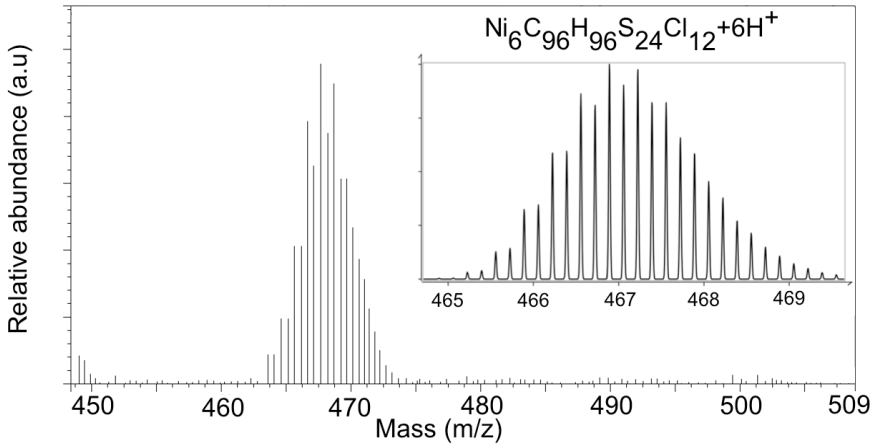

Fig. 6.7. Positive-ion ESI-MS spectrum of $[Ni_6(cpss)_{12}]$ in dichloromethane in the presence of trifluoromethanesulfonic acid; the isotopic distribution pattern simulated for $[Ni_6C_{96}H_{96}S_{24}Cl_{12}]+6H^+$ (inset).

6.2.8. Electrocatalytic H_2 Evolution by [$Ni_6(cpss)_{12}$]

Cyclic voltammograms of [$Ni_6(cpss)_{12}$] in the presence of up to twelve equivalents of protic acids, such as dichloroacetic acid and monochloroacetic acid were recorded in order to assess the electrochemical properties of the protonated [$Ni_6(cpss)_{12}$] cluster. The reduction peak of the [$Ni_6(cpss)_{12}$] wheel is slightly shifted towards more positive potential upon the protonation (–1.05 V) and a new reduction event appears around –1.5 V *vs*. Ag/AgCl; the current height of this new cathodic peak increases with increasing concentration of the acid (Fig. 6.8a).[29] This reduction is accompanied by the formation of bubbles on the surface of the electrode, confirming the production of dihydrogen gas by the electrocatalytic reduction of protons.[39,47] The positive shift in the reduction potential of the protonated [$Ni_6(cpss)_{12}$] complex is almost negligible, since the protonation of the thioether sulfur does not seem to affect the nickel(II) ion electronically, as indicated by the electronic absorption spectra. This rules out the direct protonation of the metal center prior to the reduction.[29] The definite peak-like shape of the catalytic reduction event is indicative of a diffusion-controlled electrocatalytic process and the catalytic reaction is rapid enough, so that the current is controlled by the diffusion of the substrate to the electrode surface.[39,47,48] The same experiment was carried out with monochloroacetic acid, in order to investigate the effect of the pK_a of the proton source. Despite the change in the pK_a, the reduction of the protonated [Ni_6L_{12}] complex occurs at the same potential as for dichloroacetic acid. However, the potential at which molecular hydrogen evolution occurs moved towards a slightly more negative potential of -1.6 V (Fig. 6.8b).[49]

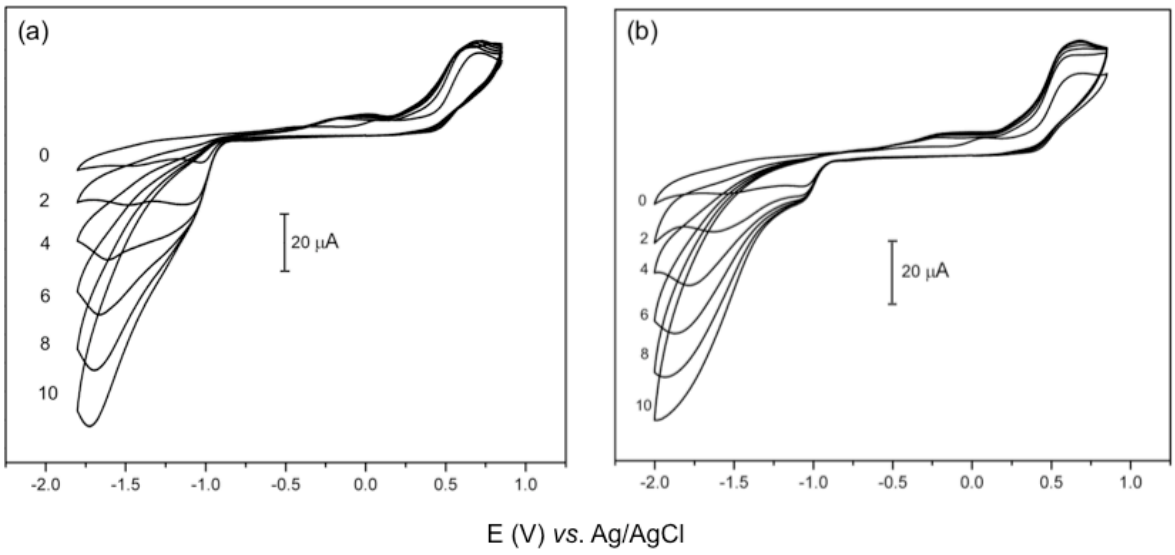

Fig. 6.8. Cyclic voltammograms of [$Ni_6(cpss)_{12}$] (0.5 mM in DMF + 0.1 M *n*-Bu_4NPF_6) in the absence (R = 0) and presence (R = [acid]/[Ni] = 2, 4, 6, 8, 10) of (a) dichloroacetic acid and (b) chloroacetic acid at a static glassy carbon working electrode with a Pt wire auxiliary electrode. Scan rate 200 mV/s.

6.2.9. Proposed Catalytic Mechanism

The axial coordination of two of the thioether sulfurs observed in the X-ray crystal structure, the protonation of the thioether sulfurs as observed with ^{1}H NMR spectroscopy and the electrochemical results described above, in combination, resulted in the following proposed catalytic cycle shown in Scheme 6.2.

Central in the proposed mechanism (Scheme 6.2) is the parent nickel(II) ion with a coordinated thioether sulfur. Protonation occurs at the thioether sulfurs as indicated by ^{1}H NMR spectroscopy and ESI-MS spectrometry. The protonated $[Ni_6(cpss)_{12}]$ complex is electrochemically reduced at –1.05 V. The second reduction observed at –1.5 V in the case of dichloroacetic acid and at –1.6 V in the case of chloroacetic acid must be accompanied by a second protonation step, thereby liberating molecular hydrogen and regenerating the catalyst. The absence of notable changes in the anodic wave in the cyclic voltammograms suggests that after the release of molecular hydrogen the oxidation part solely arises from the reformed $[Ni_6(cpss)_{12}]$ cluster. The participation of the reduced metal center in the dihydrogen evolution is further confirmed by the observation that dihydrogen evolution does not occur at around –1.5 V, when only the bidentate thioether-thiol ligand is used instead of $[Ni_6(cpss)_{12}]$.

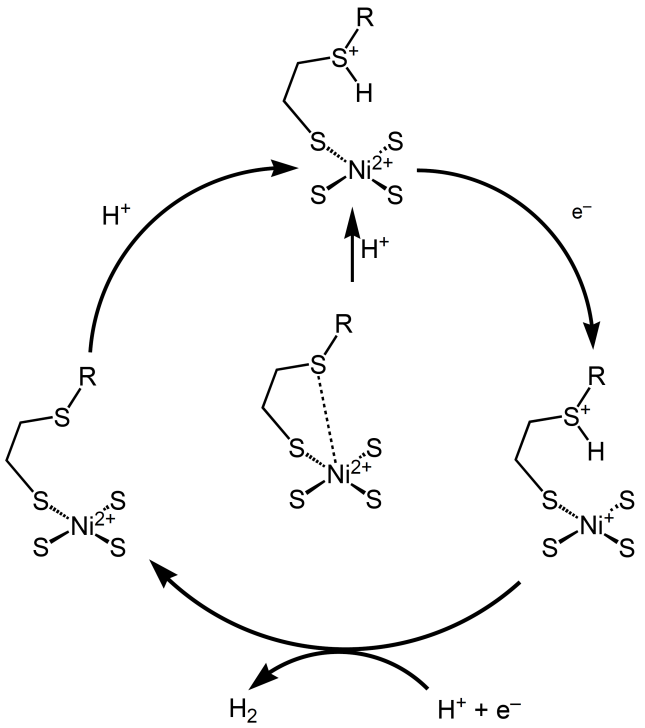

Scheme 6.2. Proposed mechanism of the catalytic cycle for the reduction of protons by $[Ni_6(cpss)_{12}]$ based on the protonation and electrochemical studies; the global charges are not indicated. Only one nickel center of the hexanuclear $[Ni_6(cpss)_{12}]$ complex is illustrated for the sake of clarity. R represents the 4-chlorophenyl group of the ligand.

6.2.10. Immobilization of [$Ni_6(cpss)_{12}$] on a Pyrolitic Graphite Electrode

In the view of possible application in proton exchange membranes[50,51] and in order to shed light on the mechanism of proton reduction, the [$Ni_6(cpss)_{12}$] cluster was immobilized on the surface of an edge plane pyrolitic graphite (EPPG) electrode using known immobilization techniques.[52] Furthermore, in this way the amount of catalyst used can be decreased and the reusability can be increased. Cyclic voltammograms of acetonitrile solutions of 0.1 M dichloroacetic were recorded using the EPPG before and after immobilization of the [$Ni_6(cpss)_{12}$] complex on the surface of the electrode.

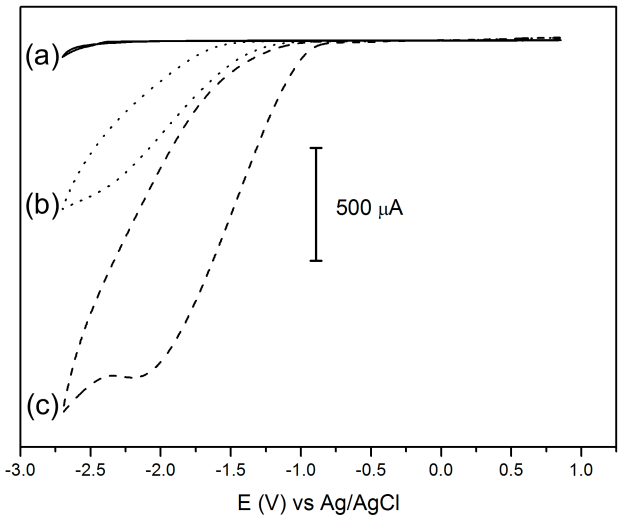

Fig. 6.9. Blank CV of acetonitrile (**a**); CV of a 0.1 M solution of dichloroacetic acid (**b**) containing 0.1 M *n*-Bu_4NPF_6 on a static edge plane pyrolitic graphite electrode; CV of 0.1 M solution of dichloroacetic acid (**c**) on a [$Ni_6(cpss)_{12}$]-immobilized static edge plane pyrolitic graphite electrode with a Pt wire auxiliary electrode (see experimental section for the details of immobilization). Scan rate 200 mV/s.

Reduction of dichloroacetic acid occurs around –2.35 V on the surface of the unmodified EPPG electrode, while the same event happens around –2.13 V after adsorption of the [$Ni_6(cpss)_{12}$] complex on the surface of the EPPG electrode (Fig. 6.1). The increase in the current height of the reduction peak and the shift in reduction potential to a more positive value by 220 mV clearly indicate the catalyzing ability of the [$Ni_6(cpss)_{12}$] cluster. The stability of the immobilized compound was checked with multiple runs of the cyclic voltammogram. After 30 scans the current height is unchanged, but the potential of the proton reduction has shifted towards slightly more negative potentials. Furthermore, a Tafel plot of the cyclic voltammogram of electrocatalytic proton reduction (log current density vs. potential), drawn between –1.2 and –1.8 V displays a slope of 75 mV/decade suggesting a Nernstian pre-equilibrium followed by a rate-determining chemical potential-independent step.[53] The deviation

from the value of 60 mV/decade may be due to a double-layer effect. Chemically this could imply that the proton binds from an equilibrium reaction and then some chemical rate-determining step, such as structural rearrangement or proton migration leads to H_2 or a precursor for H_2 formation; proton migration from the thioether sulfur to the reduced metal center may be involved in the catalytic cycle, as reported for the models of [FeFe] hydrogenases.[54-56]

6.3. Conclusions

In conclusion, the hexanuclear nickel(II)-thiolato cluster $[Ni_6(cpss)_{12}]$ has been synthesized, with NiS_4 square-planar and NiS_5 square-pyramidal units in the same molecule. The NiS_5 units resemble the Ni centre in [NiFe] hydrogenase.[44] The chemical oxidation of the $[Ni_6(cpss)_{12}]$ complex with iodine yields the dinuclear complex $[Ni_2(cpss)_2I_2]$ via an unstable intermediate as observed in the electrochemistry. The low-spin square-pyramidal nickel(II) center of the NiS_5 unit as observed from the X-ray crystal structure and from the ^1H NMR spectra of the $[Ni_6(cpss)_{12}]$ cluster, closely resembles the nickel(II) center of the [NiFe] hydrogenase in its Ni-R state.[27,57,58] The protonation of the low-spin hexanuclear nickel thiolate metallacrown $[Ni_6(cpss)_{12}]$, has been demonstrated using ^1H NMR spectroscopy and ESI-MS spectrometry. The protonated $[Ni_6(cpss)_{12}]$ complex is extremely stable, as studied by NMR and electronic spectroscopy. Furthermore, it was shown to be a functional mimic of hydrogenases, as it acts as an electrocatalyst with the evolution of dihydrogen in the presence of protons. Furthermore, the proposed catalytic cycle closely follows the route as proposed for the natural enzymatic system.[27,57,58] First, the $[Ni_6(cpss)_{12}]$ cluster is protonated and reduced (at –1.05 V vs Ag/AgCl); then, the second reduction step coupled with a protonation (at –1.5 or –1.6 V vs Ag/AgCl) induces the release of dihydrogen. In the proposed catalytic cycle of the hydrogenases, the Ni-SI state has a nickel(II) center and a protonated thiolate ligand, which undergoes reduction accompanied by proton abstraction to form the Ni-L state which contains a nickel(I) center.[27,57,58] Immobilization of the $[Ni_6(cpss)_{12}]$ cluster on an electrode surface further highlights its electrocatalytic ability.

6.4. Experimental Section

6.4.1. General

Synthesis of the ligand precursor TU-cpss is described in Chapter 2 along with the characterizations and other instrumental techniques.

6.4.2. Synthesis of $[Ni_6(cpss)_{12}]$

To a suspension of $[Ni(acac)_2]$ (0.51 g, 2 mmol) in 30 ml of toluene was added two equivalents of TU-cpss (1.13 g, 4 mmol). After the addition of two equivalents of NMe_4OH

(0.72 g, 4 mmol), the solution was refluxed for 2 h. The resulting brown solution was filtered and the solvent was evaporated under reduced pressure to give a dark brown oil. Ethanol (5 ml) was added to the dark brown oil yielding 0.63 g of a reddish–brown solid (yield 72%). Rectangular shaped tiny reddish–brown crystals suitable for X-ray diffraction were isolated from a solution of methanol and acetone (1 : 1) after standing for one day at room temperature. **^{1}H NMR**: δ_H [300.13 MHz, CD_2Cl_2, 298 K]) 7.31 (d, 2H, phenyl ring, chelate), 7.24 (d, 2H, phenyl ring, chelate), 7.12 (s, 4H, phenyl ring, monodentate), 3.18 (t, 2H, Ph-S-C*H*$_2$-CH$_2$-S-, chelate), 2.87 (t, 2H, Ph-S-C*H*$_2$-CH$_2$-S-, monodentate), 2.32 (t, 2H, Ph-S-CH$_2$-C*H*$_2$-S-, chelate), 2.01 (t, 2H, Ph-S-CH$_2$-C*H*$_2$-S-, monodentate). **^{13}C NMR:** δ_C [75.47 MHz, CD_2Cl_2, 298 K] 131.32 (Ph-C2, chelate), 130.64 (Ph-C2, monodentate), 129.58 (Ph-C3, chelate), 129.42 (Ph-C3, monodentate), 37.42 (Ph-S-*C*H$_2$-CH$_2$-S-, chelate), 34.59 (Ph-S-*C*H$_2$-CH$_2$-S-, monodentate), 32.25 (Ph-S-CH$_2$-*C*H$_2$-S-, chelate), 26.52 (Ph-S-CH$_2$-*C*H$_2$-S-, monodentate). **Elemental analysis (%):** calculated for $C_{96}H_{96}Cl_{12}Ni_6S_{24}$ (2796.95): C 41.23, H 3.46, S 27.51, found C 40.97, H 3.53, S 27.24.

6.4.3. Synthesis of [$Ni_2(cpss)_2I_2$]

To a solution of [$Ni_6(cpss)_{12}$] (0.28 g, 0.1 mmol) in 30 ml of dichloromethane was added a solution of three equivalents of iodine (0.076 g, 0.3 mmol) in 30 ml of dichloromethane and the reaction mixture was stirred for one hour at room temperature. After filtration of the white precipitate and evaporation of the solvent in open air for two days dark brown block-shaped crystals suitable for X-ray diffraction were isolated in 83% yield corresponding to [$Ni_2(cpss)_2I_2$]. **^{1}H NMR:** δ_H [300.13 MHz, CD_2Cl_2, 298 K] 7.30 (dd, 8H, phenyl ring), 3.19 (t, 4H, Ph-S-C*H*$_2$-CH$_2$-S-), 2.83 (t, 4H, Ph-S-CH$_2$-C*H*$_2$-S-). **^{13}C NMR:** δ_C [75.47 MHz, CD_2Cl_2, 298 K] 131.26 (Ph-C2), 129.32 (Ph-C3), 37.23 (Ph-S-*C*H$_2$-CH$_2$-S-), 32.03 (Ph-S-CH$_2$-*C*H$_2$-S-). **Elemental analysis (%):** calculated for $C_{16}H_{16}Cl_2I_2Ni_2S_4$ (778.65): C 24.68, H 2.07, S 16.47, found C 24.53, H 1.98, S 16.29.

6.4.4. Crystallographic data for [$Ni_6(cpss)_{12}$]

Reflections were measured on a Nonius Kappa CCD diffractometer with rotating anode (graphite monochromator, λ = 0.71073 Å) at a temperature of 150 K. The structures were solved with automated Patterson methods using the program DIRDIF[59] and refined with SHELXL-97[60] against F^2 of all reflections. Non-hydrogen atoms were refined with anisotropic displacement parameters. Hydrogen atoms were refined with a riding model. Geometry calculations and checking for higher symmetry was performed with the PLATON program.[61]

$C_{96}H_{96}Cl_{12}Ni_6S_{24}$, Fw = 2796.95, 0.28 × 0.04 × 0.02 mm^3, triclinic, P-1 (no. 2), a = 11.8667(12), b = 13.9186(12), c = 18.843(2) Å, α = 75.996(11), β = 76.080(11), γ =

74.991(13)°, V = 2863.7(5) Å^3, Z = 1, D_x = 1.622 g cm^{-3}, μ = 1.73 mm^{-1}. 55 395 Reflections were measured up to a resolution of (sin $\theta/\lambda)_{max}$ = 0.60 Å^{-1}. An absorption correction based on multiple measured reflections was applied (0.64–0.0.97 correction range). 10 355 Reflections were unique (R_{int} = 0.1398), of which 6121 were observed [$I > 2\sigma(I)$]. 622 Parameters were refined with no restraints. $R1/wR2$ [$I > 2\sigma(I)$]: 0.0596/0.0863. $R1/wR2$ [all refl.]: 0.1311/0.1048. S = 1.049. Residual electron density between −0.47 and 0.54 eÅ^{-3}.

6.4.5. Crystallographic data for $[Ni_2(cpss)_2I_2]$

$C_{16}H_{16}Cl_2I_2Ni_2S_4$, Fw = 778.65, 0.36 × 0.21 × 0.03 mm^3, monoclinic, $C2/c$ (no. 15), a = 16.4582(5), b = 15.0185(6), c = 9.8037(2) A°, β = 110.134(2)◦, V = 2275.16(13) Å^3, Z = 4, D_x = 2.273 g cm^{-3}, μ = 4.97 mm^{-1}. 20 584 Reflections were measured up to a resolution of (sin θ/λ)max = 0.65A° Å^{-1}. An absorption correction based on multiple measured reflections was applied (0.33–0.0.86 correction range). 2622 Reflections were unique (R_{int} = 0.0311), of which 2179 were observed [$I > 2\sigma(I)$]. 118 Parameters were refined with no restraints. $R1/wR2$ [$I > 2\sigma(I)$]: 0.0203/0.0387. $R1/wR2$ [all refl.]: 0.0319/0.0413. S = 1.056. Residual electron density between −0.42 and 0.37 eÅ^{-3}.

6.5. References

1. V. Artero and M. Fontecave, *Coord. Chem. Rev.*, 2005, **249**, 1518-1535.
2. S. P. Best, *Coord. Chem. Rev.*, 2005, **249**, 1536-1554.
3. C. Zhang, S. Takada, M. Kolzer, T. Matsumoto and K. Tatsumi, *Angew. Chem.-Int. Edit. Engl.*, 2006, **45**, 3768-3772.
4. E. Bouwman and J. Reedijk, *Coord. Chem. Rev.*, 2005, **249**, 1555-1581.
5. P. M. Vignais, *Coord. Chem. Rev.*, 2005, **249**, 1677-1690.
6. R. Cammack, R. Frey and R. Robson, *Hydrogen as a Fuel. Learning from Nature*, Taylor & Francis, London, 2001.
7. M. Murugesu, F. Wernsdorfer, K. A. Abboud and G. Christou, *Angew. Chem.-Int. Edit.*, 2005, **44**, 892-896.
8. S. Piligkos, G. Rajaraman, M. Soler, N. Kirchner, J. van Slageren, R. Bircher, S. Parsons, H. U. Gudel, J. Kortus, W. Wernsdorfer, G. Christou and E. K. Brechin, *J. Am. Chem. Soc.*, 2005, **127**, 5572-5580.
9. A. J. Tasiopoulos, A. Vinslava, W. Wernsdorfer, K. A. Abboud and G. Christou, *Angew. Chem.-Int. Edit.*, 2004, **43**, 2117-2121.
10. C. M. Zaleski, E. C. Depperman, J. W. Kampf, M. L. Kirk and V. L. Pecoraro, *Angew. Chem.-Int. Edit.*, 2004, **43**, 3912-3914.
11. F. K. Larsen, J. Overgaard, S. Parsons, E. Rentschler, A. A. Smith, G. A. Timco and R. E. P. Winpenny, *Angew. Chem.-Int. Edit.*, 2003, **42**, 5978-5981.
12. L. E. Jones, A. Batsanov, E. K. Brechin, D. Collison, M. Helliwell, T. Mallah, E. J. L. McInnes and S. Piligkos, *Angew. Chem.-Int. Edit.*, 2002, **41**, 4318-4321.
13. A. L. Dearden, S. Parsons and R. E. P. Winpenny, *Angew. Chem.-Int. Edit.*, 2001, **40**, 151-154.
14. S. X. Liu, S. Lin, B. Z. Lin, C. C. Lin and J. Q. Huang, *Angew. Chem.-Int. Edit.*, 2001, **40**, 1084-+.
15. S. P. Watton, P. Fuhrmann, L. E. Pence, A. Caneschi, A. Cornia, G. L. Abbati and S. J. Lippard, *Angew. Chem.-Int. Edit.*, 1997, **36**, 2774-2776.
16. J. Sletten and J. A. Kovacs, *Acta Chem. Scand.*, 1994, **48**, 929-932.

17. M. Capdevila, P. Gonzalezduarte, J. Sola, C. Focesfoces, F. H. Cano and M. Martinezripoll, *Polyhedron*, 1989, **8**, 1253-1259.
18. W. Gaete, J. Ros, X. Solans, M. Fontaltaba and J. L. Brianso, *Inorg. Chem.*, 1984, **23**, 39-43.
19. P. Woodward, L. F. Dahl, E. W. Abel and B. C. Crosse, *J. Am. Chem. Soc.*, 1965, **87**, 5251-&.
20. Z. Yu, M. Wang, P. Li, W. B. Dong, F. J. Wang and L. C. Sun, *Dalton Trans.*, 2008, 2400-2406.
21. B. Keita, S. Floquet, J. F. Lemonnier, E. Cadot, A. Kachmar, M. Benard, M. M. Rohmer and L. Nadjo, *J. Phys. Chem. C*, 2008, **112**, 1109-1114.
22. L. C. Song, Z. Y. Yang, Y. J. Hua, H. T. Wang, Y. Liu and Q. M. Hu, *Organometallics*, 2007, **26**, 2106-2110.
23. Y. Oudart, V. Artero, J. Pecaut, C. Lebrun and M. Fontecave, *Eur. J. Inorg. Chem.*, 2007, 2613-2626.
24. X. Hu, B. S. Brunschwig and J. C. Peters, *J. Am. Chem. Soc.*, 2007, **129**, 8988-8998.
25. G. A. N. Felton, A. K. Vannucci, J. Z. Chen, L. T. Lockett, N. Okumura, B. J. Petro, U. I. Zakai, D. H. Evans, R. S. Glass and D. L. Lichtenberger, *J. Am. Chem. Soc.*, 2007, **129**, 12521-12530.
26. A. M. Appel, D. L. DuBois and M. R. DuBois, *J. Am. Chem. Soc.*, 2005, **127**, 12717-12726.
27. J. C. Fontecilla-Camps, A. Volbeda, C. Cavazza and Y. Nicolet, *Chem. Rev.*, 2007, **107**, 4273-4303.
28. C. Tard, X. M. Liu, S. K. Ibrahim, M. Bruschi, L. De Gioia, S. C. Davies, X. Yang, L. S. Wang, G. Sawers and C. J. Pickett, *Nature*, 2005, **433**, 610-613.
29. S. Ott, M. Kritikos, B. Åkermark, L. C. Sun and R. Lomoth, *Angew. Chem.-Int. Edit.*, 2004, **43**, 1006-1009.
30. A. Volbeda, M. H. Charon, C. Piras, E. C. Hatchikian, M. Frey and J. C. Fontecilla-Camps, *Nature*, 1995, **373**, 580-587.
31. J. A. W. Verhagen, D. D. Ellis, M. Lutz, A. L. Spek and E. Bouwman, *J. Chem. Soc.-Dalton Trans.*, 2002, 1275-1280.
32. H. J. Kruger, G. Peng and R. H. Holm, *Inorg. Chem.*, 1991, **30**, 734-742.
33. Y. Oudart, V. Artero, J. Pecaut and M. Fontecave, *Inorg. Chem.*, 2006, **45**, 4334-4336.
34. S. Canaguier, V. Artero and M. Fontecave, *Dalton Trans.*, 2008, 315-325.
35. Y. Ohki, K. Yasumura, K. Kuge, S. Tanino, M. Ando, Z. Li and K. Tatsumi, *Proc. Natl. Acad. Sci. U. S. A.*, 2008, **105**, 7652-7657.
36. Z. L. Li, Y. Ohki and K. Tatsumi, *J. Am. Chem. Soc.*, 2005, **127**, 8950-8951.
37. X. Hu, B. M. Cossairt, B. S. Brunschwig, N. S. Lewis and J. C. Peters, *Chem. Commun.*, 2005, 4723-4725.
38. O. Pantani, E. Anxolabéhére-Mallart, A. Aukauloo and P. Millet, *Electrochem. Commun.*, 2007, **9**, 54-58.
39. I. Bhugun, D. Lexa and J. M. Saveant, *J. Am. Chem. Soc.*, 1996, **118**, 3982-3983.
40. J. P. Collman, Y. Y. Ha, P. S. Wagenknecht, M. A. Lopez and R. Guilard, *J. Am. Chem. Soc.*, 1993, **115**, 9080-9088.
41. V. Artero and M. Fontecave, *C. R. Chim.*, 2008, **11**, 926-931.
42. O. Pantani, S. Naskar, R. Guillot, P. Millet, E. Anxolabéhére-Mallart and A. Aukauloo, *Angew. Chem., Int. Ed. Engl.*, 2008, **47**, 9948-9950.
43. A. W. Addison, T. N. Rao, J. Reedijk, J. van Rijn and G. C. Verschoor, *J. Chem. Soc.-Dalton Trans.*, 1984, 1349-1356.
44. A. Volbeda, E. Garcia, C. Piras, A. L. deLacey, V. M. Fernandez, E. C. Hatchikian, M. Frey and J. C. FontecillaCamps, *J. Am. Chem. Soc.*, 1996, **118**, 12989-12996.
45. T. J. Mooibroek and P. Gamez, *Inorg. Chim. Acta*, 2007, **360**, 381-404.
46. T. J. Mooibroek, S. J. Teat, C. Massera, P. Gamez and J. Reedijk, *Cryst. Growth Des.*, 2006, **6**, 1569-1574.
47. C. P. Andrieux, C. Blocman, J. M. Dumas-Bouchiat, F. M' Halla and J. M. Savéant, *J. Electroanal. Chem.*, 1980, **113**, 19-40.
48. J. M. Savéant and K. B. Su, *J. Electroanal. Chem.*, 1984, **171**, 341-349.
49. G. A. N. Felton, R. S. Glass, D. L. Lichtenberger and D. H. Evans, *Inorg. Chem.*, 2006, **45**, 9181-9184.
50. P. Millet, F. Andolfatto and R. Durand, *Int. J. Hydrog. Energy*, 1996, **21**, 87-93.

51. P. Millet, T. Alleau and R. Durand, *J. Appl. Electrochem.*, 1993, **23**, 322-331.
52. M. T. De Groot and M. T. M. Koper, *Phys. Chem. Chem. Phys.*, 2008, **10**, 1023-1031.
53. A. J. Bard and L. R. Faulkner, *Electrochemical Methods: Fundamentals and Applications*, John Wiley & Sons, Inc., New York, 2001.
54. C. Greco, M. Bruschi, L. De Gioia and U. Ryde, *Inorg. Chem.*, 2007, **46**, 5911-5921.
55. C. Greco, G. Zampella, L. Bertini, M. Bruschi, P. Fantucci and L. De Gioia, *Inorg. Chem.*, 2007, **46**, 108-116.
56. J.-F. Capon, F. Gloaguen, F. Y. PÈtillon, P. Schollhammer and J. Talarmin, *Coord. Chem. Rev.*, 2009, **253**, 1476-1494.
57. A. L. DeLacey, V. M. Fernandez, M. Rousset and R. Cammack, *Chem. Rev.*, 2007, **107**, 4304-4330.
58. A. Pardo, A. L. De Lacey, V. M. Fernandez, H. J. Fan, Y. B. Fan and M. B. Hall, *J. Biol. Inorg. Chem.*, 2006, **11**, 286-306.
59. P. T. Beurskens, G. Admiraal, G. Beurskens, W. P. Bosman, S. Garcia-Granda, R. O. Gould, J. M. M. Smits and C. Smykalla, University of Nijmegen, The Netherlands, **1999**.
60. G. M. Sheldrick, University of Göttingen, Germany, **1997**.
61. A. L. Spek, *J. Appl. Crystallogr.*, 2003, **36**, 7-13.

7

A Molecular Cage of Ni(II) and Cu(I) Resembling the Active site of Ni-Containing Enzymes†

Abstract. A new mononuclear low-spin nickel(II) dithiolato complex, $[Ni(mpsms)_2]$ reacts with copper iodide to form the hetero-octanuclear cluster $[\{Ni(mpsms)_2\}_2(CuI)_6]$. The precursor complex $[Ni(mpsms)_2]$ and the cluster are fully characterized by physicochemical methods. The molecular structure of the cluster is determined by X-ray crystallography, which has two distorted square-planar NiS_4, four trigonal-planar CuI_2S and two tetrahedral CuI_2S_2 sites; the tetrahedrally distorted NiS_4 units resemble the nickel centre of the [NiFe] hydrogenase and the Ni–S–Cu–I cage structure is compared with the bifunctional enzyme carbon monoxide dehydrogenase/acetyl-coenzyme A synthase (CODH/ACS). Furthermore, novel anagostic Ni···H interactions are observed in the X-ray crystal structure of the molecular cage and have been confirmed to pertain in the solution employing variable temperature ^1H NMR spectroscopic studies.

---

† This chapter is based on: R. Angamuthu, L. L. Gelauff, M. A. Siegler, A. L. Spek. and E. Bouwman, *Chem. Commun.*, **2009**, 2700-2702.

7.1. Introduction

Nickel thiolato complexes, including (hetero-)multinuclear [NiFe], [NiCu], [NiZn] and [NiNi] units, are of interest in the context of their rich redox chemistry[1,2] and structural diversity in supramolecular architectures,[3] as is discussed in Chapter 6. Furthermore, they are important as synthetic models[1,4-7] for environmentally and industrially significant enzymes like hydrogenases, superoxide dismutases and CODH/ACS. The focus of attention for this Chapter is to study the chemistry involving the synthesis and reactivity of nickel thiolate complexes in relation with the structure and function of active sites in nickel-containing enzymes.[1,4-7] The mononuclear [Ni(mpsms)$_2$] discussed in Chapter 4 has now been used in a reaction with CuI resulted in a molecular cage of Ni(II) and Cu(I) resembling the active site of Ni-containing enzymes such as [NiFe] hydrogenase and the A-cluster of the CODH/ACS. This Chapter reports on the formation and structural properties of the cluster [{Ni(mpsms)$_2$}$_2$(CuI)$_6$] having two distorted square-planar NiS$_4$, four trigonal-planar CuI$_2$S and two tetrahedral CuI$_2$S$_2$ sites. In addition, the anagostic interactions between the Ni(II) ions and the *ortho*-protons of the phenyl rings of the ligands are demonstrated using both X-ray crystallography and NMR spectroscopic techniques.

7.2. Results and Discussion

7.2.1. Synthesis

The reaction of Ni(acac)$_2$ with two equivalents of the thiouronium chloride salt of the ligand, in the presence of two equivalents of tetramethylammonium hydroxide led to an immediate colour change to deep brown and the new low-spin square-planar complex [Ni(mpsms)$_2$] was isolated as flocculent reddish-brown crystals in high yield. Equimolar solutions of Ni(mpsms)$_2$ in dichloromethane and copper(I) iodide in acetonitrile were mixed under argon and stirred for an hour to yield a dark brown precipitate. A saturated solution of this product in absolute ethanol was left for slow evaporation under argon atmosphere and dark brown crystals of [{Ni(mpsms)$_2$}$_2$(CuI)$_6$] were formed over several days. The molecular structure of [{Ni(mpsms)$_2$}$_2$(CuI)$_6$], which has been determined by single crystal X-ray diffraction, shows a spectacular cage structure formed by the thiolate sulfurs and copper iodide moieties.

7.2.2. Molecular Structure of [{Ni(mpsms)$_2$}$_2$(CuI)$_6$]

The molecular structure of [{Ni(mpsms)$_2$}$_2$(CuI)$_6$] is shown in Fig. 7.1 and important bond lengths and angles are provided in Table 7.1. The asymmetric unit of [{Ni(mpsms)$_2$}$_2$(CuI)$_6$] contains one crystallographically independent ordered molecule (Fig. 7.1), and no solvent molecules are found in the crystal lattice. The two Ni(II) centers

are in slightly distorted square-planar environments with two thiolate donors and two thioether sulfurs in enforced *cis* positions. The Ni–$S_{thiolate}$ distances [2.1641(14)-2.1788(14) Å] are slightly shorter than the Ni-$S_{thioether}$ distances [2.1856(15)-2.2028(16) Å], as expected. The nickel centers have a slight tetrahedral distortion with a dihedral angle of 3.58(8)° for Ni1 (between the triangular planes S6Ni1S9 and S16Ni1S19) and 9.13(8)° for Ni1A (between the triangular planes S6ANi1S9A and S16ANi1S19A).

Table 7.1. Selected bond lengths (Å) and angles (°) of [{Ni(mpsms)$_2$}$_2$(CuI)$_6$]. Atoms that are labeled with and without 'A' are crystallographically independent.

Cu1···Cu1A	2.6032(10)	Cu2···Cu2A	4.0309(10)	Cu1···Cu3	5.3644(2)
Cu1···Cu2	3.9844(9)	Ni1···Ni1A	6.6421(9)	Ni1···Cu1	3.5495(9)
Ni1···Cu2	3.8655(9)	Ni1···Cu3	3.5982(10)	Ni1–S6	2.1641(14)
Ni1–S9	2.2028(16)	Ni1–S16	2.1757(15)	Ni1–S19	2.1932(14)
Cu1–S6	2.2925(14)	Cu2–S6	2.4417(15)	Cu1–I1	2.5955(8)
Cu1–I2	2.5271(8)	Cu2–I2A	2.6337(7)	Cu2–I3A	2.6296(7)
S6–Ni1–S9	92.17(6)	S9–Ni1–S19	90.04(6)	S16–Ni1–S19	92.08(6)
S6–Ni1–S16	85.82(6)	S6–Ni1–S19	176.89(6)	S9–Ni1–S16	176.47(6)
S6–Cu1–I1	109.11(4)	I1–Cu1–I2	124.21(3)	S6–Cu1–I2	126.61(4)
S6–Cu2–I2A	110.40(4)	I2A–Cu2–S16A	99.90(4)	I3A–Cu2–S16A	107.65(4)
S6–Cu2–I3A	98.61(4)	S6–Cu2–S16A	122.29(5)	I2A–Cu2–I3A	119.38(3)

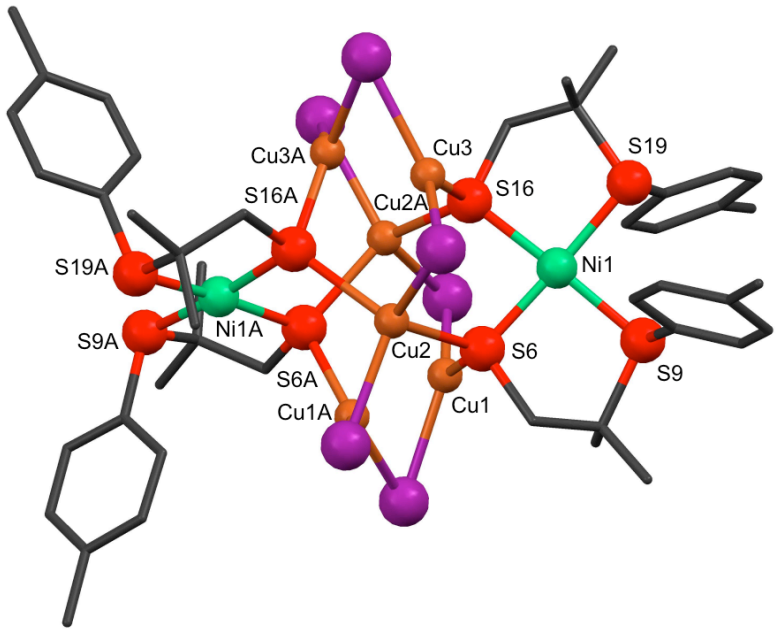

Fig. 7.1. Perspective view of [{Ni(mpsms)$_2$}$_2$(CuI)$_6$]. Ni, green; Cu, brown; S, red; I, violet; C, grey. Hydrogens are omitted for clarity.

The six copper iodide moieties are forming altogether a twelve membered Cu_6I_6 puckered-crown (Fig. 7.2) in which the six iodides are bridged between the copper ions in μ-fashion to form this crown. The two square-planar NiS_4 units are capping this crown from both sides utilizing their thiolate sulfurs to form [{Ni(mpsms)$_2$}$_2$(CuI)$_6$]; the dihedral

angle defined by these two S_4 planes is 72.10(5)°. Each thiolate sulfur is bound to two copper(I) ions, of which one is in a trigonal-planar geometry and the other possesses tetrahedral geometry. The tetrahedral copper ions are shared between the two NiS_4 units by direct S–Cu–S bridging, while the trigonal-planar copper ions are shared through a S–Cu–I–Cu–S bridge. The four thiolate sulfurs and the six copper(I) iodide units together form a cage structure in the middle of the two NiS_4 units (Fig. 7.2).

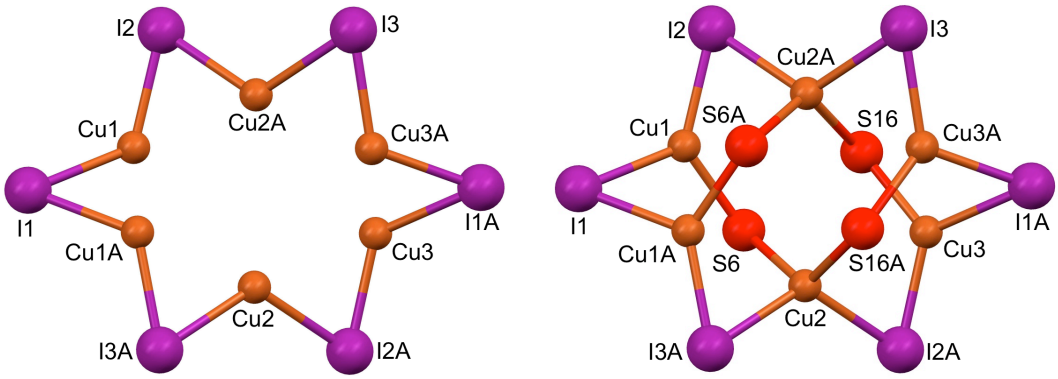

Fig. 7.2. Perspective views of the Cu_6I_6 puckered-crown (left) and $Cu_6I_6S_4$ cage (right) in $[\{Ni(mpsms)_2\}_2(CuI)_6]$.

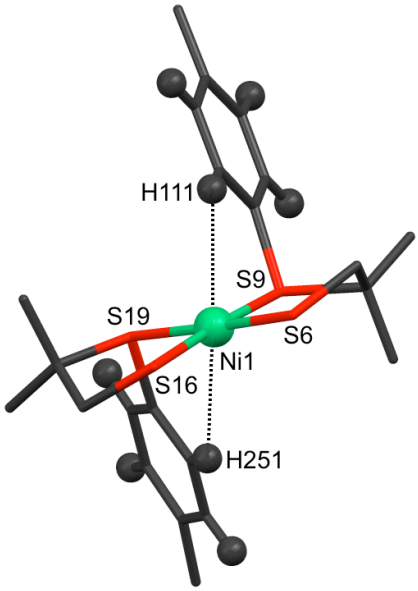

Fig. 7.3. Perspective view of one $[Ni(mpsms)_2]$ part of $[\{Ni(mpsms)_2\}_2(CuI)_6]$ with the atomic labeling of selected atoms. The nickel-to-hydrogen interactions are shown; only the hydrogens present in the 4–methylphenyl rings are shown for clarity. Ni1···H111, 2.739; Ni1···H251, 2.781; Ni1A···H152, 2.696; Ni1A···H212, 2.626 Å

The trigonal-planar copper ions, Cu1, Cu1A, Cu3 and Cu3A, are found in an I_2S coordination sphere of which one of the two iodide ions is bridged to a trigonal-planar copper ion, while the other iodide is bridged to a tetrahedral copper ion. The bond distances of iodide to copper vary due to this difference in bridging; the angles in the

trigonal-planar CuI_2S moieties are not strictly 120°. Likewise, the angles in the tetrahedral CuI_2S_2 moieties also deviate from the ideal angle of 109.5°, and range from 98.61(4)° to 122.29(5)°.

An interesting interaction between the nickel(II) ion and the *ortho*–protons of the phenyl rings is observed, with distances of about 2.7 Å in both NiS_4 units of $[\{Ni(mpsms)_2\}_2(CuI)_6]$ (Fig. 7.3). Considering these interactions as bonding, the coordination geometry of the nickel ion could be described as pseudo-octahedral, in an $H_2N_2S_2$ chromophore, in which two *ortho*–protons occupy the axial sites of the octahedron.

7.2.3. Proton NMR Spectral Studies of $[\{Ni(mpsms)_2\}_2(CuI)_6]$

To investigate whether the structure of the $[\{Ni(mpsms)_2\}_2(CuI)_6]$ is retained in solution, ^1H NMR spectra of the complex have been recorded in CD_2Cl_2 solution at different temperatures ranging from 183 to 303 K. (Fig. 7.4). Even though there are four crystallographically distinct ligands are present in the complex, the ^1H NMR spectrum at room temperature shows only a single set of signals suggesting that the four ligands are equivalent in solution. Interestingly, upon cooling the sample to 263 K the signals start to broaden and eventually split into multiple sharp signals at 183 K.

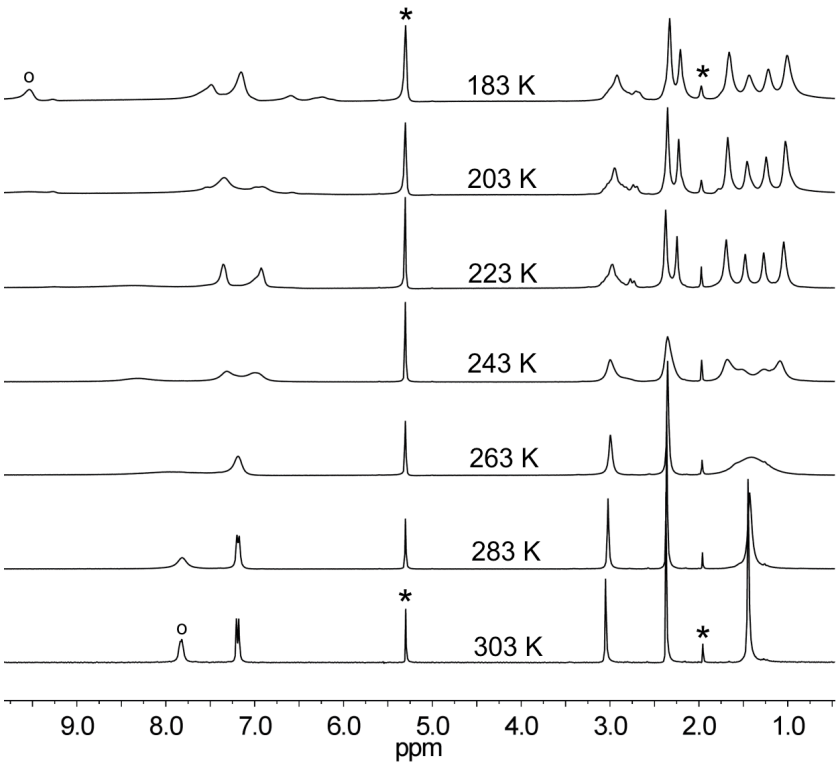

Fig. 7.4. ^1H NMR of $[\{Ni(mpsms)_2\}_2(CuI)_6]$ in CD_2Cl_2 recorded in different temperatures ranging between 183 and 303 K. ★, signals from CD_2Cl_2 (5.32 ppm) and acetone (2 ppm); **O**, signals from the *ortho*–protons of the phenyl rings.

The fluxional axial and equatorial exchange of the dimethyl groups is slow or inhibited at low temperature; the singlet of the dimethyl protons (at 1.4 ppm) consequently splits into four sharp signals. Furthermore, the two aromatic resonances (at 7.1 and 7.8 ppm) are split in a number of resonances with different intensities; the protons involved in an interaction with the nickel ions are observed at δ 9.5 ppm upon cooling to 183 K. The downfield shift of these protons in the NMR spectrum, and the fact that they are pointing in the direction of the occupied d_z^2 orbital of the nickel(II) ions (Fig. 7.3) at a distance of about 2.7 Å on average in the crystal structure, suggest that these interactions should be considered as anagostic or hydrogen bonding.[8-10]

7.2.4. Redox Properties of [{Ni(mpsms)$_2$}$_2$(CuI)$_6$]

The cyclic voltammogram of the [NiCu] cluster in a dichloromethane solution shows a number of irreversible oxidation processes (–0.273 V, –0.180 V, -0.076 V vs Ag/AgCl) and a single irreversible reduction process (–0.914 V) which are difficult to assign unequivocally due to the presence of the large number of redox non-innocent partners available in the multinuclear structure of [{Ni(mpsms)$_2$}$_2$(CuI)$_6$] (Fig. 7.5).

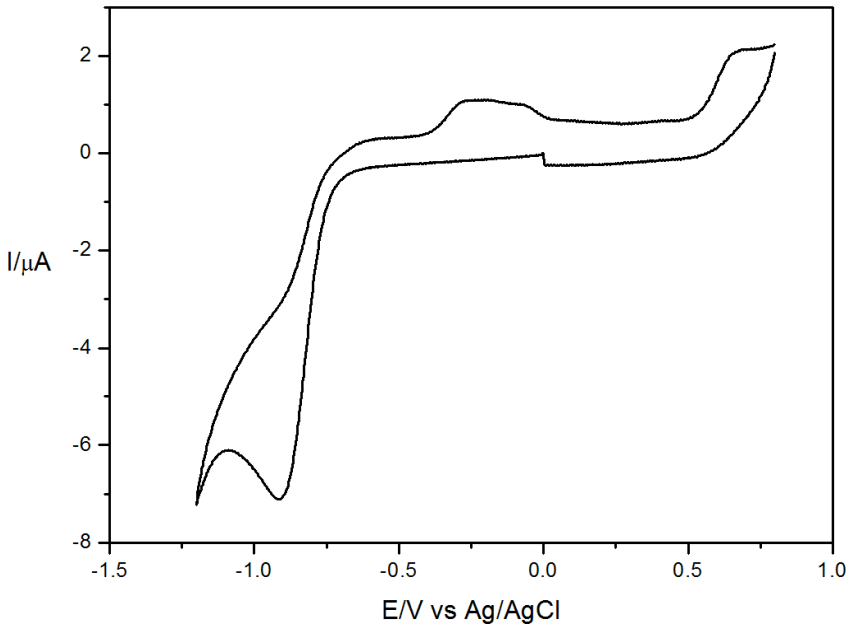

Fig. 7.5. Cyclic voltammogram of 0.5 mM solution of [{Ni(mpsms)$_2$}$_2$(CuI)$_6$] in CH_2Cl_2 containing 0.05 M $(NBu_4)PF_6$. Scan rate 100 mV s^{-1}. Static glassy carbon disc working electrode and Pt wire counter electrode used with Ag/AgCl reference electrode.

7.2.5. Relevance to the Ni-containing Enzymes

The presence of the 4-methylphenyl ring bound to the thioether sulfur paves the way to exhibit the attraction between the *ortho*–protons of the phenyl ring and the low-spin Ni(II) ion, as identified in the crystal structure and NMR spectroscopy (Fig. 7.3 and

Fig. 7.4). It appears that the cluster [{Ni(mpsms)$_2$}$_2$(CuI)$_6$] is the first compound with an NiS_4 coordination displaying the aforesaid nickel to proton anagostic interactions.

The tetrahedrally distorted NiS_4 coordination spheres of Ni1 and Ni1A in [{Ni(mpsms)$_2$}$_2$(CuI)$_6$] resemble the nickel centre of the "EPR silent active form" (Ni-SI$_a$) of [NiFe] hydrogenase with an $Ni^{II}Fe^{II}$ electronic configuration that is the starting point of the catalytic cycle of the enzymatic action; protonation of this form generates the Ni-SI$_b$ form which then turns into Ni-R state upon hydrogenation.[11-14] Development of model complexes with this kind of Ni···H interaction may help to better understand the mechanistic insights of the [NiFe] hydrogenase and further to obtain improved structural and functional mimics. Furthermore, the Ni–μ_3–S–Cu motifs forming the cage in [{Ni(mpsms)$_2$}$_2$(CuI)$_6$] resemble the A-cluster of the CODH/ACS with a low-spin square-planar nickel (Ni$_d$) and bridging μ_3–thiolates connecting the tetrahedral copper (M$_p$).

7.3. Conclusions

In summary, a novel molecular cage of hetero-octanuclear nickel(II) copper(I) cluster, [{Ni(mpsms)$_2$}$_2$(CuI)$_6$] has been isolated in good yield by the reaction of the low-spin square-planar NiS_4 complex Ni(mpsms)$_2$ with CuI and has been characterized using single-crystal X-ray diffraction, NMR and electrochemistry techniques. The anagostic interactions between the nickel and aromatic *ortho*-protons have been demonstrated by the variable temperature NMR studies also to pertain in solution.

7.4. Experimental Procedures

7.4.1. General

Synthesis of the ligand precursor TU-mpsms and the mononuclear nickel complex [Ni(mpsms)$_2$] are described in Chapters **2** and **4**, respectively, along with the characterizations.

7.4.2. Synthesis of [Ni(mpsms)$_2$(CuI)$_6$]

A solution of CuI (191 mg, 1 mmol) in 10 ml acetonitrile was added to a solution of [Ni(L)$_2$] (483 mg, 1 mmol) in 10 ml chloroform and the mixture was stirred for an hour. After evaporation of the solvent, the product was recrystallized by the slow evaporation of an ethanolic solution in an argon atmosphere. Dark-brown crystals suitable for X-ray diffraction were obtained over a few days. [Ni(mpsms)$_2$(CuI)$_6$] was reproduced in bulk by the reaction between one equivalent of complex [Ni(mpsms)$_2$] and three equivalents of CuI in acetonitrile as a brown powder (87%). **^{1}H NMR:** δ_H [300.13 MHz, CD_2Cl_2, 298 K]) 7.84 (bs, 8H, phenyl–*ortho*–*H*), 7.22 (d, 8H, phenyl–*meta*–*H*), 3.06 (s, 8H, –C*H*$_2$–S–), 2.38 (s, 12H, C*H*$_3$–Ph), 1.46 (s, 24H, –C(C*H*$_3$)$_2$–) **^{13}C NMR:** δ_C [75.47 MHz, CD_2Cl_2, 298 K] 143.52

(Ph-C4), 136.54 (Ph-C3), 131.18 (Ph-C2), 122.75 (Ph-C1), 64.35 (–*C*(CH_3)$_2$–), 49.27 (–*C*H_2–), 27.69 ((–C(*C*H_3)$_2$–), 21.94 (*C*H_3–Ph). **Elemental Analysis (%):** calculated for $C_{44}H_{60}Cu_6I_6Ni_2S_8$·3$CHCl_3$, C 22.91, H 2.58, S 10.41, found, C 22.67, H 2.54, S 10.28

7.4.3. Crystallographic Data for [{Ni(mpsms)$_2$}$_2$(CuI)$_6$]

All reflection intensities were measured at 110(2) K using a Nonius KappaCCD diffractometer (rotating anode) with graphite-monochromated Mo *K*α radiation (λ = 0.71073 Å) under the program *COLLECT*.[15] The program *PEAKREF*[16] was used to refine the cell dimensions. Data reduction was done using the program *EVALCCD*.[17] The structure was solved with the program *DIRDIF08*[18] and was refined on F^2 with *SHELXL-97*.[19] Analytical absorption corrections based on crystal face-indexing were applied to the data using *SADABS*.[19] The temperature of the data collection was controlled using the system *OXFORD CRYOSTREAM 600* (manufactured by *OXFORD CRYOSYSTEMS*). The H-atoms were placed at calculated positions (*AFIX 23* or *AFIX 43* or *AFIX 137*) with isotropic displacement parameters having values 1.2 times *U*eq of the attached C atom. Geometry calculations were performed with the *PLATON* program.[20]

$C_{44}H_{60}Cu_6I_6Ni_2S_8$, Fw = 2105.46, dark brown needles, 0.04 × 0.07 × 0.24 mm^3, triclinic, *P*-1 (no. 2), a = 11.6566(5), b = 14.1559(4), c = 19.9857(7) Å, α = 86.088(1), β = 84.143(1), γ = 70.505(2) °, V = 3090.5(2) Å^3, Z = 2, D_x = 2.263 g cm^{-3}, μ = 5.915 mm^{-1}. 67305 Reflections were measured up to a resolution of $(\sin \theta/\lambda)_{max}$ = 0.62 Å^{-1}. An absorption correction based on multiple measured reflections was applied (0.48–0.87 correction range). 12170 Reflections were unique (R_{int} = 0.063), of which 8494 were observed [$I > 2\sigma(I)$]. 607 Parameters were refined. $R1/wR2$ [$I > 2\sigma(I)$]: 0.0361/0.0553. $R1/wR2$ [all refl.]: 0.0742/0.0634. S = 1.022. Residual electron density between −0.90 and 0.98 eÅ^{-3}.

7.5. References

1. E. Bouwman and J. Reedijk, *Coord. Chem. Rev.*, 2005, **249**, 1555-1581.
2. V. Artero and M. Fontecave, *Coord. Chem. Rev.*, 2005, **249**, 1518-1535.
3. C. Zhang, S. Takada, M. Kölzer, T. Matsumoto and K. Tatsumi, *Angew. Chem.-Int. Edit. Engl.*, 2006, **45**, 3768-3772.
4. J. A. W. Verhagen, C. Tock, M. Lutz, A. L. Spek and E. Bouwman, *Eur. J. Inorg. Chem.*, 2006, 4800-4808.
5. J. A. W. Verhagen, M. Beretta, A. L. Spek and E. Bouwman, *Inorg. Chim. Acta*, 2004, **357**, 2687-2693.
6. J. A. W. Verhagen, M. Lutz, A. L. Spek and E. Bouwman, *Eur. J. Inorg. Chem.*, 2003, 3968-3974.
7. J. A. W. Verhagen, D. D. Ellis, M. Lutz, A. L. Spek and E. Bouwman, *J. Chem. Soc.-Dalton Trans.*, 2002, 1275-1280.
8. E. Bouwman, R. K. Henderson, A. K. Powell, J. Reedijk, W. J. J. Smeets, A. L. Spek, N. Veldman and S. Wocadlo, *J. Chem. Soc.-Dalton Trans.*, 1998, 3495-3499.
9. W. B. Yao, O. Eisenstein and R. H. Crabtree, *Inorg. Chim. Acta*, 1997, **254**, 105-111.
10. M. Brookhart, M. L. H. Green and G. Parkin, *Proc. Natl. Acad. Sci. U. S. A.*, 2007, **104**, 6908-6914.

11. A. L. DeLacey, V. M. Fernandez, M. Rousset and R. Cammack, *Chem. Rev.*, 2007, **107**, 4304-4330.
12. W. Lubitz, E. Reijerse and M. van Gastel, *Chem. Rev.*, 2007, **107**, 4331-4365.
13. P. E. M. Siegbahn, J. W. Tye and M. B. Hall, *Chem. Rev.*, 2007, **107**, 4414-4435.
14. P. Jayapal, M. Sundararajan, I. H. Hillier and N. A. Burton, *Phys. Chem. Chem. Phys.*, 2008, **10**, 4249-4257.
15. Nonius, Nonius BV., Delft, The Netherlands, 1999.
16. A. M. M. Schreurs, University of Utrecht, The Netherlands, 2005.
17. A. J. M. Duisenberg, L. M. J. Kroon-Batenburg and A. M. M. Schreurs, *J. Appl. Cryst.*, 2003, **36**, 220.
18. P. T. Beurskens, G. Beurskens, R. de Gelder, S. Garcia-Granda, R. O. Gould and J. M. M. Smiths, University of Nijmegen, The Netherlands, **2008**.
19. G. M. Sheldrick, *Acta Cryst.*, 2008, **A64**, 112.
20. A. L. Spek, *J. Appl. Cryst.*, 2003, **36**, 7.

8

Light-Induced C–S Bond Cleavage in a Nickel Thiolate Complex: Relevance to the Function of Methyl Coenzyme M Reductase (MCR)†

Abstract. The dinuclear complex $[Ni(ebsms)]_2$ is found to be light-sensitive; it yielded another dinuclear complex $[Ni(S_2S')]_2$ and oligoisobutylene sulfide through a C–S bond cleavage reaction provoked by the light-induced formation of a Ni(I)-S$^{\bullet}$ radical species in solution. The presence of Ni(I)-S$^{\bullet}$ radical character of $[Ni(ebsms)]_2$ is indicated by the unusual disorder observed in the X-ray crystal structure of $[Ni(ebsms)]_2$, the broad signals observed in the ^1H NMR spectra of $[Ni(ebsms)]_2$ and the products obtained from the light-induced C–S bond cleavage reaction. The results are discussed in the light of the function of methyl coenzyme M reductase.

---

† R. Angamuthu, W. Roorda, M. A. Siegler, A. L. Spek and E. Bouwman, *manuscript in preparation*.

8.1. Introduction

Metal thiolate complexes, especially nickel thiolates, are enjoying much attention among bioinorganic chemists as they are important both as structural and as functional models for environmentally and industrially significant enzymes, such as hydrogenases,[1-3] superoxide dismutases,[4,5] carbon monoxide dehydrogenase/acetylcoenzyme A synthase[6-9] and methyl coenzyme M reductase (MCR).[10,11]

MCR is the key enzyme in biological methane formation by methanogenic archaea. The coenzyme F430 in MCR, a Ni-tetrahydrocorphinoid (Scheme 8.1), catalyzes the reaction of methyl-coenzyme M (CH_3–SCoM; methylthioethyl sulfonate) and coenzyme B (HS–CoB; 7-mercaptoheptanoylthreonine phosphate) to form methane and the disulfide Co–S–S–CoB.[10-12] Two widely accepted mechanistic pathways have been proposed for this reaction, based on the results of a number of experimental and theoretical studies on F430. Yet several other hypotheses are consistent with most of the findings. The key question to be resolved is whether **(1)** the catalysis involves a nucleophilic attack of a Ni(I) center of active F430 on the methyl group of CH_3–SCoM (in the presence of H^+) to form a Ni(III)–CH_3 intermediate and HS–CoM, or **(2)** the Ni(I) center attacks the thioether sulfur of CH_3–SCoM to form a Ni(II)–SCoM intermediate and a $CH_3^{\bullet}$ radical.[11-15] Due to the limited life time of the active form of the enzyme, experimental studies to detect short-lived intermediates in order to shed light on the mechanism have so far been unsuccessful.[10]

The focus of this chapter is the chemistry and reactivity of the nickel thiolate complex $[Ni(ebsms)]_2$ reported in Chapter **3** in relation with the function of the enzyme methyl coenzyme M reductase. This chapter reports on the light-induced reactivity of the complex $[Ni(ebsms)]_2$, forming the complex $[Ni(S_2S')]_2$ and oligoisobutylene sulfide (Scheme 8.2).

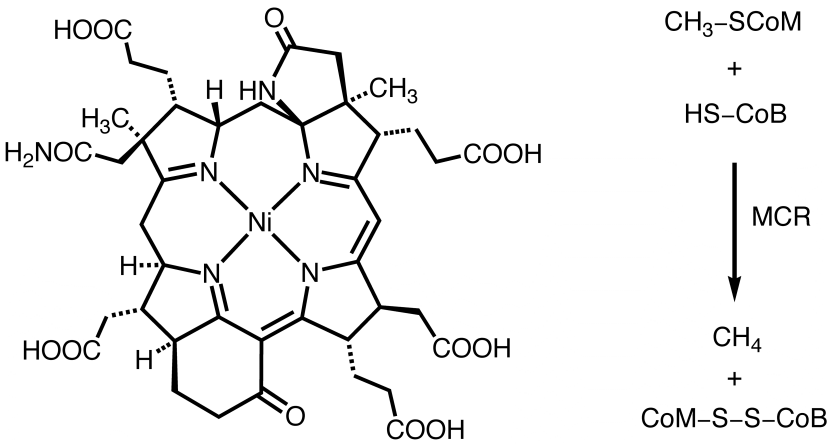

Scheme 8.1. Schematic structure of coenzyme F430 and the catalytic reaction leading to methane formation.

8.2. Results and Discussion

8.2.1. Synthesis of $[Ni(ebsms)]_2$ and the Formation of $[Ni(S_2S')]_2$

The reaction of $Ni(acac)_2$ with one equivalent of the dithiouronium dichloride salt of the ligand H_2ebsms in toluene in the presence of two equivalents of tetramethylammonium hydroxide resulted in an immediate colour change to deep brown. The new low-spin nickel complex $[Ni(ebsms)]_2$ was isolated as a reddish-brown powder in high yield (see Chapter **3**). Single crystals of complex $[Ni(ebsms)]_2$ suitable for X-ray diffraction were obtained within hours from a dichloromethane solution. The yield of the reaction was found to be very low (15%) when the reaction was performed in the presence of day light; however, it could be dramatically improved using dark conditions (63%). Crystals of different dimensionality compared to the original complex $[Ni(ebsms)]_2$ were obtained from an acetonitrile solution of the complex $[Ni(ebsms)]_2$ after two weeks and revealed the structure of the new compound $[Ni(S_2S')]_2$ as determined by X-ray diffraction (Fig. 8.1).

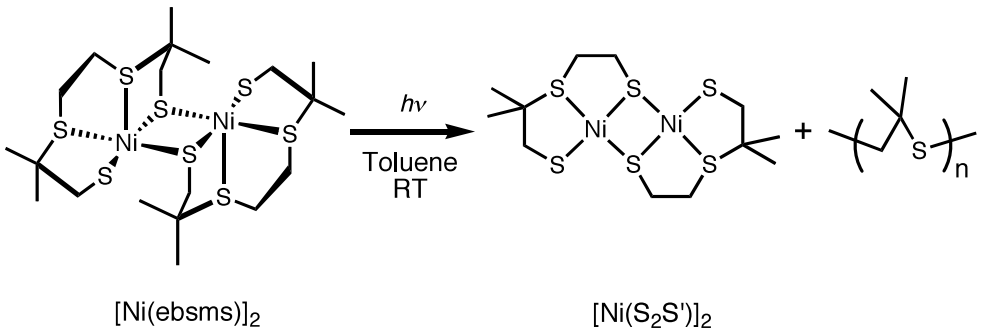

$[Ni(ebsms)]_2$ $[Ni(S_2S')]_2$

Scheme 8.2. Schematic drawing of $[Ni(ebsms)]_2$ and the formation of $[Ni(S_2S')]_2$ and oligoisobutylene sulfide upon irradiation.

8.2.2. Molecular Structures of the Complexes $[Ni(ebsms)]_2$ and $[Ni(S_2S')]_2$

Although the molecular structure of the complex $[Ni(ebsms)]_2$ has been discussed in detail in Chapter **3**, some basic molecular details of the structure are discussed here as well. The asymmetric unit of $[Ni(ebsms)]_2$ contains one molecule of the dinuclear complex $[Ni(ebsms)]_2$ and one molecule of dichloromethane. The two Ni(II) centers are in slightly distorted square-pyramidal environments with three thiolate donors and two thioether sulfurs coordinated to each nickel center (Fig. 8.1). Two thiolate sulfurs from the same ligand coordinate to a nickel center in *trans* position of each NiS_4 square plane. One of these two thiolate sulfurs is bound in a terminal position and the other sulfur is bridging to the adjacent nickel center. One thioether sulfur of the same ligand and a thiolate bridging sulfur from the other ligand occupy the remaining two *trans* positions; the remaining thioether of the ligand binds axially to the Ni(II) center. The $Ni–S_{thiolate}$

distances (bridging, 2.2096(8)–2.2344(8) Å; terminal, 2.1928(8) and 2.1965(10) Å) are shorter than the Ni–$S_{thioether}$ distances (equatorial, 2.2360(8) and 2.246(3) Å; axial, 2.6011(8) and 2.7039(9) Å), as expected. However, a surprisingly short Ni–S distance (Ni1A–S19B, 2.139(3) Å) and unusual disorder is observed for the thioether site S19 (S19A and S19B; site occupancy = 0.6 : 0.4). One of the ligands in $[Ni(ebsms)]_2$ is disordered over two conformations: the major component is related by an approximate twofold axis to the first ligand, the other is related by an approximate inversion center.

Table 8.1. Selected distances (Å) and angles (°) for $[Ni(S_2S')]_2$.

Ni1–Ni2	2.7041(3)	Ni1–S11	2.2107(6)	Ni1–S12	2.1783(5)
Ni1–S21	2.1387(5)	Ni1–S31	2.1604(6)	Ni2–S11	2.1818(6)
Ni2–S12	2.2057(5)	Ni2–S22	2.1347(5)	Ni2–S32	2.1559(5)
S11–Ni1–S12	81.53(2)	S11–Ni1–S21	89.18(2)	S11–Ni1–S31	173.30(2)
S12–Ni1–S21	170.35(2)	S12–Ni1–S31	97.55(2)	S21–Ni1–S31	91.37(2)
S11–Ni2–S12	81.57(2)	S11–Ni2–S22	169.37(2)	S11–Ni2–S32	97.51(2)
S12–Ni2–S22	89.25(2)	S12–Ni2–S32	175.06(2)	S22–Ni2–S32	91.19(2)
Ni1–S11–Ni2	75.99(2)	Ni1–S12–Ni2	76.17(2)		

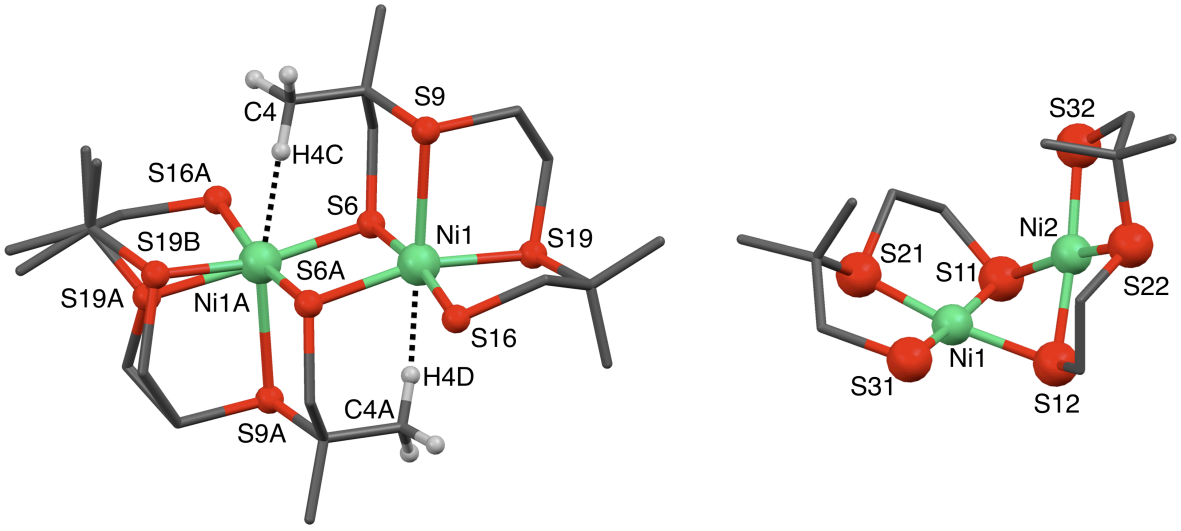

Fig. 8.1. Perspective views of $[Ni(ebsms)]_2$ (left) and $[Ni(S_2S')]_2$ (right). Ni, green; S, red; C, gray. Dichloromethane and hydrogen atoms are omitted for clarity. See Chapter 3 for further details regarding to the structure of $[Ni(ebsms)]_2$. Selected distances (Å) and angles (°) for $[Ni(S_2S')]_2$ are provided in Table 8.1.

The asymmetric unit of $[Ni(S_2S')]_2$ contains one dinuclear nickel complex of a new tridentate thioether-dithiolate (S_2S') ligand (Fig. 8.1 and Table 8.1). Two NiS_2S' units are bridged together by thiolate donors, resulting in two square-planar NiS_4 moieties. Interestingly, the Ni–$S_{thiolate}$ distances (bridging, 2.1784(5)–2.2056(6) Å; terminal, 2.1604(6) and 2.1560(6) Å) are longer than the Ni–$S_{thioether}$ distances (2.1386(5) and 2.1347(5)). This observation is in contrast to previous reports;[6,16-18] however, it is not unprecedented, as this behaviour has been reported in two previous cases in

literature.[19,20] Usually, the Ni–$S_{thioether}$ distances are longer than (or similar to) the Ni–$S_{thiolate}$ distances.[21] The dihedral angle of the two NiS_4 planes in the complex $[Ni(S_2S')]_2$ (77.78°) is slightly larger than in related molecules (75.19° and 75.73°),[19,20] which might be due to the methyl groups of the ligand. Interestingly, the S_2S' ligand of this complex formed from the $S_2S'_2$ ligand of the complex $[Ni(ebsms)]_2$ upon loss of one of the isobutylene sulfide arms. In contrast to $[Ni(S_2S')]_2$ and other oligonuclear nickel thiolate complexes[18,22] the molecular structure of the complex $[Ni(ebsms)]_2$ exhibits an unusual coplanar structure, instead of the butterfly or folded structures known for $[Ni(S_2S')]_2$ (see Chapter **3**). The dihedral angle between the two NiS_4 planes in the complex $[Ni(ebsms)]_2$ is approximately 7°. This coplanarity may be due to the dimethyl groups of the ligand, as reflected by the Ni-H_{Me} anagostic interactions (2.66 and 2.74 Å), which may be strong enough to not allow the NiS_4 planes to fold (Fig. 8.1). The first example of this kind of Ni···H anagostic interaction in a nickel thiolate (NiS_4) system, which was observed to be stable both in the solid and in solution has been described in Chapter **7**.[6]

8.2.3. ^{1}H NMR Spectra of the Complex $[Ni(ebsms)]_2$

To investigate whether the dinuclear structure and the Ni···H interactions are retained in solution, ^{1}NMR spectra of the complex $[Ni(ebsms)]_2$ have been recorded in $CDCl_3$ solution at different temperatures ranging from 223 K to 303 K (Fig. 8.2). The NMR spectra in the whole temperature range show rather broad signals indicating some paramagnetism due to high-spin Ni(II) species, possibly due to the highly strained coordination geometry. The two Ni···H interactions observed in the X-ray structure of $[Ni(ebsms)]_2$ indeed are visible in the ^{1}H NMR spectra in the presence of a broad peak at 4.15 ppm in the whole temperature range. This stability of the Ni···H interaction agrees with the observed coplanarity of the two NiS_4 planes of the complex $[Ni(ebsms)]_2$ in the crystal structure, and indicates that the dinuclear structure is largely retained in solution.

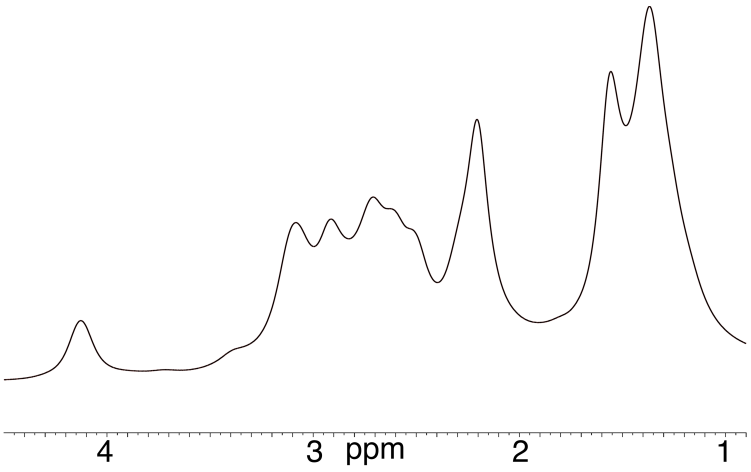

Fig. 8.2. ^{1}H NMR spectra of $[Ni(ebsms)]_2$ in $CDCl_3$ recorded at 223 K.

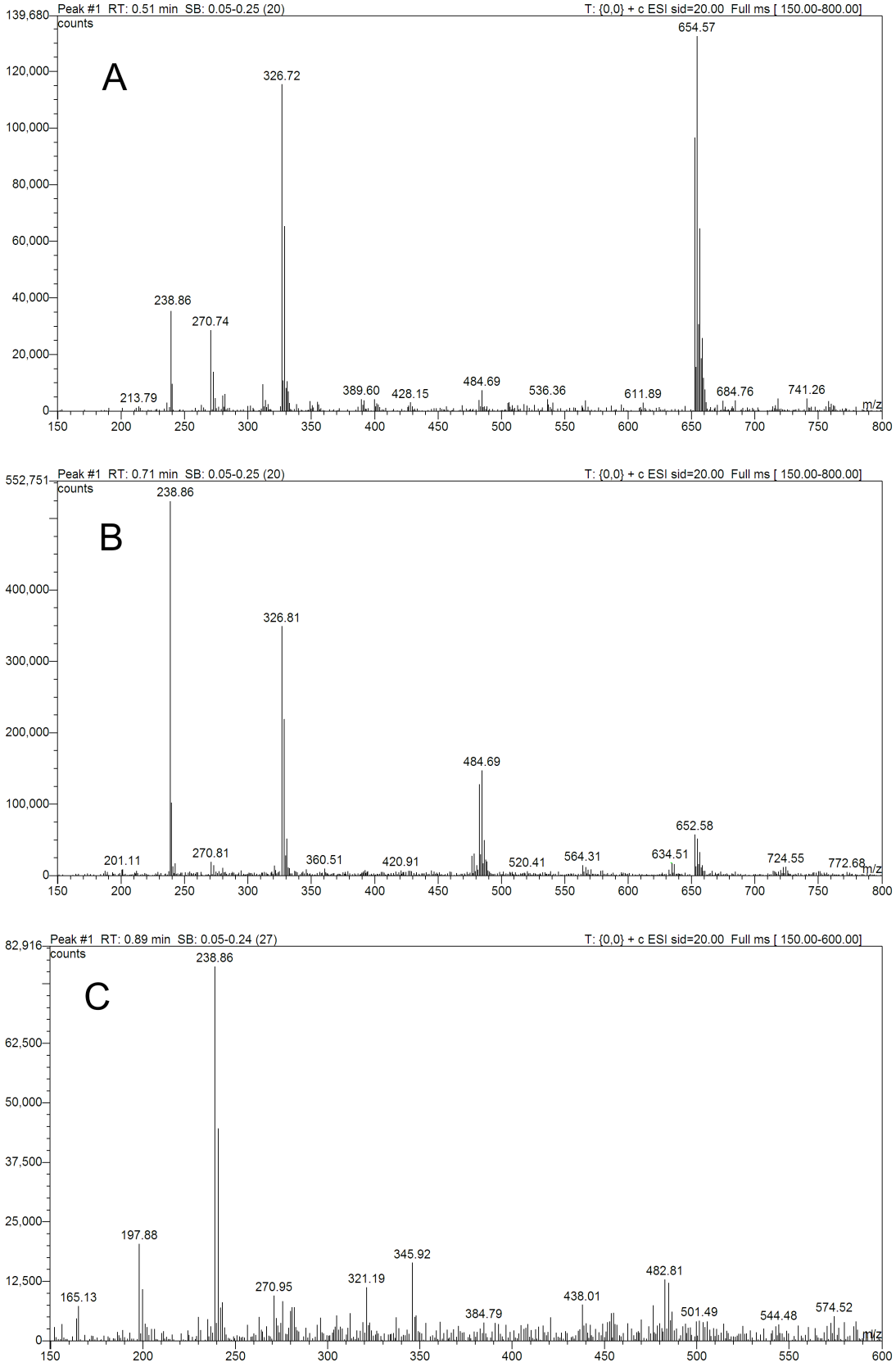

Fig. 8.3. Formation of $[Ni(S_2S')]_2$ from $[Ni(ebsms)]_2$, as followed by ESI-MS spectrometry upon irradiation on the toluene solution of $[Ni(ebsms)]_2$ at room temperature; (A) 0 hrs, (B) 6 hrs, (C) 12 hrs; *m/z* = 326.72 = $[Ni(ebsms)+H]^+$, *m/z* = 652.57 = $[Ni_2(ebsms)_2+H]^+$, *m/z* = 238.86 = $[Ni(S_2S')+H]^+$.

8.2.4. Light-Induced Disintegration of the Complex [Ni(ebsms)]$_2$ Monitored with ESI-MS Spectrometry

In order to understand the mechanism of formation of [Ni(S_2S')]$_2$ from [Ni(ebsms)]$_2$, a toluene solution of [Ni(ebsms)]$_2$ was irradiated using a mercury arc lamp; samples were collected at regular intervals and were analyzed using ESI-MS spectrometry. Interestingly, the formation of the new compound [Ni(S_2S')]$_2$ is clearly identified from the ESI-MS spectra, showing the gradual disappearance of the molecular ion peaks of [Ni(ebsms)]$_2$ with simultaneous growth of the peak corresponding to [Ni(S_2S')] (Fig. 8.3). When using the mercury lamp the decomposition reaction needs about 12 hrs for completion with the formation of [Ni(S_2S')]$_2$ and isobutylene sulfide. In an endeavour to detect the decomposition products and isolate pure [Ni(S_2S')]$_2$, the reaction mixture was distilled gently around 85 °C. A few drops of isobutylene sulfide were obtained; ESI-MS spectrometry and NMR spectra confirmed the identity of oligo-isobutylene sulfide. The remaining mixture was passed through a neutral alumina column and the pure [Ni(S_2S')]$_2$ was obtained in 87% yield.

8.2.5. Mechanistic Considerations

The unusual disorder of the nickel-thioether bond observed in the X-ray crystal structure of [Ni(ebsms)]$_2$ (Ni1A–S19A/S19B in Fig. 8.1) and the broadened signals observed in the variable temperature ^{1}H NMR spectra of the complex [Ni(ebsms)]$_2$ indicate that the Ni(I)–S$^\bullet$ radical character may already present in the complex [Ni(ebsms)]$_2$. However, when kept in the dark the compound [Ni(ebsms)]$_2$ is found to be rather stable. Therefore, the light-induced formation of [Ni(S_2S')]$_2$ and oligoisobutylene sulfide from [Ni(ebsms)]$_2$ indicates that the Ni(I)–S$^\bullet$ radical and the concurrent reactivity is formed only after irradiation of the complex [Ni(ebsms)]$_2$.

In order to investigate the radical character of the complex [Ni(ebsms)]$_2$, it was reacted with iodomethane in the presence and absence of light and the products were analysed using ESI-MS spectrometry. Usually the reaction between methyl halides and metal thiolate compounds results in the methylation of the available thiolate sulfurs only.[23,24] If the thioether sulfur of the complex [Ni(ebsms)]$_2$ has radical character it would be more reactive than the thiolates. After the reaction of [Ni(ebsms)]$_2$ with methyl iodide, a molecular ion peak at *m/z* = 268.92 was observed, matching with the calculated isotopic distribution for the fragment [[Ni(S_2S')+2CH_3] (269.00). This result was obtained both in the presence and absence of light. The three fragments 0.5×M1, M2 and M3, as shown in Scheme 8.3, are all matching the observed *m/z* value of 268.92. All these fragments suggest that the Ni1–S19 bond is highly reactive; a possible explanation for this reactivity might be the presence of partial Ni(I)–S$^\bullet$ character. Furthermore, the fragment M3 might

be the responsible species for the observed *m/z* value of 268.92 as the fragments M1 and M2 are not the most likely products due to the steric hindrance and the instability, respectively. Even though the present results support the presence of Ni(I)–S$^{\bullet}$ character, they are inadequate to confirm this hypothesis; therefore further studies are necessary.

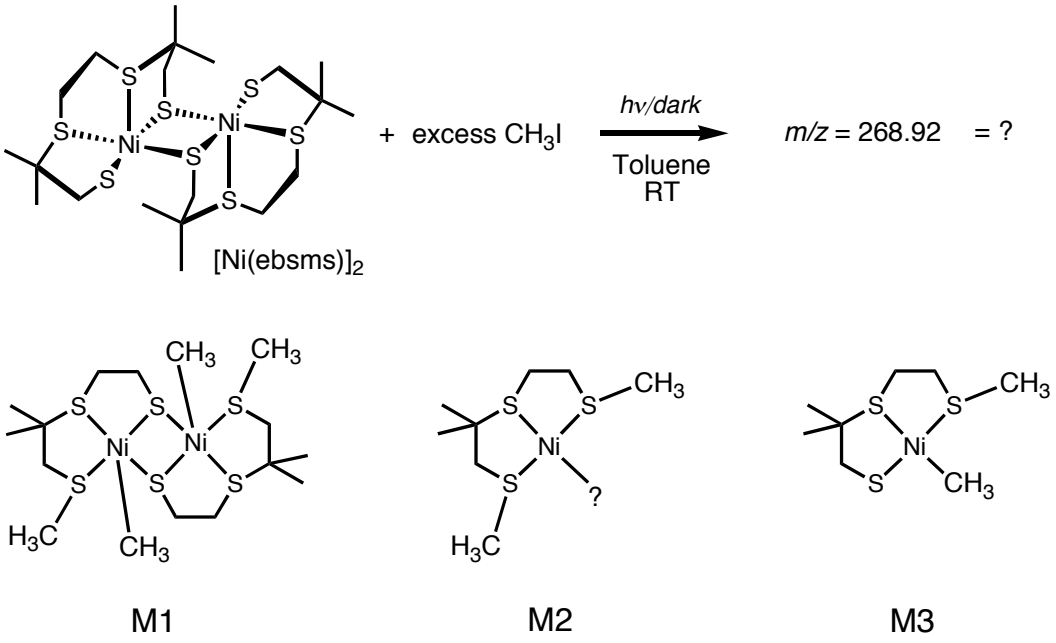

Scheme 8.3. Reaction of $[Ni(ebsms)]_2$ with excess methyl iodide in toluene and the possible products.

8.2.6. Relevance to the Function of MCR

One of the two main intermediates proposed in the catalytic mechanism of MCR is an organometallic methyl–Ni(III) F430 species (MCR_{Me}).[11] The MCR_{Me} is proposed to be formed from the reaction between the active MCR and methyl halides.[25,26] Yet the formation from the native substrate (CH_3–SCoM) has never been found. A recent paper from Siegbahn and coworkers reports the investigation of the reaction between MCR and the substrates CH_3X (X = I, Br, Cl) and CH_3–SCoM using advanced theoretical methods;[27] the reaction between MCR and CH_3X is exothermic and the CH_3–Ni(F430) species is proposed to be in a resonance state between $^{\downarrow}{}^{\bullet}CH_3$–$^{\uparrow\uparrow}$Ni(II) F430 radical and CH_3–$^{\uparrow}$Ni(III) F430. The observed broad signals in the ^{1}H NMR spectra of $[Ni(ebsms)]_2$ are supposedly due to paramagnetic species, and the reactivity of the Ni–S bond in the presence of light and with methyl iodide correlates with the theoretically observed results. Further exploration of the reaction of $[Ni(ebsms)]_2$ with substrates such as CH_3–S–CH_3 are needed to shed light on the electronic structure of both $[Ni(ebsms)]_2$ and $[Ni(S_2S')]_2$.

8.3. Conclusions

A unique reactivity of $[Ni(ebsms)]_2$ is encountered in the formation of the low-spin nickel complex $[Ni(S_2S')]_2$, which is produced upon irradiation of the complex $[Ni(ebsms)]_2$. Formation of the complex $[Ni(S_2S')]_2$ from complex $[Ni(ebsms)]_2$ is demonstrated to proceed through a C–S bond-cleavage reaction provoked by the light-induced formation of Ni(I)-$S^{\bullet}$ radical species in solution. Further exploration of this light-induced reaction with a combination of techniques and the reaction of $[Ni(ebsms)]_2$ with other substrates, or with small molecules may shed light onto the reaction pathway.

8.4. Experimental Procedures

8.4.1. General

The synthesis of the thiouronium precursor salt TU-ebsms and the complex $[Ni(ebsms)]_2$ are discussed in Chapters **2** and **3**, respectively.

8.4.2. Formation of Complex [Ni(S$_2$S')]

The complex $[Ni(ebsms)]_2$ (0.98 g, 3 mmol) was dissolved in 50 ml toluene and the solution was irradiated using a Hanau TQ81 high-pressure mercury arc lamp. Completion of the reaction was monitored by recording ESI-MS spectra of the samples collected in regular intervals. The reaction needed 12 hrs for completion and the formed isobutylene sulfide was removed from the reaction mixture by distilling the reaction mixture gently. Isobutylene sulfide started to come out when the temperature was around 85 °C and the collection flask was kept at 0 °C using an ice bath. Elemental Analysis (%): Calculated for $C_{12}H_{24}S_6Ni_2$ (478.1): C 30.15, H 5.06, S 40.24. found C 30.27, H 5.18, S 40.29. MS (ESI): (*m/z*) calculated for $C_6H_{13}S_3Ni$ $[M/2+H^+]$ requires (monoisotopic mass) 238.95, found 238.86.

8.4.3. X-ray Crystallographic Data for [Ni(S$_2$S')]

X-ray intensities were measured on a Nonius KappaCCD diffractometer with rotating anode (graphite monochromator, λ = 0.71073 Å). Intensity integration was performed with EvalCCD[28] ($[Ni(ebsms)]_2$) or HKL2000[29] ($[Ni(S_2S')]$). Absorption correction was based on multiple measured reflections. The structures were solved with SHELXS-97[30] using Direct Methods and refined against F^2 of all reflections using SHELXL-97.[30] Non-hydrogen atoms were refined freely with anisotropic displacement parameters. Hydrogen atoms were introduced in calculated positions and refined with a riding model. Geometry calculations and checking for higher symmetry was performed with the PLATON program.[31]

$C_{12}H_{24}Ni_2S_6$, Fw = 478.09, black block, 0.53 x 0.36 x 0.30 mm^3, orthorhombic, Pbca (no. 61), a = 12.9460(1), b = 22.3503(2), c = 12.9344(1) Å, V = 3742.53(5) $Å^3$, Z = 8, D_x = 1.697 g/cm^3, μ = 2.67 mm^{-1}. 45877 Reflections were measured up to a resolution of $(\sin \theta/\lambda)_{max}$ = 0.65 $Å^{-1}$ at a temperature of 150(2) K. Absorption correction range 0.32-0.45. 4284 Reflections were unique (R_{int} = 0.046), of which 3733 were observed [I>2σ(I)]. 185 Parameters were refined with no restraints. R_1/wR_2 [I > 2σ(I)]: 0.0250 / 0.0598. R_1/wR_2 [all refl.]: 0.0312 / 0.0630. S = 1.057. Residual electron density between -0.38 and 0.49 $e/Å^3$.

8.5. References

1. E. Bouwman and J. Reedijk, *Coord. Chem. Rev.*, 2005, **249**, 1555-1581.
2. V. Artero and M. Fontecave, *Coord. Chem. Rev.*, 2005, **249**, 1518-1535.
3. C. Tard and C. J. Pickett, *Chem. Rev.*, 2009, **109**, 2245-2274.
4. J. Wuerges, J. W. Lee, Y. I. Yim, H. S. Yim, S. O. Kang and K. D. Carugo, *Proc. Natl. Acad. Sci. U. S. A.*, 2004, **101**, 8569-8574.
5. J. Shearer, A. Dehestani and F. Abanda, *Inorg. Chem.*, 2008, **47**, 2649-2660.
6. R. Angamuthu, L. L. Gelauff, M. A. Siegler, A. L. Spek and E. Bouwman, *Chem. Commun.*, 2009, 2700-2702.
7. K. N. Green, S. M. Brothers, B. Lee, M. Y. Darensbourg and D. A. Rockcliffe, *Inorg. Chem.*, 2009, **48**, 2780-2792.
8. Y. Song, M. Ito, M. Kotera, T. Matsumoto and K. Tatsumi, *Chem. Lett.*, 2009, **38**, 184-185.
9. D. J. Evans, *Coord. Chem. Rev.*, 2005, **249**, 1582-1595.
10. U. Ermler, *Dalton Trans.*, 2005, 3451-3458.
11. U. Ermler, W. Grabarse, S. Shima, M. Goubeaud and R. K. Thauer, *Science*, 1997, **278**, 1457-1462.
12. R. K. Thauer, *Microbiology-(UK)*, 1998, **144**, 2377-2406.
13. V. Pelmenschikov and P. E. M. Siegbahn, *J. Biol. Inorg. Chem.*, 2003, **8**, 653-662.
14. V. Pelmenschikov, M. R. A. Blomberg, P. E. M. Siegbahn and R. H. Crabtree, *J. Am. Chem. Soc.*, 2002, **124**, 4039-4049.
15. E. C. Duin and M. L. McKee, *J. Phys. Chem. B*, 2008, **112**, 2466-2482.
16. J. A. W. Verhagen, M. Lutz, A. L. Spek and E. Bouwman, *Eur. J. Inorg. Chem.*, 2003, 3968-3974.
17. J. A. W. Verhagen, D. D. Ellis, M. Lutz, A. L. Spek and E. Bouwman, *J. Chem. Soc.-Dalton Trans.*, 2002, 1275-1280.
18. R. Angamuthu, H. Kooijman, M. Lutz, A. L. Spek and E. Bouwman, *Dalton Trans.*, 2007, 4641-4643.
19. D. Sellmann, D. Haussinger and F. W. Heinemann, *Eur. J. Inorg. Chem.*, 1999, 1715-1725.
20. R. Cao, M. C. Hong, F. L. Jiang, X. L. Xie and H. Q. Liu, *J. Chem. Soc.-Dalton Trans.*, 1994, 3459-3463.
21. M. A. Halcrow and G. Christou, *Chem. Rev.*, 1994, **94**, 2421-2481.
22. C. Zhang, S. Takada, M. Kölzer, T. Matsumoto and K. Tatsumi, *Angew. Chem.-Int. Edit. Engl.*, 2006, **45**, 3768-3772.
23. V. E. Kaasjager, E. Bouwman, S. Gorter, J. Reedijk, C. A. Grapperhaus, J. H. Reibenspies, J. J. Smee, M. Y. Darensbourg, A. Derecskei-Kovacs and L. M. Thomson, *Inorg. Chem.*, 2002, **41**, 1837-1844.
24. O. Yohan, PhD Thesis, *Structural and Functional Models for Hydrogenases*, Université Joseph Fourier-Grenoble I, 2007.
25. N. Yang, M. Reiher, M. Wang, J. Harmer and E. C. Duin, *J. Am. Chem. Soc.*, 2007, **129**, 11028-+.
26. M. Dey, J. Telser, R. C. Kunz, N. S. Lees, S. W. Ragsdale and B. M. Hoffman, *J. Am. Chem. Soc.*, 2007, **129**, 11030-+.

27. S.-l. Chen, V. Pelmenschikov, M. R. A. Blomberg and P. E. M. Siegbahn, *J. Am. Chem. Soc.*, 2009, 10.1021/ja904204g.
28. A. J. M. Duisenberg, L. M. J. Kroon-Batenburg and A. M. M. Schreurs, *J. Appl. Cryst.*, 2003, **36**, 220.
29. Z. Otwinowski and W. Minor, Processing of X-ray diffraction data collected in oscillation mode, in *Macromolecular Crystallography, Pt A*, 1997, pp. 307-326.
30. G. M. Sheldrick, *Acta Cryst.*, 2008, **A64**, 112.
31. A. L. Spek, *J. Appl. Cryst.*, 2003, **36**, 7.

9

Summary, Conclusions and Future Perspectives

9.1. Summary

The global aim of the research discussed in this thesis is the design, synthesis and characterization of suitable structural and functional models for the enzyme [NiFe] hydrogenase. Yet the thesis also describes models of other nickel-containing enzymes resulting from serendipitous findings along the main interest of the thesis.

The first part of Chapter **1** portrays a brief overview of nickel-containing enzymes with a special emphasis on the class of hydrogenases. The structural and functional properties of the enzymes and of specifically selected model complexes are also overviewed. Chapter **1** concludes with the scope of the thesis and a short summary of the strategies proposed for the structural and functional modeling of [NiFe] hydrogenases.

The design, syntheses and characterizations of new tetradentate dithioether-dithiolate ($S_2S'_2$) ligands and bidentate thioether-thiolate (SS') ligands are presented in Chapter **2**; schemes of the syntheses of the ligands and simplified code notations for the ligands and of their precursors, and intermediates have also been provided. The tetradentate ligands are designed/selected in a way that they possess systematically varied steric and electronic properties. The ligands H_2ebss, H_2pbss and H_2xbss have ethyl, propyl and xylyl bridging groups, respectively. Also, these three ligands are substituted with two electron-donating methyl groups on the β–carbons of ethylthiolate arms in order to vary the electronic properties (H_2ebsms, H_2pbsms and H_2xbsms).

The bidentate ligands possess different groups such as benzyl, 4-methylphenyl, 4-chlorophenyl, isobutyl and *n*-hexyl groups on the thioether sulfur, and have been prepared with or without the two methyl groups on the β–carbon of the ethylthiolate arm.

A library of new low-spin nickel complexes of new tetradentate dithioether-dithiolate ligands is reported in Chapter **3**. Two of these complexes, $[Ni(ebsms)]_2$ and [Ni(pbsms)], have been characterized by X-ray crystallography. $[Ni(ebsms)]_2$ is a coplanar dinuclear complex with two slightly distorted square-pyramidal NiS_5 units bridged together by two thiolates. A surprisingly short Ni–$S_{thioether}$ distance (2.139(3) Å) and interesting Ni···H_{Me} interactions (2.66 and 2.74 Å) are also observed in the crystal structure. [Ni(pbsms)] is a mononuclear compound with square-planar structure, similar to the already reported structures of [Ni(pbss)] and [Ni(xbsms)]. The Ni–$S_{thiolate}$ distances in [Ni(pbsms)] are longer than the Ni–$S_{thioether}$ distances as exhibited by [Ni(pbss)], but which is in contrast to the usual observation. These low-spin nickel complexes were reacted with $[Fe(Cp)(CO)_2I]$ to obtain [NiFe] complexes, including one reported complex; their electrocatalytic properties towards

proton reduction are also reported in Chapter **3**. All the six [NiFe] complexes show electrocatalytic activity to produce dihydrogen in the presence of acetic acid as a source of protons. Catalytic reduction of H^+ is observed at potentials as low as –1.19 V *vs*. Ag/AgCl for [Ni(pbss)Fe(CO)Cp](PF_6) in acetonitrile. It was found that increased flexibility of the bridge of the ligands leads to electrocatalysts that need lower overpotentials whereas electron-donating dimethyl-substitution of the ligands leads to the need of higher overpotentials.

The lessons learned from Chapter **3** led to the use of two bidentate SS'-donor ligands instead of one tetradentate $S_2S'_2$-donor ligand, as an increase in flexibility in the NiS_4 coordination sphere favored the lower overpotentials in the proton reduction. Chapter **4** is devoted to analogous [NiFe] complexes based on new [Ni(SS')$_2$] complexes. The [Ni(SS')$_2$] complexes reported in this chapter were obtained by the reaction of Ni(acac)$_2$ with bidentate thioether-thiolate ligands reported in Chapter **2**. The ligands substituted with two methyl groups yield stable mononuclear complexes whereas the ligands without methyl groups yield hexanuclear ([Ni_6(cpss)$_{12}$]) or insoluble oligonuclear ([Ni(mpss)]$_n$) complexes. These low-spin nickel complexes were reacted with [Fe(Cp)$(CO)_2$I] in dichloromethane with slow flow of argon gas, to obtain [NiFe] complexes; their electrocatalytic properties towards proton reduction are also reported in Chapter **3**.

The electrocatalytic proton reduction potential of these [NiFe] compounds, E_{HER} is indeed found to be lower than that of the complexes with tetradentate ligands reported in Chapter **3** (~ –0.9 V *vs*. Ag/AgCl). However, the stability of these [Ni(SS')$_2$Fe(C_5H_5)(CO)](PF_6) complexes is lower than that of the [Ni($S_2S'_2$)Fe(C_5H_5)(CO)](PF_6) complexes in the presence of protic acids; the complexes [Ni(bsms)$_2$Fe(C_5H_5)(CO)](PF_6) and [Ni(cpsms)$_2$Fe(C_5H_5)(CO)](PF_6) are readily decomposed in the presence of acid. This is likely due to the fact that the thioether sulfurs of the [Ni(SS')$_2$Fe(C_5H_5)(CO)](PF_6) complexes are easily protonated, which leads to the decomposition.

In order to make more stable and improved electrocatalysts the [Ni($S_2S'_2$)] complexes were reacted with the [Ru(bpy)$_2$(EtOH)$_2$] moiety and a new class of complexes with the general formula [Ni($S_2S'_2$)Ru(bpy)$_2$](PF_6)$_2$ have been obtained in good yield; their structures and proton reducing abilities are presented in Chapter **5**. The complex [Ni(pbss)Ru(bpy)$_2$](PF_6)$_2$ has been characterized by X-ray crystallography, whereas all the three [Ni($S_2S'_2$)Ru(bpy)$_2$](PF_6)$_2$ complexes reported in Chapter **5** have been characterized using 1D and 2D NMR techniques; the complex [Ni(pbsms)Ru(bpy)$_2$](PF_6)$_2$ is found to have two conformers in solution due to the dynamical motion of the dimethylethylene arms. These three complexes are also found to be active in proton

reduction (–1.43 to –1.01 V *vs*. Ag/AgCl) and are stable in the presence of protic acids such as trifluoroacetic acid for months.

A serendipitously obtained hexanuclear Ni_6-thiolate metallacrown, its reactivity with iodine, protonation studies and the proton reduction abilities are presented in Chapter **6**. Two square-pyramidal NiS_5 units and four NiS_4 square-planar units are bridged together *via* thiolates of the Hcpss ligands in the solid state structure, whereas all the six nickel(II) centers are found to have NiS_5 square-pyramidal geometry in solution as studied by ^{1}H NMR spectroscopy.

The hexanuclear metallacrown $[Ni_6(cpss)_{12}]$ has been demonstrated to functionally resemble the [NiFe] hydrogenases. Protonation of the $[Ni_6L_{12}]$ cluster was studied employing ^{1}H NMR spectroscopy and ESI-MS by the sequential additions of dichloroacetic acid or *p*-toluenesulfonic acid monohydrate into solutions of $[Ni_6L_{12}]$ in CD_2Cl_2 and DMF-d_7, respectively; protonation takes place on the thioether sulfurs available in the metallacrown. The electrochemical properties of both the parent and protonated $[Ni_6L_{12}]$ species have been studied using cyclic voltammetry. Protonated $[Ni_6L_{12}]$ shows an interesting electrocatalytic property as it catalyses the reduction of protons into molecular hydrogen in the presence of protic acids, such as dichloroacetic acid and chloroacetic acid at –1.5 and –1.6 V vs Ag/AgCl in DMF, respectively. A catalytic cycle has been proposed based on the observations from the NMR spectroscopic and electrochemical studies of the metallacrown. The behavior of this electrocatalyst was further studied by its immobilization on the surface of a pyrolitic graphite electrode; reduction of a dichloroacetic acid solution in acetonitrile on the surface of the modified electrode occurs at 220 mV more positive potential compared to the unmodified electrode.

The reaction of the mononuclear complex $[Ni(mpsms)_2]$ with CuI yielded a heterooctanuclear cage of formula $[\{Ni(mpsms)_2\}_2(CuI)_6]$, possessing interesting structural features including Ni···H anagostic interactions, which is reported in Chapter **7**. The molecular structure of the $[Ni_2Cu_6]$ cluster is determined by X-ray crystallography, which shows two distorted square-planar NiS_4, four trigonal-planar CuI_2S and two tetrahedral CuI_2S_2 sites; the tetrahedrally distorted NiS_4 units resemble the nickel centre of the [NiFe] hydrogenase and the Ni–S–Cu–I cage structure is compared with the bifunctional enzyme carbon monoxide dehydrogenase/acetyl-coenzyme A synthase (CODH/ACS). Furthermore, novel anagostic Ni···H interactions are observed in the X-ray crystal structure of the molecular cage and have been confirmed to pertain in solution, employing variable temperature ^{1}H NMR spectroscopic studies. These Ni···H interactions have been observed for the first time in a complex of NiS_4 coordination sphere.

A light-induced C–S bond cleavage in a nickel thiolate complex with relevance to the function of methyl-coenzyme M reductase (MCR) is presented in Chapter **8**. The dinuclear complex $[Ni(ebsms)]_2$ is found to be light-sensitive; the yield of the complex was drastically improved when it was synthesized in dark. Upon stirring a toluene solution of the complex $[Ni(ebsms)]_2$ in the presence of UV light, it yields another dinuclear complex $[Ni(S_2S')]_2$ and oligoisobutylene sulfide through a C–S bond cleavage reaction, proposedly provoked by the light-induced formation of a Ni(I)-S$^{\bullet}$ radical species in solution. The presence of Ni(I)-S$^{\bullet}$ radical character in $[Ni(ebsms)]_2$ is indicated by the unusual disorder and the short Ni–S distance (2.139(3) Å) as observed in the X-ray crystal structure of $[Ni(ebsms)]_2$, the broad signals observed in the ^{1}H NMR spectra of $[Ni(ebsms)]_2$, and the products obtained from the light-induced C–S bond cleavage reaction. The results are discussed in the light of the function of methyl coenzyme M reductase.

9.2. General Discussion, Conclusions and Future Perspectives

In contrast to the many stable nickel(II), [NiFe] and [NiRu] complexes that are reported to have tetradentate N_2S_2-donor or bidentate NS-donor ligands, the complexes reported in this thesis have been synthesized using tetradentate $S_2S'_2$-donor and bidentate SS'-donor ligands.[1-5] The thiouronium salts of both tetradentate $S_2S'_2$-donor and bidentate SS'-donor ligands have been synthesized in good yield. These thiouronium salts are found to be air stable and odorless crystalline solids, which can be stored for many months without noticeable changes; this helped to circumvent the synthesis and manipulation of oxidation sensitive, unstable and pungent smelly thiol compounds. The synthesis route followed in this thesis may be employed to make a whole range of new ligands and their complexes. Even though all the $[Ni(S_2S'_2)]$ complexes could be synthesized in toluene, some complexes have been obtained in better yield when using different solvents such as THF ([Ni(ebss)] and [Ni(xbss)]). Likewise, the $[Ni(SS')_2]$ complexes could be formed in ethanol or in toluene; however, the synthesis in toluene showed better yields and needed no further purifications.

Although not all of the X-ray crystal structures of the $[Ni(S_2S'_2)]$ and $[Ni(SS')_2]$ complexes are known, in general it is assumed that these complexes acquire slightly distorted square-planar NiS_4 coordination spheres. The $[Ni(S_2S'_2)]$ complexes possess enforced *cis* orientation of thiolates and thioether donors whereas the $[Ni(SS')_2]$ complexes possess highly preferred *trans* orientation.[6] However, the *trans* oriented $[Ni(SS')_2]$ complexes acquire *cis* orientation upon reaction with other moieties such as FeX_2, ZnX_2 (X = Cl, Br, I), CuI, $[Fe_2(CO)_9]$, $[Fe(CO)_2(NO)_2]$, $[Fe(CO)_4I_2]$, $[Fe(CO)_5]$ and $[Fe(C_5H_5)(CO)]^+$.[6-10] Even though the new $[Ni(S_2S'_2)Fe(C_5H_5)(CO)](PF_6)$ and

$[Ni(SS')_2Fe(C_5H_5)(CO)](PF_6)$ complexes are not structurally characterized, the combination of data obtained from various techniques such as ESI-MS spectrometry, FTIR spectroscopy and elemental analysis, and the reported structure of $[Ni(pbss)Fe(C_5H_5)(CO)](PF_6)$ are helpful in understanding the structures of these complexes.[1] The ^1H NMR spectroscopy and the known X-ray crystal structure of $[Ni(pbss)Ru(bpy)_2](PF_6)_2$ were very helpful in elucidating the structure of the three $[Ni(S_2S'_2)Ru(bpy)_2](PF_6)_2$ complexes in solution.

All the six $[Ni(S_2S'_2)Fe(C_5H_5)(CO)](PF_6)$ complexes are found to be active as electrocatalysts in proton reduction and also found to be relatively stable in higher concentrations of acetic acid. The increase in the flexibility of the NiS_4 coordination sphere favors the lower negative E_{HER} values whereas the electron-withdrawing dimethyl groups tend to shift the E_{HER} values to higher negative. All the three active $[Ni(SS')_2Fe(C_5H_5)(CO)](PF_6)$ complexes reduce protons around –0.9 V *vs*. Ag/AgCl; this less potential (E_{HER}) is negative than that of the $[Ni(S_2S'_2)Fe(C_5H_5)(CO)](PF_6)$ complexes. It appears – according to the available observations – that the $[Ni(SS')_2Fe(C_5H_5)(CO)](PF_6)$ complexes readily undergo protonation on the thioether sulfurs of the bidentate SS'-donor ligands; this protonation is advantageous, as this behavior assists in reducing the complexes easily; on the other hand it is disadvantageous because it leads to the decomposition of the complexes $[Ni(bsms)_2Fe(C_5H_5)(CO)](PF_6)$ and $[Ni(cpsms)_2Fe(C_5H_5)(CO)](PF_6)$.

As it was found that increased flexibility of tetradentate ligands favors proton reduction at lower potentials, but bidentate ligands are too flexible leading to decomposition, future studies should be directed to the synthesis of more flexible tetradentate ligands comprising electron-withdrawing groups. In this view tetradentate P_2S_2-donor ligands also may be useful, as the electronic and steric properties of phosphine ligands in general are easily modified.

The three active [NiRu] complexes are found to work at –1.01, –1.06 and –1.43 V *vs*. Ag/AgCl with promising stability in the presence of protic acids. Surprisingly, all three $[Ni(S_2S'_2)Ru(bpy)_2](PF_6)_2$ complexes are stable in the presence of 20 equivalents of trifluoroacetic acid for months as determined by ESI-MS spectrometry, showing the high acid tolerance of the complexes. A preliminary study yielded the complexes $[Ni(pbss)Ru(tpa)_2](PF_6)_2$ and $[Ni(pbsms)Ru(tpa)_2](PF_6)_2$ (Fig. 9.1). The tripicolylamine (tpa) ligand may dissociate one of the pyridyl rings, opening a catalytic site at the ruthenium center.[12] These [NiRu] complexes open a new avenue as they comprise both redox-active and photo-active moieties directly connected together. Future studies including the photoelectrocatalytic properties of these complexes may be highly interesting, especially in view of the development of a hydrogen economy.

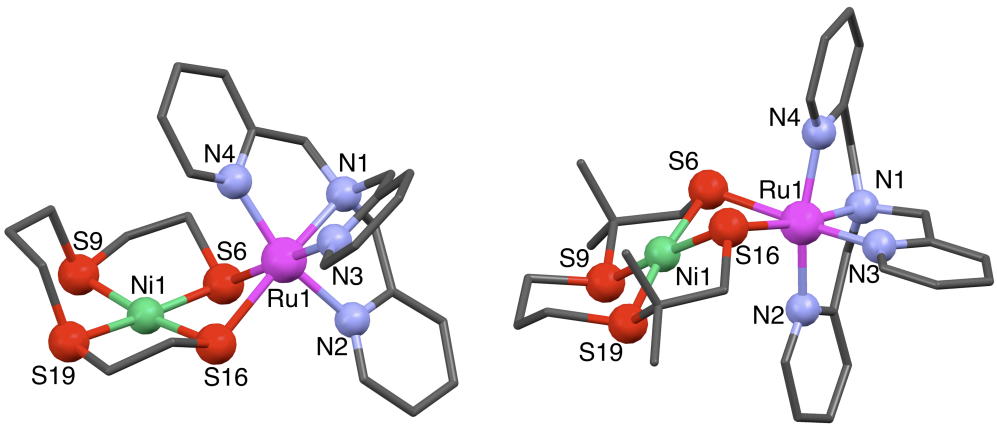

[Ni(pbss)Ru(tpa)]$^{2+}$ [Ni(pbsms)Ru(tpa)]$^{2+}$

Fig. 9.1. Perspective views of new [Ni($S_2S'_2$)Ru(tpa)](PF_6)$_2$ complexes synthesized as models for [NiFe] hydrogenases.[11]

Owing to the stability of the [Ni_6(cpss)$_{12}$] and the simple ^{1}H NMR spectra as compared to the other reported complexes, protonation studies were successfully performed shedding light on the mechanism of electrocatalytic proton reduction. The thioether sulfurs of the ligands Hcpss in the complex [Ni_6(cpss)$_{12}$] were found to be readily protonated; this observation explains both the electrocatalytic properties of this hexanuclear complex and the acid induced decomposition of the [Ni(SS')$_2$Fe(C_5H_5)(CO)](PF_6) complexes.

The heterooctanuclear cage [{Ni(mpsms)$_2$}$_2$($CuI)_6$] proved the robustness of the [Ni(SS')$_2$] complexes reported in this thesis in view of the synthesis of suitable models for hydrogenases and as well for other nickel containing enzymes. Further investigation and utilization of the secondary contacts such as Ni···H interactions observed in this cage structure may pave the way for the synthesis of future mimics with self-stabilizing intra or intermolecular frameworks.

9.3. References

1. W. F. Zhu, A. C. Marr, Q. Wang, F. Neese, D. J. E. Spencer, A. J. Blake, P. A. Cooke, C. Wilson and M. Schröder, *Proc. Natl. Acad. Sci. U. S. A.*, 2005, **102**, 18280-18285.
2. E. Bouwman and J. Reedijk, *Coord. Chem. Rev.*, 2005, **249**, 1555-1581.
3. S. Ogo, R. Kabe, K. Uehara, B. Kure, T. Nishimura, S. C. Menon, R. Harada, S. Fukuzumi, Y. Higuchi, T. Ohhara, T. Tamada and R. Kuroki, *Science*, 2007, **316**, 585-587.
4. M. A. Reynolds, T. B. Rauchfuss and S. R. Wilson, *Organometallics*, 2003, **22**, 1619-1625.
5. P. A. Stenson, A. Board, A. Marin-Becerra, A. J. Blake, E. S. Davies, C. Wilson, J. McMaster and M. Schröder, *Chem.-Eur. J.*, 2008, **14**, 2564-2576.
6. J. A. W. Verhagen, D. D. Ellis, M. Lutz, A. L. Spek and E. Bouwman, *J. Chem. Soc.-Dalton Trans.*, 2002, 1275-1280.
7. J. A. W. Verhagen, C. Tock, M. Lutz, A. L. Spek and E. Bouwman, *Eur. J. Inorg. Chem.*, 2006, 4800-4808.

8. J. A. W. Verhagen, M. Beretta, A. L. Spek and E. Bouwman, *Inorg. Chim. Acta*, 2004, **357**, 2687-2693.
9. J. A. W. Verhagen, M. Lutz, A. L. Spek and E. Bouwman, *Eur. J. Inorg. Chem.*, 2003, 3968-3974.
10. R. Angamuthu, L. L. Gelauff, M. A. Siegler, A. L. Spek and E. Bouwman, *Chem. Commun.*, 2009, 2700-2702.
11. R. Angamuthu, S. Romón-Roig, M. A. Seigler, A. L. Spek and E. Bouwman, *Manuscript under preparation*, [Ni(S2S'2)Ru(tpa)](PF6)2 Complexes.
12. T. Kojima, T. Morimoto, T. Sakamoto, S. Miyazaki and S. Fukuzumi, *Chem.-Eur. J.*, 2008, **14**, 8904-8915.

Samenvatting

Summary in Dutch

Het voornaamste doel van het onderzoek beschreven in dit proefschrift is het ontwerp, de synthese en de karakterisatie van geschikte structurele en functionele modellen voor het [NiFe]-hydrogenase-enzym. Tevens worden in dit proefschrift modellen van andere nikkelbevattende enzymen beschreven, die resulteerden uit interessante bevindingen van belang voor het hoofdonderwerp van het proefschrift.

Het eerste deel van Hoofdstuk **1** geeft een beknopt overzicht van nikkelbevattende enzymen, met nadruk op de klasse van hydrogenases. Van de structurele en functionele eigenschappen van de enzymen en van specifiek geselecteerde modelcomplexen wordt ook een overzicht geschetst. Hoofdstuk **1** wordt afgesloten met een overzicht van het proefschrift en een korte samenvatting van de voorgestelde strategieën voor de structurele en functionele modellering van de [NiFe]-hydrogenases.

Het ontwerp, de synthese en de karakterisatie van nieuwe tetradentaatliganden van het type dithioether-dithiolaat ($S_2S'_2$) en van bidentaatliganden van het type thioether-thiolaat (SS') worden beschreven in Hoofdstuk **2**; schema's van de ligandsyntheses en vereenvoudigde code-notaties voor deze liganden met hun betreffende precursors en tussenproducten worden hier ook gegeven. De tetradentaatliganden zijn op een dusdanige manier ontworpen/geselecteerd dat zij systematisch gevarieerde sterische en elektronische eigenschappen bezitten. De liganden H_2ebss, H_2pbss en H_2xbss hebben bruggende ethyl-, propyl- en xylylgroepen. Tevens zijn deze liganden gesubstitueerd met twee elektrondonerende methylgroepen op de *β*-koolstoffen van de ethylthiolaatarmen om de elektronische eigenschappen voor H_2ebss, H_2pbss en H_2xbss te variëren. De bidentaatliganden bezitten verschillende groepen, zoals benzyl, 4-methylphenyl, isobutyl en *n*-hexyl, gebonden aan de zwavel van de thioether. Deze zijn gesynthetiseerd zonder de twee methylgroepen op de *β*–koolstof van de ethylthiolaatarm.

Een serie nieuwe nikkelcomplexen in de low-spin-toestand, met nieuwe tetradentaatliganden van het type dithioether-dithiolaat wordt beschreven in Hoofdstuk **3**. Twee van deze complexen, $[Ni(ebsms)]_2$ and [Ni(pbsms)], zijn gekarakteriseerd door

middel van X-ray-kristallografie. $[Ni(ebsms)]_2$ is een co-planair dinucleair complex met twee licht verstoorde vierkant-piramidale NiS_5-eenheden, gebrugd door twee thiolaten. Een opvallend korte Ni–$S_{thioether}$-afstand (2.139(3) Å) en interessante Ni···H_{Me} interacties (2.66 and 2.74 Å) worden ook waargenomen in de kristalstructuur. [Ni(pbsms)] is een mononucleaire verbinding met een vlak-vierkante structuur, in overeenstemming met met de eerder gerapporteerde structuren van [Ni(pbss)] en [Ni(xbsms)]. De Ni–$S_{thiolaat}$-afstanden voor [Ni(pbsms)] zijn, evenals die voor [Ni(pbss)], langer dan de Ni–$S_{thioether}$-afstanden, wat in contrast staat tot de normale observatie.

Deze low-spin-nikkelcomplexen werden gereageerd met $[Fe(C_5H_5)(CO)_2I]$ om de [NiFe]-complexen te verkrijgen, waarvan één complex al in de literatuur bekend is. De elektrokatalytische eigenschappen betreffende protonreductie worden tevens beschreven in Hoofdstuk **3**. Alle zes [NiFe]-complexen laten elektrokatalytische protonreductie-activiteit zien in de aanwezigheid van azijnzuur als bron van protonen. Katalytische reductie van H^+ wordt al waargenomen bij potentialen van –1.19 V ten opzichte van Ag/AgCl voor $[Ni(pbss)Fe(CO)(C_5H_5)](PF_6)$ in acetonitril. Het blijkt dat meer flexibiliteit van de ligandbrug leidt tot elektrokatalysatoren die een lagere overpotentiaal nodig hebben, terwijl elektrondonerende dimethylsubstitutie van de liganden juist leidt tot de noodzaak van hogere overpotentialen.

De ervaringen opgedaan in hoofdstuk **3** leidde tot het gebruik van twee bidentaat SS'-donor-liganden in plaats van één tetradentaat S_2S_2-donor-ligand, omdat een toename in flexibiliteit in de NiS_4 coördinatieomgeving lagere overpotentialen mogelijk maakt bij de protonreductie. Hoofdstuk **4** is gewijd aan analoge [NiFe]-complexen gebaseerd op nieuwe $[Ni(SS')_2]$-complexen. De $[Ni(SS')_2]$-complexen beschreven in dit hoofdstuk werden verkregen door $Ni(acac)_2$ met bidentaat thioether-thiolaatliganden uit Hoofdstuk **2** te laten reageren. Het ligand dat is gesubstitueerd met twee methylgroepen geeft hexanucleaire ($[Ni_6(cpss)_{12}]$), of onoplosbare oligonucleaire $[Ni(mpss)_2]_n$-complexen. Deze low-spin-nikkelcomplexen werden gereageerd met $[Fe(C_5H_5)(CO)_2I]$ in dichloormethaan onder een trage argonstroom, om zodoende de [NiFe]-complexen te verkrijgen. De elektrokatalytische eigenschappen voor protonreductie worden ook gerapporteerd in Hoofdstuk **3**.

De elektrokatalytische protonreductiepotentiaal van deze [NiFe]-verbindingen, E_{HER} blijkt inderdaad lager te zijn dan die van de complexen met tetradentaatliganden

beschreven in Hoofdstuk **3** (~ –0.9 V *vs*. Ag/AgCl). Echter, de stabiliteit van deze $[Ni(SS')_2Fe(C_5H_5)(CO)](PF_6)$ complexen is minder groot dan die van$[Ni(S_2S'_2)Fe(C_5H_5)(CO)](PF_6)$ complexen in de aanwezigheid van protische zuren; de complexen $[Ni(bsms)_2Fe(C_5H_5)(CO)](PF_6)$ en $[Ni(cpsms)_2Fe(C_5H_5)(CO)](PF_6)$ vertoonden directe ontleding in de aanwezigheid van zuur. Dit is waarschijnlijk te wijten aan het feit dat de thioetherzwavels van de $[Ni(SS')_2Fe(C_5H_5)(CO)](PF_6)$-complexen gemakkelijk geprotoneerd worden, wat vervolgens kan leiden tot decompositie.

Om verbeterde elektrokatalysatoren te maken met hogere stabiliteit, werden de $[Ni(S_2S'_2)]$-complexen gereageerd met $[Ru(bpy)_2(EtOH)_2](PF_6)_2$. Zodoende werd een nieuwe klasse van complexen met de algemene formule $[Ni(S_2S'_2)Ru(bpy)_2](PF_6)_2$ verkregen met goede opbrengst. De structuren en protonreductie-eigenschappen worden gepresenteerd in Hoofdstuk **5**. Het complex $[Ni(pbss)Ru(bpy)_2](PF_6)_2$ is gekarakteriseerd door middel van X-ray-kristallografie, waarbij de drie complexen $[Ni(S_2S'_2)Ru(bpy)_2](PF_6)_2$ beschreven in Hoofdstuk **5,** zijn gekarakteriseerd door middel van 1D- en 2D-NMR-technieken. Hieruit blijkt dat het complex $[Ni(pbsms)Ru(bpy)_2](PF_6)_2$ in oplossing uit twee conformeren bestaat, vanwege de dynamische beweging van de dimethylethyleenarmen. Deze drie complexen zijn ook actief in het reduceren van protonen (–1.43 tot –1.01 V *vs*. Ag/AgCl) en zijn gedurende vele maanden stabiel in de aanwezigheid van protische zuren, zoals trifluorazijnzuur.

Een toevallig verkregen hexanucleaire Ni_6-thiolaat-metallakroon, zijn reactiviteit met jood, protoneringstudies en protonreductie-eigenschappen worden gepresenteerd in Hoofdstuk **6.** Twee vierkant-piramidale NiS_5-eenheden en vier vlak-vierkante NiS_4-eenheden zijn samengebrugd via de thiolaten van de Hcpss liganden in de vastefase-structuur. In oplossing hebben alle zes nikkel(II)-ionen een NiS_5-vierkant-piramidale geometrie, zoals gebleken is uit ^{1}H-NMR-spectroscopische studies.

Er is aangetoond, dat de hexanucleaire metallakroon $[Ni_6(cpss)_{12}]$ functioneel overeenkomt met [NiFe]-hydrogenases. Protonering van de $[Ni_6L_{12}]$ cluster is bestudeerd gebruikmakende van ^{1}H-NMR-spectroscopie en ESI-MS-technieken door opeenvolgende additie van dichloorazijnzuur of p-tolueensulfonzuur-monohydraat in oplossingen van $[Ni_6L_{12}]$, respectievelijk in CD_2Cl_2 en DMF-d_7. Protonatie vindt plaats op de thioetherzwavels, die beschikbaar zijn in de metallakroon.

De elektrochemische eigenschappen van $[Ni_6L_{12}]$ in zowel de niet geprotoneerde als de geprotoneerde vorm zijn bestudeerd met behulp van cyclische voltammetrie. Geprotoneerd $[Ni_6L_{12}]$ laat een interessante elektrokatalytische eigenschap zien, aangezien deze de reductie van protonen naar moleculaire waterstof katalyseert in de aanwezigheid van protische zuren, zoals dichloorazijnzuur en chloorazijnzuur bij –1.5 en –1.6 V vs Ag/AgCl in DMF. Een katalytische cyclus is voorgesteld gebaseerd op de observaties uit NMR- en elektrochemische studies van de metallakroon. Het gedrag van deze elektrokatalysator is verder bestudeerd door immobilisatie op het oppervlak van een pyrolitische grafietelektrode. Reductie van een dichloorazijnzuuroplossing in acetonitril op het oppervlak van de bewerkte elektrode vindt plaats bij een 220 mV meer positieve potentiaal dan de reductie op de ongemodificeerde elektrode.

De reactie van het mononucleaire complex $[Ni(mpsms)_2]$ met CuI leverde een hetero-octanucleaire kooiverbinding op, met de formule $[\{Ni(mpsms)_2\}_2(CuI)_6]$, die interessante structurele eigenschappen bezit, waaronder Ni···H anagostische interacties, welke gerapporteerd zijn in Hoofdstuk **7.** De moleculaire structuur van de $[Ni_2Cu_6]$ cluster is bepaald met X-ray-kristallografie. Twee verstoord vlak-vierkante eenheden NiS_4, vier vlak-trigonale CuI_2S en twee tetraëdrische CuI_2S_2 sites zijn aanwezig. De tetraëdrisch verstoorde NiS_4-eenheden zijn vergelijkbaar met het nikkelcentrum van [NiFe]-hydrogenase en de Ni-S-Cu-I-kooistructuur wordt vergeleken met het bifunctionele enzym koolstofmonooxide-dehydrogenase/acetyl-coenzym-A-synthase (CODH/ACS). Bovendien zijn er nieuwe anagostische Ni···H interacties waargenomen in de X-ray-kristalstructuur van de moleculaire kooi, welke stabiel zijn in oplossing, zoals blijkt uit ^{1}H-NMR-spectroscopische studies bij variabele-temperatuur. Dit is de eerste keer dat Ni···H interacties zijn waargenomen in een complex met een NiS_4-coordinatie-omgeving.

Een door licht geïnduceerde C–S-bandbreuk in een nikkel-thiolaatcomplex relevant voor de functie van methyl-coenzym-M-reductase (MCR) wordt gepresenteerd in Hoofdstuk **8**. Het dinucleaire complex $[Ni(ebsms)]_2$ blijkt lichtgevoelig te zijn; de opbrengst van de synthese van dit complex verbeterde drastisch, wanneer deze in het donker werd uitgevoerd. Indien een tolueenoplossing van het $[Ni(ebsms)]_2$-complex geroerd werd in de aanwezigheid van UV-licht, ontstond een alternatief dinucleair complex, $[Ni(S_2S')]_2$; tevens ontstond oligoisobutyleensulfide door een reactie waar de

C-S-band verbroken wordt, waarschijnlijk veroorzaakt doordat er een door licht geïnduceerd Ni(I)–S$^{\bullet}$ radicaal gevormd wordt in oplossing.

De aanwezigheid van een Ni(I)–S$^{\bullet}$-radicaalkarakter in $[Ni(ebsms)]_2$ blijkt uit de ongewone verstoring en de korte Ni–S-afstanden (2.139(3) Å) waargenomen in de X-ray-kristalstructuur van $[Ni(ebsms)]_2$, de brede pieken in de ^{1}H-NMR spectra van $[Ni(ebsms)]_2$ en de producten die verkregen worden in de door licht geïnduceerde afbraakreactie. De resultaten worden besproken met betrekking tot de functie van methyl-coenzyme-M-reductase.

Curriculum vitae

The author of this thesis, Raja Angamuthu, was born on 1980 in Karur (Tamil Nadu, India). After finishing his primary studies in Panchayat Union Elementary School, Vengamedu (1985-1990), he completed secondary (1990-1995) and higher secondary studies (1995-1997, mathematics, physics, chemistry and computer science) in Municipal Higher Secondary School, Karur. In 1997 he commenced with his bachelor studies in chemistry at the Government Arts College Karur affiliated to Bharathidasan University, Tiruchirappalli (Tamil Nadu, India). In 2000, he graduated (distinction) with a major in chemistry with physics and mathematics as ancillaries and stood first in the college.

He continued studying chemistry at School of Chemistry, Bharathidasan University and obtained the M.Sc. degree in Chemistry in May 2002. In the first year of the M.Sc., he was selected as Summer Visiting Student-Fellow of the Indian Academy of Sciences and worked on a project entitled "Metal Ion Reconstituted Hybrid Hemoglobin and Interactions between Hemoglobin and Nitrosohemoglobin" during April-June 2001 under the supervision of Prof. dr. P.T. Manoharan at the Regional Sophisticated Instrumentation Centre, Indian Institute of Technology, Madras (Tamil Nadu, India). In the second year of his masters, he performed a research project on the "Synthesis, Reactivity and DNA Binding Properties of Copper(II) Complexes" for Master's thesis under the supervision of Prof. dr. M. Palaniandavar at Bharathidasan University and continued his research in the same group as a research assistant until March, 2005, when he moved to Leiden University (The Netherlands).

He started his PhD project in the group of Prof. dr. Jan Reedijk in March, 2005. During the next four years, he carried out research concerning nickel-iron, nickel-ruthenium, nickel-copper, copper and zinc complexes of sulfur ligands to mimic the structure and functions of nickel-containing enzymes with special emphasis on the enzyme [NiFe] hydrogenase under the supervision of dr. Elisabeth Bouwman. He supervised four bachelor students namely, Philip Byers (Ithaca College, New York), Wouter Roorda (Leiden), Lodewijk L. Gelauff (Leiden) and Salvador Ramón-Roig (Valencia, Spain) in their research concerning the modeling chemistry of hydrogenases, superoxide dismutases and CODH/ACS. He also assisted at various inorganic and organic practical courses for bachelor students at Leiden University.

Parts of the research described in this thesis has been presented at several national and international conferences as a poster or lecture, including the 7th (2006), 8th (2007), 9th (2008) and 10th (2009) Netherlands Catalysis and Chemistry Conferences in Noordwijkerhout (The Netherlands), the 8th International Hydrogenase Conference in Breckenridge (Colorado, USA, 2007), the 38th International Conference on Coordination Chemistry in Jerusalem (Israel, 2008), the HRSMC symposia in Leiden University (2006) and in University of Amsterdam (2007), NWO meeting: Design and Synthesis, Structure and Reactivity in Biomolecular Chemistry in Lunteren (The Netherlands, 2006), and the HRSMC Autumn School-Advanced Metal-Organic Chemistry, Oegstgeest (The Netherlands, 2006).

In March 2010, Raja will commence his post-doctoral research at the University of Illinois at Urbana-Champaign (USA) in the research group of Prof. dr. Thomas B. Rauchfuss.

ஆசிரியர் குறிப்பு

இந்த ஆய்வுத் தொகுப்பின் ஆசிரியராகிய இராஜா அங்கமுத்து அவர்கள் 1980-ஆம் ஆண்டு இந்தியாவின் தமிழ்நாடு மாநிலத்தில் உள்ள கரூர் நகரத்தில் திருமதி.ஆனந்தி மற்றும் திரு.அங்கமுத்து ஆகியோரின் மகனாகப் பிறந்தார். இவர் தனது துவக்கப்பள்ளிப் படிப்புகளை கரூர் அருகில் உள்ள வெங்கமேடு பஞ்சாயத்து துவக்கப் பள்ளியிலும், மேல்நிலை மற்றும் உயர்நிலைப் படிப்புகளை கரூர் நகராட்சி மேல்நிலைப் பள்ளியிலும் பயின்றார். கரூர் அரசு கலைக் கல்லூரியில் வேதியியல் இளங்கலை பட்டப்படிப்பை 1997-ஆம் ஆண்டு துவங்கி 2000-ஆம் ஆண்டு கல்லூரியில் முதல் மாணவராக தனிச்சிறப்புடன் கூடிய முதல் வகுப்புடன் முடித்தார்.

திருச்சிராப்பள்ளியில் உள்ள பாரதிதாசன் பல்கலைக் கழகத்தில் வேதியியல் துறையில் தனது பட்ட மேற்படிப்பைத் தொடர்ந்தார். வேதியியல் முதுகலைப் படிப்பின் முதலாமாண்டு இறுதியில் "இந்திய அறிவியல் பேராயத்தின்" மூலம் தேசிய அளவில் தேர்ந்தெடுக்கப்பட்ட நூறு மாணவர்களுள் ஒருவரான சென்னை இந்திய தொழில் நுட்பக் கழகத்தின் முதுபெரும் பேராசிரியர் முனைவர் திரு.பெ.தி.மனோகரன் அவர்களுடன் இணைந்து "மைய அணு மாற்றம் செய்யப்பட்ட ஹீமோகுளோபின் உருவாக்கம் மற்றும் நைட்ரோசோஹீமோகுளோபினுடனான வினைகளை'' ஆராய்ந்தார். முதுகலைப்படிப்பின் இரண்டாமாண்டு முழுவதும் பேராசிரியர் முனைவர் திரு.ம.பழனியாண்டவர் அவர்களின் ஆய்வகத்தில் "தாமிர-ஒருங்கிணைவுச் சேர்மங்களை உருவாக்குதல், பண்பறிதல் மற்றும் உயிர் மூலக்கூறுகளுடன் (டி.என்.ஏ) வினைபுரிய வைத்தல்" என்ற தலைப்பில் ஆராய்ச்சி செய்தார். வேதியியல் முதுகலைப் பட்டத்தை முதல் வகுப்பில் 2002-ஆம் ஆண்டு பெற்றபிறகு பேராசிரியர் முனைவர் திரு.ம.பழனியாண்டவர் அவர்களின் ஆய்வுகளால் உந்தப்பட்டு தொடர்ந்து அதே உயிர் கனிமவேதியியல் ஆய்வகத்தில் ஆராய்ச்சி உதவியாளராக 2005-ஆம் ஆண்டு மார்ச் மாதம் நெதர்லாந்து நாட்டிலுள்ள லெய்டன் பல்கலைக்கழகம் செல்லும் வரை பணிபுரிந்தார்.

இராஜா அங்கமுத்து அவர்கள் தனது ஆராய்ச்சிப் படிப்பை ஒருங்கிணைவுச் சேர்மங்களின் வேதியியல் மற்றும் புற்று நோய் எதிர்ப்பு மருந்துகளின் வேதியியலில் பெயர் பெற்றவரான பேராசிரியர் முனைவர் திரு.யான் ரீடைக் என்ற டச்சு வேதியியலாரின் ஆய்வுக் குழுமத்தில் (2005-ஆம் ஆண்டு மார்ச் மாதம்) தொடர்ந்தார். ஏறக்குறைய அடுத்த நான்கு ஆண்டுகளுக்கு நிக்கல்-இரும்பு, நிக்கல்-ருத்தீனியம், நிக்கல்-தாமிரம், தாமிரம் மற்றும் துத்தநாகம் ஆகிய உலோகங்கள் கொண்ட கந்தக ஈனிகளின் சேர்மங்களை இயற்கை நொதிகளின் வடிவ மற்றும் செயல் மாதிரிகளாக உருவாக்கி அவற்றின் மூலம் நொதிகளின் செயல்வழிமுறைகளின் இரகசியங்களை முனைவர் திருமதி.எலிசபெத் பௌமன் அவர்களை வழிகாட்டியாகக் கொண்டு ஆராய்ச்சி செய்தார். இந்த நான்கு ஆண்டுகளில், ஃபிலிப் பையர்ஸ் (இதாகா கல்லூரி, நியூயார்க்), வெளத்தர் ரூர்டா (லெய்டன், நெதர்லாந்து) மற்றும் சல்வடோர் ரமோன்-ராயிஜ் (வேலன்சியா, ஸ்பெயின்) ஆகிய நான்கு மாணவர்களின் ஆராய்ச்சிகளில் வழிகாட்டியாக பணிபுரிந்துள்ளார். மேலும், பல்வேறு கரிம மற்றும் கனிமவேதியியல் செய்முறை வகுப்புகளில் பொறுப்பாளராக பணிபுரிந்துள்ளார்.

இந்த ஆய்வுத் தொகுப்பின் பல்வேறு பகுதிகளை பல்வேறு தருணங்களில் வெளிப்படுத்தும் பொருட்டு கீழ்க்கண்ட மாநாடுகளில் உரையாற்றியும், ஆய்வறிக்கை வெளியிட்டும் உள்ளார். ஏழாவது (2006), எட்டாவது (2007), ஒன்பதாவது (2008), பத்தாவது "நெதர்லாந்து தேசிய வேதியியல் மற்றும் வினைவேகவியல்" மாநாடுகளிலும், அமெரிக்காவின் கொலராடோ மாநிலத்தில் 2007-ஆம் ஆண்டு நடந்த "பன்னாட்டு ஹைட்ரஜனேஸ் மாநாட்டிலும்", இஸ்ரேல் நாட்டின் ஜெருசலம் நகரில் நடைபெற்ற "பன்னாட்டு ஒருங்கிணைவுச் சேர்ம வேதியியல் மாநாட்டிலும்", 2006-ஆம் ஆண்டு லெய்டன் பல்கலைக் கழகத்திலும், 2007-ஆம் ஆண்டு ஆம்ஸ்டர்டாம் பல்கலைக்கழகத்திலும் நடைபெற்ற "ஹாலந்து வேதியியல் ஆராய்ச்சிக் குழுமத்தின்" சந்திப்பிலும் மற்றும் பல்வேறு ஆய்வுக் கூட்டங்களிலும் கலந்து கொண்டுள்ளார். 2010-ஆம் ஆண்டு முதல் இவர் தனது ஆராய்ச்சிகளை அமெரிக்காவின் இல்லினாய்ஸ் பல்கலைக்கழகத்தின் பேராசிரியர் முனைவர் திரு.தாமஸ் பி.ரௌக்ஃபஸ் அவர்களுடன் இணைந்து தொடர்வார்.

List of Publications

1. Copper(II) complexes of tridentate pyridylmethylethylenediamines: Role of ligand steric hindrance on DNA binding and cleavage. [M.Sc. Project]

   R. Angamuthu, R. Venugopal, P. U. Maheswari, B. Ramalingam, C. A. Kilner, M. A. Halcrow, P. Mallayan, *J. Inorg. Biochem.* **2005,** *99*, 1717-1732.

2. $[Ni_6L_{12}]$ metallacrown framework consisting of NiS_4 square-planar and NiS_5 square-pyramidal building blocks. [Chapter **6**]

   R. Angamuthu, H. Kooijman, M. Lutz, A. L. Spek, E. Bouwman, *Dalton Transactions* **2007,** *41*, 4641-4643.

3. A molecular cage of nickel(II) and copper(I): a $[\{Ni(L)_2\}_2(CuI)_6]$ cluster resembling the active site of nickel-containing enzymes. [Chapter **7**]

   R. Angamuthu, L. L. Gelauff, M. A. Siegler, A. L. Spek, E. Bouwman, *Chem. Commun.* **2009,** 2700-2702.

4. Reduction of protons assisted by a hexanuclear nickel thiolate metallacrown: protonation and electrocatalytic dihydrogen evolution. [Chapter **6**]

   R. Angamuthu, E. Bouwman, *Phys. Chem. Chem. Phys.* **2009,** *11*, 5578-5583.

5. $[Ni(S_4)Fe(C_5H_5)(CO)](PF_6)$ complexes containing $S_2S'_2$-donor tetradentate ligands: Synthesis, characterization and electrocatalytic dihydrogen production. [Chapter **3**]

   R. Angamuthu, W. Roorda, M. A. Siegler, A. L. Spek, E. Bouwman, *manuscript in preparation*.

6. Synthesis, characterization and electrocatalytic properties of $[Ni(S_4)Fe(C_5H_5)(CO)](PF_6)$ complexes containing SS'-donor bidentate ligands. [Chapter **4**]

   R. Angamuthu, M. A. Siegler, A. L. Spek, E. Bouwman, *manuscript in preparation*.

7. Heterodinuclear [NiRu] complexes comprising ruthenium bis-bipyridine: Synthesis, characterisation and electrocatalytic dihydrogen production. [Chapter **5**]

   R. Angamuthu, M. A. Siegler, A. L. Spek, E. Bouwman, *manuscript in preparation*.

8. Light-induced C–S bond cleavage in nickel thiolate complex: Relevance to the function of methyl coenzyme M reductase (MCR). [Chapter **8**]

   R. Angamuthu, W. Roorda, M. A. Siegler, A. L. Spek, E. Bouwman, *manuscript in preparation*.

9. Catalytic CO_2 fixation as oxalate by a copper complex.

   R. Angamuthu, P. Byers, M. Lutz, A. L. Spek, E. Bouwman, *Submitted for publication*.

10. A zinc thiolate complex of a SN_3 tripodal ligand.

    R. Angamuthu, P. Byers, M. Lutz, A. L. Spek, E. Bouwman, *manuscript in preparation*.

11. Heterodinuclear [NiRu] complexes comprising ruthenium tris-picolylamine: Synthesis, characterisation and electrocatalytic dihydrogen production.

    R. Angamuthu, S. Ramón-Roig, M. A. Siegler, A. L. Spek, E. Bouwman, *manuscript in preparation*.

12. A trinuclear nickel to complex $S_2S'_2$-donor tetradentate ligand stabilized by novel anagostic interactions.

    R. Angamuthu, M. Lutz, A. L. Spek, E. Bouwman, *manuscript in preparation*.

Nawoord

Afterword

AT THE END of this thesis, it is time to look back the long way I have travelled to reach this point and to remember those who extended their hands - scientifically, financially, morally, and affectionately - whenever I was in need. Someone said that it is a roller coaster ride after a long period to think back to the interesting and exciting moments. So, the reader may have a blurred picture at some places as you are sitting in a roller coaster: start the tour.

HATRED AND LOVE: The first day when I came to Leiden, Uma and Sudeshna took me to the famous “Pannenkoekenhuis” (pancake house) for dinner in view of arranging some food that looks and tastes like Indian food. In 20 minutes there was pancake in front of me covered with a beautiful layer of cheese which I never tasted before. After taking three successful bites I got a feeling of throwing up. Within two years after this incident I had a library of cheese in my kitchen, as I am now addicted to the taste of cheese; “kipcorn” and “kibbeling met knoflooksaus” are the two other things, which have drawn my attention in these four years.

NEUSSPRAY EN OOGDRUPPELS: Since the spring 2006 the grass pollens have fallen in love with me. So, the doctor gave me very good “neusspray” and “oogdruppels”; the strange thing was my allergic symptoms were worsening after a week of using these two medicines. Somehow I discovered the real problem after meeting the doctor in my second visit that I had to use the oogdruppels (eye drops) on my eyes and neusspray (nose spray) in the nostrils, but not the other way around. I had just learned two new Dutch words.

THE FOUR STUDENTS whom I came across in this four-year period shaped me a lot in many ways. Phil was my first student who came from New York for a summer project of 10 weeks, but the results are worth more than that. We both were very new for the chemistry, which we planned to do. We did not get the results that we wanted; yet the results we obtained were mind blowing at the end. Wouter: the second and one of the highly motivated students who worked with me. He did work in the lab without releasing thiol smell, which I did a lot when I started to work with thiols. I still wonder how he is able to do all the things in a day of 24 hours; attending classes, private teaching for the high school kids, chess club, movies club, poker club, football club, writing articles to the student magazine etc. The project we planned for Lodewijk was highly promising; unfortunately there were no successes with the plans, yet we managed to get a beautiful Chemical Communications from the reaction, which he did in the last days of his project. Salva worked for 10 months and the chemistry resulted in two interesting structures.

Unfortunately, it was not possible to include the results of his work in the thesis in view of time. Yet there is a small piece added in the summary with the structures of the [NiRu] complexes obtained by him.

SERENDIPITY: I still remember the days when Rohan tried to explain the meaning of strange English words like serendipity. It was not easy to me to understand the different accents in a group of students from different countries in the earlier days in Leiden. So I started to watch the TV serials such as Friends. I used to laugh when my flat mates laughed; Manik and Rohan found this out one day. They were laughing when nothing was funny in the program and I was also laughing as they were laughing. Funny days… The people who made my earlier days easy in Leiden are Avila Gustavo, Franchisco, Manik, Rohan, Juan Jose, Ted, Tapan, Kannappan, Meenal, Uma, Krishnamohan, Sudeshna-kka.

MY FELLOW SCIENTISTS. Joris, Meenal, Stefania, Martha, Jimmmy, Tidddo and Prasad have made these four years go very fast. Joris' unexpected delivery of jokes, funny and stupid discussions with Marta and Jimmy, Mercury explanations of Tiddo are memorable events. I was not lucky enough to share the office with other interesting colleagues such as Patricia, Ferry, Nuria, Geoff, Susmit and Ariadna. Balamurugan, Stanley, Ramamurthy, Kallu mama, Geetha, Sivaslevi, Sasikala, Lakshmikanthan, Mathiselvam, Siva, Maheswari, Manimekalai, Sakthivel, Maheswaran, Prabha, Kavitha, Mahesh, Kathirvel, Thamilarasan, Shafiyullah, Thilagavathi, Priya, Rajakumari, Ramesh, Sridevi, SKS (sivagamasundari), Nagi, Bhuvaneswari, Jacsy (Shanthi), Loyesu, Shanthi, Morali (Muralidharan), Paraman, Balasubramani (Nile water), Keetchu, Hemakka, Mothi, GV, Naresh, Thanikachalam, Baby, Tharumarasa, Mogly (Mohan) are other important fellow scientists who ate and drunk chemistry with me.

COCHIN EXPRESS OR 06:40: Sivasubramani, Sureshbabu, Manikandan, Dr. Mohan, Dr. Raja, Nachimuthu, Vicky, Geetha, Surya, Bharathi, Neelavathi, Manju, Mani, Anni, Apsal, Fareetha, Ilhaam, Baayammaa are assisting my parents which made my stay away from home comfortable.

THE THINGS THAT PAVED THE WAY FROM K1 TO KLM: Mr. Sundarrajan and his family member's constant support, Dr. Palaniandavar's bioinorganic chemistry, Dr. Jeyaraman's retrosynthetic analysis, Dr. Panchanatheswaran's organometallic chemistry, Dr. Venuvanalingam's atom in the box, Dr. Renganathan's theories of kinetics, Dr. Arunachalam's theories of electrochemistry, Dr. Thomas Muthiah's 'metals in life' classes, Dr. Nallu's reaction mechanism classes, Dr. Jaswanth's encouragements, Palnadan sir's maths, Gowri akka's advices, Gayathri's "don't care about akka's advices", Jose akka's lunch and love, Vijaya madam's breakfast, Uma madam's support, Nesamony anna's prayers, JG and Jhon's chemistry classes in high school days, Ramu Ayya's Ramayanam and the flawless efforts made by many teachers who shed light on α, β's of life with τ, Δ, Λ's of chemistry.

VANAKKAM: Jos' "Vanakkam", Jopie's "Yes, I can measure", John's "Yes, I have time", Ge's "Jaa, we can do it", Cees' "Hij is vroeg altijd", Fons' "No problem, it is possible to measure", Yvonne and Esther's "I can do it for you", and Prof. Spek, Dr. Lutz, Dr. Kooijman and Dr. Siegler's beautiful crystal structures, and last but not least "Everything under control ?!?" and "it looks promising !!!" made the research in Leiden exciting and feasible for the past four years.

MY PARENTS - Ananthi and Angamuthu - are my first teachers. One among many interesting Tamil proverbs said frequently by my mom when I was a kid: "One can use at least his hair as a rope to pull the mountain when he has nothing else; he will get a mountain if it moves or else he will loose only the hair, but not hope".

RASU: Prasad, Lakshmi akka, Prasanna, Karthik, Ravishankar, Shiva, Jos and Loes made the life away from the lab more interesting. Babu, Siva, Satthi, Loyes, Paraman and their friends took my place and responsibilities in India while Mayes, Prabha, Shanthi and Loyes were cheering me with their mails or calls. That's it for now.